

Part I:  
miR-9/9\* regulate the tumor suppressor CAMTA1  
in glioblastoma stem cells

Part II:  
Nuclear transport of Argonaute and TNRC6 proteins

DISSERTATION

Daniel Schraivogel

Regensburg, 2015



Part I:

# miR-9/9\* regulate the tumor suppressor CAMTA1 in glioblastoma stem cells

Part II:

# Nuclear transport of Argonaute and TNRC6 proteins



DISSERTATION ZUR ERLANGUNG DES DOKTORGRADES DER  
NATURWISSENSCHAFTEN (DR. RER. NAT.) DER FAKULTÄT FÜR BIOLOGIE UND  
VORKLINISCHE MEDIZIN DER UNIVERSITÄT REGENSBURG

vorgelegt von

**Daniel Schraivogel**  
aus Ochsenhausen

Regensburg, 2015

Das Promotionsgesuch wurde eingereicht am:

13.02.2015

Die Arbeit wurde angeleitet von:

Prof. Dr. Gunter Meister

---

(Daniel Schraivogel)

*Any living cell carries with it the experience of a billion years of experimentation by its ancestors.  
You cannot expect to explain so wise an old bird in a few simple words.*

(Max Delbrück, 1949)



# Contents

Summary	11
<b>I. General introduction</b>	<b>13</b>
1. Small non-coding RNAs	14
2. Biogenesis of miRNAs in mammals	16
3. Argonaute and TNRC6 proteins	22
3.1. Argonaute proteins are key players in miRNA-mediated gene silencing . . . . .	22
3.2. TNRC6 proteins are the effector proteins recruited by Argonaute . . . . .	24
3.3. Intracellular localization of gene silencing components . . . . .	26
4. Post-transcriptional gene silencing processes	29
<b>II. miR-9/9* regulate CAMTA1 in glioblastoma stem cells</b>	<b>33</b>
1. Introduction	34
1.1. Small RNA-mediated gene regulatory pathways in cancer . . . . .	34
1.2. <i>Glioblastoma multiforme</i> . . . . .	36
1.3. Cancer stem cell hypothesis . . . . .	40
2. Aims of part II	44
3. Results	45
3.1. Small RNA profiling of GSCs . . . . .	45
3.2. miR-9/9* function as oncogenes in GBM and GSCs . . . . .	47
3.3. Identification of miR-9* targets . . . . .	50
3.4. Characterization of the novel tumor suppressor CAMTA1 . . . . .	50
3.5. Identification of CAMTA1 target genes . . . . .	58
4. Discussion of Part II	62
<b>III. Nuclear Import of Argonaute and TNRC6 proteins</b>	<b>67</b>
1. Introduction	68
1.1. Small RNA-mediated gene regulation in the nucleus . . . . .	68
1.2. Diverse nuclear small RNA-guided functions in mammals . . . . .	71
1.3. Nuclear transport processes . . . . .	72

1.4. Nuclear transport of small RNA-silencing proteins . . . . .	77
<b>2. Aims of part III</b>	<b>80</b>
<b>3. Results</b>	<b>81</b>
3.1. Nucleo-cytoplasmic distribution of human Ago2 . . . . .	81
3.2. Ago2 import and shuttling . . . . .	82
3.3. Nuclear transport of Ago2 . . . . .	85
3.4. TNRC6 proteins are nucleo-cytoplasmic shuttling proteins . . . . .	90
3.5. Nuclear import of TNRC6 proteins is mediated by Imp $\alpha$ and Imp $\beta$ . . . . .	93
3.6. Cytoplasmic Ago and TNRC6 levels influence nuclear localization . . . . .	97
<b>4. Discussion of Part III</b>	<b>100</b>
<b>IV. Materials and Methods</b>	<b>105</b>
<b>1. Materials</b>	<b>106</b>
1.1. Chemicals and Enzymes . . . . .	106
1.2. Instruments . . . . .	106
1.3. Buffers and Solutions . . . . .	107
1.4. DNA and RNA oligonucleotides . . . . .	114
1.5. Plasmids . . . . .	119
1.6. Antibodies . . . . .	120
1.7. Bacterial Strains and Media . . . . .	122
1.8. Mammalian Cell lines and Media . . . . .	123
<b>2. Molecular Biological Methods</b>	<b>127</b>
2.1. DNA cloning . . . . .	127
2.2. Working with RNA . . . . .	130
2.3. cDNA synthesis and quantitative real-time PCR . . . . .	132
2.4. miRNA target identification . . . . .	132
2.5. Transcriptome analysis after CAMTA1 overexpression . . . . .	133
2.6. Generation of small RNA libraries and Deep sequencing . . . . .	133
<b>3. Proteinbiochemical methods</b>	<b>135</b>
3.1. Immunoprecipitations . . . . .	135
3.2. Protein expression, purification and antibody production . . . . .	135
3.3. Antibody production and purification . . . . .	137
3.4. <i>in vitro</i> transcription/translation . . . . .	137
3.5. Preparation of cell extracts . . . . .	138
3.6. GST pulldowns . . . . .	138
3.7. SDS-PAGE and Western-Blot . . . . .	139
<b>4. Cell Biological Methods</b>	<b>140</b>
4.1. Cultivation of mammalian cells . . . . .	140
4.2. Cultivation of insect cells and baculovirus production . . . . .	140
4.3. Cell transfections . . . . .	141

---

4.4. Preparation of stable cell lines . . . . .	141
4.5. Investigation of nucleocytoplasmic transport processes . . . . .	142
4.6. Flow cytometry . . . . .	143
4.7. Neurosphere-formation assays . . . . .	143
4.8. Luciferase Reporter Assays . . . . .	144
<b>5. Microscopy</b>	<b>145</b>
5.1. Immunofluorescence stainings . . . . .	145
5.2. Microscopy . . . . .	145
5.3. Microscopy data analysis and quantifications . . . . .	146
<b>6. <i>In vivo</i> Experiments</b>	<b>148</b>
6.1. Mouse strains . . . . .	148
6.2. Murine xenograft model for CAMTA1 overexpression . . . . .	148
6.3. Isolation of neural stem cells . . . . .	149
6.4. Mouse genotyping . . . . .	149
<b>7. Computational methods and statistical analyses</b>	<b>151</b>
7.1. Analysis of glioblastoma patient data . . . . .	151
7.2. Prediction of classical NLS and NES sequences . . . . .	151
7.3. Statistical analyses . . . . .	152
<b>Appendix</b>	<b>153</b>
<b>Contributions</b>	<b>163</b>
<b>List of Figures</b>	<b>164</b>
<b>List of Tables</b>	<b>166</b>
<b>List of Abbreviations</b>	<b>167</b>
<b>Bibliography</b>	<b>169</b>
<b>Publications and Presentations</b>	<b>200</b>
<b>Curriculum vitae</b>	<b>202</b>
<b>Acknowledgements</b>	<b>203</b>



# Summary

Small non-coding RNAs like microRNAs (miRNAs) are important regulators of gene expression. miRNAs bind to a member of the Argonaute (Ago) protein family and guide them to partially complementary sequences on target messenger RNAs (mRNAs). Argonaute-miRNA complexes silence target mRNAs by inducing translational repression and mRNA decay. To mediate these effects, Argonaute proteins interact with a member of the TNRC6 protein family, which recruit deadenylase and decapping complexes to the mRNA.

Post-transcriptional gene regulation by miRNAs has been implicated in central processes like differentiation, development and cell proliferation. Consequently, miRNAs also play important roles in diseases including cancer. In cancer, miRNAs can regulate both tumor suppressors and oncogenes. To get deeper insights into the role of miRNAs in cancer, we analyzed the role of miRNAs in cancer stem cells. Cancer stem cells are an undifferentiated subpopulation of cancer cells with properties of normal tissue stem cells including self-renewal and multipotency. Interestingly, it is thought that cancer stem cells drive tumor growth, contribute significantly to therapy resistance and cause tumor recurrence after therapy. We therefore isolated cancer stem cells and non cancer stem cells from *Glioblastoma multiforme*, an highly malignant brain tumor, which is thought to be driven by a cancer stem cell population. We analyzed miRNA expression between cancer stem cells and their non stem cell counterpart and identified miRNAs including miR-9, miR-9\* and miR-17 to be preferentially expressed in glioblastoma stem cells. Inhibition of these miRNAs led to significantly reduced tumor growth *in vitro*, decreased the cancer stem cell pool and stimulated cell differentiation. To further characterize the function of miR-9\*, we identified target genes including the putative transcription factor Calmodulin-binding transcription activator 1 (CAMTA1). CAMTA1 was validated as novel tumor suppressor in *Glioblastoma multiforme*, as overexpression of CAMTA1 led to strongly reduced tumor growth *in vitro* and *in vivo* and CAMTA1 expression correlated with patient survival. As CAMTA1 is a putative transcription factor, we further characterized potential CAMTA1 regulated genes. We identified the anti-proliferative cardiac hormone natriuretic peptide A (NPPA), which might at least in part mediate the tumor suppressive effects of CAMTA1. Therefore, these findings provide deep insights into novel players in *Glioblastoma multiforme* and cancer stem cell biology and could provide a basis for therapeutic strategies.

Although miRNAs, Ago and TNRC6 proteins are expected to function in the cytoplasm by regulating mRNAs, they have also been identified in the cell nucleus. However, whereas the post-transcriptional mechanisms in the cytoplasm are well understood, not much is known on their nuclear functions. Furthermore, it is totally unknown how they reach the nucleus to fulfill their nuclear functions. To better understand these processes, we characterized nuclear transport pathways of Ago and TNRC6 proteins. We show that Ago and TNRC6 proteins mainly localize to the cytoplasm but can be also identified in the nucleus of human cells. We provide direct evidence for nuclear import of Ago proteins and show that both Ago and TNRC6 shuttle between the nucleus and cytoplasm. We suggest that Ago proteins are imported by multiple redundant importins and show that TNRC6 proteins are imported via Importin-beta (Imp $\beta$ ). Therefore, both protein families are imported via different import routes. Nuclear export of both Ago and TNRC6 proteins was de-

pendent on Crm1. Finally, we show that both protein families can regulate each others import by a cytoplasmic retention mechanism. In this mechanism, Ago-TNRC6 interaction prevents nuclear import, whereas free Ago and TNRC6 pools can be imported into the nucleus. We further provide evidence that Ago prevents the nuclear import of TNRC6 proteins by masking nuclear localization signals in TNRC6. We therefore suggest that nuclear import balances cytoplasmic Ago-TNRC6 levels, a mechanism that might be important for cytoplasmic miRNA-mediated gene silencing as well as possible nuclear Ago and TNRC6 functions.

## **Part I.**

# **General introduction**

# 1. Small non-coding RNAs

Whether genes are transcribed and translated is strictly regulated by diverse transcriptional and post-transcriptional mechanisms. Transcriptional mechanisms include epigenetic regulation by chromatin modification and binding of transcription factors. Whether the transcribed gene is indeed translated into a protein is additionally regulated on the post-transcriptional level. These mechanisms determine the stability of the messenger RNA (mRNA) and can repress translation by the ribosome. Of these variable post-transcriptional mechanisms, especially the biology of post-transcriptional gene silencing (PTGS) by small non-coding RNAs (ncRNA) caught special interest and is a major topic of this work.

Small ncRNAs were originally identified in *Caenorhabditis elegans* (*C. elegans*). Victor Ambros and Gary Ruvkun discovered that the unusual *lin-4* gene produces a small ncRNA, that can suppress *lin-14* protein translation via a proposed 'antisense RNA-RNA interaction' mechanism (Lee et al., 1993, Wightman et al., 1993). Andrew Fire and Craig Mello then made the observation that long double-stranded RNAs (dsRNA) can function as highly potent triggers that silence complementary genes (Fire et al., 1998). This process, called RNA interference (RNAi) made it theoretically possible to knockdown each gene with known sequence in *C. elegans*. The first RNAi experiments in mammalian cells were carried out years later in the Tuschl lab using shorter dsRNAs, overcoming the interferon response of mammalian cells against long dsRNAs (Elbashir et al., 2001). The actual boost in the field came with the discovery of another small ncRNA *let-7* (Reinhart et al., 2000). Strikingly, it was found that *let-7* is not restricted to nematodes but is rather conserved throughout animals, including humans (Pasquinelli et al., 2000). The same was true for *lin-4* and subsequently, other small ncRNAs were identified in diverse organisms (Lagos-Quintana et al., 2001).

The minimal triggers for RNAi are called small interfering RNAs (siRNA) (Elbashir et al., 2001). siRNAs are approximately 21 nucleotides long and double-stranded. They bind to perfect complementarity target sites on mRNAs and function through induction of endonucleolytic cleavage. Small ncRNAs like *let-7* and *lin-4* on the other side are called micro RNAs (miRNAs) (Lagos-Quintana et al., 2001, Lau et al., 2001, Lee and Ambros, 2001). miRNAs are approximately 21 to 24 nucleotides long and double-stranded, i.e. very similar to siRNAs. The difference however is their mode of target RNA binding, as miRNAs bind to only partially complementary target sites. In mammals, miRNA binding sites are located within 3' untranslated regions (UTR) of the target mRNA and binding induces either translational repression or exonucleolytic degradation (Huntzinger and Izaurralde, 2011). Of note, during PTGS of mRNAs in mammals, small ncRNAs generally function as miRNAs and not as siRNAs, i.e. they do not mediate target mRNA cleavage (Fabian et al., 2010). How mammalian miRNAs are generated will be described in part I section 2.

Both siRNAs and miRNAs need associated proteins to mediate their effects. These protein components are targeted sequence-specifically to the miRNA or siRNA binding site on the target mRNA. Argonaute proteins are the key players in siRNA- and miRNA-mediated gene silencing processes (Meister, 2013). Argonautes and siRNAs form an RNA-induced silencing complex (RISC), with Argonaute being the catalytically active component that mediates target RNA cleav-

age. Gene silencing by miRNAs is mediated by the miRNA-induced silencing complex (miRISC). To mediate silencing, miRISC contains not only the miRNA and Argonaute, but additionally another key protein component, which are the so-called TNRC6 proteins (Braun et al., 2013). TNRC6 proteins recruit downstream factors including deadenylase and decapping complexes, which then mediate both translational repression and mRNA degradation. How Argonaute and TNRC6 proteins function and how translational repression and mRNA degradation are induced will be presented in part I sections 3 and 4 of this introduction.

Since their discovery, small RNA-mediated gene silencing processes have been identified in many organisms including *C. elegans*, mammals, plants and yeast (Bartel, 2004). The cellular functions that are under miRNA control are broad and include central processes like differentiation, cell proliferation, metabolism and apoptosis (Peters and Meister, 2007, Bushati and Cohen, 2007). Consequently, miRNAs have also been identified to play important roles in disease processes including cancer (Esquela-Kerscher and Slack, 2006). How miRNAs regulate cancerous processes is one major part of this thesis and will be presented in part I section 1.1.

While it became obvious that miRNAs regulate important cellular processes by mediating PTGS of target mRNAs, the small ncRNA world has been further expanded by the discovery of novel small RNA classes. One example are Piwi-interacting RNAs (piRNAs), which are exclusively expressed in the germ line where they silence transposons (Weick and Miska, 2014). Major contributions to the discovery of novel miRNAs had the availability of the complete genomic sequences of model organisms like *C. elegans*, *Drosophila*, human and mouse, allowing annotation of novel small RNA species (Bartel, 2004). Furthermore, the applicability of deep-sequencing technologies enabled fast and simultaneous sequencing of complete RNomes. Along with the discovery of new small ncRNA classes, also other mechanisms have been identified by which the small RNA mediates its gene regulatory effects. One example is transcriptional gene silencing, in which small RNAs travel into the nucleus bound to Argonaute proteins and induce epigenetic chromatin modifications (Castel and Martienssen, 2013). As nuclear small RNA-mediated functions will introduce to the second major part of this thesis, they will be presented in part I section 1.1.

## 2. Biogenesis of miRNAs in mammals

The processes described in this section generate miRNAs in an ordered multistep biogenesis pathway. The generated miRNAs are then loaded onto Argonaute proteins to build up miRISC, which can bind to target mRNAs to induce silencing. Of note, only the mammalian miRNA biogenesis pathway will be described here, as all work during this study has been done in the human cells. In addition, it will be shown how siRNAs are loaded onto Argonaute and where siRNAs can originate from in the mammalian system.

### miRNA genes and transcription

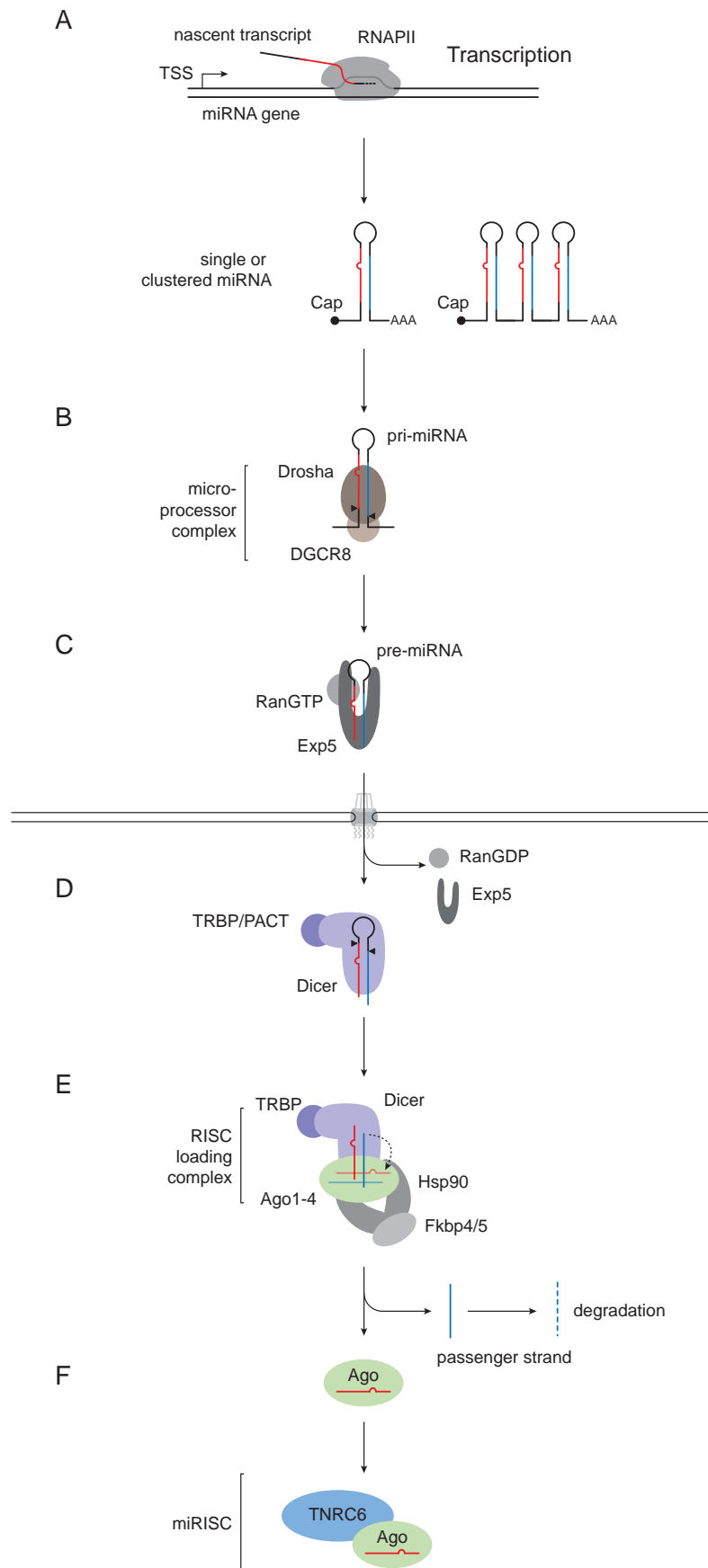
Most mammalian miRNA genes are transcribed by RNA polymerase II (RNAP II) (Lee et al., 2004). The primary transcripts of miRNA-containing genes are called primary miRNA (pri-miRNA). These pri-miRNA transcripts are capped and polyadenylated and of variable length (Cai et al., 2004). The miRNA sequence is part of a stem-loop structure within the pri-miRNA, which serves as substrate for a sequential processing pathway (Figure 1.2.1).

miRNA genes can be found in diverse patterns of genomic organization. Intragenic miRNAs are mostly located within introns or rarely exons of protein-coding or non-coding host genes that have additional functions beyond miRNA expression (Rodriguez et al., 2004). They are mostly transcribed as part of the host gene but can also be expressed from own independent promoters (Ramalingam et al., 2014). Intergenic miRNAs are encoded in previously unannotated regions of the human genome and do require an own promoter. Of note, a clear differentiation between intergenic and intragenic miRNAs is sometimes problematic, especially regarding non-coding hosts genes. In these cases, it is often not clear whether the non-coding transcript solely encodes the miRNA (i.e. intergenic miRNA gene) or has additional functions (i.e. intragenic miRNA gene).

Many miRNAs are multiply encoded within the genome (Kim et al., 2009). One example is hsa-miR-9 (hsa, *Homo sapiens*), which is highly expressed in human brain and encoded in three separate loci miR-9-1, miR-9-2 and miR-9-3. Another important property of genomic miRNA organization are so-called miRNA clusters, i.e. one miRNA transcription unit gives rise to several different miRNAs. Indeed, most mammalian miRNAs are encoded within those clusters, which are expressed as a common polycistronic transcript, are presumably coregulated but independently processed (Altuvia et al., 2005, Lagos-Quintana et al., 2001, Chaulk et al., 2011). One of

---

**Figure 1.2.1. (following page) Biogenesis pathway of miRNAs in mammals.** **A**, pri-miRNA transcripts are capped (Cap) and polyadenylated and contain single or clustered miRNA stem-loops. **B**, The microprocessor complex comprising Drosha and DGCR8 bind the pri-miRNA stem-loop and Drosha cleaves near the stem to release the pre-miRNA. The 5p arms is indicated in red, the 3p arms in blue. **C**, Exp5 bound to RanGTP binds the pre-miRNA and exports as trimeric complex to the cytoplasm. In the cytoplasm, Exp5 and RanGDP release the pre-miRNA. **D**, Dicer and one of its cofactors TRBP and PACT bind the pre-miRNA and Dicer cleaves near the pre-miRNA loop. The product is a mature miRNA heteroduplex. **E**, The RISC loading complex senses the guide (here: 5p arm) and passenger strand and mediates handover of the miRNA to one of the four human Argonaute proteins (Ago1-4). The passenger strand is removed and degraded, whereas the guide strand stays within Argonaute. **F**, Functional miRISC minimally contains the miRNA guide strand, one Argonaute protein and a member of the TNRC6 family proteins. TSS, transcriptional start site; ►, endonucleolytic cleavage site.



the best characterized examples is the miR-17~92 cluster. It is expressed as a single intergenic polycistronic pri-miRNA that contains six tandem stem-loop structures yielding miR-17, miR-18a, miR-19a, miR-20a, miR-19b-1 and miR-92-1. Furthermore, most of the mammalian miRNAs are assigned to so-called miRNA families, which are miRNAs with the same seed sequence (Kim et al., 2009). The seed sequence of a miRNA includes nucleotides 2 to 8 and base pairing of this seed sequence has been shown to be sufficient for miRNA-mRNA binding (Lewis et al., 2003). It is expected that members of a miRNA family have redundant or partially redundant functions. Members of one miRNA family are marked with an alphabetical character suffix, as for example miR-18a and miR-18b.

### **Primary miRNA processing by Drosha**

The first step of the miRNA processing pathway is catalyzed by the so called microprocessor complex (Figure 1.2.1 B). In this step, the stem-loop structure that harbors the miRNA sequence is cut out from the pri-miRNA transcript. The microprocessor complex consists of the RNaseIII enzyme Drosha and its cofactor DiGeorge Syndrome Critical Region Gene 8 (DGCR8) (Gregory et al., 2004, Denli et al., 2004, Han et al., 2004, Landthaler et al., 2004). DGCR8 harbors two double-stranded RNA-binding domains (dsRBDs) and senses the junction of double-stranded and single-stranded (ds, ss) sequences at the base of the pri-miRNA hairpin. DGCR8 seems to recruit and position Drosha on the hairpin, whose RNase III domains mediate cleavage about 11 nucleotides away from the junction (Han et al., 2006b). This cleavage releases the so-called precursor miRNA (pre-miRNA), which has a median length of 70 nucleotides and comprises a single stem-loop.

Drosha processing occurs cotranscriptionally and seems to be linked to splicing (Morlando et al., 2008, Pawlicki and Steitz, 2008, Siomi and Siomi, 2010). In case of intronic miRNAs, pri-miRNA processing is thought to occur before splicing and indeed, splicing is not prerequisite for pri-miRNA processing (Kim and Kim, 2007). However, both processes seem to be highly interconnected, as introns with a miRNA hairpin are spliced more slowly and the early spliceosome complex seems to tether introns during Drosha cleavage (Kataoka et al., 2009). However, the molecular mechanisms that link transcription, splicing and pri-miRNA processing are not characterized in detail. While processing of intronic miRNAs does not obviously affect the expression levels of the host gene (Kim and Kim, 2007), exonic miRNAs processing should affect host gene expression. However, this has not been characterized comprehensively.

### **Precursor miRNA export by Exp5 and processing by Dicer**

The pre-miRNA is exported from the nucleus by the karyopherin Exp5 in a RanGTP-dependent manner (Yi et al., 2003, Bohnsack et al., 2004, Lund et al., 2004, Figure 1.2.1 C). The crystal structure of Exp5 in complex with RanGTP and pre-miR-30a has been resolved and shows that the Exp5-RanGTP complex recognizes the two nucleotide 3'-overhang generated by Drosha cleavage and parts of the hairpin stem (Okada et al., 2009, Figure 1.2.1 C right panel). After transition of the pre-miRNA-Exp5-RanGTP complex through the nuclear pore complex, RanGTP hydrolysis occurs which releases the pre-miRNA.

In the cytoplasm, the pre-miRNA is bound by Dicer and one of its cofactors TAR RNA binding protein 2 (TRBP) and protein activator of PKR (PACT) (Haase et al., 2005, Chendrimada et al., 2005, Lee et al., 2006c). Dicer is, similar to Drosha, an RNaseIII enzyme, i.e. it cleaves dsRNA. TRBP and PACT are dsRNA binding proteins (dsRBPs) with three dsRBDs. TRBP interacts directly with the helicase domain of Dicer and functions in substrate binding and product

length determination (Fukunaga et al., 2012). The exact role of PACT and whether PACT directly contacts Dicer is not known (Lee et al., 2013, Kim et al., 2014a). Both components, Dicer and TRBP contact the pre-miRNA loop and stem and Dicer's RNase III domains mediate cleavage (Zhang et al., 2004, Macrae et al., 2006, Taylor et al., 2013, Wilson et al., 2015, Figure 1.2.1 D right panel). The product of this step is a short dsRNA of about 21 nucleotides with 2 nucleotides 3'-overhangs, a 5'-phosphate and a 3'-hydroxyl group, i.e. a mature miRNA heteroduplex. The two strands within the miRNA heteroduplex are called miR-X-5p and miR-X-3p, with 5p and 3p defining the respective 5' and 3' arm of the pre-miRNA where the strand derives from (X is any miRNA).

### **miRNA-loading onto Argonaute proteins**

To function in PTGS, miRNAs are loaded onto Argonaute proteins (Figure 1.2.1 E). Interestingly, isolated Argonaute proteins hardly bind dsRNAs, indicating that loading of miRNAs onto Argonaute is an assisted mechanism (Meister et al., 2005, Lima et al., 2009, Hauptmann and Meister, 2013). In addition, Argonaute proteins associate with only one strand of the miRNA heteroduplex. Therefore it must be somehow decided which strand stays associated with Argonaute and the other strand must be displaced.

The proteins that assist miRNA-loading include the microprocessor components Dicer and TRBP and a multi-protein chaperone machinery (Dueck and Meister, 2014). Dicer and TRBP directly associate with Argonaute proteins to form the so-called RISC loading complex (Figure 1.2.1 E). Both loading and strand selection occurs within this complex. TRBP is thought to sense the correct strand, whereas Dicer hands over the miRNA heteroduplex to Argonaute (Maniataki and Mourelatos, 2005, Gregory et al., 2005, Noland et al., 2011). Furthermore, Argonaute proteins associate with the chaperone heat shock protein 90 (Hsp90) and the FK506-binding immunophilins Fkbp4/5, which can function as co-chaperones (Frohn et al., 2012, Martinez et al., 2013, Pare et al., 2013). It has been suggested from the investigation of Argonaute loading in plants and flies, that these chaperones keep Argonaute in an open conformation that can accommodate the miRNA duplex (Iki et al., 2010, Iwasaki et al., 2010, Johnston et al., 2010, Martinez et al., 2013). By a not completely understood mechanism, the miRNA duplex is unwound and one miRNA strand is removed (Dueck and Meister, 2014). By definition, the miRNA strand that resides in Argonaute is the guide strand, whereas the discarded strand is the passenger strand, also often referred to as miRNA\* (star) strand.

One important determinant for strand selection is the stability of miRNA ends. The so-called asymmetry rule describes that the strand with the less thermodynamically stable 5'-end is preferentially loaded (Khvorova et al., 2003, Schwarz et al., 2003). Furthermore, Ago proteins have a strong preference for uridine and adenosine at the 5'-position, which might also contribute to strand selection (Frank et al., 2010). Whether other determinants of strand selection exist or if strand selection has a randomized component is not well understood.

### **Formation of functional silencing complexes**

Ago proteins are part of larger effector complexes also known as miRNA-induced silencing complex (miRISC). Although the exact composition of miRISC is still a matter of debate, miRISC is commonly defined by its minimal components consisting of the miRNA guide strand, one Ago protein and one TNRC6 protein (Kim et al., 2009). Whether miRISC assembly follows an ordered

sequence and which mechanisms regulate the assembly of miRISC are not known in detail. Details on Argonaute and TNRC6 proteins and their function within miRISC are described in part I section 3. Furthermore, section 4 will discuss the current knowledge on miRISC assembly and target mRNA binding.

### Origins and mode of function of siRNAs

Whereas miRNAs mediate gene silencing by inducing translational repression and mRNA degradation, siRNAs function by inducing endonucleolytic cleavage of the target RNA. In the mammalian system, siRNAs either originate from endogenous sources or enter the cell from exogenous sources as experimentally transfected siRNAs or viral siRNAs for example.

Endogenous siRNAs (endo-siRNAs) have been identified in mouse oocytes and embryonic stem cells, however their detailed function is not clear (Tam et al., 2008, Babiarz et al., 2008, Watanabe et al., 2008). Endo-siRNAs can originate from various genomic sources, which include hybridized sense-antisense transcripts, transcripts from inverted repeat regions and spliced transcripts from protein-coding genes that hybridize with antisense transcripts from homologous pseudogenes (Figure 1.2.2 A, Tam et al., 2008, Watanabe et al., 2008). The resulting longer dsRNAs are then processed by Dicer into 21 nucleotide long siRNAs (Figure 1.2.2 B). After loading onto Argonaute, endo-siRNAs are thought to induce endonucleolytic cleavage of target RNAs.

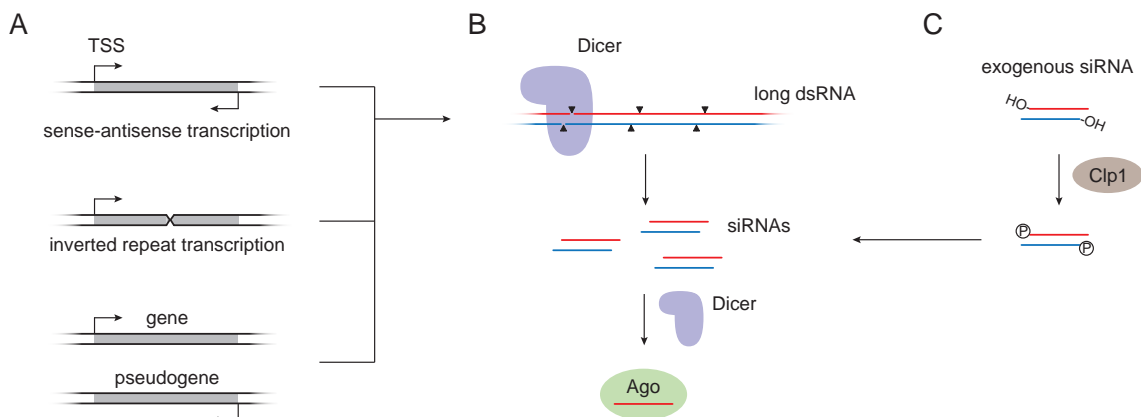


**Figure 1.2.2. Sources of siRNAs in mammals.** **A**, Endogenous siRNAs can originate from various sources, that generate long dsRNAs. These include sense-antisense transcription, transcription of inverted repeat regions and transcription from gene-pseudogene pairs. **B**, Long dsRNAs are cleaved by Dicer proteins into short siRNAs, that are loaded onto Argonaute. **C**, Exogenous experimentally transfected siRNAs are phosphorylated at the 5' end by Clp1 and loaded onto Argonaute in a Dicer-dependent manner. TSS, transcriptional start site; ►, endonucleolytic cleavage site.

For experimental RNAi, siRNAs are synthesized and supplied as 21 nucleotide long RNA duplexes (Elbashir et al., 2001). These chemically synthesized siRNAs generally possess a 5'-hydroxyl moiety and consequently, must get first phosphorylated for stable Argonaute interaction (Figure 1.2.2 C). Indeed, immediately after entry into the cell, the siRNA 5'-hydroxyl groups are phosphorylated by the human RNA kinase Clp1 (Weitzer and Martinez, 2007). Loading of siRNAs seems to depend on Dicer and also follows the asymmetry rule (Khvorova et al., 2003, Schwarz et al., 2003, Sakurai et al., 2011). The resulting RISC, minimally consisting of an siRNA and an Argonaute protein then binds the mRNA and induces mRNA cleavage. The cleavage products are degraded by the exosome from their 3' ends or by the exonuclease Xrn1 from their 5' ends (Orban and Izaurralde, 2005). Of note, the long dsRNAs that have been used in the first effective RNAi experiments in *C. elegans* (part I section 1, Fire et al., 1998) are processed by the

*C. elegans* dicer protein DCR-1 into siRNAs, which then associate with Argonaute (Parrish et al., 2000, Zamore et al., 2000, Hammond et al., 2000, Ketting et al., 2001).

In nematodes, plants and insects, RNAi can function as an antiviral defense mechanism, that generates siRNAs from and consequently against viral genomes or their dsRNA intermediates (Ding and Voinnet, 2007). This mechanism however does not seem to be active in mammals, although conflicting reports show that this is still under debate (Jeang, 2012, Maillard et al., 2013, Li et al., 2013).

## 3. Argonaute and TNRC6 proteins

### 3.1. Argonaute proteins are key players in miRNA-mediated gene silencing

Argonaute proteins are the key protein components in all sRNA-mediated gene silencing processes that have been characterized so far (Meister, 2013). Argonaute proteins are the direct binding partners of small ncRNAs, which target the Argonaute protein to complementary or partially complementary target RNAs.

Argonaute proteins are highly conserved from prokaryotes to eukaryotes. All eukaryotes analyzed so far contain minimally one Argonaute protein, with the exception of *Saccharomyces cerevisiae* (*S. cerevisiae*) (Swartz et al., 2014). Phylogenetically, Argonaute genes cluster into three distinct clades: the Ago clade, Piwi clade and the worm-specific Wago clade (Meister, 2013). Ago clade members interact with miRNAs and siRNAs and are components of miRISC and RISC. Piwi clade members bind to a distinct small ncRNA class, called Piwi-interacting RNAs (piRNAs). Both Piwi and piRNAs are specifically expressed in testes, are mainly nuclear and repress transposable elements in the male germ line (Siomi et al., 2011). Wago proteins bind diverse small ncRNA classes and have similarly diverse functions including siRNA-guided gene silencing and epigenetic transcriptional silencing (Ketting, 2011). The number of Argonaute proteins varies substantially between organisms. Mammals contain four Ago and four Piwi clade members, *Arabidopsis thaliana* (*A. thaliana*) contains ten Ago proteins, *Schizosaccharomyces pombe* (*S. pombe*) one Ago protein, *C. elegans* 23 Ago and three Piwi clade proteins and *Drosophila melanogaster* contains two Ago and three Piwi proteins (Peters and Meister, 2007, Tolia and Joshua-Tor, 2007, Hutvagner and Simard, 2008, Höck and Meister, 2008).

The four human Ago clade members are Ago1, Ago2, Ago3 and Ago4. Of central importance, only Ago2 is able to cleave target mRNAs, whereas Ago1, Ago3 and Ago4 are catalytically inactive (Meister et al., 2004b, Liu et al., 2004). Therefore, only Ago2 mediates siRNA-guided gene silencing by endonucleolytic cleavage. The reason for this functional divergence of Ago2 and Ago1/3/4 is not known in detail. The largely uniform expression pattern of human Ago1-4 would suggest largely redundant functions. Furthermore, experiments in mouse embryonic stem cells suggested redundancy at least in this cellular system, as each Ago protein is able to rescue the phenotype of Ago1-4 deficient cells (Su et al., 2009). Interesting hints towards non-redundant functions came from the analysis of Ago knockout mice. Whereas Ago2 knockouts are embryonic lethal, Ago1, Ago3 and Ago4 knockouts as well as Ago1/3 double knockouts are viable (Liu et al., 2004, Morita et al., 2007, Cheloufi et al., 2010, Van Stry et al., 2012, Modzelewski et al., 2012). During embryonic development, Ago2 has an essential function in extra-embryonic tissue independent of its cleavage activity (Cheloufi et al., 2010). In addition, Ago2 cleavage activity is important for hematopoiesis, as Ago2 knockout mice which carry a transgene with a cleavage deficient Ago2 mutant, overcome the early embryonic lethality but die shortly after birth due to anemia (Cheloufi et al., 2010). This might at least in part result from the erythropoietic miR-451,

which is Dicer-independently processed by Ago2-mediated cleavage of the precursor (Yang et al., 2010, Cheloufi et al., 2010, Cifuentes et al., 2010, Rasmussen et al., 2010). Ago4 has been attributed with non-redundant functions in the male germ line, as Ago4 knockouts have defects in spermatogenesis although the other Ago proteins are expressed in the germ line (Modzelewski et al., 2012). Taken together, both redundant and non-redundant functions seem to be attributed to mammalian Ago clade members with cell type and developmental stage-specific effects.

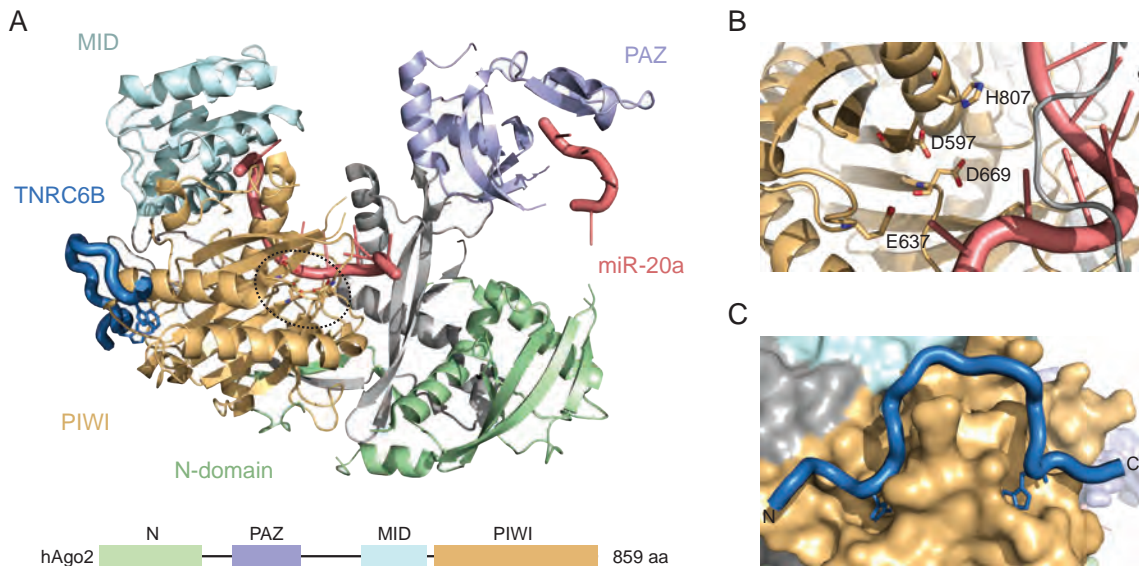


**Figure 1.3.1. Structure of human Ago2 and binding to TNRC6 proteins.** **A**, Structure of human Ago2 bound to miRNA. Ago2 consists of N (green), PAZ (violet), MID (light blue), and PIWI (brown) domain. The PAZ and MID domain bind to the 3'- and 5'-ends of the miRNA (miR-20a is shown in red). Of note, nucleotides 11 to 15 of miR-20a were not resolved in the crystal. The active center of Ago2 is indicated with a broken circle. The lower panel shows the domain architecture of human Ago2 (hAgo2). **B**, Active center of Ago2 with DEDH catalytic tetrad and the miRNA guide strand. **C**, Modeling of the Ago2-binding peptide of TNRC6B with two tryptophans (depicted as line-angle formula) binding to tryptophan binding pockets of the Ago2 PIWI domain. Figure adapted from Schraivogel and Meister, 2014.

Ago proteins are characterized by a unique domain architecture, which is highly conserved between species. Functional studies of Ago proteins have been complicated in the past as truncation and even point mutations in most cases lead to partial or complete loss-of-function and severely affect expression levels and protein stability. The crystal structure of human Ago2 was solved recently and provided important insights into Ago protein function and the mechanisms of miRNA-mediated PTGS (Schirle and MacRae, 2012, Elkayam et al., 2012, Schirle et al., 2014). The Ago protein adopts a bilobal structure with an N-terminal and C-terminal lobe and a nucleic acid binding channel between the two lobes (Figure 1.3.1 A). Beginning at the amino terminal end, Ago proteins are built of a N domain, the Piwi-Argonaute-Zwille (PAZ) domain, the middle (MID) domain and the PIWI domain (Meister, 2013). The PAZ domain anchors the 3'-end of the sRNA, whereas the MID domain anchors the 5'-phosphorylated end. The Piwi domain possesses cleavage activity, and is structurally similar to RNaseH, which cleaves the RNA strand of an RNA-DNA duplex. Cleavage by Ago2 is achieved by the residues DEDH (D597, E637, D669, and H807), which form a catalytic tetrad in the active center of Ago2 (Figure 1.3.1 B). Linker domains, designated as L1 to L3, are located between N, PAZ, MID and PIWI domains, interconnect the domains and also contribute to RNA binding (Schirle and MacRae, 2012).

How do miRNAs bind the target mRNA within the Ago complex? Some nucleotides of the miRNA sequence are more important for target recognition than others. The so-called seed region, which comprises nucleotides 2 to 8 from the 5' end of the miRNA must form perfect

Watson-Crick base pairs, whereas the surrounding nucleotides are not essential for target mRNA recognition (Schirle et al., 2014). Interestingly, the crystal structure of hAgo2 revealed that the seed nucleotides 2 to 6 are conformationally prearranged within Ago2 for pairing with the target mRNA, whereas the nucleotides outside the seed region are not accessible. Only after formation of the ternary complex by binding to the target RNA, a conformational change in Ago2 makes nucleotides 14 to 18 accessible for pairing. However it still remains to be answered how the non-seed nt contribute to target recognition, specificity and silencing. The remaining nt at the 3'- and 5'-end are not accessible to the target but are associated with Ago2.

How does Ago2 mediate endonucleolytic cleavage? Endonucleolytic cleavage occurs in the phosphodiester bond opposite of nucleotides 10 and 11 of the siRNA guide, which form the active center together with the catalytic tetrad (Figure 1.3.1 B). Perfect complementarity inside and outside of the seed seems to be necessary to properly orient the scissile phosphate for cleavage (Ipsaro and Joshua-Tor, 2015). Cleavage is catalyzed by a  $Mg^{2+}$ -dependent, not fully understood mechanism (Schwarz et al., 2004, Tolia and Joshua-Tor, 2007, Schirle et al., 2014). The cleavage step leaves a 5'-phosphate and a 3'-hydroxylated end, whereas the siRNA guide strand itself remains unaffected.

## 3.2. TNRC6 proteins are the effector proteins recruited by Argonaute

During miRNA-mediated PTGS, Ago proteins interact with a member of the TNRC6 protein family, also known as GW proteins or GW182 family proteins. *Drosophila* contains one GW protein (GW182), *C. elegans* contains two paralogs (AIN-1 and AIN-2) and mammals contain three paralogs referred to as TNRC6 (trinucleotide repeat containing 6) A, B and C (Pfaff and Meister, 2013). TNRC6A is the closest mammalian homolog of *Drosophila* GW182. Here, the domain structure of TNRC6 proteins will be presented together with the binding mechanism of Ago and TNRC6 proteins.

TNRC6 proteins contain an N-terminal Ago-binding domain and a C-terminal silencing domain (Figure 1.3.2). The N-terminal domain, also designated as GW domain, mediates interaction with Ago clade proteins. This domain is characterized by multiple GW (Glycine-Tryptophan) repeats. The interaction between Ago and TNRC6 proteins is mediated by specific tryptophans of these GW-repeats, that bind into tryptophan binding pockets on the surface of the Ago Piwi domain (Figure 1.2.1 A and C) (Till et al., 2007, Eulalio et al., 2009a, Baillat and Shiekhattar, 2009, Chekulaeva et al., 2010, Pfaff et al., 2013). Although the GW domain of TNRC6 proteins contains multiple tryptophans, studies suggest that only a limited set of tryptophans mediate interaction. Furthermore, Ago2 and eventually Ago1/3/4 contain two distinct tryptophan binding pockets and indeed, binding of two tryptophans is required for stable Ago2-TNRC6 interaction (Baillat and Shiekhattar, 2009, Chekulaeva et al., 2010, Pfaff et al., 2013). Furthermore, it has been shown for Ago2, that the two tryptophan binding pockets require a tryptophan distance of about 10 amino acids, which might at least in part mediate specificity of the interaction (Pfaff et al., 2013). TNRC6B for example contains two tryptophans pairs that can mediate Ago2 interaction (Figure 1.3.2). One is located in the central part of the GW domain, the second one, also referred to as 'Ago2-hook', is located in the C-terminal part close to the end of the GW domain (Till et al., 2007, Pfaff et al., 2013). Regarding TNRC6A, three possible Ago2 binding hot spots have been identified that partially overlap with those in TNRC6B, indicating similar binding mech-

anisms (Nishi et al., 2013). Whether multiple tryptophan pairs function cooperatively by a not yet identified mechanism or whether there are regions with high and low Ago2 affinity remains to be investigated. In addition, many tryptophans within TNRC6 are separated by 10 amino acids distance. Therefore, it is not yet known which mechanisms further determine specificity of this interaction.

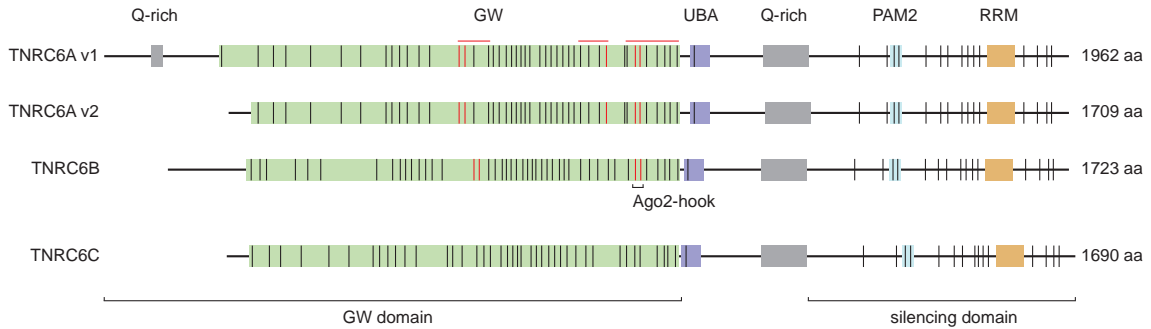


**Figure 1.3.2. Domain organization of human TNRC6A-C with indicated tryptophan residues.** A, Domain organization of human TNRC6A variant v1 (NP\_055309), TNRC6A v2 (NP\_001136112), TNRC6B (NM\_001162501) and TNRC6C (NP\_001136112). Starting from the N-terminus, TNRC6 proteins contain a GW domain (green), UBA domain (violet), Q-rich domain (grey), PAM2 motif (light blue) and RRM (brown). For abbreviations, please refer to the main text. TNRC6A v1 contains an additional Q-rich domain at the N-terminus. Vertical lines indicate the exact positions for each tryptophan residue. Validated Ago2 binding sites in TNRC6A and TNRC6B were mapped to amino acid position (red vertical line) or region (red horizontal line). In TNRC6A, three possible Ago2 binding hot spots have been identified (Takimoto et al., 2009, Nishi et al., 2013), whereas TNRC6B contain two possible Ago2 binding regions (Till et al., 2007, Pfaff et al., 2013). The four schemes were aligned to the Ago2-hook (Till et al., 2007).

The C-terminal silencing domain consists of a ubiquitin-associated (UBA)-like domain, a glutamine (Q)-rich domain, a poly-A binding protein interacting motif 2 (PAM2) and an RNA-recognition motif (RRM). The UBA-like domain as well as the RRM domain are the only structured sequences in this large 180 kDa protein (Huntzinger and Izaurralde, 2011, Eulalio et al., 2009b). How this hall-marking unstructured conformation contributes to TNRC6 function remains to be answered. UBA domains are usually present in proteins involved in the ubiquitin-proteasome system. However, a function for the TNRC6 UBA domain has not been identified yet and it seems to be dispensable for silencing (Lazzaretti et al., 2009). The RRM of *Drosophila* GW182 seems to lack RNA binding activity but contributes to miRNA-mediated gene silencing by a yet unknown mechanism (Eulalio et al., 2009b). In human TNRC6B, the RRM seems to be important for protein function as well, however the underlying mechanism is unknown as well (Baillat and Shiekhatar, 2009). The PAM2 is responsible for the interaction with PABP (Huntzinger et al., 2010, Jinek et al., 2010). The Q-rich region is necessary for P-body localization but dispensable for silencing (Lazzaretti et al., 2009). How the C-terminal silencing domain functions during PTGS will be described in part I section 4.

TNRC6 proteins are thought to function redundantly during miRNA-mediated PTGS. Indeed, knockdown of one or two of the three human TNRC6 paralogs does not have severely affect PTGS, whereas depletion of all three proteins results in a strong derepression of miRNA-reporter constructs (Zipprich et al., 2009, Chekulaeva et al., 2011, Hannus et al., 2014). Furthermore, artificial tethering of the C-terminal domains of TNRC6A-C showed that all three TNRC6 proteins are capable of activating PTGS (Lazzaretti et al., 2009). TNRC6A, TNRC6B and TNRC6C associate with all four human Ago proteins and a common set of miRNA targets and miRNAs (Landthaler et al., 2008, Baillat and Shiekhatar, 2009, Lazzaretti et al., 2009). However, whether indeed all 12 possible Ago-TNRC6 combinations are formed and functional *in vivo*, and whether some Ago-TNRC6 combinations are predominantly formed, remains to be investigated.

### 3.3. Intracellular localization of gene silencing components

mRNAs are localized in the cytoplasm and consequently, Ago proteins as well as TNRC6 proteins have also been shown to be mainly localized within the cytoplasm (Jakymiw et al., 2005, Liu et al., 2005b, Sen and Blau, 2005, Leung et al., 2006, Rüdél et al., 2008). In addition, the miRNA loading machinery has been exclusively found in the cytoplasm, indicating that Ago loading is also a cytoplasmic process (Ohrt et al., 2008, Gagnon et al., 2014). Ago and TNRC6 proteins show a granular and equally distributed signal pattern in the cytoplasm when stained with antibodies detecting the endogenous protein (Rüdél et al., 2008, Gagnon et al., 2014). Of importance, different cell lines, antibodies and staining protocols lead to different Ago2 patterns and localization (Rüdél et al., 2008, Azuma-Mukai et al., 2008, Benhamed et al., 2012, Gagnon et al., 2014).

Biochemical fractionations confirm this cytoplasmic Ago and TNRC6 pool, however also detect significant amounts of Ago protein in nuclear fractions of mammalian cells (Robb et al., 2005, Rüdél et al., 2008, Chu et al., 2010, Gagnon et al., 2014). Of note, impurities of nucleocytoplasmic fractionations might partially falsify the amount of nuclear Ago2 and therefore have to be interpreted carefully. Within nuclear fractions, Ago2 was found in soluble as well as chromatin-associated fractions, indicating a chromatin-bound and free nuclear Ago2 pool (Ameyar-Zazoua et al., 2012). The exact amount of nuclear Ago2 is not characterized in detail. Nuclear Ago2 is estimated to be approximately five times lower in concentration compared to cytoplasmic Ago2, as determined by fluorescence correlation spectroscopy of overexpressed eGFP-Ago2 (Ohrt et al., 2008). Functions have been attributed to nuclear Ago2 and will be discussed in part I section 1.1.

The intracellular distribution of TNRC6 proteins is far less clear. In biochemical fractionations, endogenous TNRC6A has been identified to be enriched in the cytoplasm but also in the nucleus, using different antibodies and unknown amounts of extracts in Western Blots (Nishi et al., 2013, Gagnon et al., 2014). By immunofluorescence, overexpressed TNRC6A-C are almost exclusively cytoplasmic (Lazzaretti et al., 2009). A similar predominantly cytoplasmic localization has been observed for TNRC6A, however without clear validation of antibody specificity (Eystathioy et al., 2002, Eystathioy et al., 2003a, Jakymiw et al., 2005, Li et al., 2014). Taken together, the exact intracellular localization of TNRC6 proteins is not clear.

#### **P-bodies and stress granules as cytoplasmic sites of miRNA-mediated PTGS**

It is not yet fully understood how miRISC finds target mRNAs in the cytoplasm. RNA granules, such as P-bodies, have been implicated in this process, however they are not essential for miRNA-mediated PTGS as well as for RNAi (Chu and Rana, 2006, Eulalio et al., 2007a, Eulalio et al., 2009a). P-bodies are thought to be sites where central processes like mRNA decay, nonsense-mediated decay and PTGS by miRNAs come together, because they contain proteins associated with those processes (Eulalio et al., 2007a). Of importance, P-bodies are visible especially under conditions of an overexpressed P-body component and are almost absent without overexpression. Different reports, cell lines and antibodies lead to conflicting results regarding the presence of P-bodies without protein overexpression (Eulalio et al., 2007b, Rüdél et al., 2008). *Vice versa*, the formation of P-bodies seems to depend on the presence of factors including TNRC6, miRNAs, Lsm1, DCP1 and DDX6 (Liu et al., 2005a, Rehwinkel et al., 2005, Chu and Rana, 2006, Pauley et al., 2006, Eulalio et al., 2007b).

It has been proposed that within P-bodies, Ago2 is bound to translationally repressed and temporally stored mRNAs (Kulkarni et al., 2010, Brengues et al., 2005, Cougot et al., 2013). P-body

localized mRNAs are not bound by ribosomes but can reenter polyribosomes; in addition, mRNA degradation seems to be active in P-bodies (Bhattacharyya et al., 2006, Eulalio et al., 2007a). Only a very minor pool of human Ago2 seems to localize to visible P-bodies and in addition, only a minor pool of P-bodies are Ago2-positive. Therefore the major portion of Ago2 is present in a free cytoplasmic pool in the above mentioned granular pattern (Leung et al., 2006, Leung and Sharp, 2013). The proportion of TNRC6 proteins within P-bodies has not been quantified comprehensively, but similar P-body associated and free TNRC6 pools can be expected (Yang et al., 2004). Ago2 seems to be trapped within P-bodies as only a very slow exchange of Ago2 between the P-body localized and the free Ago2 pool was observed (Aizer et al., 2008). In contrast to this invariable Ago2 association, P-bodies are of dynamic size and seem to be disassembled during mitosis, however, a direct interconnection between these dynamics and Ago protein function has not been shown yet (Yang et al., 2004). Of note, not only Ago2, but also Ago1, Ago3 and Ago4 are localized to P-bodies when the proteins are overexpressed (Liu et al., 2005b, Pillai et al., 2005, Sen and Blau, 2005). Similar to human Ago proteins, TNRC6A-C overexpression leads to the formation of P-bodies as well (Meister et al., 2005, Jakymiw et al., 2005, Pillai et al., 2005, Lazzaretti et al., 2009). The frequently mentioned GW-bodies, which are also visible upon overexpression of TNRC6 proteins, are very probably identical to P-bodies (Eystathioy et al., 2003b).

Stress granules (SGs) are another type of cytoplasmic bodies, which appear under stress conditions. Stress conditions are for example induced by heat shock or oxidative stress and are expected to at least in part resemble stress conditions *in vivo*. The detailed function of SGs during stress reponse is not known, but similar to P-bodies, SGs are enriched in non-translating mRNAs (Anderson and Kedersha, 2008). Therefore, it has been supposed that SGs might function as storage centers for untranslated mRNAs, which can be activated again after stress relieve (Anderson and Kedersha, 2008). Interestingly, Ago2 has been found to localize in SGs during stress conditions and quantifications revealed that about 1 to 10 % of Ago2 is present in SGs (Leung et al., 2006, Leung and Sharp, 2013). Furthermore, miRNA-mediated repression was relieved upon stress induction while mRNA stability consequently increased, which is in line with the hypothesized mRNA storage function of SGs (Detzer et al., 2011). Whether Ago2 is still associated with mRNA in SGs is not known, as well as whether TNRC6 proteins localize to SG.

Of note, the physiological significance of P-bodies and SGs has not been shown and is difficult to prove experimentally. Therefore, these bodies might still be experimental artifacts, eventually created by protein aggregation or precipitation under completely unphysiological conditions (see also discussion in part III section 4). On the other side, it might be thinkable that the granularity of the Ago2 immunofluorescent signal might present submicroscopical P-body like structures. This hypothesis also includes, that submicroscopical P-body like structures might result in visible P-bodies under special conditions like protein expressions. However, whether this is indeed the case, has not been investigated so far.

### **miRISC loading, function and degradation can be associated with the endomembrane system**

miRNA-mediated post-transcriptional gene silencing components have been associated with the endomembrane system (Kim et al., 2014b). The main components of the animal endomembrane system are the endoplasmic reticulum (ER), Golgi complex, trans-Golgi network, endosomes and lysosomes. Cytoplasmic fractionations and immunofluorescence experiments identified a significant proportion of Ago2 protein being associated with the rough ER, together with siRNA guide

strand and target mRNAs (Cikaluk et al., 1999, Stalder et al., 2013). Interestingly, the remaining components of the RISC loading complex Dicer, TRBP and PACT, were also associated with the rough ER (Stalder et al., 2013). This suggested that both miRISC loading as well as miRNA-mediated PTGS can be associated with the ER.

miRISC turnover has been associated with other components of the endomembrane system. Autophagy is a degradation pathway for components such as proteins and organelles in the cytoplasm. These components are sequestered within autophagosomes, that fuse with lysosomes forming an organelle in which proteins and organelles are degraded. Ago2, miRNAs and Dicer, but not TNRC6, have been found to associate within autophagosomes in which they are subjected to degradation (Gibbings et al., 2012, Martinez and Gregory, 2013).

The proportion of the described gene silencing components that are associated with the ER and how much Ago is degraded via autophagy is not known so far. It would be conceivable that there are target-specific effects, as mRNAs exist that are preferentially translated at the rough ER. In addition, external stimuli like for example serum and nutrient starvation, strongly regulate the extend of autophagy, which also might have implications for Ago turnover.

## 4. Post-transcriptional gene silencing processes

miRNAs mediate post-transcriptional gene silencing by translational repression and mRNA decay. Both processes are induced by TNRC6 proteins, which are guided to 3' UTRs via interaction with Ago proteins. Interestingly, it has been shown that the C-terminal silencing domain of TNRC6A-C is able to mediate translational repression and mRNA degradation alone (Eulalio et al., 2009c, Lazzaretti et al., 2009, Zipprich et al., 2009). Therefore, all downstream processes described here are mediated by this C-terminal domain.

To induce translational repression and mRNA decay, miRISC binds miRNA-target sites in a sequence-specific manner. The miRNA-binding sites are mostly located in the 3'-UTR of target mRNAs (Figure 1.4.1 A). miRNA binding sites within the open reading frame (ORF) or the 5' UTR seem to exist and some seem to be functional, however, they are controversially discussed especially regarding the silencing mechanism (Lytle et al., 2007, Orom et al., 2008, Hafner et al., 2010, Hausser et al., 2013). Whether Ago binds TNRC6 prior or after mRNA binding is not known in detail and observations differ between reports (Baillat and Shiekhataar, 2009, Rüdell et al., 2011, Frohn et al., 2012, Schirle et al., 2014).

Upon association with the target mRNA, translational repression and mRNA degradation are induced. Translational repression seems to act on the initiation phase of translation. To understand the underlying processes, the mechanism of canonical translation initiation will be described in short. During translation initiation, 5'-Cap and poly(A) tail cooperate to recruit the 43S pre-initiation complex. The pre-initiation complex then scans for the start codon and initiates translation (Jackson et al., 2010). The Cap structure is recognized by eIF4F, a complex that consists of the cytoplasmic Cap-binding protein eIF4E, the scaffolding protein eIF4G and the RNA helicase eIF4A (Figure 1.4.1 A, eIF4A not shown). The poly-(A) tail is bound by the cytoplasmic poly(A)-binding protein PABPC. PABPC binding regulates both poly(A) tail length and translation initiation. For effective translation initiation, PABPC interacts with eIF4G, bringing both mRNA termini together to form a closed loop state (Jackson et al., 2010).

PABPC is one important interaction partner of TNRC6 proteins (Zekri et al., 2013). The PAM2 of TNRC6 proteins directly associates with the PABC domain in PABPC (Fabian et al., 2009, Figure 1.4.1 A). The corresponding crystal structure of human TNRC6 PAM2 peptide in complex with the PABC domain of PABPC has been solved (Jinek et al., 2010). For fly GW182, additional contacts between tryptophan motifs in the silencing domain and PABPC have been identified (Chekulaeva et al., 2011). Despite the importance of these interactions, the detailed mechanism of PABPC function in miRNA-mediated PTGS is not yet clear. One controversially discussed scenario suggests that TNRC6 inhibits interaction between PABPC and eIF4G, therefore preventing closed loop formation (Fabian et al., 2009, Zekri et al., 2009). Alternative scenarios propose that translational repression functions independent of PABPC, eventually by recruitment of the CCR4-NOT complex (see below). Indeed, some studies suggest that TNRC6-PABPC interaction is dispensable for silencing and CCR4-NOT can induce translational repression independent of

its deadenylase activity (Braun et al., 2011, Chekulaeva et al., 2011, Huntzinger et al., 2013). This might be mediated via recruitment of DDX6, a known translational repressor and decapping factor (Mathys et al., 2014, Chen et al., 2014). Whether DDX6 mainly mediates translational repression or decapping is still unclear. Additionally to PABPC-dependent and CCR4-NOT-dependent translational repression, mRNA deadenylation might contribute to translational repression, as successive poly(A) tail shortening diminishes PABPC interaction and consequently translation initiation (Fabian and Sonenberg, 2012, Subtelny et al., 2014).

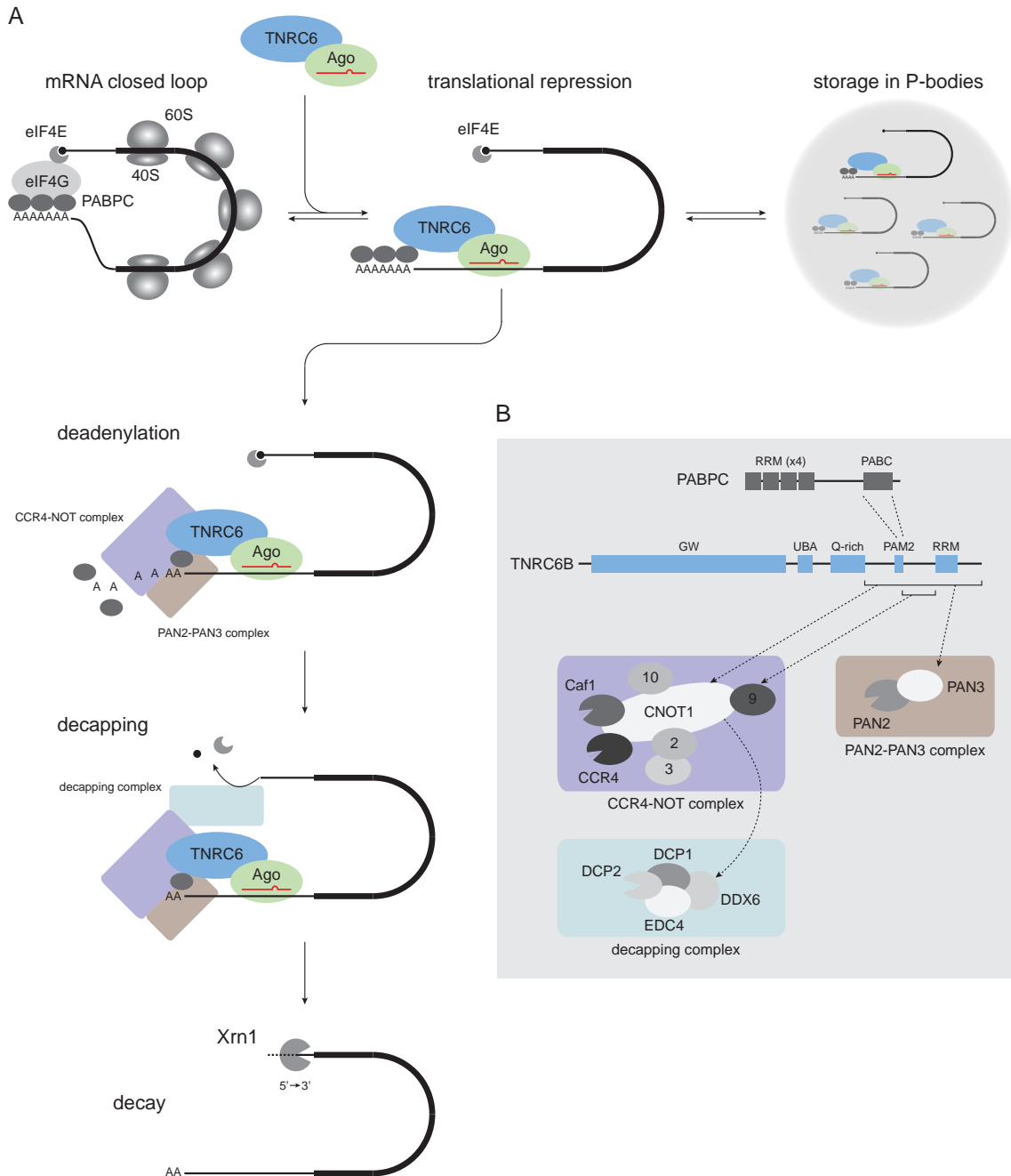


**Figure 1.4.1. Mechanisms of miRNA-mediated PTGS in mammals.** **A**, Multistep process of PTGS in mammals. miRISC binds to a target mRNA and induces translational repression and mRNA decay. Alternatively, translationally repressed mRNAs can be storage in P-bodies (upper right panel). For more detailed information, please refer to the main text. **B**, Detailed view of the interactions between TNRC6B C-terminal silencing domain, PABPC, CCR4-NOT and PAN2-PAN3 complex. CCR4-NOT recruits the decapping complex via Ddx6.

Degradation of mRNAs is mediated by deadenylation, which causes mRNAs to undergo decapping and finally 5'→3' decay (Behm-Ansmant et al., 2006, Chen et al., 2009). Deadenylation is mediated primarily by the CCR4-NOT complex and to a lesser extent by the PAN2-PAN3 complex, whereas decapping is catalyzed by the decapping-complex (Figure 1.4.1 A and B, Fabian et al., 2010, Huntzinger and Izaurralde, 2011). It is not yet clear whether both deadenylase complexes are redundant or fulfill separate functions, which so far have not been functionally dissected (Braun et al., 2013). Via their C-terminal silencing domain, TNRC6 proteins act as docking platform for both deadenylase complexes (Braun et al., 2011). A direct interaction of the decapping complex with TNRC6 proteins has not been identified so far, instead it seems to be recruited by CCR4-NOT (Chen et al., 2014, Mathys et al., 2014). The CCR4-NOT complex is a multimodular complex composed of several independent modules. Modules bind to the CNOT1 subunit, which functions as a scaffold for complex assembly. The catalytic active components are the two deadenylases CAF1 and CCR4a. Two redundant modes of CCR4-NOT interaction with mammalian TNRC6 proteins have been suggested so far. First, the silencing domain of TNRC6 can interact directly with the scaffold protein CNOT1 via its tryptophan residues (Fabian et al., 2011, Braun et al., 2011, Chekulaeva et al., 2011). Second, TNRC6 can contact CNOT9 via a tandem tryptophan motif in its C-terminal silencing domain, between the PAM2 motif and the RRM domain (Chen et al., 2014, Mathys et al., 2014). CNOT9 is bound to CNOT1 and therefore mediates CCR4-NOT recruitment by TNRC6 proteins (Figure 1.4.1). Both interactions rely on tryptophan insertion into binding pockets on the respective protein partner, similar to the mechanism of Ago-TNRC6 interaction. The two-subunit PAN2-PAN3 deadenylation complex contains Pan3 and the exonuclease component Pan2. Pan3 mediates association with RNA, either by directly binding poly-(A) RNA or indirectly via PABPC (Siddiqui et al., 2007, Wolf et al., 2014). During miRNA-mediated PTGS, TNRC6 proteins have been shown to recruit the PAN2-PAN3 complex by direct interaction of Pan3 with the TNRC6 silencing domain (Braun et al., 2011, Christie et al., 2013).

While mediating deadenylation, the CCR4-NOT complex component CNOT1 recruits the DEAD-box ATPase DDX6 (also known as p54/RCK), a known general activator of decapping (Chu and Rana, 2006, Mathys et al., 2014, Chen et al., 2014). DDX6 interacts with the DCP1-DCP2 decapping complex, which consists of the catalytic subunit DCP2 and additional activators including DCP1, EDC4 and DDX6 (Huntzinger and Izaurralde, 2011). After decapping, mRNAs are rapidly degraded by the 5'→3' exonuclease Xrn1 (Figure 1.4.1 A). 5'→3' degradation is the predominant degradation pathway of miRNA silenced transcripts (Huntzinger and Izaurralde, 2011). Depletion of Xrn1 results in defective miRNA silencing and deadenylated miRNA target mRNAs accumulate when decapping is blocked (Behm-Ansmant et al., 2006, Nishihara et al., 2013). The recruitment of the decapping complex is thought to occur before completion of deadenylation, which might explain why degradation does not occur from the 3' end by the exosome.

Alternatively to mRNA degradation, miRNA-mediated PTGS can result in storage of translationally repressed mRNAs (Figure 1.4.1 A right, Fabian et al., 2010). Stored mRNAs dissociate from ribosomes and have been shown to contain shorter poly(A) tails, indicating deadenylation prior to mRNA storage (not indicated in Figure 1.4.1 A). Storage of mRNAs is thought to be reversible, i.e. translationally repressed mRNAs can be activated again upon external stimuli. What regulates a possible degradation-or-storage decision is not characterized so far, as well as how much mRNA is stored and degraded (Kulkarni et al., 2010).

### **Relative contribution of translational repression and mRNA decay**

Whether translational repression or mRNA decay might be the dominant effect of miRNA-guided regulation is still under discussion (Wilczynska and Bushell, 2015). Initial evidence from *C. elegans* suggested that mammalian miRNAs mediate target repression on the level of translation, with little or no influence on mRNA stability (Wightman et al., 1993, Olsen and Ambros, 1999). However, recent studies suggest that mRNA degradation might be the dominant effect of mammalian miRNAs (Huntzinger and Izaurralde, 2011, Fabian and Sonenberg, 2012). The overall effect of translational repression in these studies was relatively weak, so that around 70 to 80 % of the effects on protein expression are attributed to mRNA destabilization (Eichhorn et al., 2014). However this has been challenged again by other studies, which suggest a more significant role for translational repression (Larsson and Nadon, 2013).

There is strong evidence that translational repression and mRNA decay are timely ordered processes (Djuranovic et al., 2012, Bazzini et al., 2012, Béthune et al., 2012, Eichhorn et al., 2014). Translational repression seems to be activated rapidly after miRISC binding and to occur before mRNA destabilization. Indeed, translational repression has been shown to be independent of deadenylation and decapping (Bazzini et al., 2012). One important determinant, which results in the shift from translational repression to mRNA decay could be the poly(A) tail length. In mammalian cells, intermediate poly(A) tail length is approximately 80 nt and translation rate correlates with poly(A) tail length (Subtelny et al., 2014). Within this model, deadenylation might start immediately after miRISC binding, resulting in initial translational repression, but with ongoing successive poly(A) shortening, decapping and consequently destabilization are induced (Subtelny et al., 2014).

**Part II.**

**miR-9/9\* regulate CAMTA1 in  
glioblastoma stem cells**

# 1. Introduction

In this study, we analyze miRNA functions in cancer stem cells. As a model system, we use *Glioblastoma multiforme*, a highly aggressive brain tumor that is thought to be driven by a cancer stem cell population. Here, I will first present how miRNAs function in cancerous processes in general. To get insights into the biology of *Glioblastoma multiforme* and cancer stem cells, I will then give a short overview on important aspects of *Glioblastoma multiforme* and how cancer stem cells are thought to drive tumor growth.

## 1.1. Small RNA-mediated gene regulatory pathways in cancer

The identification and characterization of miRNA-target pairs have shown that miRNAs regulate the expression of proteins implicated in diverse biological processes, including cell proliferation, differentiation and metabolism. Consequently, miRNAs have also been implicated in disease processes including cancer (Esquela-Kerscher and Slack, 2006). There they regulate important tumorigenic processes like apoptosis, invasion, vascularization, metastasis and proliferation. Furthermore, due to the ability to regulate various target mRNAs, the deregulation of one or a few miRNA genes could potentially promote diverse cancer-associated processes (Di Leva et al., 2014). As is the case for proteins, miRNAs can function as oncogenic miRNAs (oncomiRs) or tumor suppressors, depending on the respective target proteins: A miRNA functions as tumor suppressor, when a major target mRNA has oncogenic function; or it functions as oncogene, when a major target mRNA is a tumor suppressor.

The diverse mechanisms by which miRNAs support tumor-formation and growth will be represented here in short, along with the most prominent cancer-related miRNAs. These miRNAs include let-7, miR-21, miR-9, miR-29, miR-34 and miR-155 and the miRNA clusters miR-17~92, miR-15a~16 and miR-221~222 (Esquela-Kerscher and Slack, 2006, Croce, 2009, Jansson and Lund, 2012, Di Leva et al., 2014). Of note, many of these miRNAs have been reported to function as tumor suppressor in one cancer type but as oncogene in another. In the coming sections, the different mechanisms that affect miRNA function in cancer will be presented along with the most prominent cancer-related miRNAs.

### Abnormal miRNA expression by genetic aberration of miRNA genes

miRNA genes are frequently deleted or amplified in cancers. The first evidence for a deleted miRNA gene was the miR-15a~16 cluster in chronic lymphocytic leukemia (CLL) (Calin et al., 2002). In CLL, miR-15a and miR-16 function as tumor suppressors by regulating the oncogene BCL2, which is consequently derepressed. Interestingly, deletion of the miR-15a~16-1 cluster locus is sufficient for CLL development in mice (Croce, 2009). Further prominent tumor suppressor miRNAs come from the let-7 family, whose members are frequently deleted in various types of cancer (Di Leva et al., 2014). Members of the let-7 family regulate the important oncogenes RAS, MYC and HMGA2, which are overexpressed when let-7 is lost (Johnson et al., 2005, Lee and

Dutta, 2007). Amplification of miRNA genes has been reported for the oncomiRs miR-155 and miR-17~92 cluster in various types of cancer (Di Leva et al., 2014). Members of the miR-17~92 cluster regulate tumor suppressors including PTEN, P21 and components of the TGF- $\beta$  tumor suppressor pathway (Di Leva et al., 2014). Translocation of miRNA genes into different genomic contexts has been reported and could potentially increase or decrease miRNA expression (Di Leva et al., 2014). However, so far there is no reported evidence for an ultimate tumorigenic effect of these miRNA translocations.

Point mutations within mature miRNA sequences have only been very sporadically reported and recent large scale sequencing studies in various types of cancer did not identify mutated miRNAs (Jansson and Lund, 2012). One exception is miR-142, which is frequently mutated in B-cell lymphomas (Kwanhian et al., 2012). Point mutations within the pri- and pre-miRNA sequences which result in reduced miRNA processing have also been reported. One example is the miR-15a~16-1 cluster, which can show reduced processing efficiency by a single base substitution immediately downstream of the miR-16-1 sequence (Calin et al., 2005).

### **Aberrant regulation of miRNA expression by transcriptional and epigenetic mechanisms**

It has been shown that cancer-related transcription factors can modulate miRNA expression. The tumor suppressor TP53, for example, can induce expression of the miR-34 family by direct binding to miR-34 family promoters in various types of cancer (Chang et al., 2007, He et al., 2007, Tarasov et al., 2007). Therefore, at least a part of the TP53 tumor suppressive effects could be mediated by this miRNA family. The miR-34 family represses well known oncogenes like for example BCL2, HMGA2 and MYC (Di Leva et al., 2014). The oncogene MYC has been shown to transactivate the miR-17~92 cluster and to repress the miR-15a~16-1 cluster in different types of cancer.

Epigenetic silencing of miRNA loci has been reported as well. A large proportion of miRNA genes are associated with CpG islands, indicating regulation by DNA methylation. One example is the CpG island controlled let-7a-3 locus, which is hypomethylated in some lung cancers and consequently let-7a expression is increased (Brueckner et al., 2007). Of note, let-7a had oncogenic function in the investigated lung cancer cases.

### **Deregulation of miRNA expression by miRNA biogenesis defects**

Reported evidence for single miRNAs that are downregulated or lost in cancer is more frequent than overexpressed miRNAs. Similarly, losing of a (protein) tumor suppressor seems to be a more frequent event in cancer than the acquisition of an oncogene (Hanahan and Weinberg, 2011). Surprisingly, some studies also showed that global downregulation of mature miRNAs occurs with high incidence in various cancer types (Lu et al., 2005). The underlying mechanisms seem to be aberrations in the miRNA processing machinery including Drosha, Dicer, DGCR8, TRBP and Exp5 (Jansson and Lund, 2012). The most frequently observed aberration is a heterozygous loss of Dicer, which occurs in almost one third of tumors of various tissue origins (Kumar et al., 2009, Lambert et al., 2010). Another example is a functional loss of Exp5 by a premature stop codon, resulting in a C-terminally truncated protein that cannot bind pre-miRNAs any more (Melo et al., 2010). Consequently, inactivation of Exp5 resulted in globally nuclear trapped pre-miRNAs and derepressed oncogenes including BCL2 (Melo et al., 2010).

Numerous factors have been shown to regulate miRNA biogenesis in a general way or by affecting the processing of single miRNAs (Ha and Kim, 2014). Aberrations of these miRNA biogenesis regulators have also been reported in cancer. One example is the RNA-binding protein LIN28,

which binds pri-let-7 and pre-let-7 at the terminal loop and suppress Drosha- and Dicer-processing (Ha and Kim, 2014). In malignant germ cell tumors, LIN28 has been found to be highly expressed and to downregulate let-7 expression, which contributed significantly to malignancy (Murray et al., 2013).

Reports that show cancer-related deregulation of the miRISC components Ago and TNRC6 are rare. In malignant melanomas for example, Ago2 expression seems to be strongly decreased by a so far unidentified post-transcriptional mechanism (Völler et al., 2013). However, how increased Ago2 levels might influence tumorigenicity of malignant melanomas is unknown.

### **Aberrant miRNA function by altered miRNA binding sites**

In various types of cancers, rearrangements within 3' UTRs have been identified and directly linked to miRNA-mediated regulation of the affected mRNA. In almost all cases reported so far, these rearrangements result in a loss of miRNA-mediated repression of an oncogene. In many cancers, 3' UTRs seem to be frequently shortened, mainly resulting from the choice of alternative polyadenylation signals (Mayr and Bartel, 2009). 3' UTR shortening directly affected miRNA-mediated regulation, which partially explained the observed increase in protein expression. Recent large scale sequencing efforts also revealed translocations, interchanges or deletions of 3' UTRs of specific genes (Brennan et al., 2013). For example, translocations within the 3' UTR of HMGA2 oncogene remove functional let-7 seed-match sequences (Mayr et al., 2007, Lee and Dutta, 2007). This has been found to explain overexpression of the HMGA2 oncoprotein in various types of cancer (Mayr et al., 2007).

In addition to 3' UTR rearrangements, mechanisms exist that affect single miRNA binding sites in cancers (Ryan et al., 2010). One example is a single nucleotide polymorphism (SNP) within a let-7 miRNA binding site of the KRAS 3' UTR in lung cancers (Chin et al., 2008). miRNA target sites can also be regulated by diverse RNA binding proteins. The ubiquitously expressed RNA-binding protein Pumilio (PUM1), for example, binds the mRNA of the p27 tumor suppressor and is mutated in various cancers (Jansson and Lund, 2012). By binding, it favors association of miR-221 and miR-222, resulting in a suppression of p27 and consequently a decrease in cell cycle progression (Kedde et al., 2010).

## **1.2. *Glioblastoma multiforme***

Brain tumors include a large variety of different tumor types and although incidence is fairly low compared to other types of cancer, the vast majority of brain tumors are highly malignant. Brain tumors start either in the brain as primary tumors or can spread into the brain from a cancer somewhere else in the body as secondary metastatic tumors. Gliomas are the most common type of brain tumor and are defined as tumors that display histological and immunohistochemical evidence of glial differentiation. However, from which cellular origins gliomas derive from is indeed unknown.

*Glioblastoma multiforme*, also referred to as glioblastoma, grade IV astrocytoma or short GBM is the most common and simultaneously the most malignant and lethal type of primary brain tumor. GBM occurs in both child age as well as adults with an incidence of about three cases per 100,000 people (Siegel et al., 2014). Without therapy, median survival is about 4 months after initial diagnosis, whereas current multimodal therapy by surgical resection, irradiation and

chemotherapy increases median survival in selected therapy studies to about 13 months (Stupp et al., 2005, Gilbert, 2011).

GBMs either develop as primary or secondary GBM. 90 % of GBM cases are primary GBM which develop rapidly *de novo* and mainly in older patients. The remaining cases are secondary GBM which arise within 5 to 10 years from lower-grade gliomas in younger patients (Ohgaki and Kleihues, 2007). Despite their different pathology, primary and secondary GBM are clinically and histochemically not distinguishable, however, they accumulate partially different sets of mutations and genomic aberrations (Brennan et al., 2013).

Important pathological properties of GBM include high infiltrative growth patterns (Cloughesy et al., 2014, Cuddapah et al., 2014). Tumor cells migrate deeply into adjacent non-neoplastic brain tissue, thereby preventing complete surgical resection. Furthermore, GBM is among the most vascularized of all solid tumors and tumor growth strongly depends on vascularization (Jain et al., 2007). Another hallmarking property of GBM is its cellular and morphological heterogeneity and the parallel detection of cell populations with different grades of differentiation (Chen et al., 2012b). This heterogeneity has been shown to contribute to tumor growth and therapy resistance.

### 1.2.1. Molecular pathology

GBM, and cancer in general, is a disease of accumulated genetic and epigenetic aberrations (Hanahan and Weinberg, 2011). Recent studies integrating large scale genome, exome and RNA sequencing data, as well as copy-number, transcriptomic, epigenomic and targeted proteomic profiling provided deep insight into alterations associated with GBM (TCGA, 2008, Brennan et al., 2013). In addition to the presented data from the TCGA consortium, molecular analysis and classification of GBM patient samples have been performed in other studies not presented here in detail (Gravendeel et al., 2009, Li et al., 2009, Parsons et al., 2008).

These studies revealed that recurrent genetic alterations occur in a limited number of three core pathways: Receptor tyrosine kinase (RTK), TP53 and RB1 signaling pathways (Figure 2.1.1). Components within these pathways show a statistical tendency towards mutual exclusivity, i.e. in GBM patients, only a single component within each of the three pathways is affected. Furthermore, most tumors show aberrations in all three pathways, suggesting that deregulation of these pathways is a core requirement for GBM pathogenesis (TCGA, 2008). Consistently, transgenic and knockout mouse models developed GBM-like tumors after cooperative lesion in minimally two of the three presented core pathways (Chen et al., 2012b).

The RTK pathways integrate extracellular signals and activate transcriptional programs that affect proliferation, migration and survival. Frequent aberrations of RTK pathways in GBM are mutation and amplification of EGFR or PDGFRA and mutation or deletion of PTEN, less frequent are deletion or mutation of NF1 itself (Figure 2.1.1 B left panel). The TP53 pathway regulates senescence and apoptosis and integrates signals from various upstream pathways like DNA repair mechanisms. Inactivation of the TP53 pathway most frequently occurs via deletion or mutation of ARF or TP53 itself (Figure 2.1.1 B middle panel). The RB pathway regulates cell cycle arrest and G1/S progression. In most cases, the CDKN2A/B locus is deleted or CDK4 amplified. Deletion or mutation of RB1 itself is not frequent (Figure 2.1.1 B right panel).

Clustering of the TCGA data revealed different subclasses of GBM that, interestingly, resemble stages in neurogenesis and mesenchymal lineage (Phillips et al., 2006, Verhaak et al., 2010, Huse et al., 2011). This means, that gene expression programs typically active in those lineages are activated in the different subtypes in addition to their glial expression profiles, as for example

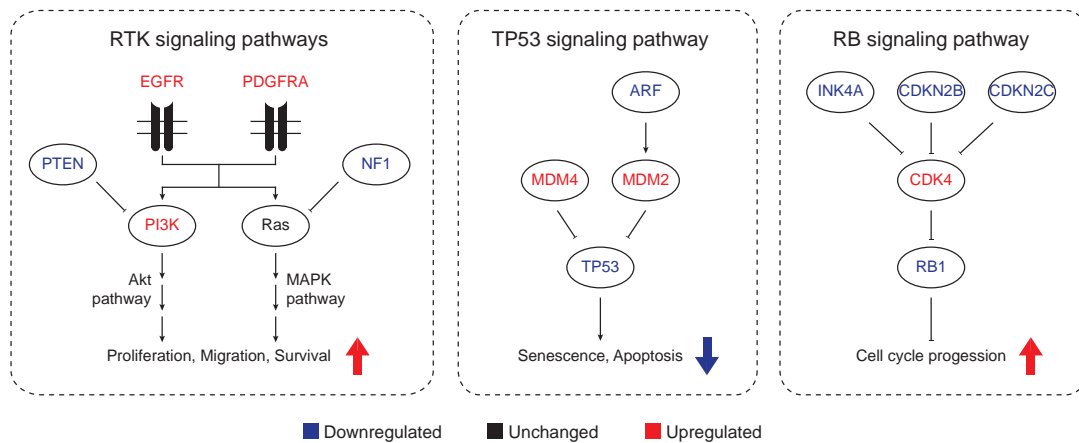


**Figure 2.1.1. Alterations in RTK, TP53 and RB signaling pathways in GBM.** Shown are recurrent genetic aberrations in RTK, TP53 and RB signaling pathways. Genetic aberrations either lead to decreased (blue) or increased (red) function. Most frequent aberrations affect EGFR, PDGFRA or PTEN in RTK signalling, ARF or TP53 in TP53 signalling and CDKN2A/B or CDK4 in RB signalling. In RTK signaling pathways, effects are mediated in large part through downstream Akt- and MAPK-signaling pathways, which themselves are only rarely direct targets of mutational events in GBM. Figure was partially adapted from Brennan et al., 2013.

shown by GFAP expression (Brennan et al., 2013). These subclasses include proneural, neural, classical and mesenchymal lineage which are shown with representative genetic aberrations and lineage signature genes in Figure 2.1.2 A. The proneural subclass exhibits frequent PDGFRA, TP53 and IDH1 mutation and expresses genes associated with neurogenesis. The mesenchymal subclass shows frequent aberration of NF1 and increased expression of components in the NF $\kappa$ B pathway. Mesenchymal GBM displays expression of mesenchymal and astrocytic signature genes. Interestingly, increased expression of two transcription factors C/EBP $\beta$  and STAT3 has been identified as potential driver for mesenchymal transformation in GBM (Carro et al., 2010). GBM of the classical subclass is associated with exceptionally high rates of EGFR amplification and mutation or loss of CDKN2A. The neural subclass is characterized by aberrations in many of the genes also found in other groups and cannot be clearly separated. It shows gene expression signatures that resemble those of neurons. Despite these deep insights, the prognostic value of the different subclasses is low. Only the proneural subclass correlated with marginally improved patient survival (Figure 2.1.2 B) but seems to be largely resistant to temozolomide, an alkylating agent used as chemotherapy drug in GBM patients (Stupp et al., 2005). On the other hand, mesenchymal and classical subclasses show increased necrosis and vascularization and increased therapy response, which might be a result of higher proliferation rate observed in these classes.

Due to the lack of efficient therapies for GBM, these molecular profiling and classification studies are an important basis for development of targeted therapy strategies, i.e. towards unique gene changes for patient specific treatment (Cloughesy et al., 2014).

### 1.2.2. miRNAs regulate hallmarks of GBM

The presented large-scale genomic and transcriptomic datasets gained deep insight into the mutational landscape underlying GBM. However, despite epigenetic, genomic and transcriptomic abnormalities, also post-transcriptional and even post-translational regulatory mechanisms have strong impact on protein outcome and function. As this thesis investigates post-transcriptional gene regulation by miRNAs, important roles of miRNAs in GBM will be presented here.

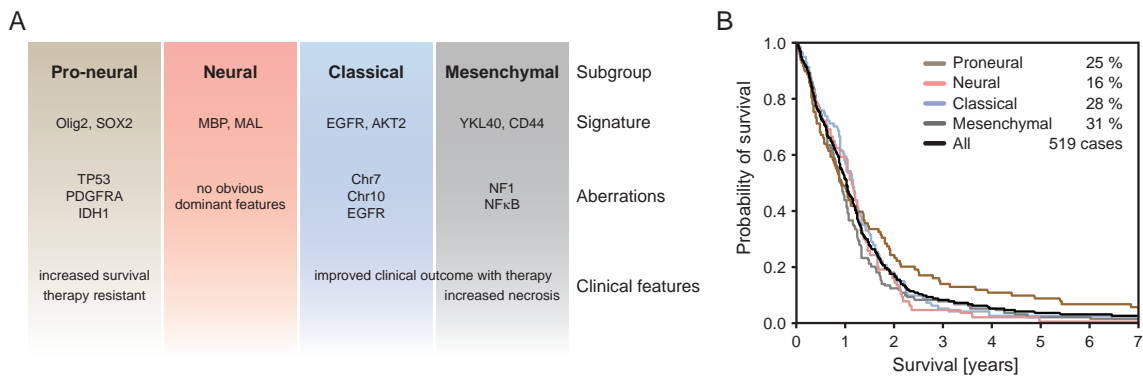


**Figure 2.1.2. Molecular subclasses of GBM.** **A**, Four different subclasses of GBM as identified in Verhaak et al., 2010 are shown with subclass signature genes. Aberrations are shown that are unique selling points for each subclass. Proliferative and mesenchymal subtype show improved clinical outcome by radiation and temozolomide therapy. Therapy resistance of the proneural subtype includes chemotherapy by temozolomide. **B**, Kaplan-Meier survival analysis of four GBM subclasses from 519 GBM patient samples. TCGA datasets were used to extract patient survival data and gene signatures. Only patients with known survival time were included into analysis. Percentage show the proportion of patients falling into either one of the four molecular subclasses. Figure part A was partially adapted from Brennan et al., 2013.

A tremendous number of studies tried to identify differentially expressed miRNAs in GBM and to link those to GBM pathogenesis and molecular pathways (reviewed in Mizoguchi et al., 2012, Møller et al., 2013, Henriksen et al., 2014). A selection of miRNAs that repeatedly appeared to be differentially expressed in GBM include miR-21, miR-10b, miR-26a, miR-34a, miR-124, miR-128, miR-181b and the miR-221~222 and miR-17~92 cluster. Therefore, also typical cancer-associated miRNAs like miR-21, miR-34a and the two clusters miR-221~222 and miR-17~92 seem affected in GBM (see part I section 1.1). However, conflicting results have for example been reported for the oncomiR cluster miR-221~222, which was repeatedly identified to be down- as well as upregulated in different GBM profiling studies. Whether this might depend on different GBM subclasses and tumor heterogeneity is not known so far. Thus, despite the high number of published miRNA expression data, an exhaustive as well as reliable profile of GBM-associated miRNAs is still lacking.

Many of the identified miRNAs have been implicated into central cancerous processes including cell cycle control, growth suppressor signaling, apoptosis, regulation of immune responsive signaling, angiogenesis and invasion. In addition, some of those miRNAs can target components of the three GBM core pathways including RTK signaling, TP53 signaling and RB signaling (Mizoguchi et al., 2012, Møller et al., 2013, Henriksen et al., 2014). Although this shows principal importance of miRNAs for GBM, only very few studies comprehensively and reliably analyzed how single miRNAs influence these cancer-associated processes. miR-26a for example promotes GBM growth by targeting PTEN, RB1 and MAP3K2/MEKK2 (Huse et al., 2009, Kim et al., 2010). miR-10b is a miRNA not expressed in non-neoplastic brain tissue, but highly expressed in GBM; miR-10b might contribute to GBM tumorigenicity by directly targeting the tumor suppressors TP53, NOTCH1, CDKN1A and CDKN2A (Gabriely et al., 2011, Lin et al., 2012). miR-21 was the first miRNA identified as an oncomiR in GBM and was elevated in cancer tissue (Chan et al., 2005). miR-21 targets include multiple important components of the TP53 tumor suppressor pathways (Zhou et al., 2010). miR-18, a miRNA of the miR-17~92 cluster which is lower expressed in GBM, targets oncogenic Smad3 which is consequently increased and positively regulates TGF- $\beta$  signaling (Fox et al., 2013).

A recent study used miRNA expression profiles from the TCGA network to classify human GBM (Kim et al., 2011b). According to their miRNA expression profiles which resembled different

neural precursors at multiple stages of differentiation, patient samples were separated into five classes: Neural, oligoneural, multipotent, astrocytic and neuromesenchymal GBM. Interestingly, miRNA expression-derived subclasses showed stronger correlation with patient survival than the above presented mRNA subclasses presented in II section 1.2.1. A comparison of the five miRNA-derived GBM classes with the four mRNA-derived GBM classes revealed only partial overlap. For example, the neural miRNA class contains a mixture of all four mRNA classes, whereas the oligoneural miRNA class matches well with the proneural mRNA class (Kim et al., 2011b). It is however not clear, why for example tumors with neural miRNA expression profiles do not similarly show neural mRNA expression profiles.

### 1.3. Cancer stem cell hypothesis

As detailed knowledge on cancer development is often lacking, models have been formulated that implement known aspects and processes of tumor-formation. Cancers are thought to be of monoclonal origin, i.e. a founding driver mutation occurs in a single cell-of-origin (Hanahan and Weinberg, 2011). This cell undergoes clonal expansion and accumulates further aberrations by increased genome instability (Figure 2.1.3 A). Therefore cancerous diseases preclude a multistep progression with intermediate stages of increasing aggressiveness (Greaves and Maley, 2012). Of note, recent evidence also suggested that complex genomic rearrangements frequently observed in many cancers can occur in a single cellular catastrophe and not by accumulation of aberrations, a process referred to as chromothripsis (Stephens et al., 2011).

The cancer stem cell model, also described as the hierarchical model, assumes that some cancers are additionally organized in a hierarchical manner with cells of different grades of differentiation that resemble the hierarchical structure of non-neoplastic tissues (Figure 2.1.3 B and C,

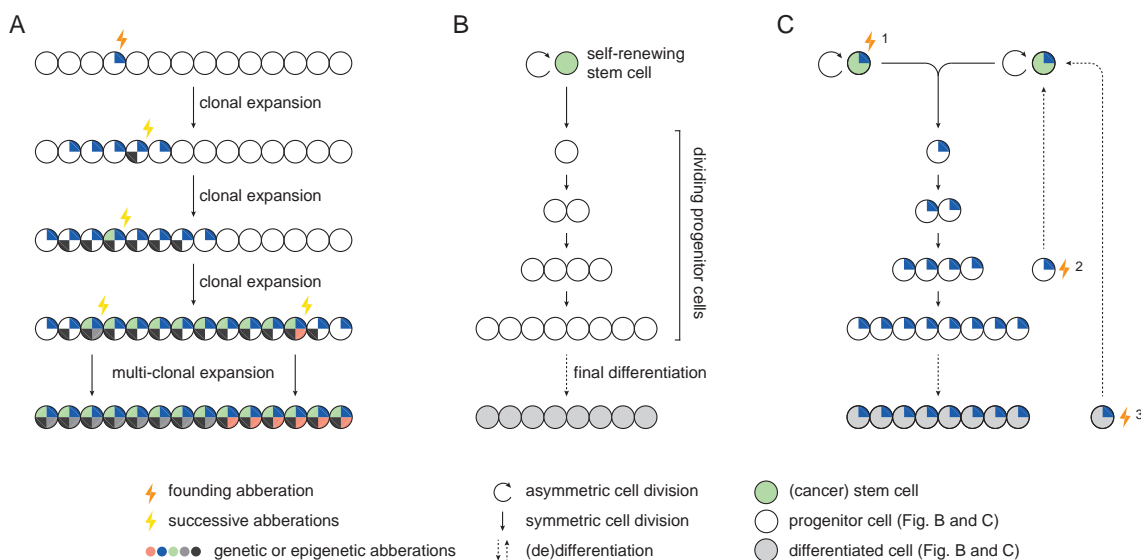


**Figure 2.1.3. Sources of intratumoral heterogeneity and models of tumor growth.** **A**, Heterogeneity by clonal evolution of cells resides on the stochastic nature of genetic aberrations. Selection within the tumor leads to clonal or multi-clonal expansion of dominant subpopulations. This results in a total population of increasing aggressiveness. **B**, Stem cell hierarchy within non-neoplastic tissue with a self-renewing and multipotent stem cell on the top. Symmetric cell division leads to progenitor cells with restricted multipotency which finally differentiate into specialized mostly post-mitotic cells. **C**, Schematic representation of the cancer stem cell model including founding aberrations, that might occur in differentiated cells (3), progenitor cells (2) or stem cells (1). Subfigures A and B are partially adapted from Weinberg, 2013.

Kreso and Dick, 2014). Adult stem cells of non-neoplastic tissues are essential for tissue homeostasis and have been identified in diverse tissues like hematopoietic lineages, digestive tract, muscle, brain and skin. They carry long-term self-renewal capacity and multipotency and divide by relatively rare, periodic and asymmetric divisions or give rise to more committed progeny by symmetric cell divisions. In a simplified view, the resulting progenitor cells proliferate by many symmetrical divisions before becoming fully differentiated and eventually post-mitotic (Figure 2.1.3 B). Cancer stem cells, from now on referred to as CSCs, are defined by self-renewal and multipotency as well. CSCs are isolated by cell sorting using cell surface markers of normal tissue stem cells. Stem cell characteristics are then experimentally tested by repeated xenotransplantations, clonogenic assays *in vitro* and expression of marker proteins typically expressed in non-neoplastic stem cells, progenitor cells or differentiated cells.

Cancer stem and progenitor cells have been implicated in various aspects of tumor-formation and growth: First, they are thought to be essential for tumor growth, as differentiated cells of many tumors do not proliferate any more and like in normal tissues, self-renewal of stem cells might also ensure life long feed with proliferative cells in tumors as well. Second, processes like formation of metastases and relapse after therapy might depend on cancer stem cells in some cancers. Third, it has been proposed that normal stem and progenitor cells are candidates for tumor cells of origin. This however remains to be characterized and recent evidence for dedifferentiation of tumor cells to CSCs provide an alternative explanation where CSCs might arise from. These dedifferentiation processes can occur from progenitor cells or even differentiated cells of various tissues (Figure 2.1.3 C, Friedmann-Morvinski and Verma, 2014).

Although the cancer stem cell model provides explanations for various cancerous processes, it still must be considered as a model. Indeed, the detailed function of CSCs *in vivo* within the patient is still controversially discussed. However, numerous *in vitro* studies and *in vivo* animal models provide strong evidence that CSCs might at least in part be drivers for the above mentioned processes.

### 1.3.1. GBM cancer stem cells

CSCs have been identified in GBM as one of the first CSCs in solid tumors (Singh et al., 2004) and have since then been characterized mainly phenotypically and functionally. GBM CSCs, from now on referred to as GSCs, are thought to be implicated in GBM growth, therapy resistance and tumor regrowth after therapy (Sundar et al., 2014). Furthermore, they have been implicated in processes like tumor vascularization and the high infiltrative behavior of GBM (Ricci-Vitiani et al., 2010, Wang et al., 2010). Last but not least, non-neoplastic neural stem cells (NSCs) have been suggested as a possible cell-of-origin for GBM by generating a GSC population (Chen et al., 2012a). However, because direct evidence for GSCs within the parent tumor is still lacking, the extend of their contribution to the mentioned processes is still a matter of debate.

GSCs have been originally characterized to express the surface marker CD133, but since now, various additional marker proteins have been introduced for GSCs as for example CD44, Integrin  $\alpha 6$  and CD36 (Singh et al., 2004, Sundar et al., 2014). Whether these markers are coexpressed on GSCs or whether different studies isolate different GSC subpopulations has not been analyzed comprehensively but might be possible. Furthermore, despite the broad spectrum of available marker proteins, none of the mentioned markers has indeed been shown to be exclusively expressed on GSCs and to be expressed on all GSCs. CD133, for example, is the most frequently used marker for GSC isolation, however, cells with GSC properties have also been identified that

do not express CD133 (Beier et al., 2007, Lottaz et al., 2010, Beier et al., 2012).

Where are GSCs located within the tumor and how do they contribute to GBM growth? Although numerous studies provide interesting insights into these important questions, only a short overview will be given here. GSCs were initially thought to be rare within GBMs. However, due to varying results between studies and markers used for sorting, it is not exactly known how many cells are indeed *bona fide* GSCs and if all GBMs contain GSCs (Singh et al., 2004, Beier et al., 2007, Günther et al., 2008, Chen et al., 2010). Within GBM, the GSC subpopulation has been found to reside in two different niches, a perivascular and perinecrotic location, with extensive regulatory crosstalk between GSCs and the respective niche cells (Calabrese et al., 2007, Seidel et al., 2010). GSCs have been suggested to contribute to vascular proliferation through a variety of mechanisms, including hypoxia-induced stimulation of endothelial cell growth, recruitment of endothelial progenitor cells and transdifferentiation into endothelial cells (Ricci-Vitiani et al., 2010, Wang et al., 2010). Although the proliferative behavior of GSCs within the primary tumor is not characterized comprehensively, most GSCs are expected to be quiescent and only periodically activated, and indeed, a second smaller subpopulation of proliferative GSCs has been identified (Chen et al., 2012a, Patel et al., 2014, Codega et al., 2014). Despite this restricted proliferative behavior of GSCs, they are thought to drive tumor growth by generating a highly proliferative progeny, which contributes largely to tumor growth (Kreso and Dick, 2014). In addition to the proposed role in tumor growth, GSCs have been implicated in rapid tumor recurrence after therapy and show increased resistance to both radiotherapy and chemotherapy. This resistance is thought to be ensured both by increased DNA-damage response and by the low proliferative behavior of most GSCs, which are consequently less responsive to chemotherapy (Bao et al., 2006, Chen et al., 2012a). In addition, recurrent tumors after chemotherapy in GBM mouse models have been shown to largely derive from GSCs, further supporting their importance for this inevitable process in GBM (Chen et al., 2012a).

### **Molecular characterization of GSCs**

Whether the stem cell-like properties of GSCs are intrinsic to early founding tumor cells or whether they are an acquired property is not clear, as well as the underlying molecular mechanisms. A recent study provided insights into stemness maintenance mechanisms of GSCs (Suva et al., 2014). The authors characterize epigenetic profiles and gene expression programs in GSCs versus non-GSCs. Interestingly, they identify four neurodevelopmental transcription factors POU3F2, SOX2, SALL2 and OLIG2, that can reprogram differentiated GBM tumor cells into cells that resemble *bona fide* GSCs regarding epigenetic marks, gene expression data, neurosphere growth and tumor propagating potential. Strikingly, these transcription factors were more highly expressed in CD133<sup>+</sup> cells, indicating that the observed reprogramming might indeed occur *in vivo*. Similar attempts of artificial dedifferentiation have been used in induced pluripotent stem cell (iPSC) generation from non-neoplastic cells (Takahashi and Yamanaka, 2006).

Taken together, although GSCs seem to be important for GBM tumorigenicity, a detailed and comprehensive understanding of the molecular mechanisms that are important for GSC function is lacking. Therefore, future studies will be needed, that for example compare GSCs with non-GSCs from many patient samples, similar as it has been done for total GBM samples described above in part II section 1.2.1.

### **miRNAs with GSC-specific functions**

miRNAs have been implicated as important regulators in stem cell biology by regulating differentiation and stem cell maintenance (Gangaraju and Lin, 2009, Gruber and Zavolan, 2013, Shenoy and Blelloch, 2014). Such roles for miRNAs have been identified in embryonic stem cells, germline stem cells and various somatic tissue stem cells including those of the central nervous system. In addition, miRNAs also regulate central processes during neurogenesis (Shen and Temple, 2009). However, although many miRNAs have been suggested to specifically function in CSCs and GSCs, comprehensive miRNA profiles and detailed functional analyses are still lacking (reviewed in DeSano and Xu, 2009, Liu and Tang, 2011, Takahashi et al., 2013, Katsushima and Kondo, 2014, Rathod et al., 2014).

The vast majority of studies investigated single miRNAs that have been previously associated with stem cell functions in non-neoplastic brain cells. In addition, miRNA targets are mostly picked from *in silico* predicted lists according to previously reported roles in NSCs or neurogenesis. This, however, questions conclusions regarding the *bona fide* miRNA function in the respective cellular context. These studies suggest for example miR-34a, miR-124, miR-128, miR-137, miR-138, miR-451 and the miR-17~92 cluster to function in GSCs (Silber et al., 2008, Gal et al., 2008, Godlewski et al., 2008, Ernst et al., 2010, Guessous et al., 2010, Xia et al., 2012, Chan et al., 2012, Peruzzi et al., 2013). The identified miRNAs seem to have targets that function in stem cell-specific processes and some of those miRNAs were also differentially expressed in GSCs.

Taken together, although miRNAs have been implicated in differentiation and stem cell maintenance, not much is known how miRNAs regulate GSC function and how they contribute to GSC-driven tumor growth.

## 2. Aims of part II

A molecular characterization of the highly malignant brain tumor *Glioblastoma multiforme* (GBM) has comprehensively been done from isolated tumor samples. Genetic programs, however, that are specifically important in GBM cancer stem cells (GSCs) are underrepresented in those datasets. Additionally, conventional chemotherapeutic therapies are designed to target rapidly proliferating cells, which might be a major reason why the relatively rare and periodic divisions allow survival of GSCs after therapy. Therefore, a more detailed characterization of GSCs is necessary to better understand their regulation and to develop novel targeted therapies.

microRNAs (miRNAs) have been shown to play important roles in cancer and normal stem cells, however their role in cancer stem cells has not been characterized in detail. Therefore, the aim of this thesis is to analyze miRNA expression in GSCs. miRNAs which are differentially expressed in GSCs might be important for GSC biology and therefore GBM in general. To understand how these miRNAs contribute to GSC maintenance and GBM growth, *in vitro* tumor formation assays will be used. This should uncover miRNAs as a basis for the development of future targeted therapy strategies by miRNA- or siRNA-based therapeutical agents.

To get deep insights into the function of the identified miRNAs, miRNA target mRNAs will be identified. Interesting target mRNAs will be subjected to further cell biological and biochemical analysis, with the aim to better understand how the identified miRNA-mRNA pairs contribute to GSCs and GBM. This should finally allow the identification of novel regulatory pathways in GBM and GSCs.

Taken together, the specific aims in part I of this work include:

1. Identification of miRNAs differentially expressed between GSCs and non-GSCs.
2. Characterization of GSC-enriched miRNAs by *in vitro* assays.
3. Experimental identification and validation of target mRNAs.
4. Characterization of the function of miRNA targets *in vitro* and *in vivo*.

## 3. Results

### 3.1. Small RNA profiling of GSCs

To analyze miRNA expression in GSCs and to identify differentially expressed miRNAs, glioblastoma cell lines were used, that derived from patients suffering from primary GBM. The R11 cell line was cultivated in stem cell medium conditions to enrich for GSCs and to prevent rapid differentiation, which would occur under serum conditions (Lottaz et al., 2010).

To separate GSCs from non-GSCs we used CD133 as surface marker for fluorescence activated cell sorting (FACS). Cluster of differentiation 133 (CD133), also known as prominin-1, is a transmembrane glycoprotein of unknown function expressed on adult neural stem cells and diverse stem cells of other tissues (Cheng et al., 2009). CD133 was used for the first identification and isolation of cancer stem cells from GBM and has been shown to effectively enrich for GSCs from R11 (Singh et al., 2004, Beier et al., 2007). CD133<sup>+</sup> cells were stained with a phycoerythrin (PE) coupled anti-CD133 antibody and positive cells were gated out from negative cells to get CD133<sup>+</sup>- and CD133<sup>-</sup>-enriched subpopulations. These subpopulations were used for total RNA isolation and miRNA deep sequencing (Figure 2.3.1 A). FACS analysis revealed a CD133<sup>+</sup> subpopulation of 11,8 % in R11 (Figure 2.3.1 B). This GSC content was in line with published results for CD133-sorted GSCs from R11 (Beier et al., 2007). RNA was extracted from both fractions, cloned and analyzed by deep sequencing. Sequences from datasets were annotated and library composition is shown in Figure 2.3.1 C.

We then identified differentially expressed miRNAs. Therefore, the number of reads for each miRNA was normalized to the total number of miRNA reads in each sample and the log<sub>2</sub> ratio was calculated for each miRNA between CD133<sup>+</sup> and CD133<sup>-</sup> cells. Candidate miRNAs were selected from the 20 miRNAs with the highest read number and therefore highest expression and are presented in Figure 2.3.1 D. A value above zero shows that a miRNA is more abundant in CD133<sup>+</sup> cells and a value below zero shows a miRNA that is more abundant in CD133<sup>-</sup> cells. The size of the dots represents the read number. miR-17, miR-9\* and miR-106b showed the strongest upregulation and were therefore chosen for further analysis. As miR-9, the complementary strand to miR-9\*, also was one of the 20 miRNAs with the highest read number, miR-9 was also chosen for further analysis.

The sequencing data for the selected miRNAs was further validated by Northern Blot. Signals for miR-9, miR-9\*, miR-17 and miR-106b were much stronger in CD133<sup>+</sup> cells (Figure 2.3.1 E) indicating that these miRNAs are indeed differentially expressed in GSCs versus non-GSCs.

miR-9 and miR-9\*, from now on also referred to as miR-9/9\* since they originate from the same precursor, were both highly expressed in CD133<sup>+</sup> cells. Therefore, the expression levels of miR-9/9\* were analyzed in CD133<sup>+</sup> cells from a broader range of human primary GBM-derived cell lines. R11, R28, R44 and R54 are Type I GSC lines, which were shown to contain a CD133<sup>+</sup> cell population with GSC properties and neurosphere growth and express proneural signature genes (Beier et al., 2007). The additionally used cell lines R20, R40 and R52 are not characterized in detail but were shown to contain a CD133<sup>+</sup> cell population as well. Consistent with the data

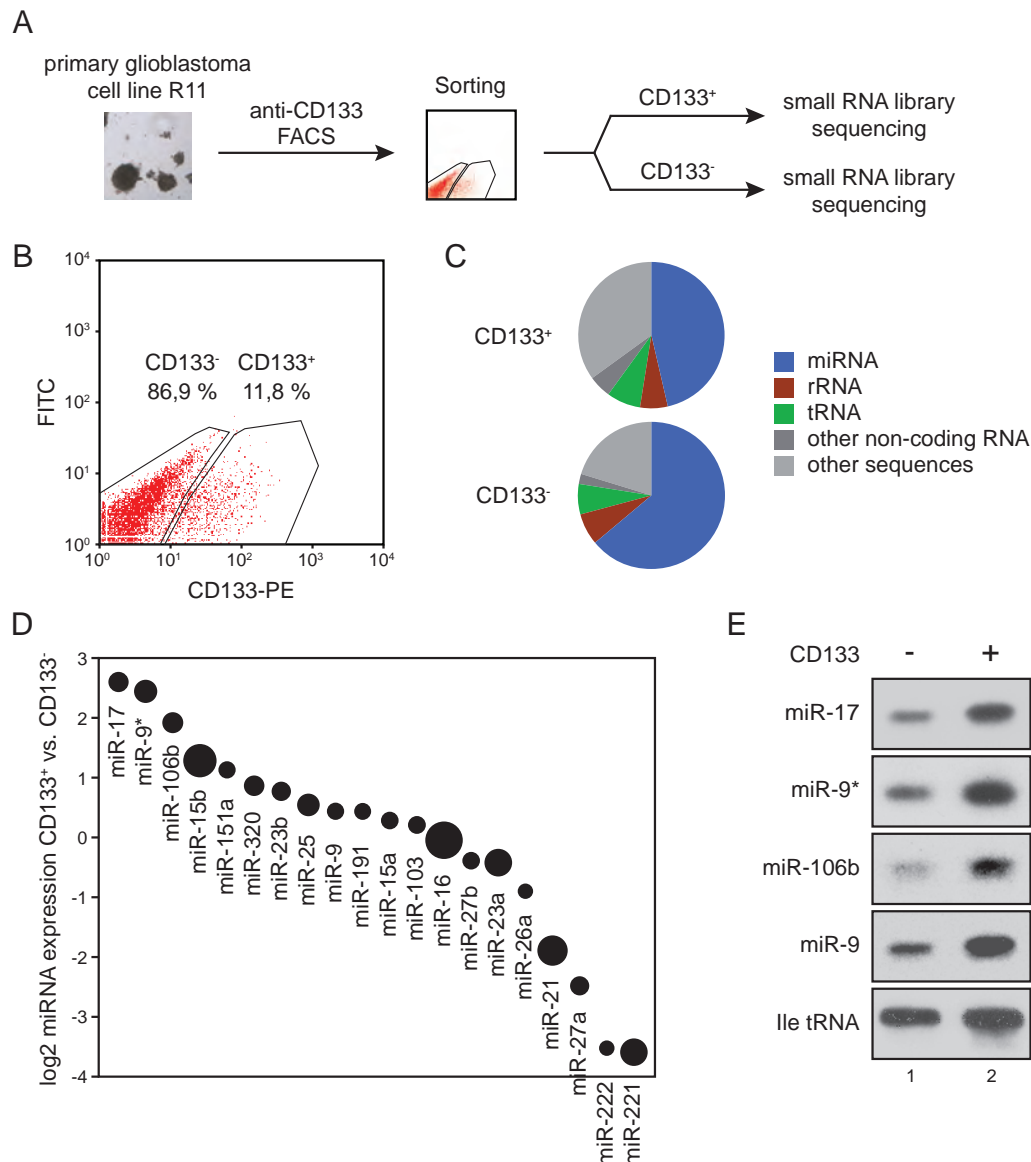


**Figure 2.3.1. miRNA expression profiling of glioblastoma cancer stem cells versus non-cancer stem cells.** **A**, Schematic representation of workflow. Primary glioblastoma cell line R11 was cultivated in stem cell medium and sorted into CD133<sup>+</sup> and CD133<sup>-</sup> subpopulations. Small RNAs were cloned and analyzed by deep sequencing. **B**, Representative FACS analysis of R11 cells shows a subpopulation of 11,8 % CD133-positive (CD133<sup>+</sup>) cells. **C**, Small RNA library composition. **D**, Selected miRNA candidates differentially expressed in CD133<sup>+</sup> versus CD133<sup>-</sup> cells. Positive values indicate higher expression in CD133<sup>+</sup> cells, negative values indicate higher expression in CD133<sup>-</sup> cells. **E**, Validation of differential expression of miR-17-5p, miR-9\*, miR-106b and miR-9 by Northern Blot in R11 cells. Isoleucine (Ile) tRNA was used as loading control.

obtained from R11, miR-9/9\* expression was significantly higher in CD133<sup>+</sup> cells from almost all cell lines tested (Figure 2.3.2 A and B). miR-34a, a miRNA which was detected in the deep sequencing data and more highly expressed in CD133<sup>-</sup> cells, was used as control. Indeed, miR-34a was either more highly expressed in CD133<sup>-</sup> cells or equally expressed, with the exception of R28 (Figure 2.3.2 C).

Taken together, we sorted CD133<sup>+</sup> and CD133<sup>-</sup> cells from the primary human GBM-derived cell line R11 to enrich for a subpopulation that contains or lacks GSCs. We found miRNAs differentially expressed in CD133<sup>+</sup> and CD133<sup>-</sup> cells and validated miR-9/9\*, miR-17 and miR-106b as candidates to be specifically upregulated in CD133<sup>+</sup> cells.

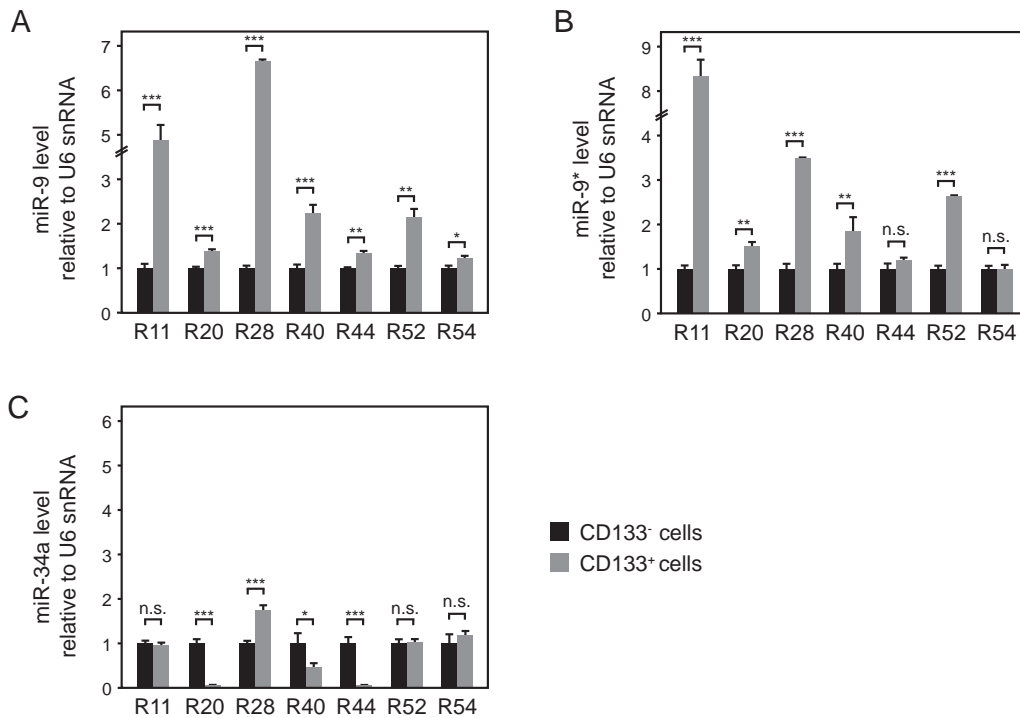


**Figure 2.3.2. Quantification of miR-9 and miR-9\* in different GBM cell lines.** miR-9 (A) and miR-9\* (B) were analyzed by quantitative real-time PCR in CD133<sup>+</sup> and CD133<sup>-</sup> GBM subpopulations. As control, miR-34a (C) was analyzed accordingly. Data are shown as mean plus SEM. P-values are shown as \*P < 0.05; \*\*P < 0.005; \*\*\*P < 0.0005; n.s., not significant.

## 3.2. miR-9/9\* function as oncogenes in GBM and GSCs

### 3.2.1. miR-9/9\* and miR-17 regulate GBM growth *in vitro*

To analyze the functions of the CD133<sup>+</sup>-enriched miRNAs in GBM, we blocked the activity of miRNAs by chemically modified miRNA inhibitors or increased the abundance of these miRNAs by introducing miRNA mimicking RNAs. We analyzed neurosphere-formation, the proportion of CD133<sup>+</sup> cells and differentiation markers.

The activity of a miRNA can be blocked by transfection of chemically modified oligonucleotides which can base pair with the targeted miRNA strand. We used inhibitors with a 2'-O-methylated ribose sugar backbone and the 21 nucleotide antisense sequence of the target miRNA strand (Meister et al., 2004a). One broadly accepted experimental approach used to characterize GSCs is a clonogenic assay, that quantifies the formation of so called neurospheres. Neurospheres are a cell culture phenomenon originally observed when adult neural stem cells are cultivated under defined growth factor and non-adherent conditions (Reynolds and Weiss, 1992). They are free-floating heterogeneous cell aggregates, that are thought to develop by clonal expansion from neural stem cells (Reynolds and Weiss, 1992). Indeed, although GSCs seem to be largely quiescent *in vivo*, the defined culture conditions *in vitro* result in high proliferation of GSCs. GSCs form large neurospheres, whereas progenitor cells have restricted neurosphere-forming potential, the more differentiated GBM cells instead do not form neurospheres (Beier et al., 2007, Singh et al., 2004).

To characterize the role of the identified miRNAs in GBM and GSCs, we analyzed neurosphere-formation after inhibition of miR-9/9\*, miR-17 or miR-106b. As a control, an inhibitor against miR-122 was used as miR-122 is not expressed in brain tissue but has been shown to be liver-specific

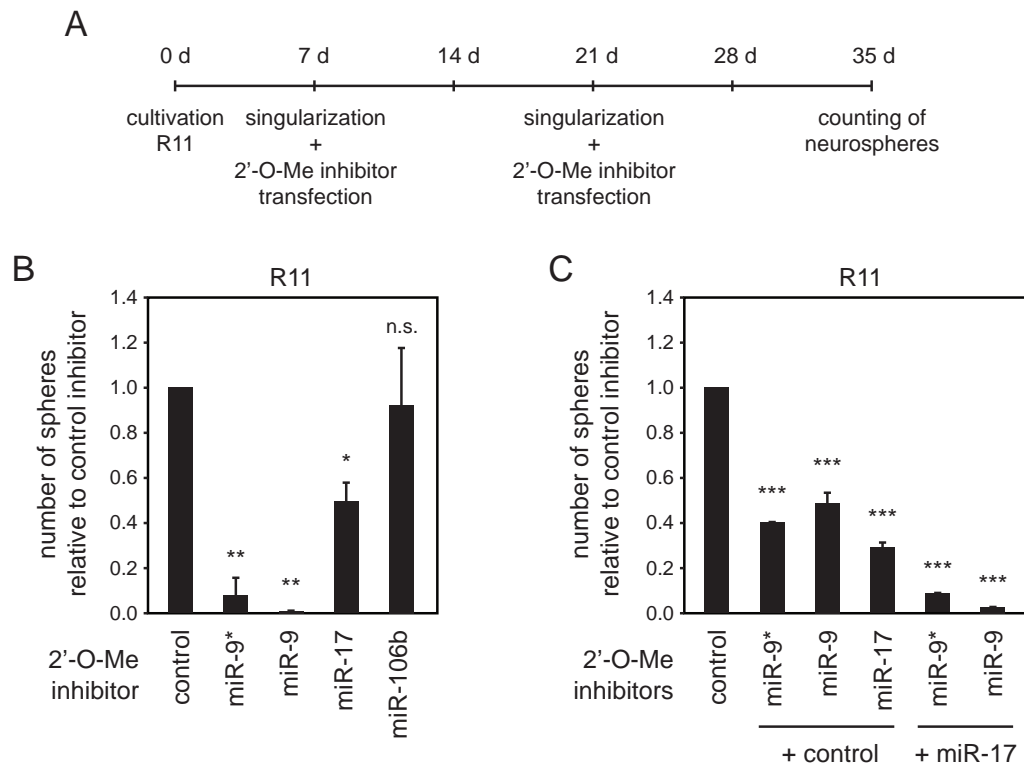


**Figure 2.3.3. miR-9/9\* inhibition affects neurosphere-formation.** **A**, Schematic presentation of workflow for miRNA inhibition experiments. **B**, miR-9, miR-9\*, miR-17-5p and miR-106b were inhibited using 2'-O-methylated inhibitors and neurosphere-formation was analyzed in R11 cells. **C**, Inhibitors against miR-9, miR-9\* and miR-17-5p were transfected at lower concentration or cotransfected with a miR-17-5p inhibitor to show additive effects of miRNA inhibition. Neurosphere-formation in panel B and C is shown normalized to a miR-122 control inhibitor. miR-122 is a liver-specific miRNA. Data are shown as mean plus SEM. \* $P < 0.05$ ; \*\*\* $P < 0.0005$ ; n.s., not significant.

(Lagos-Quintana et al., 2002). Cells were transfected twice with miRNA inhibitors in 7 day intervals and neurosphere-formation was analyzed 14 days after the second transfection (Figure 2.3.3 A). Of note, a double transfection was done to increase the duration of the transient effect of the miRNA inhibitors. Inhibition of miR-9 and miR-9\* let to a strongly reduced neurosphere-formation, inhibition of miR-17 reduced neurosphere-formation to about 50 % and miR-106b had no effect (Figure 2.3.3 B). Since inhibition of both miR-9/9\* and miR-17 affected neurosphere-formation, we tested whether simultaneous inhibition of two different miRNAs shows additive effects. Indeed, the effect of simultaneous inhibition of two different miRNAs was significantly stronger compared to samples in which only one of the three miRNAs was inhibited (Figure 2.3.3 C). Of note, only 50 % of the inhibitor concentration in Figure 2.3.3 B was used for the simultaneous inhibition of two miRNAs, which explains the intermediate effects of miR-9/9\* in Figure 2.3.3 C. Simultaneous transfection of miR-9 and miR-9\* was not tested, as both inhibitors can anneal and would probably neutralize each other.

We next increased the amount of mature miRNA. This can for example be achieved by transfecting so called miRNA mimics, which are annealed mature miRNA sense and antisense strands. We analyzed neurosphere-formation after miR-9/9\* mimic transfection in two different cell lines (R11 and R28). As expected from the miRNA inhibition experiments, the transfection of miRNA mimics conversely increased neurosphere-formation (Figure 2.3.4).

Taken together, we have shown that inhibition of miR-9/9\* and miR-17 strongly decreases whereas overexpressing miR-9/9\* enhances neurosphere-formation of GBM-derived cell lines. Therefore, miR-9/9\* and miR-17 have oncogenic function in this cellular system.

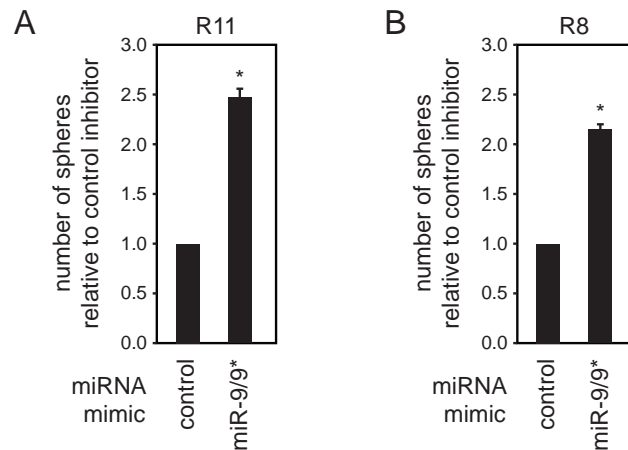


**Figure 2.3.4. Transfection of miR-9/9\* mimics increases neurosphere-formation.** GBM cell lines R11 (A) and R8 (B) were transfected with miR-9/9\* mimics as shown in Figure 2.3.3 A. Neurosphere-formation was analyzed. As control miR-122 mimics were transfected and used for normalization. Data are shown as mean plus SEM. \*P < 0.05.

### 3.2.2. miR-9/9\* affect the CD133<sup>+</sup> GSC pool and differentiation

Since miR-9/9\* are highly expressed in CD133<sup>+</sup> cells and strongly affect neurosphere-formation, we analyzed whether miR-9/9\* directly affect the CD133<sup>+</sup> subpopulation. GSCs are thought to be the major driver for the formation of neurospheres and therefore a reduced CD133<sup>+</sup> pool could explain the effects of miR-9/9\* on neurosphere-formation. We transfected R11 cells with miR-9/9\* inhibitors as described above and analyzed the CD133<sup>+</sup> subpopulation by flow cytometry. Indeed, inhibition of miR-9 or miR-9\* led to a reduction of the CD133<sup>+</sup> subpopulation to about 50 to 60 % compared to the control inhibitor, suggesting that these miRNAs are important for maintenance of the GSCs status (Figure 2.3.4 A).

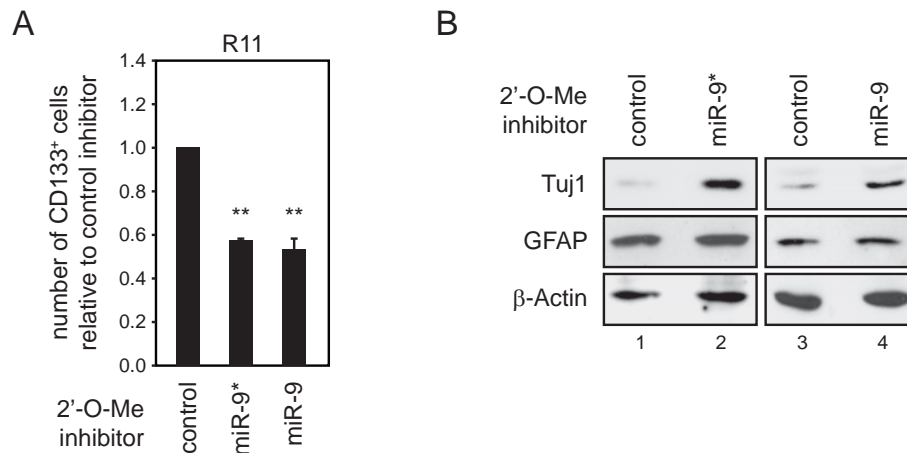


**Figure 2.3.5. miR-9/9\* inhibition affects GSC population.** A, miR-9 and miR-9\* were inhibited using 2'-O-methylated antisense oligonucleotides as shown in Figure 2.3.3 A. Cells were analyzed with CD133-FACS five days after second inhibitor transfection. B, miR-9 (lane 2) and miR-9\* (lane 4) were inhibited as described above and neuronal differentiation marker Tuj1 (upper panels) and glial differentiation marker GFAP (middle panels) were analyzed by Western Blot. β-Actin (lower panels) was used as loading control and miR-122 inhibitor was used as control inhibitor (lanes 1 and 3). Data are shown as mean plus SEM. \*\*P < 0.005.

Reduced stem cell maintenance might result in increased cell differentiation. We therefore tested neuron-specific class II β-Tubulin (Tuj1) and glial fibrillary acidic protein (GFAP) by Western Blot upon miR-9 or miR-9\* inhibition. Tuj1 functions as a neuronal marker and is specifically expressed in differentiating neuronal progenitors and GFAP is a glial marker which is mainly

expressed in differentiated astrocytes (reviewed in von Bohlen Und Halbach, 2007). A marker for oligodendrocytes, as for example MBP, PDGFR $\alpha$  and Olig1/2 has not been tested. Indeed, Tuj1 was clearly increased upon miR-9/9\* inhibition, showing induced neuronal differentiation (Figure 2.3.4 B). The glial differentiation marker GFAP instead was not increased.

Taken together, we found that miR-9/9\* and miR-17 strongly affect neurosphere-formation of primary human GBM-derived cell lines. miR-9/9\* probably function in maintaining GSC-status by preventing differentiation.

### 3.3. Identification of miR-9\* targets

#### 3.3.1. miR-9\* mRNA target identification

As miRNAs function by regulating the expression of other genes, we identified target genes of miR-9\* by analysis of mRNA enrichment in Ago2-immunoprecipitations upon miRNA inhibition (Beitzinger et al., 2007, Karginov et al., 2007, Easow et al., 2007). We selected miR-9\*, since it showed strong upregulation in CD133<sup>+</sup> cells and prominent effects in neurosphere-formation assays presented in part II section 3.2. R11 cells were transfected with miR-9\* or control inhibitors and immunoprecipitated Ago2-bound mRNAs were detected by microarray. The miRNA inhibitor prevents mRNA binding and therefore miR-9\* targets are selectively lost in the immunoprecipitates compared to control transfections and the input RNA (Figure 2.3.6 A). The top twenty candidates are shown in Figure 2.3.6 B. miR-9\* target mRNA candidates that were more than 10-fold depleted in the miR-9\* inhibitor sample compared to the control sample were PGBD2, NEFM, MALT1, CAMTA1, OASL and PPIP5K1.

PiggyBAC transposable element derived 2 (PGBD2) is not characterized so far, but is predicted to encode for a transposase. Neurofilament medium polypeptide (NEFM, NF-M) is a neurofilament protein of the axonal cytoskeleton and functions as neuronal differentiation marker. Mucose-associated lymphoid tissue lymphoma translocation gene 1 (MALT1) is a caspase-like protein and plays a role in NF- $\kappa$ B activation during T-cell receptor signalling (Thome, 2008). Calmodulin-binding transcription activator 1 (CAMTA1) encodes for a potential transcription activator involved in neuroblastoma and is located on 1p36, a region frequently deleted in GBM (Henrich et al., 2011). 2'-5'-Oligoadenylate synthase-like (OASL) encodes for a protein which activate RNaseL as a viral defense mechanism (Thome, 2008). Diphosphoinositol pentakisphosphate kinase 1 (PPIP5K1, HISPPD2A) encodes for a largely uncharacterized inositol kinase.

Taken together, we have identified several possible miR-9\* target mRNAs. These included CAMTA1, a transcription factor with an interesting genomic localization.

### 3.4. Characterization of the novel tumor suppressor CAMTA1

#### 3.4.1. CAMTA1 is a putative tumor suppressor in 1p36 and frequently deleted in GBM

For further analysis, we focused on CAMTA1, as it is expressed from the 1p36 locus which is frequently deleted in gliomas, including anaplastic astrocytoma, oligodendroglioma and the unrelated neuroblastoma (Ichimura et al., 2007, Henrich et al., 2011). Reported frequencies of 1p36 deletions in GBM range from 1 to 20 % between different reports (Weller et al., 2009, Brennan

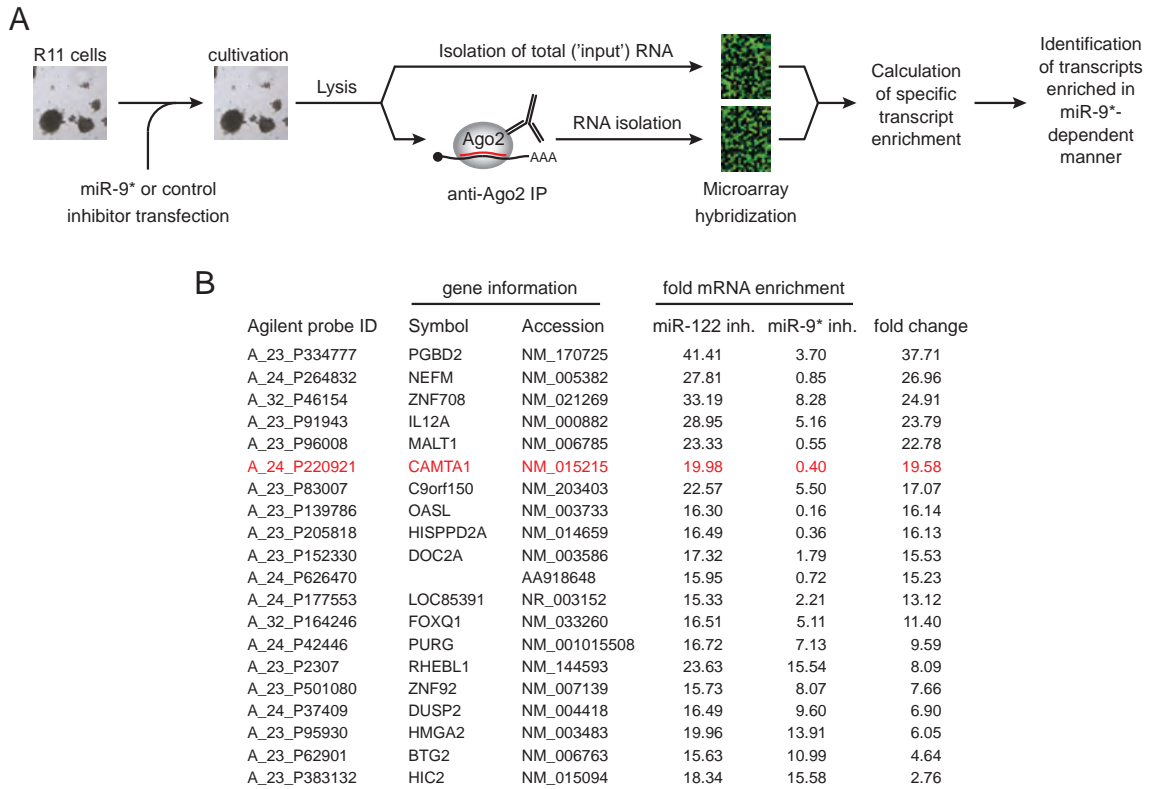


**Figure 2.3.6. Identification of miR-9\* target mRNAs.** **A**, Strategy to identify miR-9\* target mRNAs based on Ago2 immunoprecipitation and microarray analysis. **B**, List of the twenty most strongly Ago2-associated transcripts in the presence of control inhibitor (inh.) with simultaneous lower abundance in the miR-9\* inhibition sample. List is sorted according to fold change as calculated by subtracting fold mRNA enrichment in miR-9\* and miR-122 inhibitor samples. CAMTA1 is shown in red.

et al., 2013, Figure 2.3.7 A). For astrocytoma and oligodendroglioma, CAMTA1 has been reported to be located within a minimally deleted region of 1p36 (Dong et al., 2004, Barbashina et al., 2005). Therefore, CAMTA1 might be important for different glioma types.

The human CAMTA1 gene spans a region of almost 1 Mb and contains 23 exons. N- and C-terminally truncated non-coding and protein-coding transcript variants are predicted, in addition to splice variants of the full length CAMTA1. Clear evidence for the expression of single transcript variants is largely lacking. Human CAMTA1 mRNA has been detected in non-neoplastic adult brain tissue as an 8 kb transcript, which corresponds to full length CAMTA1 mRNA, and an additional 3 kb transcript, which might correspond to a C-terminally truncated variant (Barbashina et al., 2005). Mouse CAMTA1 mRNA is strongly expressed in brain tissue and weakly in heart (Song et al., 2006), which is in line with our own quantitative real-time PCR experiments (data not shown).

The human CAMTA1 gene encodes for a 1673 amino acid protein with a molecular weight of about 180 kDa (Appendix Figure A1). Domain predictions suggest a CG-1 DNA-binding domain, a transcription factor immunoglobulin-like (TIG) domain that can mediate sequence-independent DNA contacts, calmodulin-binding motifs (IQ), a calmodulin-binding domain (CaMBD) and ankyrin domains that may mediate protein-protein interactions (Figure 2.3.7 B). CAMTA1 is therefore predicted to be a Calmodulin-regulated transcription factor. Additionally, CAMTA1 contains two nuclear localization signals and is therefore predicted to be nuclear (Figure 2.3.7 B). Evidence for functionality of those domains and localization of the human protein is largely lacking, except for the DNA-binding activity of the N-terminal CG-1 domain (Long et al., 2014).

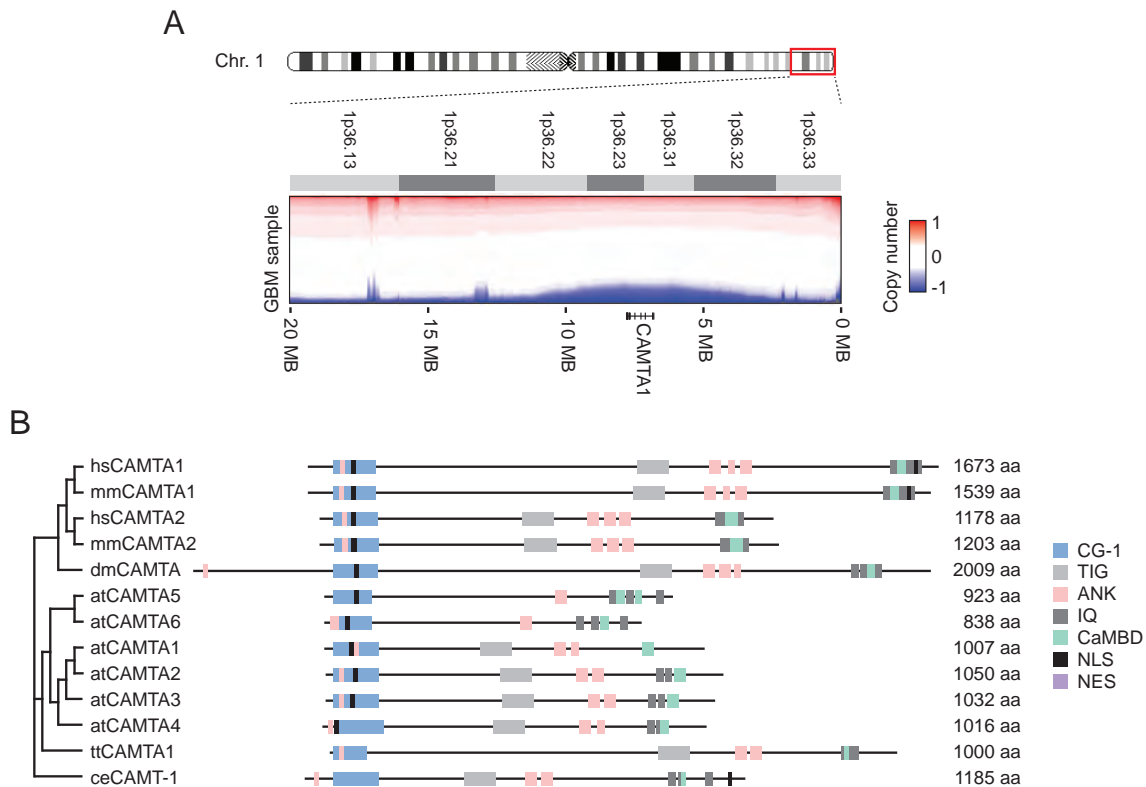


**Figure 2.3.7. CAMTA1 shows a conserved domain structure and is located at 1p36.** **A**, CAMTA1 is located at 1p36 which is deleted in some GBM patients. Genomic copy number aberrations at the terminal 20 MB of chromosome arm 1p are shown from 578 GBM patient samples. Blue represents regions that are more frequently deleted. CAMTA1 is schematically shown with Introns and Exons. **B**, CAMTA1 homologs and paralogs in different organisms. CAMTA proteins consist of multiple predicted domains as described in the main text. Phylogenetic tree was built with Clustal W2, domains were identified with ELM Tool or adapted from Finkler et al., 2007. Accessions are as follows: hsCAMTA1 (NP\_056030), hsCAMTA2 (AAI44233), mmCAMTA1 (AAI50741), mmCAMTA2 (AAH56395), dmCAMTA (ABI94369), atCAMTA1 (Q9FY74), atCAMTA2 (Q6NPP4), atCAMTA3 (Q8GSA7), atCAMTA4 (Q9FYG2), atCAMTA5 (Q23463), atCAMTA6 (Q9LSP8), ttCAMTA1 (THERM\_00145410), ceCAMT-1 (H2KY84). Abbreviations: hs, *Homo sapiens*; mm, *Mus musculus*; dm, *Drosophila melanogaster*; at, *Arabidopsis thaliana*; tt, *Tetrahymena thermophila*; ce, *Caenorhabditis elegans*.

### 3.4.2. Validation of CAMTA1 as a miR-9/9\* target mRNA

To show that CAMTA1 is indeed regulated by miR-9\*, we searched for miR-9\* binding sites in the 3'-UTR of CAMTA1. Interestingly, we not only identified potential binding sites for miR-9\*, but also for miR-9, miR-17 and miR-106b, which were also highly abundant in CD133<sup>+</sup> cells (Figure 2.3.8 A). Therefore, CAMTA1 might be regulated by multiple miRNAs in GSCs.

To validate those binding sites, we cloned and fused the CAMTA1 3'-UTR to firefly luciferase and cotransfected miRNA inhibitors. Therefore, firefly luciferase is under control of the CAMTA1 3'-UTR and its expression should be influenced by miRNA inhibitor transfection. Renilla luciferase was detected as internal control, which is expressed from the same reporter plasmid. Inhibition of a miRNA that regulates CAMTA1 would result in an increase in firefly signal. As control for miR-9 and miR-9\* we mutated CAMTA1 3'-UTRs in all predicted miR-9 or miR-9\* binding sites, respectively. Indeed, inhibition of miR-9 and miR-9\* resulted in a significant derepression of the wildtype CAMTA1 3'-UTR reporter but not of mutated CAMTA1 3'-UTR reporters, indicating that the predicted miRNA binding sites are indeed functional (Figure 2.3.8 B).

Inhibition of miR-106b or miR-17 also resulted in a derepression of the CAMTA1 3'-UTR reporter (Figure 2.3.8 C), indicating that miR-9, miR-9\*, miR-106b and miR-17 regulate CAMTA1

expression. Of note, compared to the weak increase in CAMTA1 mRNA levels (Figure 2.3.8 D), CAMTA1 protein was much stronger increased (Figure 2.3.8 E), suggesting that miR-9/9\* may preferentially inhibit CAMTA1 translation, rather than mRNA stability.

Taken together, we have shown that CAMTA1 is indeed regulated by miR-9/9\*, miR-17 and miR-106b.

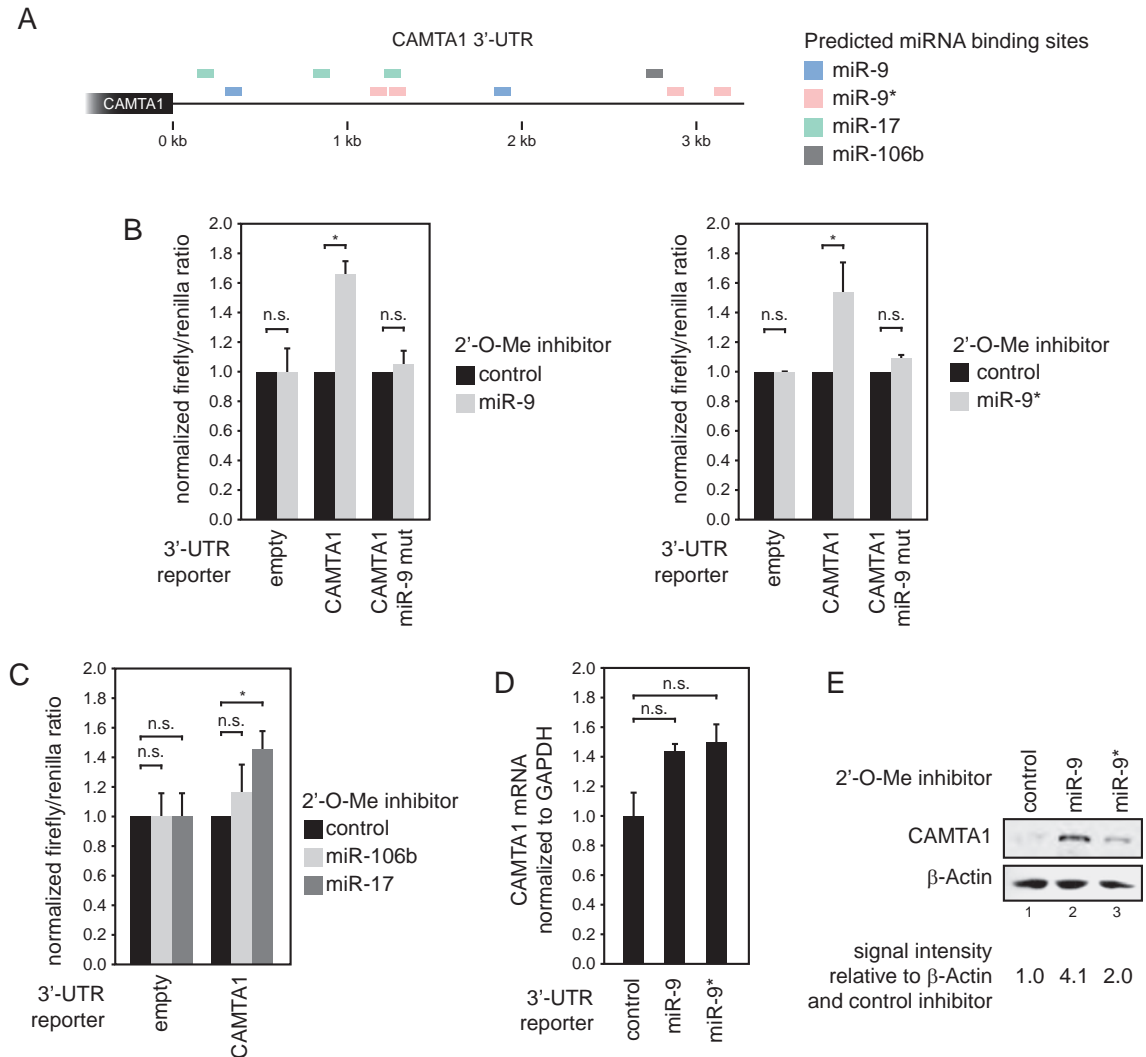


**Figure 2.3.8. miR-9, miR-9\*, miR-106 and miR-17-5p regulate CAMTA1 expression.** **A**, Location of miR-9, miR-9\*, miR-17-5p and miR-106b binding sites in the 3'-UTR of CAMTA1 as predicted with TargetScan and manual sequence analysis. **B**, CAMTA1 3'-UTR and variants with mutations in miR-9 (left panel) or miR-9\* (right panel) binding sites were fused to firefly luciferase and expression was analyzed in the presence or absence of miR-9 (left panel) or miR-9\* (right panel) inhibitors or control inhibitors in T98G cells. **C**, CAMTA1 3'-UTR was analyzed as described in the presence or absence of miR-106 or miR-17-5p inhibitors. **D**, **E**, mRNA (D) and protein (E) levels of CAMTA1 were analyzed by quantitative real-time PCR and Western Blot after miR-9 (lane 2) and miR-9\* (lane 3) inhibition or transfection of a control inhibitor (lane 1) in R11 cells. GAPDH was measured and used for normalization of quantitative real-time PCR.  $\beta$ -Actin (lower panel in E) was used as loading control for Western Blot. Data are shown as mean plus SEM. \*P < 0.05; n.s., not significant.

### 3.4.3. CAMTA1 impairs glioblastoma growth *in vitro*

Because neurosphere-formation assays suggested an oncogenic function of miR-9/9\*, CAMTA1 should function as a tumor suppressor if miR-9/9\* and CAMTA1 expression are functionally coupled. To investigate the function of CAMTA1 in GBM growth *in vitro*, we first characterized the

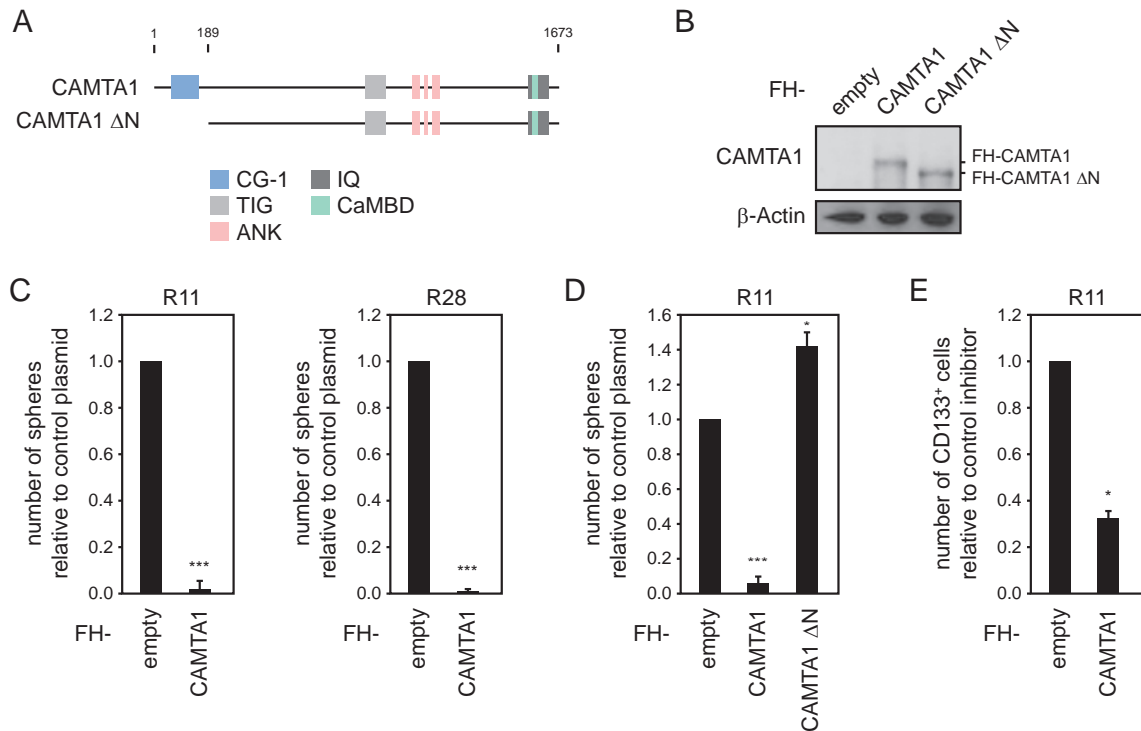


**Figure 2.3.9. CAMTA1 has tumor suppressor activity *in vitro*.** **A**, Domain organization of CAMTA1 and CAMTA1 ΔN, in which the putative CG-1 DNA-binding domain has been deleted. **B**, Flag/HA-tagged (FH) CAMTA1 and CAMTA1 ΔN were expressed in HEK 293T cells and protein expression was analyzed by Western Blot using anti-CAMTA1 antibody. **C**, FH-CAMTA1 was expressed in R11 (left panel) and R28 (right panel) and neurosphere-formation was analyzed. **D**, FH-CAMTA1 and FH-CAMTA1 ΔN were expressed in R11 cells and neurosphere-formation was analyzed. **E**, FH-CAMTA1 was expressed in R11 cells and CD133<sup>+</sup> subpopulation was quantified by FACS analysis. An empty plasmid, expressing FH only was used as control in **C**, **D** and **E**. Data are shown as mean plus SEM. \*P < 0.05; \*\*\*P < 0.0005.

effects of CAMTA1 overexpression on neurosphere-formation of GBM-derived cell lines. It has already been shown for mouse CAMTA2, that the N-terminal CG-1 domain is essential for protein function (Song et al., 2006). Therefore, we included a N-terminally truncated mutant CAMTA1 ΔN into our analyses (Figure 2.3.9 A) and tested overexpression in HEK 293T cells (Figure 2.3.9 B). Of note, endogenous CAMTA1 was not detectable in HEK293T cells (Figure 2.3.9 B).

Strikingly, expression of CAMTA1 in both GBM-derived cell lines tested led to an almost complete loss of neurosphere-formation capacity (Figure 2.3.9 C). Interestingly, expression of CAMTA1 ΔN had no inhibitory effect on neurosphere-formation, indicating that expression of a functional CAMTA1 only inhibits neurosphere-formation (Figure 2.3.9 D). Of note, expression of CAMTA1 ΔN resulted in a slight increase in neurosphere-formation (Figure 2.3.9 D). However, because the effects of CAMTA1 ΔN were not reproducible in GBM cell line R28, we so far do not suggest that CAMTA1 ΔN might exhibit dominant-negative functions (data not shown).

We have shown that miR-9/9\* inhibition results in a decrease of CD133<sup>+</sup> cells in the GBM-derived cell line R11. To investigate whether CAMTA1 overexpression decreases the CD133<sup>+</sup> subpopulation, we overexpressed CAMTA1 and submitted these cells for FACS analysis. Indeed we observed a strong reduction of CD133<sup>+</sup> cells to about 30 % of the control sample upon CAMTA1 overexpression (Figure 2.3.9 E) indicating that low CAMTA1 levels are beneficial for the CD133<sup>+</sup> subpopulation.

Taken together, CAMTA1 functions as a tumor suppressor in GBM *in vitro* and affects the CD133<sup>+</sup> GSC pool, which might at least in part explain its tumor suppressor function.

### 3.4.4. miR-9/9\* effects and CAMTA1 expression are functionally coupled

We found that miR-9 and miR-9\* inhibition as well as CAMTA1 overexpression block neurosphere-formation. Therefore, we hypothesized that miR-9/9\* effects might result from induced CAMTA1 protein after miR-9/9\* inhibition. If this hypothesis is correct, it should be possible to rescue the effects of miR-9/9\* inhibition on neurosphere-formation by decreasing levels of CAMTA1. Additionally, we wanted to test whether the decrease of endogenous CAMTA1 levels has the opposite effects on neurosphere-formation compared to CAMTA1 overexpression.

We therefore depleted CAMTA1 by RNAi and validated successful reduction of the endogenous protein with anti-CAMTA1 Western-Blot and two different siRNAs (Figure 2.3.10 A). Knockdown of CAMTA1 alone (i.e. without miR-9/9\* inhibition) only resulted in a weak increase of neurosphere-formation for one siRNA (Figure 2.3.10 B, black bars). Therefore, we did not observe a supportive effect of decreased CAMTA1 levels on neurosphere-formation capacity.

We subsequently transfected inhibitors against miR-9, miR-9\* or a control inhibitor and knocked down CAMTA1 simultaneously (Figure 2.3.10 B, grey bars). Indeed, reduction of neurosphere-formation upon miR-9 and miR-9\* inhibition was strongly reduced in CAMTA1 knockdown samples, although the rescue of miR-9\* inhibition was not as efficient as for miR-9.

Taken together, these data show that CAMTA1 protein mediates the miR-9/9\*-dependent effects on neurosphere-formation.

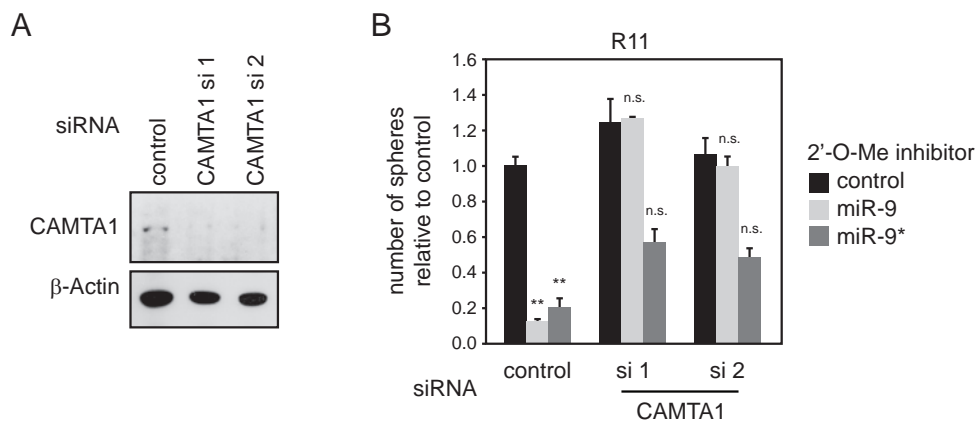


**Figure 2.3.10. Knockdown of CAMTA1 rescues neurosphere-formation defects upon miR-9/9\* inhibition.** **A**, R11 cells were treated with two different CAMTA1 siRNAs and CAMTA1 protein expression was determined by Western Blot using anti-CAMTA1 antibody. Antibody against  $\beta$ -Actin was used as loading control. **B**, R11 cells were pretreated with CAMTA1 siRNAs and subsequently transfected with miR-9 and miR-9\* or a control inhibitor. neurosphere-formation was analyzed after miRNA inhibitor transfection. Data are shown as mean plus SEM. \*\*P < 0.005; n.s., not significant.

### 3.4.5. CAMTA1 functions as a tumor suppressor *in vivo*

The striking effects of CAMTA1 overexpression on neurosphere growth of GBM-derived cell lines led us to investigate whether CAMTA1 also functions as a tumor suppressor *in vivo*. To do so, we used a well established xenograft model, in which human GBM-derived cell lines are injected orthotopically (i.e. at its naturally occurring position) into brains of nude mice NU/NU-Foxn1<sup>nu</sup> (NU/NU) (Figure 2.3.11 A). NU/NU mice show a strong thymus dysgenesis with a severely diminished immune response. We used the GBM-derived cell line R28, because it showed strong effects on CAMTA1 overexpression and has already been shown to form reproducible and fast growing tumors when orthotopically implanted into mouse brains (Beier et al., 2007). To be able to follow tumor growth in the living animal, R28 was transduced to stably express firefly luciferase

and as expected, luciferase expression correlated with cell number *in vitro* (Figure 2.3.11 B). After transfection with CAMTA1 plasmid or empty plasmid as control, cells were injected into mice and tumor growth was analyzed 15 days after transfection by measuring luciferase signal after luciferin injection. In agreement with the *in vitro* data, cells transfected with CAMTA1 showed strongly decreased tumor growth (Figure 2.3.11 C and D), whereas control cells rapidly formed tumors. Of note, the color scale in Figure 2.3.11 C is different between both groups, making weak signals in the CAMTA1 transfected group more intense.

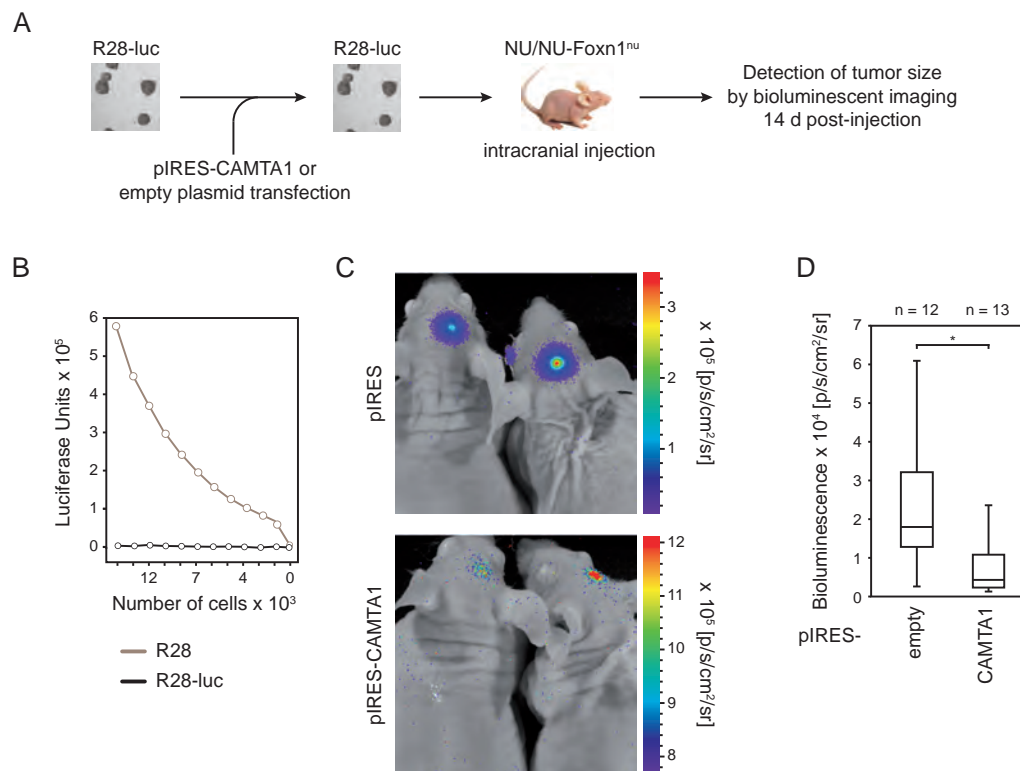


**Figure 2.3.11. CAMTA1 functions as a tumor suppressor *in vivo*.** **A**, Schematic representation of the used xenograft model. **B**, Human GBM cell line R28 was transfected with a construct containing firefly luciferase (*luc*) to generate stable R28-*luc* cell line. Luciferase expression was analyzed by detection of luciferase activity. **C**, **D**, R28-*luc* was transiently transfected with pIRES-CAMTA1 or an empty plasmid followed by orthotopic implantation into nude mice (NU/NU-Foxn1<sup>nu</sup>) brain. Tumor size was analyzed by bioluminescent imaging 14 d post implantation. Two representative mice of each experimental group are shown in panel C. The color scales indicate signal intensity recorded as total photons per second, square centimeter and steradian. Box-Whisker-Diagram of the quantified dorsal signals from both experimental groups is shown in panel D with a significance of \*P < 0.05. n represents group size. Data in D are shown as mean plus/minus SEM.

### 3.4.6. Initial characterization of a CAMTA1 knockout mouse model

As CAMTA1 showed striking effects on tumor growth *in vitro* and *in vivo*, we decided to use a previously reported conditional CAMTA1 knockout mouse model (Long et al., 2014, see Appendix Figure A2). As expected for a tumor with highly diverse and multiple genetic aberrations, spontaneous formation of GBM or other brain tumors has not been identified in CAMTA1 knockout mice (Long et al., 2014). This indicates that a homozygous loss of CAMTA1 alone is not able to induce GBM or other brain tumors. As it has been shown that GBM-like tumors can develop from neural stem cells (NSCs), we decided to generate an inducible CAMTA1 knockout specifically in NSCs (Sanai et al., 2005, Stiles and Rowitch, 2008, Zong et al., 2012, Chen et al., 2012b). Furthermore, we developed tools for detailed analysis of the mouse model and for future crossings with

other GBM-prone mouse models. This should finally allow to determine whether loss of CAMTA1 increases the frequency of spontaneous GBM-like tumors together with other aberrations.

To do so, we did embryo transfers to establish two founding pairs for the CAMTA1<sup>fl/fl</sup> line. Adult NSCs reside within the subventricular zone and the subgranular zone of the dentate gyrus and are characterized by expression of the intermediate filament protein Nestin. Therefore, we crossed CAMTA1<sup>fl/fl</sup> mice with Nestin-CreERT2 driver lines, which allow for tamoxifen (TAM) inducible CAMTA1 knockouts during variable developmental stages or in adult animals (Lagace et al., 2007). TAM application results in a nuclear translocation of the cytoplasmic Nestin-CreERT2 fusion protein and consequently knockout of CAMTA1. Five sequential administrations of TAM intraperitoneally were used (Lagace et al., 2007). Genotyping after TAM administration did not allow direct identification of the CAMTA1 knockout allele via brain biopsies from different brain regions. However, we showed successful CAMTA1 knockout after cultivation of subventricular zone-derived NSCs under stem cell cultivation conditions (data not shown). Whether we were able to knockout CAMTA1 in all NSCs is probable, because no wildtype allele was visible by genotyping after TAM administration. However, this has to be further investigated. Three month after tamoxifen injection, mice did not show the observed long-term effects of the published CAMTA1-knockout mice, including severe ataxia (data not shown). Furthermore, the mice did not show other obvious behavioral abnormalities and no weight loss (data not shown). Therefore, we are able to knockout CAMTA1 in adult NSCs without the previously observed abnormalities, which is a beneficial condition for long-term observation of tumor development and growth. This provides a solid basis for future analysis of this mouse model system.

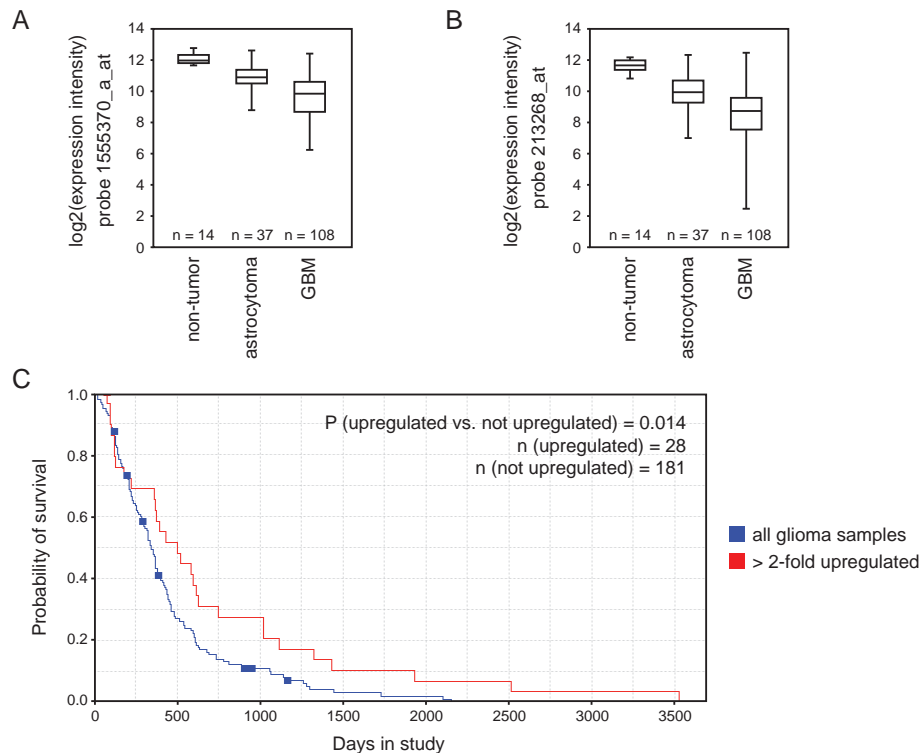


**Figure 2.3.12. CAMTA1 expression correlates with patient survival.** **A, B**, CAMTA1 mRNA expression was analyzed in non-tumor brain tissue, astrocytoma (WHO grade I-III) and GBM using the indicated Affymetrix probes. **C**, Kaplan-Meier survival plot for GBM patients with high (red) and normal (blue) CAMTA1 mRNA expression, as determined using Affymetrix probe 213268. Data in A are shown as mean plus/minus SEM. Data in A and B were obtained and P-value in C was calculated using REMBRANDT database.

### 3.4.7. CAMTA1 expression correlates with patient survival

As CAMTA1 overexpression showed striking effects on GBM growth *in vitro* and *in vivo* and because 1p36 deletions are frequent in glioma patients, we asked whether CAMTA1 expression correlates with survival of patients suffering from different classes of gliomas. As source material, we accessed the Repository of Molecular Brain Neoplasia Data (REMBRANDT), a database that integrates clinical data, copy number information and gene expression data from glioma patients out of clinical trials (Madhavan et al., 2009). Here, CAMTA1 mRNA expression was decreased in GBM and WHO grade I to III astrocytoma samples compared to healthy individuals (Figure 2.3.12 A and B). Interestingly, GBM showed lower CAMTA1 expression than the less malignant astrocytomas. We next analyzed whether patients with high CAMTA1 expression might have beneficial prognosis for a longer survival. Indeed, patients with high CAMTA1 levels in tumor tissue showed a significantly longer survival compared to all other patients (Figure 2.3.12 C). Of note, we only found a very low number of GBM patients with high CAMTA1 levels (data not shown), therefore survival data were analyzed from patients suffering from GBM, astrocytomas, oligodendrogliomas and gliomas with mixed histology. Taken together, analysis of patient data indicates that CAMTA1 might act as a tumor suppressor in GBM and other gliomas. In addition, CAMTA1 might function as a marker with potential prognostic value.

## 3.5. Identification of CAMTA1 target genes

CAMTAs have been shown to function as transcription factors in various organisms (reviewed in Finkler et al., 2007). To further characterize CAMTA1, we identified potential target genes of CAMTA1 by CAMTA1 overexpression and target mRNA quantification.

### 3.5.1. CAMTA1 regulates the natriuretic peptide hormone system

It has been previously shown, that mouse CAMTA2 activates transcription of the atrial natriuretic peptide (ANP) in the heart (Song et al., 2006). ANP belongs to the natriuretic peptides, which are

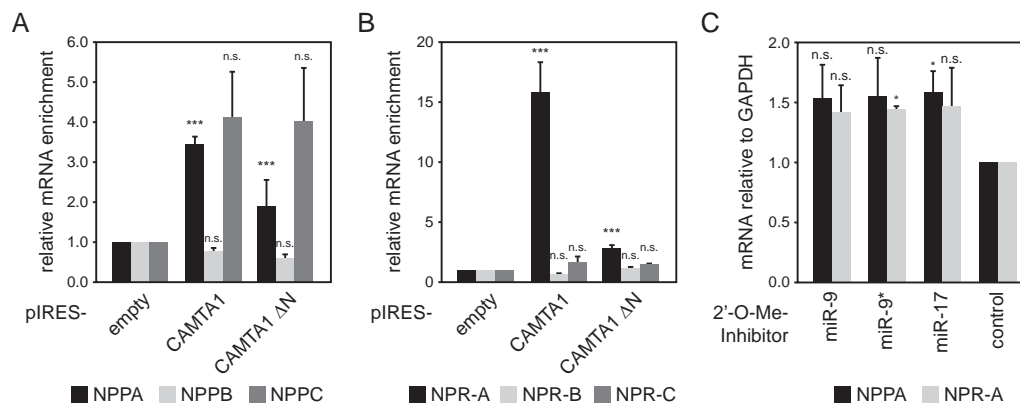


**Figure 2.3.13. CAMTA1 positively regulated NPPA and NPR-A.** **A, B**, R28 cells were transiently transfected with CAMTA1 or CAMTA1 ΔN expressing plasmids or an empty plasmid as control. Natriuretic peptide precursor (NPP) A, B and C mRNA was analyzed by quantitative real-time PCR in panel **A**. Quantification of natriuretic peptide receptor (NPR) A, B and C mRNA is shown in panel **B**. **C**, LN-229 cells were transfected with miR-9, miR-9\* or miR-17-5p inhibitors and NPPA and NPR-A mRNA was quantified by quantitative real-time PCR. GAPDH was used as internal control for normalization in A, B and C. Data are shown as mean plus SEM. \*P < 0.05; \*\*P < 0.005; \*\*\*P < 0.0005; n.s., not significant.

mainly secreted by the heart, but have also been found to be synthesized in the brain and other organs (Anand-Srivastava, 2005). Two structurally related proteins brain natriuretic peptide (BNP) and C-type natriuretic peptide (CNP) belong to the same family of peptide hormones. Despite its name, BNP is mainly expressed in heart but has also been identified in brain, as it is the case for ANP and CNP. ANP, BNP and CNP are expressed as inactive precursors from the natriuretic peptide precursor (NPP) genes NPPA, NPPB or NPPC, respectively. ANP and BNP are agonists of the natriuretic peptide receptor A and C (NPR-A, NPR-C), CNP is agonist of NPR-B. Interestingly, it has been shown that ANP has antiproliferative effects on GBM cell lines *in vitro* (Vesely et al., 2007). To investigate whether CAMTA1 activates the expression of NPPA in GBM-derived cell lines, CAMTA1 or CAMTA1  $\Delta$ N was expressed in LN-229 cell line followed by quantification of peptide hormone precursor and receptor mRNAs. CAMTA1 overexpression increased NPPA mRNA levels, whereas transfection of CAMTA1  $\Delta$ N had a much weaker effect, however the induction was still significant (Figure 2.3.13 A). NPPB did not respond to CAMTA1 overexpression, NPPC was increased to a similar degree in CAMTA1 and CAMTA1  $\Delta$ N transfected cells; additionally, induction of NPPC was variable between biological replicates (Figure 2.3.13 A). Among the receptors, NPR-A was strongly induced upon CAMTA1 overexpression, whereas NPR-B and NPR-C did not increase (Figure 2.3.13 C).

Because miR-9/9\* and miR-17 inhibition increased CAMTA1 expression, we asked whether inhibition of miR-9/9\* and miR-17 also increase expression of NPPA and NPR-A. Indeed, NPPA and NPR-A mRNA levels were increased upon miR-9/9\* and miR-17 inhibition, presumably by CAMTA1 expression (Figure 2.3.13 C). Although the results were reproducible, induction of NPR-A

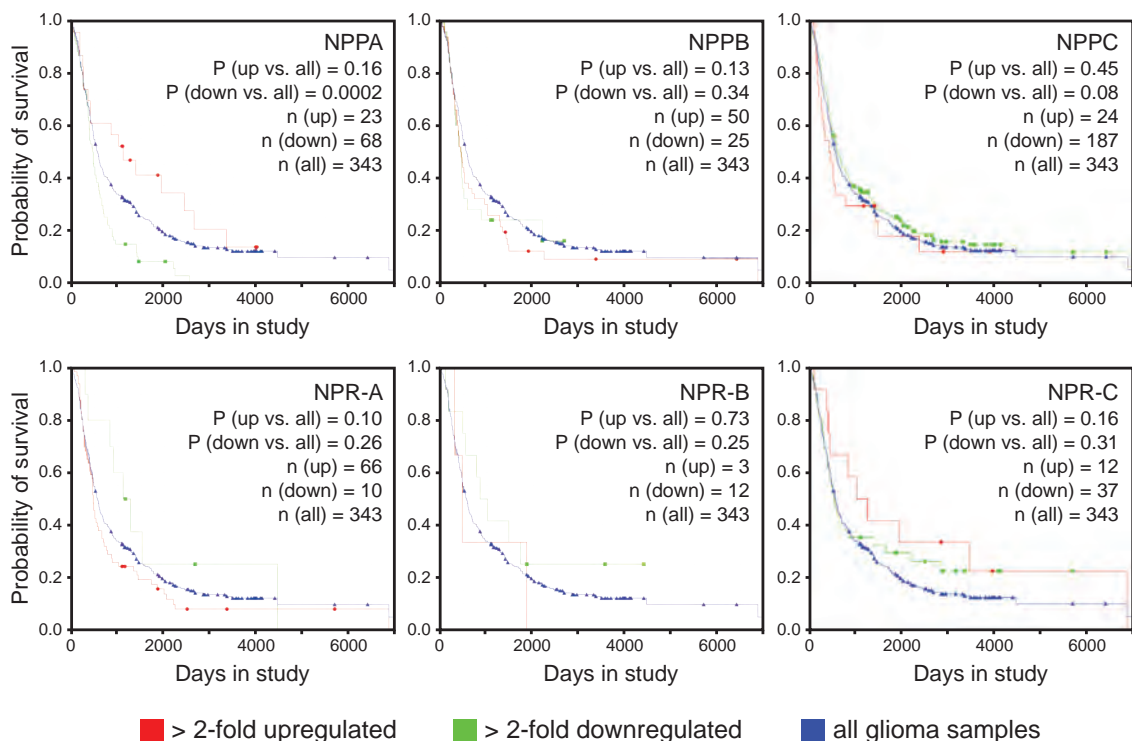


**Figure 2.3.14. NPPA expression correlates with patient survival.** NPPA, NPPB, NPPC and the receptors NPR-A, NPR-B and NPR-C were analyzed in patient samples. Kaplan-Meier plots were generated from glioma patients including GBM, oligodendroglioma and astrocytoma. Samples were sorted into high (red) or low (green) expression of each mRNA and compared to survival data of all samples (blue) used for analysis. Only NPPA showed a significant correlation with patient survival. Analyses were performed using REMBRANDT database and P-values were calculated by REMBRANDT software. n represents group size.

and NPR-A upon miRNA inhibition were not statistically significant.

We next analyzed whether NPPA and the other components of the natriuretic peptide hormone system show correlation with GBM patient survival. We again used REMBRANDT database for our analysis. Consistently with our *in vitro* data, low NPPA expression correlated significantly with patient survival (Figure 2.3.14). Of note, only GBM patients have been included into the analysis, because enough patients were available with altered NPPA expression and ANP has been previously shown to have antiproliferative function on GBM-derived cell lines (Vesely et al., 2007). All other components NPPB, NPPC, NPR-A, NPR-B and NPR-C did not significantly correlate with patient survival.

Because the role of the natriuretic peptide hormone system in the brain is still a matter of debate and we did not test yet whether ANP indeed has inhibitory effects on GBM growth, we can only state so far that ANP might play a role downstream of CAMTA1 for GBM but an exact role of the natriuretic peptide system has to be further analyzed.

### 3.5.2. Transcriptome response upon CAMTA1 overexpression

To get deeper insights into CAMTA1 function, we characterized the transcriptome response after CAMTA1 overexpression. Genes regulated directly or indirectly by CAMTA1 should be either lower or higher expressed in the CAMTA1 transfected sample compared to an empty plasmid transfected sample. RNA was hybridized to an Affymetrix GeneChip Human Gene 1.1 ST Ar-

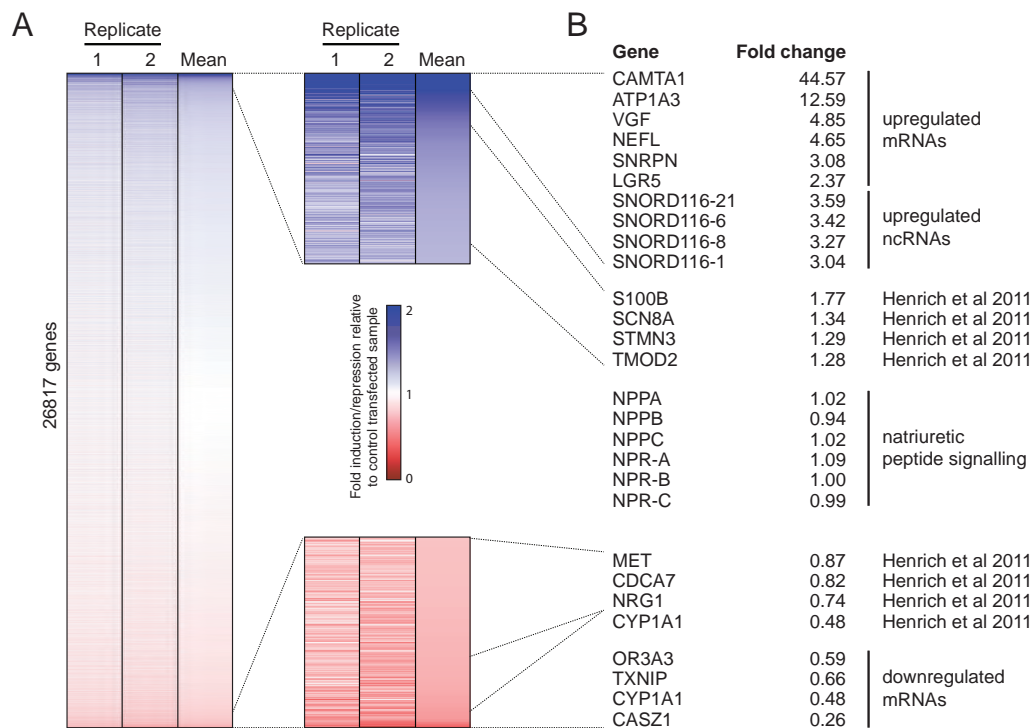


**Figure 2.3.15. Transcriptome response after CAMTA1 overexpression.** **A**, GBM cell line R28 was transiently transfected with CAMTA1 or empty plasmid. RNA samples were processed and hybridized on an Affymetrix Human Gene 1.1 ST Arrays in biological duplicates. Expression ratio CAMTA1 to control was calculated for each transcript in both duplicates (lane 1 and 2). Mean value was calculated from biological duplicates and genes were sorted according to decreasing mean ratio. Blue indicates higher, red indicates lower expression after CAMTA1 overexpression, whereas the value 1 corresponds to unchanged levels. **B**, Candidates were selected from the top up- or down-regulated mRNAs and non-coding RNAs (ncRNAs). Additionally, previously described potential CAMTA1 target genes from Henrich et al., 2011 and the natriuretic peptide hormone system (this work) were detected in the microarray data and listed together with the measured mean fold change.

ray designed to cover the whole human transcriptome in two biological replicates (Figure 2.3.15 A). Analysis revealed strongly up- and downregulated genes with CAMTA1 being the most strongly upregulated candidate. To validate the data, NPPA and NPR-A were analyzed, however, neither NPPA nor NPR-A were elevated in the microarray (Figure 2.3.15 B), although an increase of NPPA and NPR-A mRNA was confirmed by quantitative real-time PCR in the same biological replicates (data not shown). We therefore included possible CAMTA1 transcriptional targets from Henrich et al., 2011 into our analysis, and consistently, putative targets from Henrich et al., 2011 were also elevated or reduced in our microarray (Figure 2.3.15 B). Of note, whether the up- and down-regulated genes are direct transcriptional targets or indirectly regulated is not known. Interestingly, the top-downregulated gene castor zinc finger 1 (CASZ1) has been shown to function as tumor suppressor in neuroblastoma and will be an interesting candidate for further analysis (Liu et al., 2011, Virden et al., 2012).

## 4. Discussion of Part II

MiRNAs have been implicated in all types of cancer analyzed so far by regulating important tumor suppressors and oncogenes. In addition, they play pivotal roles in stem cell biology, differentiation and neurogenesis. Although this immediately suggests that miRNAs also regulate stemness and differentiation in cancer stem cells (CSCs), comprehensive analyses of miRNAs in CSCs have not been done so far. However, this is of central interest, as CSCs can drive tumor growth, therapy resistance and tumor relapse after therapy. To get a deeper insight into these processes, we have chosen to study GBM, a highly malignant brain tumor that lacks effective therapy strategies and which is thought to be driven by a GBM cancer stem cell (GSC) subpopulation.

### **miR-9/9\* are differentially expressed in GSCs and may function as oncomiRs**

To obtain GSC and non-GSC subpopulations for miRNA deep sequencing, we used the primary GBM patient-derived cell line R11. Previous studies have shown that CD133-positive (CD133<sup>+</sup>) cells of R11 indeed correspond largely to the *bona fide* GSC subpopulation, allowing efficient enrichment of GSC and non-GSC subpopulations. Of note, the identification of a small CD133<sup>-</sup> GSC subpopulation has been reported, however, we did not try to further separate these cells from the non-GSC subpopulation used for our analysis (Beier et al., 2007). R11 forms well-defined neurospheres and previously determined transcriptome data showed that R11 is genetically and transcriptionally stable, allowing in depth downstream analyses (Beier et al., 2007, Beier et al., 2008).

We found that miR-9 and its corresponding miR-9\* are strongly expressed in GSCs compared to the non-GSC subpopulation, as shown by miRNA deep sequencing and Northern Blot analysis. miR-9/9\* is almost exclusively expressed in brain and both strands have been shown to be functional (Landgraf et al., 2007). Interestingly, miR-9/9\* has been found to be highly expressed in diverse primary brain tumors including astrocytomas, oligodendrogliomas and GBM (Nass et al., 2009, Huse et al., 2009, Malzkorn et al., 2010, Kim et al., 2011a). This indicates that miR-9/9\* might be important for a broad spectrum of brain tumors. Furthermore, it has been shown that miR-9/9\* play important roles during neurogenesis, neural stem cell (NSC) fate determination and for proliferation and migration of neural progenitor cells (Sempere et al., 2004, Yoo et al., 2009, Zhao et al., 2009, Delaloy et al., 2010). In addition to GBM, miR-9/9\* expression is increased in other cancer types including lymphomas, breast cancers, cervical cancers, colon cancers and stomach cancers (Coolen et al., 2013). Besides miR-9/9\*, we identified additional cancer-associated miRNAs to be differentially expressed in GSCs, including miR-17, miR-21, miR-221 and miR-222. These miRNAs have previously been shown to be frequently highly expressed in various types of cancer (Esquela-Kerscher and Slack, 2006, Croce, 2009, Jansson and Lund, 2012). The identification of miRNAs that are increased in cancer is consistent with the pre-selection of miRNAs with the highest number of reads in our deep sequencing data. In addition, the identification of important cancer-related miRNAs within the top-regulated candidates indicates that our miRNA expression profiling provides a solid basis for further analysis. Our data

were further confirmed by validation of the top upregulated miRNAs by Northern Blot and analysis of miR-9/9\* expression in a broad spectrum of GBM-derived cell lines. Due to the previous implication of miR-9/9\* into GBM and neurogenesis, we have chosen miR-9/9\* for further analysis.

The mechanisms that regulate differential expression of miRNAs in cancer are not known in most cases. This is also true for miR-9/9\*, which can be expressed from three genomic loci (hsa-mir-9-1, hsa-mir-9-2, hsa-mir-9-3). Which locus or loci are active in GBM and which mechanisms regulate expression of miR-9/9\* is not known. Of note, an initial analysis of genomic GBM data from the TCGA consortium did not reveal significant genomic amplification of the three miR-9/9\* loci (data not shown). Regarding the regulatory mechanisms that mediate differential miRNA expression in GSCs versus non-GSCs, transcriptional programs might be probable candidates, as genetic differences between GSCs and their differentiated progeny are not expected. One study showed that miR-9 expression is stimulated by MYCN in breast cancer (Ma et al., 2010). It is therefore tempting to speculate, if MYCN might contribute to miR-9/9\* expression in GBM/GSCs as well. In addition to MYCN, hypoxia has been shown to induce expression of miR-9/9\* from mir-9-1 and mir-9-3 but not mir-9-2 by the hypoxia-associated transcription factor HIF-1 $\alpha$  (Shan et al., 2014). Interestingly, hypoxia plays important roles in GBM and influences GSC activity within its niche (Seidel et al., 2010, Heddleston et al., 2012). Furthermore, Lin28a regulates neuronal differentiation and controls miR-9/9\* processing by inducing the degradation of its precursor through poly-U tailing, mediated by a so far unknown TUTase (Nowak et al., 2014).

Functional analysis of miR-9/9\* revealed that miR-9/9\* function as oncogenes in GBM. Taking advantage of the neurosphere-formation assay, we observed severely affected growth of several GBM-derived cell lines *in vitro* when miR-9/9\* were inhibited. On the other side, neurosphere-formation increased upon transfection of miR-9/9\* mimics. The observed effects might at least in part be explained by GSC-specific functions of miR-9/9\*, as a loss of miR-9/9\* resulted in reduced CD133<sup>+</sup> cells and increased differentiation. This is in line with the previously reported roles of miR-9/9\* to exhibit oncogenic function in GBM and other types of cancer and to function as regulator of differentiation (Coolen et al., 2013). Differentiation upon miR-9/9\* inhibition was driven towards the neuronal lineage, however, we did not investigate whether cells also differentiated along the oligodendrocytic lineage. Seemingly inconsistent with our observations, miR-9/9\* has been previously implicated as positive regulator of neural differentiation during neurogenesis and miR-9-2/miR-9-3 double knockouts, which express about 20 to 30 % of the wildtype miR-9/9\* levels, show severe neurodevelopmental defects and die within one week after birth (Shibata et al., 2011). Despite these findings, other studies suggested that miR-9/9\* does not directly support differentiation but functions to keep cells in a state that is prone to differentiation, but can also be pushed in the other direction by inhibiting differentiation (Coolen et al., 2013). This reversal might be regulated by other factors not identified so far. Therefore, whether miR-9/9\* supports or inhibits differentiation seems to be highly context-specific.

Apart from their role in cell differentiation, not much is known on miR-9/9\* function. Interestingly, a study found miR-9 and miR-17 to play important roles in secondary GBM progression (Malzkorn et al., 2010). This study analyzed miRNAs in secondary GBM compared to their lower-grade precursor neoplasms. A small set of miRNAs including miR-9 and miR-17 has been found to be repeatedly increased in GBM relative to the precursor neoplasm, indicating that these miRNAs are deregulated either during progression to GBM or late within GBM.

Another study has analyzed miRNA expression profiles from 261 TCGA GBM patient samples (Kim et al., 2011a). Tumors were clustered according to their miRNA expression profiles and classified using cell lineage marker genes. This revealed neural, oligoneuronal, multipotent, as-

trocytic and neuromesenchymal classes (Kim et al., 2011a). Interestingly, miR-9/9\*, miR-17 and miR-106b were all found in the oligoneuronal subclass, suggesting that these miRNAs are especially important for this subclass of GBM. This is an expected finding because of the pronounced tumor heterogeneity in GBM, represented by different genetic aberrations and gene expression profiles. Furthermore, tumor heterogeneity on the level of miRNA expression would explain why miRNA profiles from GBM often differ between studies (see part II section 1.2.2 and 1.3.1). The oligoneuronal miRNA cluster overlaps well with the proneural mRNA class, which shows slightly increased survival but resistance to chemotherapy with temozolomide (Phillips et al., 2006, Verhaak et al., 2010, Brennan et al., 2013). This is in line with miR-9 and miR-17 being highly expressed in secondary GBM, which largely cluster into the proneural group (Verhaak et al., 2010). However, whether miR-9/9\*, miR-17 and miR-106b expression correlates with patient survival and therapy resistance in these subgroups is not known. In addition, we do not know whether the described subclasses contain different proportions of GSCs. Taken together, these observations suggest that, in addition to the heterogeneous miRNA expression profiles between tumors, also GSCs of different tumors might express different miRNAs. It is also conceivable that different GSC subpopulations within the same tumor express different sets of miRNAs. This has important implications for possible miRNA-based therapy strategies, as not all tumors would respond to the same miRNA-targeting therapy.

### **Identification of miR-9/9\* targets and characterization of the novel tumor suppressor CAMTA1**

To better understand miR-9/9\* function in GBM and GSCs, we identified miR-9\* target mRNAs in R11. The list of putative targets contained several factors that might be interesting candidates for further analysis. For example, FoxQ1 is a member of the forkhead transcription factor family that is involved in differentiation in various cell types (Feuerborn et al., 2011). Another member, FoxG1, has previously been shown to function as a miR-9 target in mice and to contribute to the pro-differentiating effects of miR-9/9\* during neurogenesis (Shibata et al., 2011). The putative miR-9/9\* target mRNA NEFM encodes for the neurofilament protein medium polypeptide NF-M, which is exclusively expressed in finally differentiated neurons (Antic et al., 1999). Identification of this neuronal differentiation marker supports our observation that miR-9/9\* expression functions as a negative regulator of differentiation in GBM. Among the targets, CAMTA1 caught our special interest and was selected for further characterization. CAMTA1 has been reported to function as a putative tumor suppressor in neuroblastoma and to be located within 1p36, a region frequently deleted in various brain tumor types (Barbashina et al., 2005, Ichimura et al., 2007, Weller et al., 2009, Henrich et al., 2011). Although 1p36 seems to be less frequently deleted in GBM compared to other gliomas and neuroblastoma, the suppression of CAMTA1 expression by miR-9/9\* would be a possible mechanism to silence this putative tumor suppressor in GBM. Interestingly, we did not only identify and validate binding sites for miR-9\*, but also miR-9 and miR-17, both of which were upregulated in GSCs. Therefore, these miRNAs might function cooperatively to efficiently silence CAMTA1.

CAMTA proteins share a series of domains and motifs, including a CG-1 DNA binding motif, a TIG domain implicated in non-specific DNA-binding and dimerization, ankyrin repeats that can mediate oligomerization and calmodulin-binding IQ motifs. Mammals contain two CAMTA genes that encode the highly homologous CAMTA1 and CAMTA2 proteins. CAMTA1 and CAMTA2 expression partially overlaps in mice: CAMTA2 is mostly expressed in heart and brain and to lower

levels in liver, kidney and testis. CAMTA1 is expressed at high levels in brain and low levels in heart and was not detected in any other tissue (Song et al., 2006). We found that CAMTA1 tumor suppressor activity strictly depends on the CG-1 DNA binding domain. This is in line with published results showing that CAMTA1 protein indeed functions as transcription factor in mammalian cells and binds DNA via its CG-1 domain (Henrich et al., 2011, Long et al., 2014). Functional characterization of the other CAMTA1 domains is lacking. Studies of mouse CAMTA2 showed that CAMTA2 is kept in an inactive state by binding of class II histone deacetylases to CAMTA2 ankyrin repeats (Song et al., 2006). In addition, CG-1 is not only able to directly bind DNA but can also associate with the transcriptional coactivator Nkx2-5, supported by the TIG domain. Reported evidence that mammalian CAMTA1 and CAMTA2 function are regulated by calcium signalling through calmodulin binding is lacking, however, calmodulin binding has been shown for plant and fly CAMTA proteins (Bouché et al., 2002, Han et al., 2006a).

Due to their high sequence homology, especially within the DNA-binding domain, we looked for published CAMTA2 regulated genes which could be targets for CAMTA1 as well. CAMTA2 can activate the expression of the natriuretic peptide hormone precursor NPPA in the heart during hypertrophic signaling (Song et al., 2006). Interestingly, the processed product of NPPA has antiproliferative functions in various types of cancer including GBM (Vesely et al., 2005, Vesely et al., 2007). Strikingly, we have shown that CAMTA1 activates NPPA expression in GBM cells as well. Moreover, CAMTA1 also stimulates the expression of the NPPA receptor NPR-A. Whether both NPPA and NPR-A expression indeed mediate CAMTA1 tumor suppressor effects and if their coactivation enables autocrine signalling remains to be analyzed. Interestingly, the NPPA gene is located in the 1p36 locus, and it is indeed deleted in a number of gliomas (Ichimura et al., 2007).

To get deeper insights into CAMTA1 regulated genes in GBM, we investigated transcriptome changes after CAMTA1 overexpression. Although the microarray did not show changes in NPPA and NPR-A expression, we found further putative CAMTA1-regulated genes. Among those, we have identified numerous genes that have previously been shown to be up- or downregulated by CAMTA1 in neuroblastoma (Henrich et al., 2011). This overlap indicates that our dataset provides a solid basis for further analysis. Of note, CAMTA1 overexpression increases endogenous levels of neuronal markers like TUBB3, MAP2 and NEFL in neuroblastoma cell lines, which could at least in part explain the observed effects of miR-9/9\* inhibition on differentiation (Henrich et al., 2011). Among the putative CAMTA1 targets, CASZ1 was the top-downregulated gene. CASZ1 is an highly interesting candidate for further analysis, as it has been shown to function as tumor suppressor in neuroblastoma and is also located in 1p36 (Liu and Tang, 2011, Virden et al., 2012).

### **Model and outlook**

The identified pathway consisting of miR-9/9\*, CAMTA1 and the NPPA/NPR-A prompted us to propose the following model (Figure 2.4.1). In GSCs, miR-9/9\* and miR-17 expression is high compared to non-GSCs, which results in low CAMTA1 expression in GSCs. Of note, it is likely that miR-9/9\* regulate other target mRNAs as well which might also contribute to the observed phenotypes. This is also true for the identified putative CAMTA1 targets. CAMTA1 functions as a transcription factor to induce the expression of NPPA and its receptor. Coexpression of both NPPA and NPR-A potentially allows autocrine signaling with antiproliferative function. By increasing miR-9/9\* levels, GSCs repress CAMTA1 and the anti-proliferative NPPA. In addition miR-9/9\* negatively regulates neuronal differentiation.

One major future perspective is a deeper understanding of miRNA targets in GSCs, including

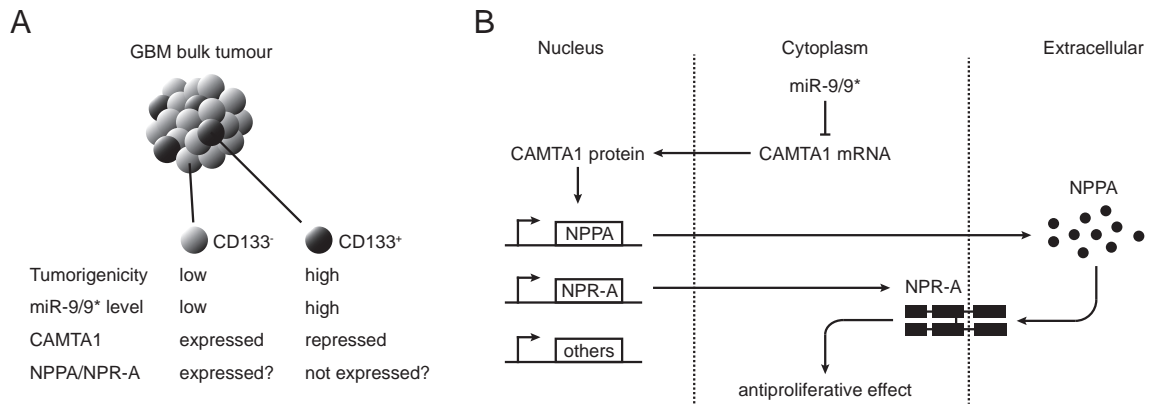


**Figure 2.4.1. A model for miR-9/9\*, CAMTA1 and NPPA/NPR-A function in GBM. A,** Schematic representation of miR-9/9\*, CAMTA1, and NPPA/NPR-A expression in GSC and non-GSCs. **B,** Model of miR-9/9\*, CAMTA1 and NPPA/NPR-A function in GBM. In GSCs, miR-9/9\* are elevated and repress CAMTA1 expression by miRNA-mediated gene silencing. This prevents transcriptional activation of NPPA and NPR-A, which have anti-proliferative function. Whether miR-9/9\* and CAMTA1 have other target genes is not known, but might also contribute to the observed oncogenic effects of miR-9/9\* and tumor suppressor effects of CAMTA1.

the tumor suppressor CAMTA1. One might speculate whether CAMTA1 might function as potential therapy target, however, as a deeper understanding of CAMTA1 function is still lacking, this remains to be analyzed. It should be investigated how CAMTA1 regulates its target genes and whether CAMTA1 is depleted in a broad spectrum of tumors. The generated CAMTA1 knockout mouse model could provide important insights into these processes. For example, it could be investigated whether loss of CAMTA1 in  $p53^{+/-}$  mice,  $PTEN^{+/-}$  mice and other GBM prone mouse models further increases tumor-formation.

There is extensive scientific effort to develop targeted and patient-specific therapy approaches as an alternative to conventional radio- and chemotherapy. GSCs have been suggested as important driver of GBM growth and novel therapeutic approaches try to target the GSC pool (Stupp and Hegi, 2007). It would therefore be tempting to see whether GSC-specific miRNAs can be inhibited *in vivo* to reduce GBM growth, as observed in our *in vitro* studies. This could be tested by xenograft mouse models that are treated orthotopically with miRNA inhibitors. Our study provided further evidence that the application of miRNA inhibitor combinations might be effective to reduce tumor growth. These inhibitor cocktails could be designed patient-specifically to target multiple GSC-specific miRNAs.

## **Part III.**

# **Nuclear Import of Argonaute and TNRC6 proteins**

# 1. Introduction

Argonaute and TNRC6 proteins are the key players in post-transcriptional gene silencing (PTGS) pathways. Argonaute proteins bind small non-coding RNAs (ncRNAs) and are then guided to a target messenger RNA (mRNA). Argonaute proteins further associate with TNRC6 proteins, which recruit deadenylase and decapping complexes. Although these cytoplasmic processes are reasonably well understood, Argonaute and TNRC6 proteins have also been identified in the nucleus of mammalian cells. However, which transport routes are used to reach the nucleus are not characterized so far.

This introduction will give an overview on nuclear functions small RNA-guided gene silencing components. Then, nuclear transport pathways will be presented and the current knowledge on nuclear transport of small RNA-mediated gene silencing components.

## 1.1. Small RNA-mediated gene regulation in the nucleus

Nuclear functions of small RNA-guided gene regulatory proteins have been investigated in diverse organisms. So far, these nuclear functions have only been well characterized in lower organisms including worms, plants and yeast. I will restrict this section to the nuclear functions in somatic cells.

### 1.1.1. Small RNA-guided transcriptional gene regulation

Transcriptional gene regulation by small RNAs has been identified in diverse organisms and has so far been characterized in *S. pombe*, plants and worms (Castel and Martienssen, 2013). Central principles of small RNA-guided transcriptional regulation are common between organisms: An Argonaute protein binds via an associated sRNA sequence-specifically to a nascent transcript. This tethers the Argonaute protein to specific genomic loci. Argonaute then recruits histone or DNA methylases that place repressive chromatin marks. This finally leads to transcriptional gene silencing of the respective loci (TGS). Of importance, apart from this basic principle, different kinds of sRNAs, Argonautes and accessory proteins like RNA-dependent RNA polymerases (RdRP) participate in TGS in different organisms.

#### Small RNA-guided TGS in *S. pombe*

*S. pombe* contains only one Ago protein, referred to as Ago1, which mediates TGS. Furthermore, *S. pombe* contains a single Dicer protein (Dcr1) and one RdRP (Rdp1). Ago1, the chromodomain protein Chp1 and Tas3, which bridges Ago1 and Chp1, form the so-called RNA-induced transcriptional silencing complex (RITS) (Figure 3.1.1, Verdell et al., 2004). RITS is responsible for TGS and induces heterochromatin-formation around centromeres by methylation of histones (Castel and Martienssen, 2013). First, a non-coding centromeric transcript (cenRNA) is produced from centromeric repeat regions. RITS recognizes and binds the nascent cenRNA by base pairing

(Motamedi et al., 2004). RITS is additionally tethered to chromatin via Chp1, which binds H3K9 methylated histones. The sRNAs that mediate base pairing with the cenRNA are derived from the cenRNA itself: The RNA-directed RNA polymerase complex (RDRC) containing the RdRP Rdp1, is recruited by RITS, leading to the synthesis of a long dsRNA from the single-stranded cenRNA (Colmenares et al., 2007). This dsRNA is then processed by Dcr1 into siRNAs, which are loaded in a signal amplification loop onto Ago1 (Bühler et al., 2007). RITS also recruits the Clr4 H3K9 methyltransferase complex (CLRC) to the centromeric chromatin, which leads to H3K9 methylation and heterochromatin-formation (Bayne et al., 2010).

Interestingly, recent work has shown that RITS not only associates with centromeric heterochromatin, but also many other loci including retrotransposons and non-coding RNA genes, which are also under transcriptional control of RITS under specific cellular conditions (Woolcock et al., 2011). The origin of the priming siRNAs for RITS-cenRNA association is so far unknown.

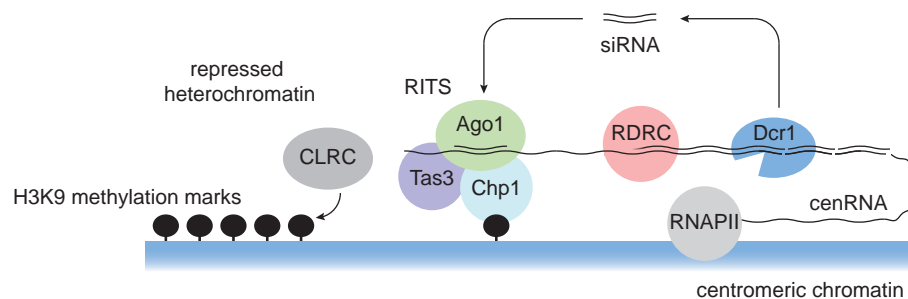


**Figure 3.1.1. TGS of centromeric chromatin in *S. pombe*.** RNA-induced transcriptional silencing (RITS) complex, consisting of Ago1, Tas3 and Chp1, binds to nascent transcripts from centromeric chromatin (cenRNA). RITS leads to transcriptional silencing by placing chromatin marks and recruiting the RNA-dependent RNA polymerase complex (RDRC). RDRC produces dsRNA, which serves as substrate for siRNA processing by Dcr1. The Clr4 methyltransferase complex (CLRC) is recruited by RITS and methylates H3K9. Figure taken from Schraivogel and Meister, 2014.

### RNA-directed DNA methylation in plants

In *A. thaliana*, four Dicer-like proteins (DCL1-4) and ten different Argonaute proteins (AGO1-10) exist. These proteins are involved in various different sRNA-mediated pathways including siRNA-guided PTGS and TGS by RNA-directed DNA methylation (RdDM) (Bologna and Voinnet, 2014). RdDM transcriptionally represses a subset of transposons and genes by placing repressive DNA methylation marks and is implicated in various processes including pathogen defense and stress response (Matzke and Moshier, 2014). Plant RdDM is a highly complex nuclear pathway that involves DCL3 and AGO4 and eventually AGO6 and AGO9 (Zheng et al., 2007, Havecker et al., 2010). Furthermore, RdDM requires a specialized transcription machinery and numerous accessory proteins. As RdDM is not fully understood, it will be depicted here in a very simplified way (Matzke and Moshier, 2014).

First, the plant-specific RNA polymerase IV produces a long dsRNA, which is processed by the nuclear protein DCL3 into siRNAs (Daxinger et al., 2009). These siRNAs are also referred to as heterochromatic (hc-) siRNAs. By a yet unknown mechanism, hc-siRNAs are exported to the cytoplasm, one strand is loaded onto AGO4, which is then re-imported into the nucleus. In the nucleus, the AGO4-hc-siRNA complex targets a nascent transcript produced by another plant-specific RNA polymerase V (Wierzbicki et al., 2008). This targeting then triggers the recruitment

of DNA methyltransferases to mediate *de novo* DNA methylation. These repressive chromatin marks result in transcriptional silencing of Pol V transcribed loci, which are mostly transposons and other repetitive DNA elements (Wierzbicki et al., 2012).

### **TGS in *C. elegans***

When worms are fed with dsRNAs that are complementary to an endogenous gene, not only does RNAi silence mRNAs post-transcriptionally in the cytoplasm, but also nuclear RNAi mediates TGS of the respective target locus. This nuclear RNAi pathway in somatic cells of *C. elegans* promotes TGS by histone methylation and inhibition of RNA polymerase II (Guang et al., 2008, Guang et al., 2010). The key players of TGS in somatic cells of *C. elegans* is the Ago protein NRDE-3, the RdRP RRF-1 and the Dicer protein DCR-1.

Small RNA-guided TGS in *C. elegans* is induced by cytoplasmic PTGS. During PTGS, diverse Ago proteins silence transcripts in the cytoplasm but can also recruit RdRPs like RRF-1 to target mRNAs. RRF-1 produces long dsRNAs which are processed by DCR-1 into so called secondary siRNAs (Gent et al., 2010). These secondary siRNAs are subsequently loaded onto the Ago protein NRDE-3. NRDE-3 is imported into the nucleus where it binds to nascent transcripts of complementary gene loci (Guang et al., 2008). This association leads to TGS by inhibition of RNA polymerase II and formation of heterochromatin by histone methylation (Guang et al., 2010). Of note, in contrast to *S. pombe* and *Arabidopsis*, the nuclear processes of this pathway in *C. elegans* are far less understood.

### **What about TGS by small RNAs in mammals?**

Argonaute proteins and associated small RNAs have been suggested to mediate TGS in mammals (Morris et al., 2004, Janowski et al., 2006, Kim et al., 2006, Morris et al., 2008, Chu et al., 2010, Ahlenstiel et al., 2012, Huang et al., 2013). So far, not much is known on this process in mammalian cells and there is no consensus regarding the underlying mechanisms. Therefore, TGS by small RNAs in mammals is still controversially discussed.

To mediate TGS, mammalian Argonaute proteins are thought to associate with chromatin (Morris et al., 2004, Janowski et al., 2006, Schwartz et al., 2008, Matsui et al., 2013). Indeed, chromatin immunoprecipitation (ChIP) suggested association of Ago1 and Ago2 with chromatin and Ago2 has been identified at sequences including gene promoter regions (Huang and Li, 2014). How Argonaute proteins bind chromatin is not fully understood. So called promoter-associated transcripts have been suggested to function as putative nuclear target RNAs in this process. Promoter-associated transcripts can be in sense or antisense orientation relative to gene promoters and are thought to be tethered to promoters in *cis* by yet unknown mechanisms (Janowski et al., 2006). Ago proteins are then expected to associate with these transcripts by not yet characterized sRNA populations (Schwartz et al., 2008). These sRNA populations might derive from the cellular miRNA pool, as for example miR-589 has been suggested to function in transcriptional regulation (Matsui et al., 2013). How the downstream processes regulate transcription differs between reports: On the one hand, it has been suggested that Ago-binding leads to degradation of the promoter-associated transcript (Schwartz et al., 2008, Matsui et al., 2013). Degradation of the promoter-associated RNA can mediate TGS (Janowski and Corey, 2010). Of note, in addition to TGS, degradation of the promoter-associated RNA can also mediate transcriptional activation (Chu et al., 2010). Alternatively, Ago binding might lead to recruitment of DNA methylases that

methylate CpG islands in gene promoters, which represses transcription initiation (Morris et al., 2004).

## 1.2. Diverse nuclear small RNA-guided functions in mammals

Besides transcriptional gene regulation, a diverse spectrum of other small RNA-guided functions has been suggested to be active in human nuclei. These include silencing of nuclear localized RNAs, DNA damage repair-associated mechanisms and regulation of alternative splicing.

### Silencing of nuclear RNAs

It has been suggested early, that human Ago2 can be active in the nucleus of human somatic cells. Indeed, it was shown that nuclear localized RNAs like the nuclear RNA 7sk can be efficiently knocked down by transfection of siRNAs (Robb et al., 2005). Subsequently, several reports showed active nuclear RNAi by targeting other presumably nuclear long non-coding RNAs like MALAT-1 and NEAT-1 (Nishi et al., 2013, Gagnon et al., 2014). Although this provides strong evidence for active Ago proteins in the nucleus, whether miRNA-mediated PTGS is also active in human nuclei remains to be demonstrated.

Presuming that miRNA-mediated PTGS is active in the nucleus, nuclear enriched miRNAs should exist that associate with Ago and TNRC6 proteins. Several studies analyzed miRNA profiles from nuclear and cytoplasmic extracts and indeed found nuclear enriched miRNAs (Jeffries et al., 2011, Gagnon et al., 2014). However, whether the identified profiles indeed overlap between studies and whether nucleo-cytoplasmic extractions can efficiently separate nuclear and cytoplasmic RNAs has not been demonstrated. It is also unknown whether these presumably nuclear enriched miRNAs indeed associate with Ago and TNRC6 proteins in the nucleus. In addition, studies were so far not able to link the nuclear enriched miRNAs to specific nuclear RNA targets. One interesting scenario would be that miRNAs could target the 3'-UTRs of precursor-mRNAs already in the nucleus, however this has to be investigated in future studies.

### Small RNA-guided DNA double-strand break repair

It has been suggested that human Dicer, Drosha, Ago proteins and a new class of small RNAs might be involved in DNA double-strand break (DSB) repair. In cells with artificially generated DSBs, so-called DSB-induced small RNAs, also referred to as diRNAs, have been identified (Wei et al., 2012). diRNAs are produced in a Dicer-dependent manner and align to sequences around DSB sites. Interestingly, DSB repair efficiency decreased upon knockdown of Ago2 and Dicer, suggesting that diRNAs could associate with Ago2 which somehow supports DSB repair. Which dsRNAs might function as precursor for diRNA production however remains to be elucidated. Furthermore, it is not clear how Ago2 and diRNAs should support DSB repair. A recent study suggested that diRNAs recruit Ago2 to DSB sites and Ago2 further recruits Rad51, a protein that functions in DSB repair by homologous recombination (Gao et al., 2014). Another study showed similar results by identification of a small RNA population similar to diRNAs (Francia et al., 2012). In this study, DSB repair was Drosha- and Dicer-dependent but independent of TNRC6A-C, whereas Ago dependency has not been investigated.

Although this might provide an highly interesting mechanism, these findings were recently challenged by a study showing that Dicer knockdown in human cells increases the resistance towards

DNA-damaging agents (Liu et al., 2015). However, as Dicer seems to be essential for diRNA production, this is not in line with the suggested small RNA-guided DSB repair mechanism.

### Regulation of alternative splicing

The spectrum of nuclear Ago functions has additionally been broadened by several studies investigating a possible role of Ago1 and Ago2 in alternative splicing (Alló et al., 2009, Liu et al., 2012, Ameyar-Zazoua et al., 2012). These studies reported that transfected siRNAs targeting exonic or intronic sequences proximal to splice junctions can regulate alternative splicing. Both Ago1 and Ago2 might be involved in this process. In the current model, Ago1 or Ago2 are targeted to specific gene loci by a so far not yet identified naturally occurring small RNA population. How Ago-chromatin interaction might work in this case is also unknown, but might involve an intragenic antisense transcript that base-pairs with the nascent transcript. Ago1 and Ago2 then function by placing repressive histone methylation marks, which slow down RNA polymerase II during transcriptional elongation. In addition, Ago1 and Ago2 might recruit spliceosome complex components. Both slowdown of RNA polymerase II and recruitment of the spliceosome then can allow for different splicing patterns.

The implicated slowdown of RNA polymerase II is a well known mechanism that regulates alternative splicing *in vivo* (de la Mata et al., 2003). However, the upstream effects and possible interactions with the spliceosome are not characterized sufficiently. Therefore, whether this mechanism indeed functions *in vivo* is not known.

## 1.3. Nuclear transport processes

The nuclear envelope (NE) separates nucleoplasm and cytoplasm and is composed of an outer and an inner nuclear membrane. To allow transport of proteins and RNA between nucleus and cytoplasm, nuclear pore complexes (NPC) form partially selective channels that pass through both nuclear membranes (Wente and Rout, 2010). Small molecules like metabolites and small proteins can freely diffuse through the NPC. In contrast, proteins and ribonucleoprotein particles (RNPs) that exceed the exclusion size between 20 to 40 kDa must be actively transported (Görlich and Kutay, 1999). Nuclear import and export of the vast majority of large cargo proteins is facilitated by so-called karyopherins or nuclear transport receptors (Görlich and Kutay, 1999). Karyopherins are subdivided into importins and exportins, depending on the transport direction. In humans, eleven importins and five exportins have been identified, which recognize unique sets of proteins or RNA, thus creating multiple transport pathways across the nuclear pore (Chook and Blobel, 2001). To increase the cargo spectrum of the different karyopherins, they recognize so-called nuclear localization (NLS) or nuclear export (NES) signals that function as universal adaptor sequences (Görlich and Kutay, 1999).

Nuclear transport directionality and energy demand is driven by a GTP gradient across the nuclear membrane. The proportion of cellular GTP/GDP that drives nucleo-cytoplasmic transport is associated with the small Ras-related GTPase Ran (Moore and Blobel, 1993). Ran cycles between a GTP-bound and GDP-bound state and only in its GTP-bound state, Ran is active and binds karyopherins. Ran's intrinsic GTPase activity is low and depends on the GTPase activating protein RanGAP (Bischoff et al., 1994). RanGAP is cytoplasmic and coupled to the NPC, thus activating GTP hydrolysis when RanGTP enters the cytoplasm. In the nucleus, the Ran guanine nucleotide exchange factor RCC1 catalyzes the exchange of GDP to GTP (Bischoff and Ponstingl,

1991). RCC1 is anchored to chromatin and generates high nuclear levels of RanGTP. Therefore, the asymmetric distribution of RanGAP and RCC1 build up a RanGTP/GDP gradient across the nuclear envelope. The direction of nuclear transport is determined by RanGTP binding to the karyopherin: Whereas importins have low affinity to their cargo when bound to RanGTP, exportins have high affinity to the cargo in their RanGTP-bound state (Görlich and Kutay, 1999). Consequently, importins recruit cargo in the cytoplasm and release cargo in the nucleus, whereas exportins work the other way around.

How do importins and exportins mediate nuclear import and export? Nuclear import is mediated by binding of an importin to the NLS sequence of a cargo protein at low RanGTP concentration in the cytoplasm (Figure 3.1.2 A) (Stewart, 2007). The dimeric complex then translocates through the NPC. In the nucleus, RanGTP binding to the importin results in dissociation of the importin-cargo complex. This is mediated by conformational changes within the importin upon RanGTP binding, that lowers the affinity to the cargo protein. The resulting importin-RanGTP complex is then recycled back to the cytoplasm. In the cytoplasm, GTP is hydrolyzed, resulting in release and recycling the importin. Exportins on the other side, have high affinity to the cargo NES when bound to RanGTP in the nucleus (Figure 3.1.2 B) (Stewart, 2007). The ternary complex composed of cargo-exportin-RanGTP is transported through the NPC and disassembled in the cytoplasm by GTP hydrolysis of Ran-bound GTP. The exportin is then recycled back into the nucleus.

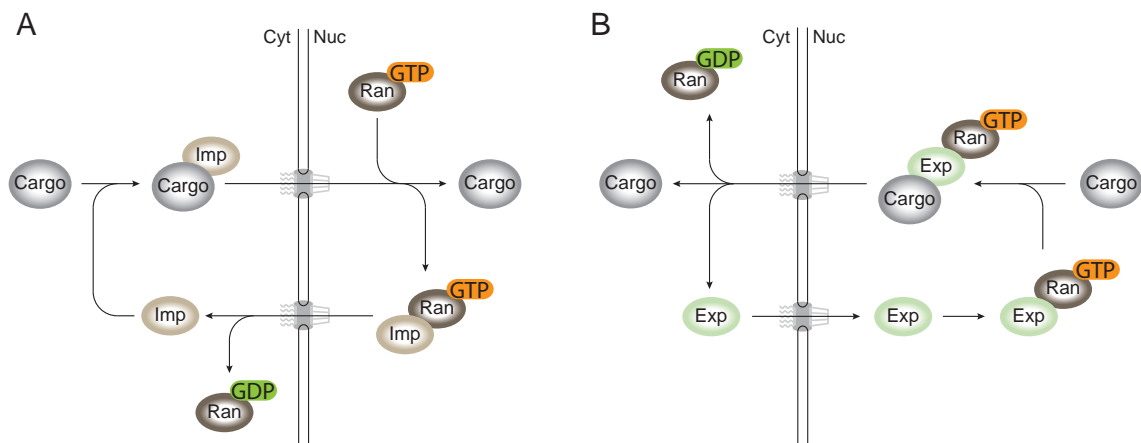


**Figure 3.1.2. Principles of nuclear import and export pathways. A,** Nuclear import of a cargo protein is mediated by importins (Imp). In the nucleus, the trimeric transport complex is disassembled by binding of RanGTP. **B,** Nuclear export of proteins is mediated by exportins (Exp). RanGTP in the nucleus mediates binding to the cargo, whereas the export complex is disassembled in the cytoplasm by GTP hydrolysis.

It should be noted, that the RanGTP/GDP gradient does not directly supply energy into the translocation process through the NPC. Instead, the RanGTP/GDP gradient determines directionality by the described mechanisms, as the direction of cargo flux through the NPC can for example be reversed by RanGTP/GDP gradient reversion (Nachury and Weis, 1999). Additional directionality seems to occur during the actual NPC passage by a yet unknown mechanism (Pyhtila and Rexach, 2003). Whether nuclear transport processes need a driving force in addition to Ran-mediated directionality is controversially discussed. It might be possible that concentration gradients of importins and exportins, RanGTP and RanGDP, the cargo itself and other components can additionally drive transport in and out of the nucleus. However, it has also been suggested that the Ran affinity switches alone provide all energy for cargo delivery and release (Wente and Rout, 2010).

The NPC is a macromolecular assembly of approximately 30 different proteins, termed nucle-

oporins (Nup). Nups are arranged in a symmetric ring that forms a central channel (Brohawn et al., 2009). From the ring, filaments extend flexibly into the cytoplasm which carry the Ran-GAP protein. On the nuclear side, nucleoplasmic filaments form a nuclear basket, which supports disassembly of the import complexes (Wente and Rout, 2010). How translocation through the nuclear pore is mediated mechanistically is an unresolved issue (Wente and Rout, 2010, Grossman et al., 2012). The permeability barrier within the NPC is formed by a subset of Nups with phenylalanine/glycine-rich repeats (FG-repeats). FG-repeat domains contain up to 50 repeat units of hydrophobic FG-rich patches, which are separated by hydrophilic spacer sequences. FG-repeat domains within these Nups are considered to be unfolded and to reach into the central channel of the NPC. Translocation is then mediated by interactions between FG-repeats and multiple binding sites on karyopherins (Wente and Rout, 2010).

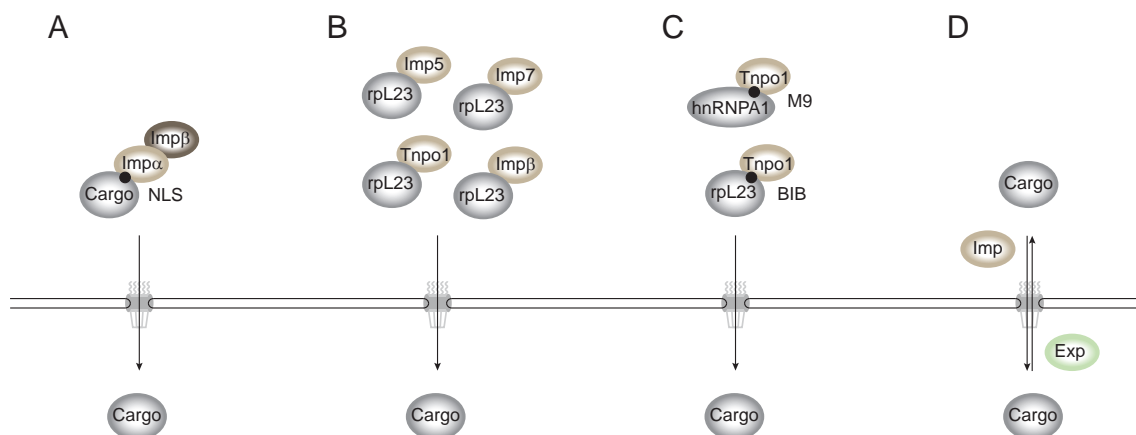


**Figure 3.1.3. Hallmarking properties of nuclear import pathways.** **A**, Many importins function as dimeric complexes, while other can mediate transport as single importin. In both cases, nuclear localization signals (NLS) are recognized on the cargo protein. **B**, many cargo proteins are imported by redundant import pathways, as for example ribosomal protein of the large subunit 23 (rpL23). **C**, Single importins can recognize different NLS sequences, as for example Transportin 1 (Tnp1), which recognizes the M9 sequence in hnRNPA1 and the beta-like import receptor binding (BIB) domain in rpL23. **D** Many proteins shuttle between the cytoplasm by alternating interaction with importins and exportins.

Hallmarking properties of nuclear transport processes are shown in Figure 3.1.3. First, many importins function as heterodimers in which one importin mediates interaction with the cargo protein NLS, whereas another importin mediates translocation through the NPC. This is for example the case during classical nuclear transport pathway described in part III section 1.3.1 (Figure 3.1.3 A). Second, many cargo proteins can interact with a broad spectrum of importins, resulting in multiple redundant import pathways. This has for example been shown for most histones and ribosomal proteins, like rpL23, which can be imported by four different importins (Figure 3.1.3 B, Jäkel and Görlich, 1998). Third, many importins can recognize variable NLS sequences, like for example Tnp1. Tnp1 interacts with the M9 sequence of hnRNPA1 but also with the BIB domain in rpL23 (Figure 3.1.3 C, Pollard et al., 1996, Jäkel and Görlich, 1998). Last but not least, many cargo proteins are alternately imported and exported, a process also referred to as nucleo-cytoplasmic shuttling. Depending on the respective transport rates during nuclear import and export, shuttling proteins are predominantly nuclear or cytoplasmic (Gama-Carvalho and Carmo-Fonseca, 2001). One well-studied example is heterogeneous nuclear ribonucleoprotein A1 (hnRNPA1), an mRNA binding protein and important splicing regulator. hnRNPA1 is mainly nuclear, but constantly shuttles out of the nucleus bound to precursor mRNAs and is imported back after dissociation from the mature mRNA (Piñol-Roma and Dreyfuss, 1992).

### 1.3.1. Classical nuclear import by Importin alpha/beta

The vast majority of eukaryotic proteins are imported into the nucleus by a well characterized nuclear import pathway mediated by Importin-alpha ( $\text{Imp}\alpha$ ) and Importin-beta ( $\text{Imp}\beta$ ) (Görlich et al., 1995, Radu et al., 1995, Moroianu et al., 1996).  $\text{Imp}\alpha$  functions as an adaptor karyopherin by binding to a cargo NLS, whereas  $\text{Imp}\beta$  binds  $\text{Imp}\alpha$  and interacts with the NPC (Figure 3.1.3 A).

The classical NLS that is recognized by  $\text{Imp}\alpha$  is enriched in basic residues, mostly lysine (K) and arginine (R). These basic sequences can be arranged in different ways: Monopartite NLS sequences are single short clusters, like the SV40 large T antigen NLS with the sequence PKKKRKV for example. Bipartite NLS sequences, like KR[PAATKKAGQA]KKKK within nucleoplasmin, are composed of two basic clusters spaced by approximately 10 less conserved amino acids. Interestingly, NLS sequences seem to be largely independent of their localization within the protein and can experimentally be transferred to a heterologous protein or within the same protein without losing function (the same is true for NES sequences, which will be described below).

Unlike other karyopherins,  $\text{Imp}\alpha$  is represented by six family proteins in humans, which are  $\text{Imp}\alpha 1$ ,  $\text{Imp}\alpha 3$ ,  $\text{Imp}\alpha 4$ ,  $\text{Imp}\alpha 5$ ,  $\text{Imp}\alpha 6$  and  $\text{Imp}\alpha 7$  (Malik et al., 1997). Each  $\text{Imp}\alpha$  family member can bind both types of classical NLS sequences, however with partially different affinities. Indeed, cargo proteins have been identified that bind to all  $\text{Imp}\alpha$  subtypes, or bind a specific subset of  $\text{Imp}\alpha$ s or are highly specific for a single  $\text{Imp}\alpha$  (Köhler et al., 1999).

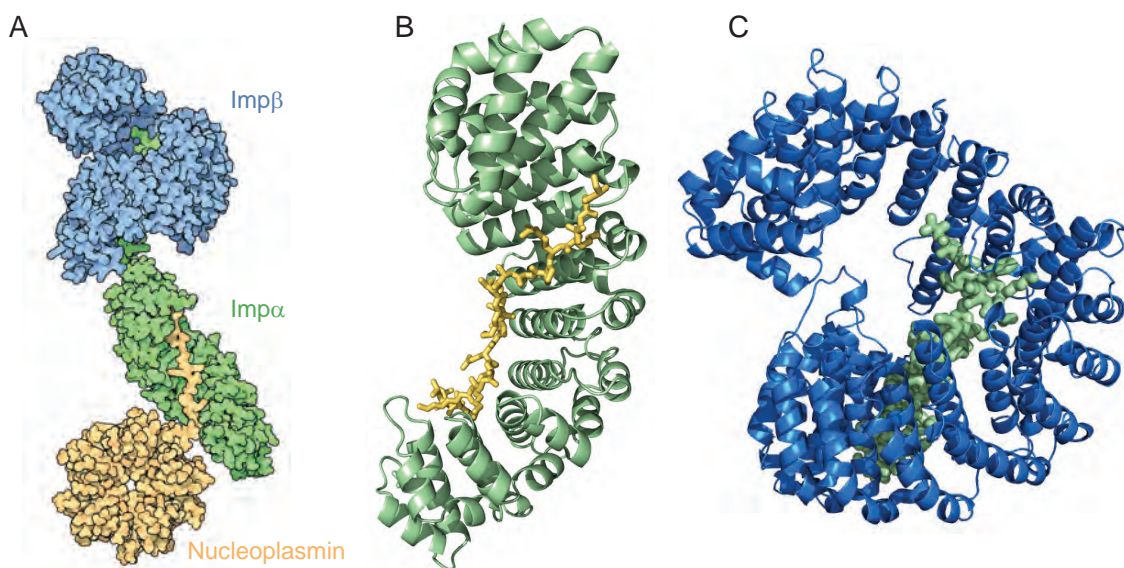


**Figure 3.1.4. Structural properties of  $\text{Imp}\alpha/\text{Imp}\beta$  bound to a classical nuclear localization sequence.** **A**, Complex of  $\text{Imp}\alpha$  (green),  $\text{Imp}\beta$  (blue) and nucleoplasmin with its classical NLS (yellow) is shown. **B**, Structure of  $\text{Imp}\alpha$  bound to the classical NLS of nucleoplasmin (yellow). Individual ARM repeats consist of three alpha-helices organized in a helical structure. **C**, Structural view of  $\text{Imp}\beta$  that wraps around the Importin-beta binding domain (IBB) of  $\text{Imp}\alpha$  (green). HEAT repeats are composed of pairs of antiparallel alpha-helices. Figure A has been taken from PDB structural views of biology section and includes PDB entries 1qgk, 1ee5 and 1k5j. Structures in B and C have been published in Marfori et al., 2012 (PDB entry 3UL1) and Cingolani et al., 1999 (PDB entry 1QGK).

The structure of  $\text{Imp}\alpha/\text{Imp}\beta$  with nucleoplasmin, as exemplary cargo protein for classical import is shown in Figure 3.1.4.  $\text{Imp}\alpha$  is composed of a core domain with 10 Armadillo (ARM) repeats and an N-terminal importin-beta binding domain (IBB) (Fontes et al., 2000, Figure 3.1.4 B). The ARM repeats form two NLS binding sites whereas the IBB domain functions as  $\text{Imp}\beta$  docking site (Conti et al., 1998, Cingolani et al., 1999). Without bound  $\text{Imp}\beta$ , the IBB functions as NLS

for Imp $\alpha$  itself and outcompetes binding of cargo-derived NLS sequences. Therefore, the IBB has an autoinhibitory function that blocks cargo binding without Imp $\beta$  and releases cargo upon Ran-mediated Imp $\beta$  dissociation (Kobe, 1999, Fanara et al., 2000). Imp $\beta$  is composed of 19 HEAT repeats (Figure 3.1.4 C). These HEAT repeats wrap around the Imp $\alpha$  IBB and are therefore responsible for Imp $\alpha$  binding (Cingolani et al., 1999). On the opposite surface, the HEAT repeats provide multiple binding sites for interaction with the FG-repeats of the NPC.

How Imp $\beta$  mediates translocation through the NPC is not yet known in detail. After translocation through the NPC, the trimeric cargo-Imp $\alpha$ -Imp $\beta$  complex remains attached to the NPC. Finally, binding of RanGTP leads to extensive conformational changes in Imp $\beta$  that result in cargo release and dissociation from the NPC (Bayliss et al., 2000). Imp $\beta$  returns to the cytoplasm bound to RanGTP without the need for export factors. Imp $\alpha$  instead is exported by specialized exportin termed Cas (Kutay et al., 1997).

### 1.3.2. Non-classical import pathways

It has been estimated for yeast, that around half of the nuclear proteins contain a classical NLS and are imported via Imp $\alpha$ /Imp $\beta$ . The remaining proteins must therefore be imported by other means via non-classical nuclear import.

The best characterized non-classical pathway is mediated by Imp $\beta$  and Transportin 1 (Tnp1, Imp2, KPNB2). Imp $\beta$  can function independently of Imp $\alpha$  by directly interacting with the cargo protein, as in the case of rPL23 and many other proteins (Chook and Süel, 2011). Furthermore, Imp $\beta$  can also use other adaptor proteins besides Imp $\alpha$ , as for example Imp7 or even non-karyopherin adaptors like Snurportin (Huber et al., 1998). Tnp1 uses NLS sequences of which some share common characteristics that defined a new class of NLS sequences, termed PY-NLS. However, PY-NLS sequences are highly diverse and are not predictable as it is the case for classical NLS sequences (Lee et al., 2006a). Well characterized targets of Tnp1 are c-Jun, hnRNPA1 and several RNA-binding proteins including HuR (Chook and Süel, 2011).

Much less is known of the specific functions of other importins including Imp4, Imp5, Imp7, Imp8, Imp9, Imp11 and Imp12 (reviewed in Görlich and Kutay, 1999, Chook and Süel, 2011). Although some of those importins have numerous known targets, NLS sequences are not uniform and consequently not predictable. Another unconventional nuclear transport pathway is mediated by karyopherins that transport cargo in both directions. These importins/exportins include Imp13 and Exp4. Of note, the cargos that are exported are different from the imported cargos and in addition, are not obviously functionally related (Mingot et al., 2001).

Interestingly, recent studies identified specific double-stranded RNA binding domains (dsRBD) as unconventional NLS sequences. These dsRBDs not only mediate RNA-protein interaction, but can also serve as protein-protein interaction domains for importin binding for example. The RNA-editing enzyme ADAR1 contains three dsRBDs, of which one mediates nuclear import via Tnp1. RNA binding and Tnp1 interaction seems to be mutually exclusive (Barraud et al., 2014). Furthermore, the dsRBD of human Dicer has been suggested to function as NLS. However, how importins are bound is not characterized so far (Doyle et al., 2013). The dsRBD of fission yeast Dicer (Dcr1) seems to be involved in nuclear localization of Dcr1 as well (Barraud et al., 2011).

The vast majority of large molecules are imported in an importin-dependent manner. However, some proteins can mediate their own import by direct interaction with the NPC, a process also referred to as karyopherin-independent transport (Colwell et al., 2010, Sharma et al., 2012). A well

studied example is  $\beta$ -Catenin, which is structurally very similar to Imp $\beta$  and indeed,  $\beta$ -Catenin's ARM repeats mediate its translocation through the NPC in *in vitro* nuclear import assays (Sharma et al., 2012). Other studies even propose that a broad spectrum of related HEAT repeat proteins or even proteins that simply contain extended hydrophobic surfaces or amphiphilic alpha helices might be capable of karyopherin-independent import (Naim et al., 2009, Kumeta et al., 2012, Yoshimura et al., 2014).

### 1.3.3. Nuclear export of proteins

Several exportins have been identified in human cells. These include Crm1 (Exp1), Cas (Exp2), Exp-t (Exp3), Exp5, Exp6 and Exp7. These exportins mediate transport of proteins, tRNAs and pre-miRNAs (Köhler and Hurt, 2007). Nuclear export of mRNAs is mediated by another non-karyopherin system, for which I want to refer to reviews Köhler and Hurt, 2007 and Carmody and Wentz, 2009. The classical protein export mechanism by Crm1 will be described here in short. Other alternative nuclear protein export pathways include piggyback mechanisms with mRNA and the export of large nuclear particles by nuclear envelope budding (Parton et al., 2014, Hatch and Hetzer, 2014).

Like the other exportins and the majority of importins, Crm1 is a HEAT repeat containing protein. Crm1 is a highly versatile nuclear transport receptor that recognizes a broad spectrum of structurally unrelated proteins. The simplest Crm1-dependent NES, also termed classical NES or leucine rich NES, is a short peptide of four spaced hydrophobic residues which are mostly lysines (L) (Fukuda et al., 1997). Prototypical representatives are the PKI NES (LALKLAGLDI) and the MAPKK NES (LQKKLEEELELD). Leucine rich NES sequences bind the outer convex surface of Crm1, whereas RanGTP binds to the inner concave surface (Dong et al., 2009). It has been shown that RanGTP and NES binding are cooperative, i.e. Crm1 only binds to the cargo in its RanGTP-bound state and NES binding further strengthens the RanGTP binding (Monecke et al., 2013). Although the classical leucine-rich NES seems to be present in the vast majority of Crm1 substrates and consequently on most exported proteins, other export signatures are known. One example is a complete structured domain in the case of Snurportin (Paraskeva et al., 1999, Monecke et al., 2009).

## 1.4. Nuclear transport of small RNA-silencing proteins

To fulfill their possible nuclear functions, Argonaute proteins and other small RNA-guided gene silencing pathway components have to reach the nucleus (Schraivogel and Meister, 2014). Although the underlying nuclear transport pathways could shed light on the interesting nuclear functions, they still remain largely elusive. Furthermore, nuclear transport might have critical implications for nuclear and cytoplasmic small RNA-guided functions as it could provide a simple but effective mechanism to regulate protein activity. Therefore, I will summarize the current knowledge of nuclear transport processes of small RNA-guided gene silencing components. In addition, it will be discussed how their nuclear localization is regulated and how nuclear transport might regulate their function.

### Nuclear import of Argonaute proteins is often regulated by small RNA-binding

It is believed, that small RNAs are loaded onto Argonaute proteins in the cytoplasm, independent of nuclear or cytoplasmic small RNA-function (Guang et al., 2008, Ohrt et al., 2008, Noto et al., 2010, Olivieri et al., 2010, Ye et al., 2012, Gagnon et al., 2014). Interestingly, it has been shown that many Argonaute proteins that function in the nucleus are only imported when they are loaded with small RNAs. This was the case for the Ago clade members *A. thaliana* AGO4, *C. elegans* NRDE-3 and *Tetrahymena thermophila* Twi1p and Twi12p (Guang et al., 2008, Noto et al., 2010, Couvillion et al., 2012, Ye et al., 2012). Furthermore, the same observations were made for the Piwi clade proteins Mouse Miwi2 and *Drosophila* Piwi (Reuter et al., 2009, Saito et al., 2009, Olivieri et al., 2010). The underlying mechanism has been characterized in more detail for *C. elegans* NRDE-3 (Figure 3.1.5) and *Arabidopsis* AGO4. NRDE-3 contains a bipartite classical NLS and associates with secondary siRNAs that are generated in the cytoplasm. Without bound siRNA, the NLS is not accessible, however, upon small RNA loading, the NLS is exposed and loaded NRDE-3 gets imported (Guang et al., 2008). *Arabidopsis* AGO4 import is regulated in a similar way but additionally, the correct removal of the passenger strand has been shown to be prerequisite for activation of the NLS (Ye et al., 2012). Therefore, nuclear transport seems to function as quality control step that allows only correctly assembled small RNA-Argonaute complexes to be imported.

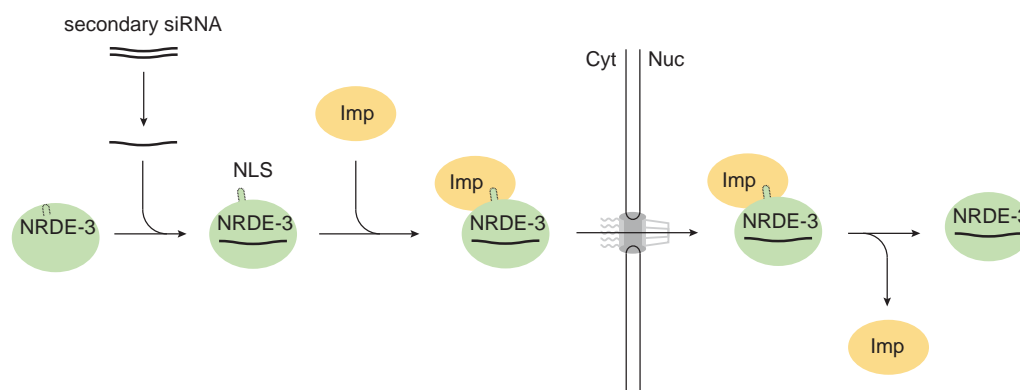


**Figure 3.1.5. Nuclear import of *C. elegans* Argonaute protein NRDE-3 requires small RNA binding.** In the cytoplasm, secondary siRNAs are produced that guide NRDE-3 to complementary nascent transcripts in the nucleus. NRDE-3 nuclear import is mediated by a nuclear localization signal (NLS) and so far unknown importins (Imp). Without bound siRNA, nuclear import is inhibited by masking the NLS sequence, however, after binding the secondary siRNA, the NLS gets accessible resulting in nuclear import. Figure adapted from Schraivogel and Meister, 2014.

### Nucleo-cytoplasmic shuttling of small RNA-guided gene silencing components

A restricted set of gene silencing components including human TNRC6A, TNRC6B, Dicer and *S. pombe* Dicer (Dcr1) have been identified to be nucleo-cytoplasmic shuttling proteins (Till et al., 2007, Emmerth et al., 2010, Doyle et al., 2013, Nishi et al., 2013). Whereas nothing is known on the functional significance of shuttling of the human gene silencing factors, recent studies suggest a model for *S. pombe* Dcr1 shuttling (Figure 3.1.6, Emmerth et al., 2010). Dcr1 is mainly nuclear and is anchored to centromeric chromatin which is localized at the inner nuclear membrane around nuclear pores. Together with centromeric chromatin, heat-shock response genes are also located at the nuclear periphery. Nuclear Dcr1 silences these heat-shock response genes by functioning in small RNA-guided transcriptional gene silencing processes (part I section 1.1). After

heat shock, Dcr1 is released from chromatin and exported to the cytoplasm. The effect of this process is the expression of heat-shock response genes (Woolcock et al., 2012). The mechanisms that prevent Dcr1 export under steady-state conditions are not yet understood, but might depend on nuclear export signals that are only exposed upon heat shock (Woolcock et al., 2012).

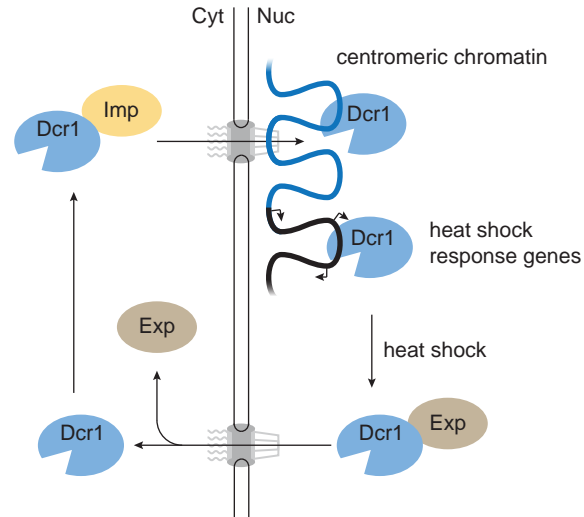


**Figure 3.1.6. *S. pombe* Dcr1 is a nucleo-cytoplasmic shuttling protein and shuttling is activated by heat shock.** Dicer 1 (Dcr1) shuttles between the cytoplasm (Cyt) and nucleus (Nuc) but is mainly nuclear under steady-state conditions. Import is mediated by an unknown importin (Imp), export by an also unknown exportin (Exp). Nuclear Dcr1 is anchored at centromeric chromatin, which is localized to the inner nuclear membrane. Heat-shock response genes are also localized at the nuclear periphery and are silenced by Dcr1. Upon heat-shock, Dcr1 is released from these regions and is subsequently exported, whereas heat-shock response genes can now be expressed. Figure adapted from Schraivogel and Meister, 2014.

### Nuclear transport mechanisms

So far, nuclear import receptors that guide Argonaute and other gene silencing pathway components to the nucleus are largely unknown. Many proteins like *Arabidopsis* AGO4, DCL1, DCL4, *Drosophila* Piwi, *C. elegans* NRDE-3 and human TNRC6A-C contain classical NLS sequences, which would indicate import via the classical Imp $\alpha$ /Imp $\beta$  pathway (Schauer et al., 2002, Hiraguri et al., 2005, Guang et al., 2008, Ye et al., 2012, Nishi et al., 2013). Indeed, this transport pathway and the recognized NLS consensus sequences are conserved among species. However, direct evidence for classical import of these components is completely lacking and therefore, the import receptors remain to be identified.

For several other gene silencing components, however, specific importins have been suggested to mediate nuclear import. Human Dicer contains a dsRBD at its C-terminus that can function as NLS, at least when expressed as an isolated domain (Doyle et al., 2013). Interestingly, the three importins Imp $\beta$ , Imp7 and Imp8 function redundantly in Dicer nuclear import. However, whether this non-canonical NLS is also used in the full-length context remains elusive. In the case of human Ago2, knockdown of Imp8 seems to reduce the nuclear Ago2 pool, however, whether Imp8 is directly involved in nuclear Ago2 transport is not known (Weinmann et al., 2009, Wei et al., 2014). Instead, Imp8 has shown to be implicated in cytoplasmic Ago2 functions (Weinmann et al., 2009). Last but not least, the *S. pombe* RNA-dependent RNA polymerase Rdp1, that is involved in small RNA-mediated transcriptional gene silencing in the nucleus, has been shown to be imported by Sal3, the *S. pombe* homolog of human Imp5 (Park et al., 2012).

## 2. Aims of part III

The cytoplasmic functions of Argonaute (Ago) and TNRC6 proteins are well understood. However, both protein families have also been identified in the nucleus of mammalian cells. Whereas the nuclear functions of TNRC6 proteins are unknown, diverse functions have been attributed to nuclear Ago including transcriptional gene regulation, regulation of mRNA splicing and DNA repair.

To fulfill their nuclear functions, Ago and TNRC6 proteins must reach the nucleus. Therefore, the aim of this thesis is to analyze nuclear transport pathways of both protein families. We will use nuclear transport assays to directly show nuclear transport of Ago and TNRC6 proteins and to further characterize these transport pathways. We will then apply diverse biochemical, cell biological and functional assays to identify import receptors that mediate nuclear transport of Ago and TNRC6 proteins.

Nuclear transport processes can be regulated by diverse mechanisms and they provide an effective way to regulate nuclear and cytoplasmic protein function. Therefore, we want to investigate how nuclear transport of Ago and TNRC6 proteins is regulated. Furthermore, we want to investigate how nuclear transport influences nuclear and cytoplasmic function of Ago and TNRC6 proteins.

Our findings should provide important insights into nuclear transport processes of Ago and TNRC6 proteins. These processes are important for the understanding of Ago and TNRC6 protein function, especially those in the nucleus. Further more, they might provide novel but so far uncharacterized steps in miRNA-guided gene regulatory pathways.

Taken together, the specific aims in part II of this work include:

1. Identification of nuclear transport processes of Ago and TNRC6 proteins.
2. Investigation of the underlying nuclear import and export mechanisms.
3. Characterization of how nuclear transport of Ago and TNRC6 is regulated.
4. Identification of the functional significance of nuclear Ago2 and TNRC6 transport.

## 3. Results

### 3.1. Nucleo-cytoplasmic distribution of human Ago2

Here, we analyze nuclear transport pathways of Ago and TNRC6 proteins and how these processes are regulated. To investigate these questions, the nucleo-cytoplasmic distribution of Ago proteins will be investigated first.

In immunofluorescence (IF) stainings, the vast majority of Ago2 is located in the cytoplasm (Jakymiw et al., 2005, Liu et al., 2005b, Sen and Blau, 2005, Leung et al., 2006, Rüdél et al., 2008). To get comprehensive insights into Ago2 localization in a broad spectrum of cells, we stained endogenous Ago2 in 26 cell lines (Figure 3.3.1 and Appendix Figure A3). As antibody against Ago2, we used a previously reported monoclonal antibody (Rüdél et al., 2008). For quantitative information on nuclear and cytoplasmic Ago2 signals, we measured signals from cytoplasmic and nuclear regions and calculated a nucleo-cytoplasmic ratio from the mean signal intensities (for technical details, see Materials and Methods section 5.3). The mean nucleo-cytoplasmic ratio over all 26 cell lines was  $0.55 \pm 0.12$ , i.e. the mean signal in the cytoplasm was about twice as intense as the nuclear signal normalized over all cell lines. Interestingly, we identified a cell line from human pulmonary artery smooth muscle cells (HPASMC) and the melanoma cell line Sk-Mel-28 to have exceptionally high nucleo-cytoplasmic ratios (Figure 3.3.1 A and B). The cell lines HEK 293T and HeLa, that were subsequently used during this study, contained rather low

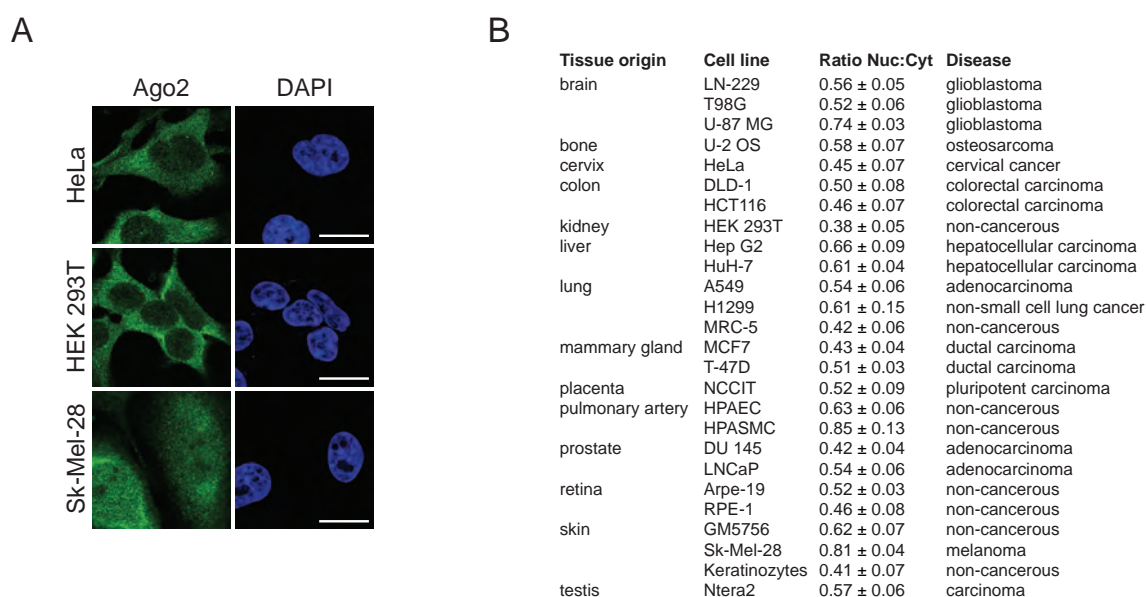


**Figure 3.3.1. Ago2 localization in different human cell lines from various tissue origins** **A**, Ago2 was stained in HeLa, HEK 293T and Sk-Mel-28, three exemplary cell lines from overall 26 cell lines that were tested for Ago2 localization (Figure is continued as Appendix Figure A3). DAPI was used to stain nuclei. **B**, Tabular summary of Ago2 signal quantifications from the 26 different human cell lines. To calculate nucleus-to-cytoplasm ratio, Ago2 signal was quantified from nuclear and cytoplasmic regions. Scale bars in A represent 20  $\mu\text{m}$ . Data in B are shown as mean  $\pm$  SEM.

nuclear Ago2 levels. No correlation with specific tissue-origins was observed. Additionally, we did not observe correlation with passage number and plating density in HeLa and HEK 293T as well as differentiation in primary keratinocytes (data not shown).

Although specificity of the used anti-Ago2 antibody has been shown before (Rüdel et al., 2008), we again verified the obtained Ago2 IF signal (Figure 3.3.3 A, D and E). We performed Ago2 knockdowns in HeLa cells, followed by the comparison of anti-Ago2 antibody signals in IF and Western Blot. For knockdown of Ago2, we used so called siPools, which are mixtures of multiple siRNAs against the same target mRNA, which increases specificity of the knockdown (Hannus et al., 2014). Although we observed a clear signal decrease in IF and Western Blot, the knockdown efficiency with the used Ago2 siPools was low with about 50 % remaining protein. However, upon Ago2 knockdown we measured almost identical Ago2 signal reductions in the total cell lysates used for Western as well as in cytoplasmic and nuclear regions quantified from IFs. The Western signal for Ago2 was further validated with a polyclonal anti-Ago2 antibody and again, we measured a very similar signal reduction. Therefore, we conclude that we detect Ago2 in both the nuclear and cytoplasmic compartments with high specificity in IF and Western experiments.

## 3.2. Ago2 is imported into the nucleus and shuttles between nucleus and cytoplasm

### 3.2.1. Heterokaryon assays provide direct evidence for Ago2 nuclear import

To solidify that Ago2 is indeed found in the nucleus, we wanted to investigate whether Ago2 is imported into the nucleus. We therefore applied a modified heterokaryon assay. In the classical heterokaryon assay, mouse NIH 3T3 cells are fused with human HeLa cells and the redistribution

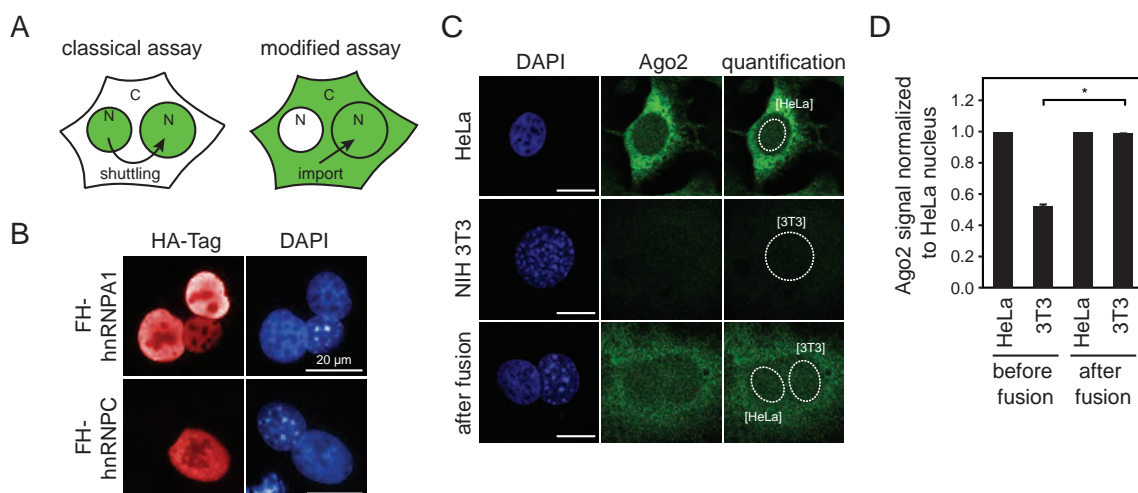


**Figure 3.3.2. Ago2 is imported into the nucleus of human cells.** **A**, Schematic diagram showing classical and modified heterokaryon assay as described in the main text. **B**, HeLa cells transfected with FH-hnRNPA1 and FH-hnRNPc were fused to mouse NIH 3T3 cells. Proteins were observed to appear in the mouse nucleus after fusion. Nuclei from 3T3 can be distinguished by the intense speckled DAPI staining. **C**, HeLa was fused to 3T3 and endogenous Ago2 was detected with monoclonal anti-Ago2 antibody. Microscopy shows Ago2 staining in unfused HeLa cells and no signal in unfused 3T3 cells. After fusion, Ago2 can be detected in heterokaryon cytoplasm and both human and mouse nuclei. **D**, Diagram shows quantification of Ago2 signal HeLa and 3T3 nuclei before and after fusion with data normalized to human nucleus. N, nucleus; C, cytoplasm; FH, Flag/HA tag. Scale bars in B and C represent 20  $\mu$ m. Data in D are shown as mean plus SEM. \*P < 0,05.

of a human nuclear protein into the mouse nucleus is observed. As Ago2 is mainly cytoplasmic, we modified the assay readout and investigated the redistribution of cytoplasmic Ago2 into the mouse nucleus (Figure 3.3.2 A). To validate functionality of our assay, we performed classical heterokaryon assay with the shuttling protein hnRNPA1 as positive control and the non-shuttling protein hnRNPC as negative control (Figure 3.3.2 B). Indeed, we observed hnRNPA1 in the mouse nucleus after 4 hours, whereas hnRNPC remained in the human nucleus. Of note, for classical and modified heterokaryon assays, the cells were treated with cycloheximide to prevent synthesis of new protein in the cytoplasm, which would falsify the readout of the assay. Strikingly, when endogenous Ago2 was analyzed, we found that human Ago2 levels increased slightly but clearly measurable over background signal in the mouse nucleus (Figure 3.3.2 B). The increase of Ago2 in the mouse nucleus corresponded to the Ago2 levels that have been measured in the human nucleus. Therefore, Ago2 is transported from the cytoplasm into the mouse nucleus.

### 3.2.2. Ago2 is a nucleo-cytoplasmic shuttling protein

Based on the above mentioned results, we conclude that Ago2 is mainly cytoplasmic but can be imported into the nucleus. Next we tested whether Ago2 can shuttle between the nucleus and cytoplasm and applied two different transport assays.

First, we analyzed endogenous Ago2 localization upon inhibition of Crm1-mediated nuclear export by Leptomycin B (LMB). LMB is a metabolite of *Streptomyces* and has been found as

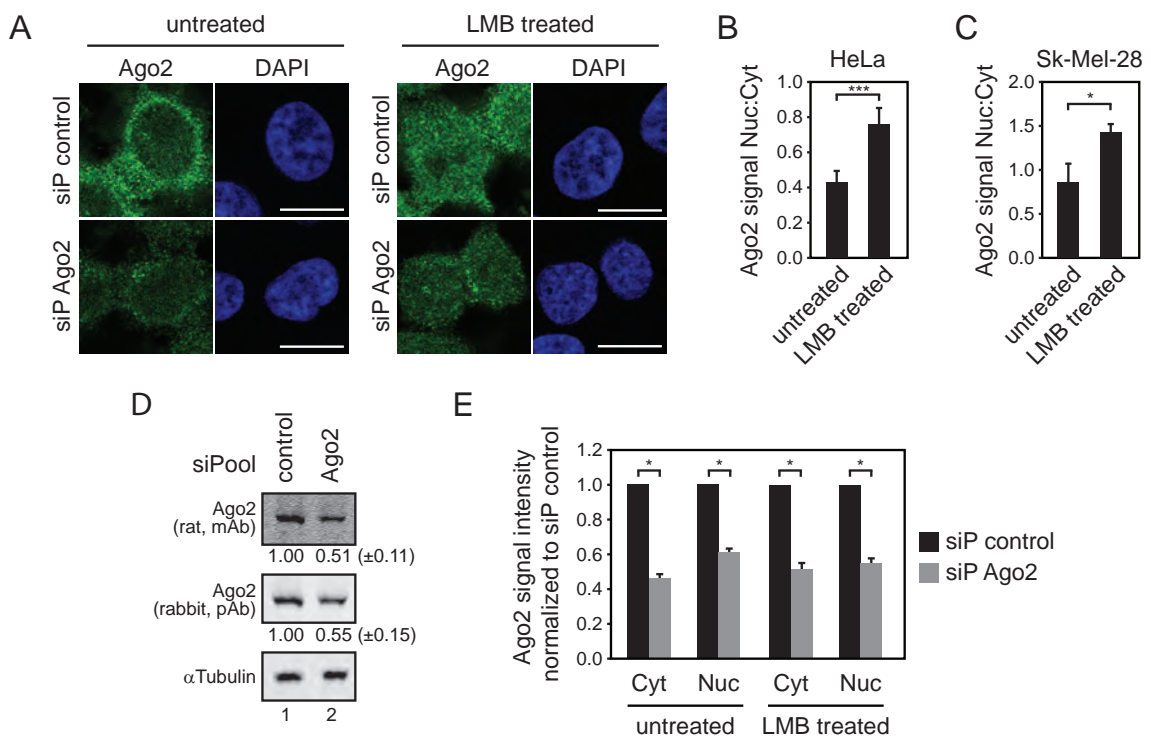


**Figure 3.3.3. Ago2 shuttles between the nucleus and cytoplasm.** **A**, Endogenous Ago2 signal was detected in HeLa cells treated with Leptomycin B or control treated. Cells were transfected with control or Ago2 siPool. **B** and **C**, Signal quantification and calculation of nucleus-to-cytoplasm ratio in untreated or Leptomycin B treated HeLa (**B**) and Sk-Mel-28 (**C**) cells. **D**, Ago2 protein was analyzed upon knockdown of Ago2 or transfection of a control siPool with two different antibodies. Signal quantification of knockdown versus control was normalized to  $\alpha$ Tubulin. **E**, Ago2 signal was quantified from nucleus and cytoplasm in untreated or Leptomycin B treated cells upon knockdown of Ago2 or transfection of a control siPool. Signals were normalized to control siPool. siP, siPool; LMB, Leptomycin B. Scale bars in **A** represent 10  $\mu$ m. Data in **B** to **E** are shown as mean plus SEM. \* $P < 0,05$ ; \*\*\* $P < 0,0005$ .

potent nuclear export inhibitor that covalently binds Crm1 within its NES-binding site (Nishi et al., 1994, Fornerod et al., 1997, Kudo et al., 1999, Sun et al., 2013). Of note, LMB seems to be highly specific for Crm1, as biotinylated LMB specifically pulls down a single protein from HeLa cell lysate and the cytotoxic effect of LMB can be completely reversed with a LMB-insensitive Crm1 mutant (Nishi et al., 1994, Kudo et al., 1999). Nucleo-cytoplasmic shuttling proteins which are exported from the nucleus in a Crm1-dependent manner, accumulate in the nucleus upon LMB treatment. We treated HeLa cells with LMB and detected endogenous Ago2 in the nucleus and cytoplasm (Figure 3.3.3 A and B). Strikingly, we observed a clear increase of Ago2 in the nucleus, as shown by a higher nucleo-cytoplasmic ratio upon treatment with LMB. Again, Ago2 signal seems to be specific, as knockdown of Ago2 leads to partial signal loss in both the nucleus and cytoplasm (Figure 3.3.3 A, D and E). To validate this finding, we tested another independent cell line Sk-Mel-28 and indeed, we again detected an increase in nuclear Ago2 upon LMB treatment (Figure 3.3.3 C). In both cell lines HeLa and Sk-Mel-28, the nucleo-cytoplasmic Ago2 signal ratio almost doubled and in Sk-Mel-28, the signal intensity after LMB treatment was stronger in the nucleus compared to the cytoplasm. As LMB affected Ago2 export from the nucleus, we conclude that Ago2 nuclear export is probably mediated by Crm1, the classical nuclear export factor that is used by the vast majority of proteins.

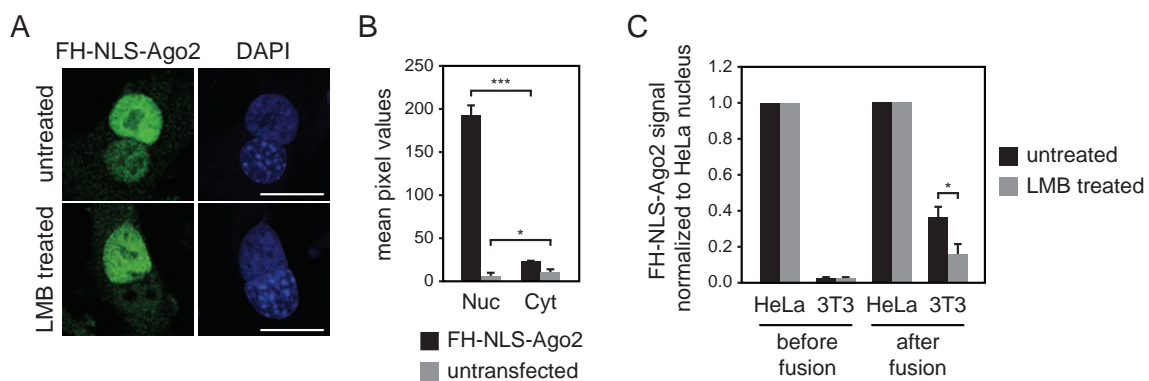


**Figure 3.3.4. Classical heterokaryon assay with a nuclear trapped Ago2 fusion confirms Ago2 shuttling activity.** **A**, HeLa cells stably transfected with FH-NLS-Ago2 with or without Leptomycin B treatment were used for heterokaryon assay. Ago2 was detected by anti-HA IF. **B**, FH-NLS-Ago2 was quantified from nucleus and cytoplasm before fusion with 3T3. **C**, Quantification of Ago2 signal from HeLa and 3T3 nuclei before and after fusion of untreated or Leptomycin B treated cells. FH, Flag/HA tag; NLS, SV40 nuclear localization sequence; LMB, Leptomycin B. Scale bars in A represent 10  $\mu$ m. Data are shown as mean plus SEM. \*P < 0.05; \*\*\*P < 0.0005.

To further solidify the observed nucleo-cytoplasmic shuttling activity of Ago2, we performed heterokaryon assays. As the readout from the classical heterokaryon assay depends on strictly nuclear proteins, we fused Ago2 to the strong SV40 nuclear localization sequence (NLS). This resulted in nuclear trapped Flag/HA-tagged NLS-Ago2 that can be detected in IF with an anti-HA antibody. To achieve a uniform NLS-Ago2 expression, we generated a stable monoclonal HeLa cell line. We then investigated whether the generated cell line contains residual NLS-Ago2 in the cytoplasm, as this might lead to unspecific observations regarding nucleo-cytoplasmic shuttling. We quantified anti-HA signal from the NLS-Ago2 cell line and compared it to background signal from an untransfected HeLa cell line. We observed a very weak NLS-Ago2 signal in the cytoplasm which could, at least in part, mimic the readout from the heterokaryon assay. When these cells were fused with NIH 3T3 cells, NLS-Ago2 signal clearly increased in the mouse nucleus. To show that this is indeed NLS-Ago2 that shuttles from the human to the mouse nucleus, we treated heterokaryons with LMB to prevent nuclear export from the human nucleus. Strikingly, significantly

less nuclear NLS-Ago2 was found in the mouse nucleus after LMB treatment, demonstrating that NLS-Ago2 indeed shuttled from the human nucleus to the mouse nucleus.

Taken together, we have shown that human Ago2 is mainly cytoplasmic but can also be found in the nucleus. Ago2 can be imported into the nucleus and is a nucleo-cytoplasmic shuttling protein. Nuclear export of Ago2 seems to depend on Crm1.

### 3.3. Nuclear transport of Ago2

#### 3.3.1. A functional assay suggests redundant import routes for Ago2

Importins mediate nuclear import of a wide spectrum of proteins by recognition of nuclear localization sequences on the cargo protein and interaction with the nuclear pore complex. To identify importins that mediate nuclear transport of Ago2, we designed an siRNA library against each human importin (Imp) identified so far. We did not generate siRNAs against the Imp $\alpha$  family of import factors, as it is thought that Imp $\alpha$  function strictly depends on Imp $\beta$  (see part III section 1.3). For all other importins, except for Imp4, the siRNA library contained two independent siRNAs designated as si1 and si2. The siRNA library was validated by quantitative real-time PCR to detect importin mRNA levels after knockdown (Figure 3.3.5 C). Except for si1/2 Imp3, si1/2 Imp9 and si2 Tnpo1, all siRNAs showed knockdown efficiencies of around 10 % remaining mRNA levels and therefore provide a solid basis for further analysis.

The importin siRNA library was then screened by anti-Ago2 IF upon importin knockdown. If a single importin is needed for Ago2 import, knockdown should lead to a decrease in nuclear Ago2. Therefore, HeLa cells were transfected with the Importin siRNA library and two days and three days post-transfection, Ago2 localization was analyzed (data not shown). However, we did not observe any decrease in nuclear Ago2 when single Importins were knocked down. To our surprise, also the knockdown of Imp8, which has been previously reported to slightly decrease the nuclear Ago2 pool, did not show effects in our analysis (Weinmann et al., 2009). Taken together, these data indicate that single importin knockdown does not significantly change the nuclear Ago2 pool.

As the performed loss-of-function analysis with direct readout of Ago2 localization did not prove informative, we tested the requirement for import receptors by another independent method. As the steady-state pool of Ago2 is low in the used cell system, we established an assay with a functional readout for nuclear Ago2 activity. It has been shown that nuclear localized RNAs like the 7sk RNA can be knocked down by RNAi (Robb et al., 2005). In addition, siRNA loading seems to be a cytoplasmic process (Ohrt et al., 2008, Gagnon et al., 2014). Therefore, if importin knockdown affects Ago2 import, less 7sk siRNA loaded Ago2 should be present in the nucleus and knockdown efficiency of 7sk should consequently be affected (Figure 3.3.5 A). To validate this system, we depleted Ago1-4 and analyzed 7sk knockdown efficiency (Figure 3.3.5 B). 7sk levels were determined by Northern Blot and normalized to U6 RNA. As expected, 7sk knockdown efficiency was clearly reduced only after depletion of Ago2. This demonstrates that the measured effects are Ago2-dependent and the assay is suitable for the analysis of Ago2 import routes. Of note, similar to the observed knockdown efficiency of Ago2 siPools, the used Ago2 siRNAs in this experiment did not allow complete Ago2 knockdown (data not shown). However, we were still able to see clear elevation of 7sk snRNA levels upon 7sk siRNA transfection. Subsequently, we knocked down Imp $\beta$ , Imp3-5, Imp7-9, Imp11-13 and Tnpo1 and measured 7sk knockdown efficiency as described (Figure 3.3.5 D). However, none of the tested knockdown conditions resulted

in a significant change in 7sk knockdown efficiency. Of note, we measured slight effects with one of two siRNAs for Imp5, however si2 Imp5 did not show the same effects although it reduced Imp5 mRNA level more efficiently than si1 Imp5. Taken together, we conclude that knockdown of single import receptors is not sufficient to prevent nuclear Ago2 transport. This is in line with the results from Ago2 IF experiments. It is therefore conceivable that several import receptors function redundantly in transporting Ago2 to the nucleus.

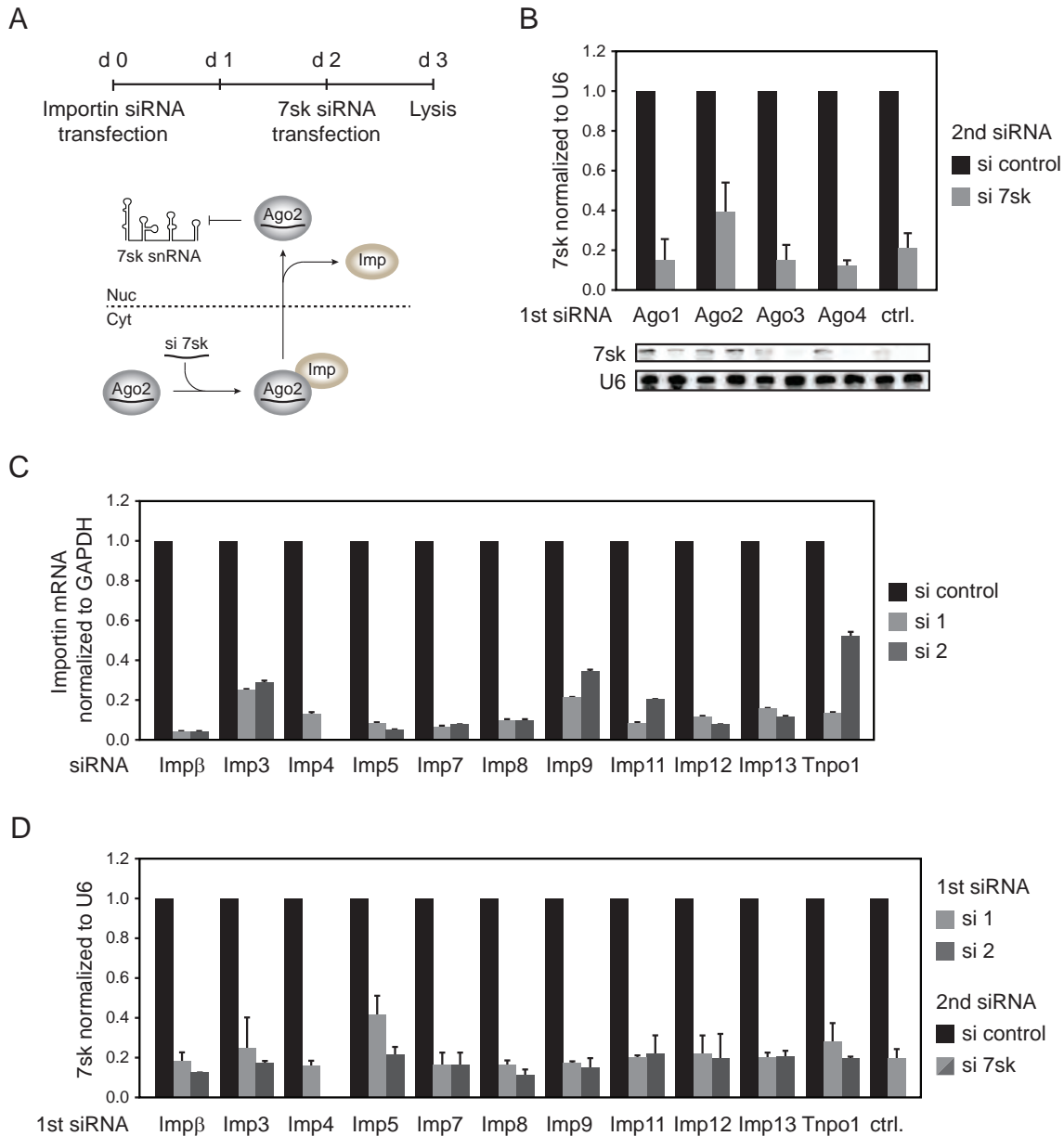


**Figure 3.3.5. A functional assay suggests redundant importins for Ago2 nuclear import.** **A**, Schematic representation of the experimental procedure for the 7sk assay to measure nuclear Ago2 activity upon Importin knockdown. Nuclear Ago2 activity is measured as knockdown efficiency of the nuclear RNA 7sk. was determined from knockdown efficiency of the nuclear located 7sk snRNA. **B**, Knockdown of human Ago1-4 was used to validate functionality of the assay. 7sk knockdown efficiency was only decreased upon Ago2 knockdown. Data were analyzed by Northern Blot for 7sk and the loading control U6. 7sk signal was then normalized to the U6 signal in the corresponding sample and control siRNA transfected sample. **C**, Quantitative real-time PCR was used to validate a siRNA library against each human Importin, except for Imp $\alpha$ . Data were normalized to GAPDH mRNA and control transfected sample. **D**, The importin siRNA library was used for 7sk assay and data were analyzed as described in B. snRNA, small nuclear RNA; d, days. Data are represented as mean plus SEM.

### 3.3.2. Ago2 is probably not imported via the classical Imp $\alpha$ /Imp $\beta$ -dependent pathway

Many human proteins are imported via the classical Imp $\alpha$ /Imp $\beta$ -dependent nuclear transport pathway. This import mechanism includes binding of Imp $\alpha$  to a short monopartite or bipartite stretch of largely basic amino acids (Görlich and Kutay, 1999). Since it is possible to predict these classical nuclear localization signals (NLS), we used *in silico* linear motif prediction to search for a classical NLS sequences in mammalian Ago proteins. In addition, as nuclear export of Ago2 seems to be Crm1-dependent, we also looked for classical nuclear export sequences (NES). We found an NLS within the Ago PAZ domain and an NES within the Piwi domain (Figure 3.3.6 A). Both sequences including the critical basic and hydrophobic residues were conserved among human and mouse Ago1-4.

Using the recently published Ago2 structure in complex with miR-20a, we observed that both sequence stretches are located on the surface of Ago2 and should therefore be accessible for karyopherin binding (Figure 3.3.6 B). Regarding the NLS, structural analysis revealed that miRNA-binding might conceal the NLS. Therefore, we did site-directed mutagenesis of critical residues within the predicted NLS and NES in Ago2 wildtype and Y529E mutant background (Figure 3.3.6 C and E). Ago2 Y529E mutant does not bind miRNAs anymore, as shown previously (Rüdel et al., 2008). Localization of the generated mutants revealed that mutagenesis of the NLS did not reduce the nuclear Ago2 pool and mutagenesis of the NES did not increase the nuclear Ago2 pool (Figure 3.3.6 C and E). To solidify our results, we fused the predicted Ago2 NLS and NES to eGFP and investigated localization of the generated eGFP fusions (Figure 3.3.6 D and F). Of note, eGFP can passively diffuse into the nucleus due to its limited size, therefore eGFP alone is located in both the nucleus and cytoplasm. While the strong SV40 NLS resulted in a clear accumulation of eGFP in the nucleus, the predicted Ago2 NLS had no effect. Similarly, the strong MAPKK NES resulted in exclusively cytoplasmic eGFP, whereas the predicted Ago2 NES had no effect. Therefore we conclude that the predicted NLS and NES are probably not functional. In addition this hints towards an Imp $\alpha$ /Imp $\beta$ -independent transport pathway for Ago proteins. Regarding the nuclear export pathway, we suggest an additional NES that is not predictable in Ago2.

Although these data suggest that classical NLS sequences are not present in Ago2, the obtained data do not finally prove independency of Imp $\alpha$ /Imp $\beta$ . However, this observation is further supported by the finding that Imp $\beta$  knockdown did not decrease the nuclear pool of endogenous Ago2 (see section 3.3.1). As the nuclear Ago2 pool is low under steady state-conditions, the expected effects might be below the detection limit of Ago2 IF quantification. We therefore investigated whether the nuclear import of Ago2 is affected by Imp $\beta$  knockdown under conditions of increased nuclear Ago2 localization, as observed upon LMB treatment (Figure 3.3.7). However, even after LMB addition, Imp $\beta$  knockdown did not affect nuclear accumulation of Ago2.

Therefore, we conclude that nuclear import of Ago2 is most likely not mediated by classical Imp $\alpha$ /Imp $\beta$ -dependent transport pathway. Furthermore, because Imp $\beta$  knockdown did not affect Ago2 localization, nuclear import of Ago2 also seems to be independent of non-classical Imp $\beta$ -mediated pathways.

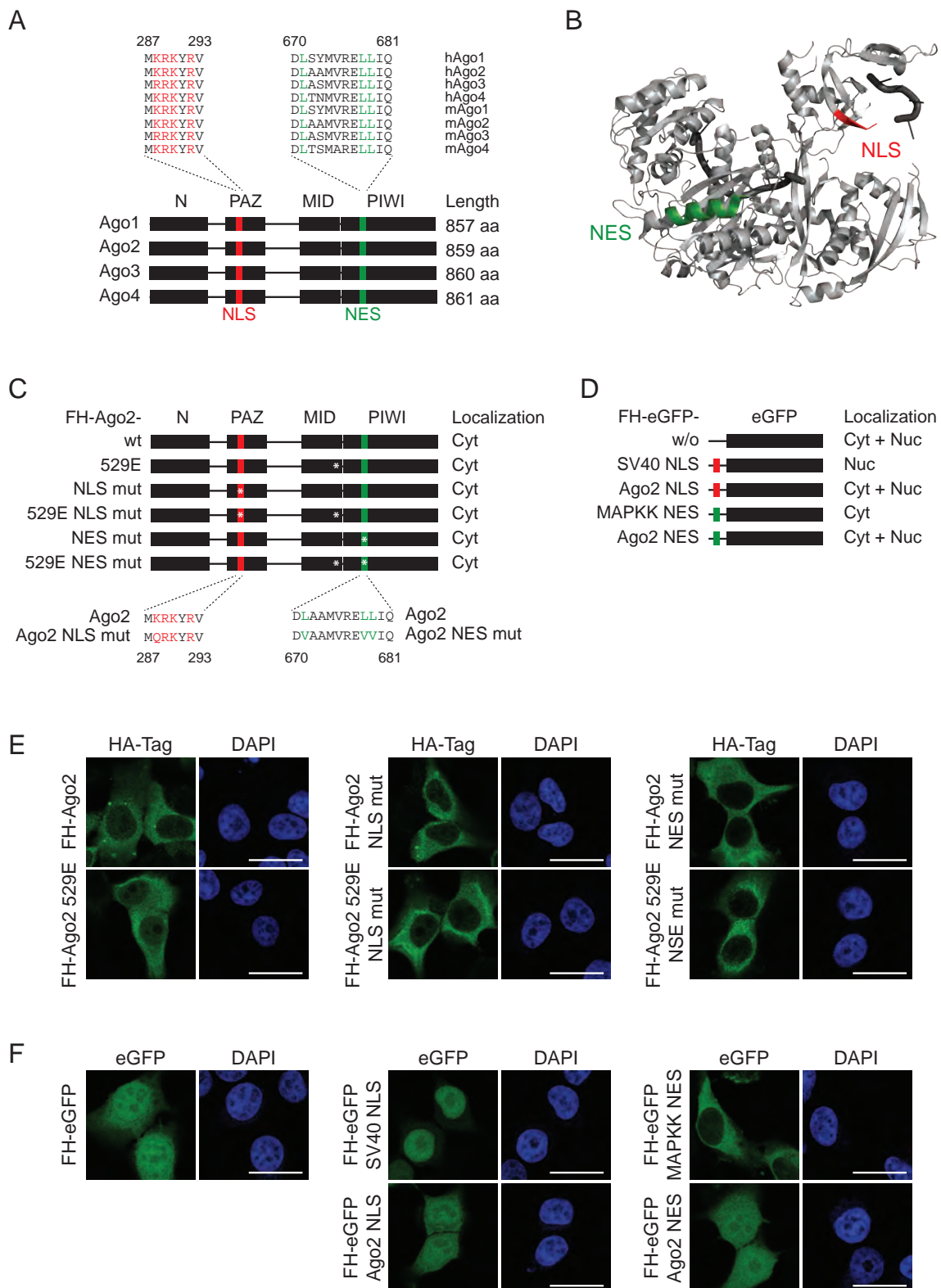


**Figure 3.3.6. *In silico* predicted classical NLS and NES sequences in Ago2 are not functional. A**, Linear motif prediction identified classical NLS and NES within conserved regions of human and mouse Ago1-4 PAZ and PIWI domain. **B**, The predicted NLS and NES lie on the surface of human Ago2 and were mutated within the critical residues. Human Ago2 is shown in light gray, miR-20a is shown in dark gray. **C** and **E**, NLS and NES were mutated in Ago2 wildtype and 529E background and used for microscopic analysis. Schematic representation of the generated mutations and the resulting predominant localization in C. Corresponding IF pictures are not shown in E. **D** and **F**, Ago2 NLS and NES were fused to eGFP and localization of the generated fusions was investigated. SV40 NLS and MAPKK NES served as controls for nuclear and cytoplasmic localization, respectively. Scale bars in E and F represent 20  $\mu$ m.

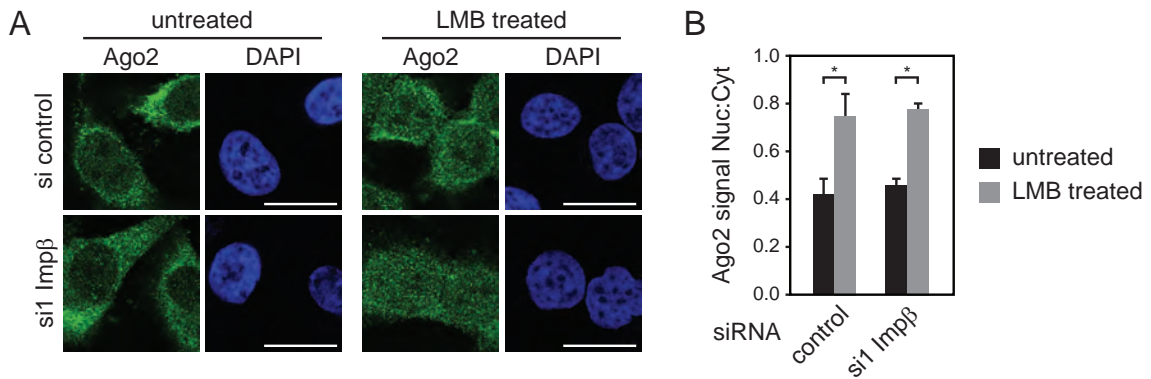


**Figure 3.3.7. Shuttling of human Ago2 is Imp $\beta$ -independent.** **A**, Imp $\beta$  was knocked down in HeLa cells followed by treatment of LMB. Untreated cells and cells transfected with a control siRNA were used as controls. Endogenous Ago2 was detected with anti-Ago2 antibody. **B**, Quantification of nuclear and cytoplasmic Ago2 signal was used to calculate nucleus-to-cytoplasm ratios. Scale bars in **A** represent 20  $\mu$ m. Data in **B** are represented as mean plus SEM. \*P < 0.05

### 3.3.3. Biochemical analyses did not show Ago2-associated import factors

As our loss-of-function analyses by knockdown of import factors did not identify single importins that might contribute to Ago2 import, we performed biochemical analyses to identify import factors that associate with Ago2. We cloned human importins *de novo* from HeLa cDNA, including Imp $\beta$ , Imp3, Imp11, Imp13 and Tnp1. Imp4 and Imp8 expression constructs were available (Weinmann et al., 2009). Cloning of Imp5, Imp7 and Imp12 was not successful. These constructs were then used for co-immunoprecipitation with Ago2 with importins as bait, Ago2 as bait as well as with overexpressed and endogenous Ago2 (data not shown). However, none of the tested importins did efficiently coimmunoprecipitate with Ago2. PABPC was used as positive control and has been found in Ago2-immunoprecipitations (Fabian et al., 2009), indicating successful immunoprecipitations.

In order to investigate Ago2-importin interaction in another independent system, we collaborated with Oliver Gruss (ZMBH, Heidelberg, Germany) to perform Ago2-pulldowns from *Xenopus* oocyte extracts. Homology between human and *Xenopus* importins is high and almost identical sets of importins exist in both organisms. In addition, *Xenopus* oocytes express comparably high amounts of import factors. As importin-cargo interaction is negatively regulated by RanGTP, we additionally depleted RanGTP from the extracts. Supplementing RanGTP back to this system should then allow to identify Ran-dependent Ago2 interactors. We first expressed HA-tagged Ago2 (HA-Ago2) in insect cells and obtained highly pure Ago2 protein (Figure 3.3.8 A to C). Oocyte extract with or without RanGTP was incubated with HA-Ago2, Ago2 interacting proteins were isolated by anti-HA antibody and pulled down proteins were identified by mass spectrometry. As we enriched numerous known RNA-dependent and -independent Ago2 interaction partners, we conclude that the pulldown was successful. However, we did not identify any import factors that significantly increased in the Ran-free sample.

Taken together, we did not identify Ago2 interacting importins biochemically in different systems. However, Ago2 is a mainly cytoplasmic protein and only a subpopulation of Ago2 seems to be imported as shown by nuclear transport assays. Therefore, Ago2-importin interaction might only occur in a small Ago2 subpopulation. Furthermore, cargo-importin interaction is transient and only occurs during import, which might complicate biochemical identification. Therefore further analyses are needed to investigate Ago2 import in more detail.

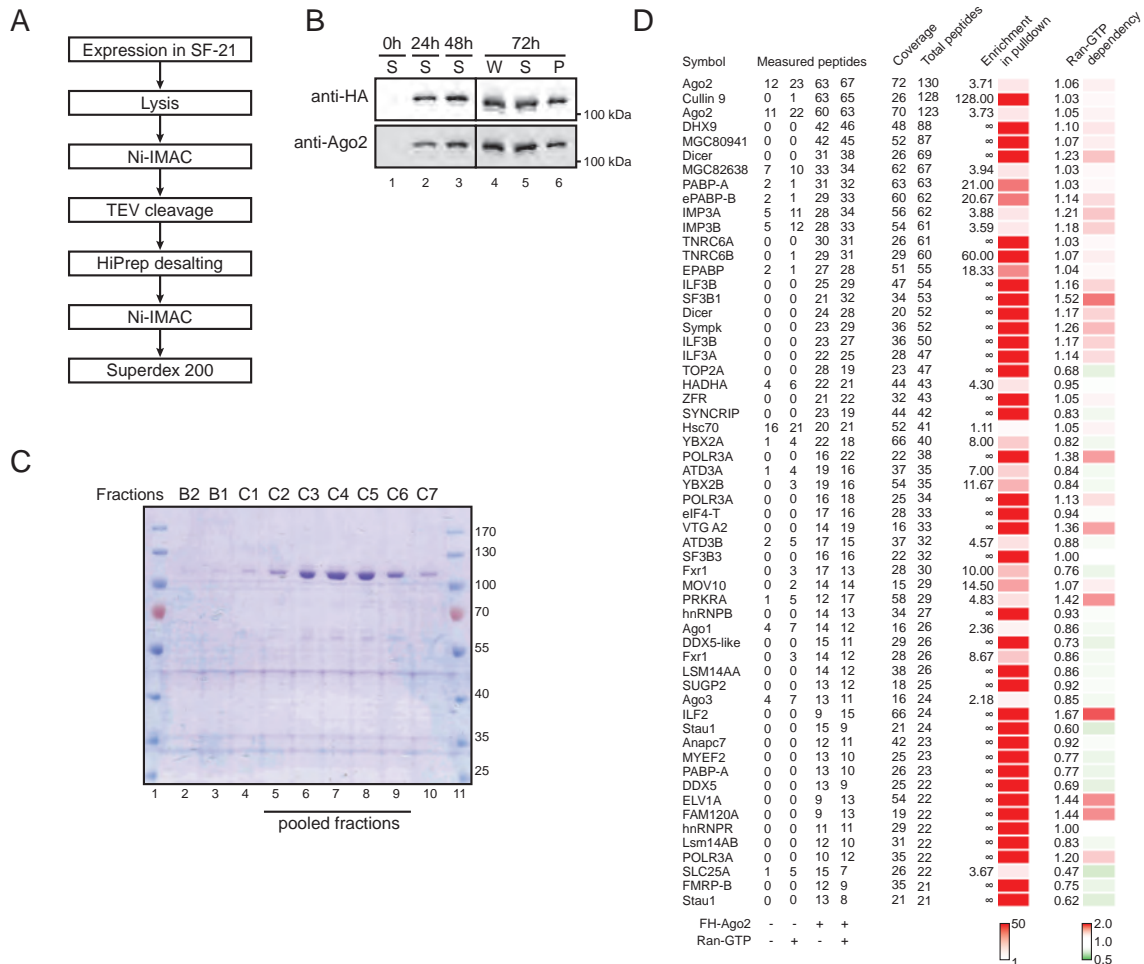


**Figure 3.3.8. Identification of Ran-dependent Ago2 interactors did not reveal Ago2-associated import factors. A,** Purification strategy of human HA-tagged Ago2 from SF-21 insect cells. **B,** Identity of the expressed protein was determined by Western Blot from lysed insect cells with anti-HA and anti-Ago2. Shown are four time points (0, 24, 48 and 72 h) with soluble (S), whole-cell (W) and insoluble/pelleted (P) protein fractions. **C,** After gel filtration, purity of the elution fractions was assessed by Coomassie staining. Marked are fractions that were used for pulldown experiments. **D,** Pull-downs of FH-Ago2 with anti-HA antibody from Ran-depleted oocyte extracts that were supplemented with GTP-loaded Ran or not. The left heat map shows the IP versus control ratio of measured peptides independent of Ran-addition (enrichment in pulldown). The heat map on the right compares enrichment ratios with and without addition of Ran, i.e. green color would show proteins that are less abundant in the Ago2-pulldowns upon addition of Ran (Ran-GTP dependency). Of note, Ago2 peptides were annotated to both *Xenopus tropicalis* and *Xenopus laevis*; therefore, Ago2 is listed twice in the table. Color code shows enrichment in pulldown compared to input sample and relative enrichment in RanGTP samples. ∞, infinite value.

### 3.4. TNRC6 proteins are nucleo-cytoplasmic shuttling proteins

TNRC6 proteins interact with Ago proteins during miRNA-mediated post-transcriptional gene silencing. It has been previously shown that TNRC6A and TNRC6B can localize in the nucleus upon inhibition of Crm1-dependent export by LMB (Till et al., 2007, Nishi et al., 2013). Therefore, at least TNRC6A and TNRC6B seem to shuttle between the nucleus and cytoplasm. Furthermore, TNRC6A contains functional classical NLS and NES sequences (Nishi et al., 2013). To get further insights into TNRC6 nuclear transport processes, we initially investigated whether all three human TNRC6 proteins shuttle. We expressed Flag/HA-tagged TNRC6A-C and treated cells with LMB for inhibition of Crm1-dependent nuclear export (Figure 3.3.9 A and B). Under

steady state-conditions, overexpressed TNRC6A-C localizes in cytoplasmic foci which probably resemble P-bodies (Kulkarni et al., 2010). When cells were treated with LMB, however, TNRC6A-C exclusively localized in the nucleus indicating that all three human TNRC6 proteins constantly shuttle between the nucleus and cytoplasm. Similar to the observed cytoplasmic foci, TNRC6A-C localized in distinct foci in the nucleus upon LMB treatment. This was in agreement with previous observations, observing similar nuclear foci for nucleus-trapped TNRC6A and TNRC6B (Till et al., 2007, Nishi et al., 2013).

As overexpression of proteins can lead to unspecific effects, we generated a monoclonal antibody against TNRC6B in cooperation with Elisabeth Kremmer (Helmholtz Center, Munich, Germany). To show that the antibody is specific for TNRC6B, we transfected siPools against TNRC6B (Figure 3.3.9 C and E). The generated antibody specifically detected TNRC6B in Western Blot and IF experiments, as shown by complete signal loss upon TNRC6B knockdown (Figure 3.3.9 C and E). We then performed LMB treatment as described above but detected endogenous TNRC6B (Figure 3.3.9 C to E). Strikingly, TNRC6B accumulated in the nucleus upon LMB treatment, showing shuttling activity and Crm1-dependent export. Of note, the cytoplasmic pool of TNRC6B as well as the nuclear accumulated pool did not generate such discrete foci as observed for the over-expressed protein. In addition, we did not observe a quantitative shift of the complete cytoplasmic

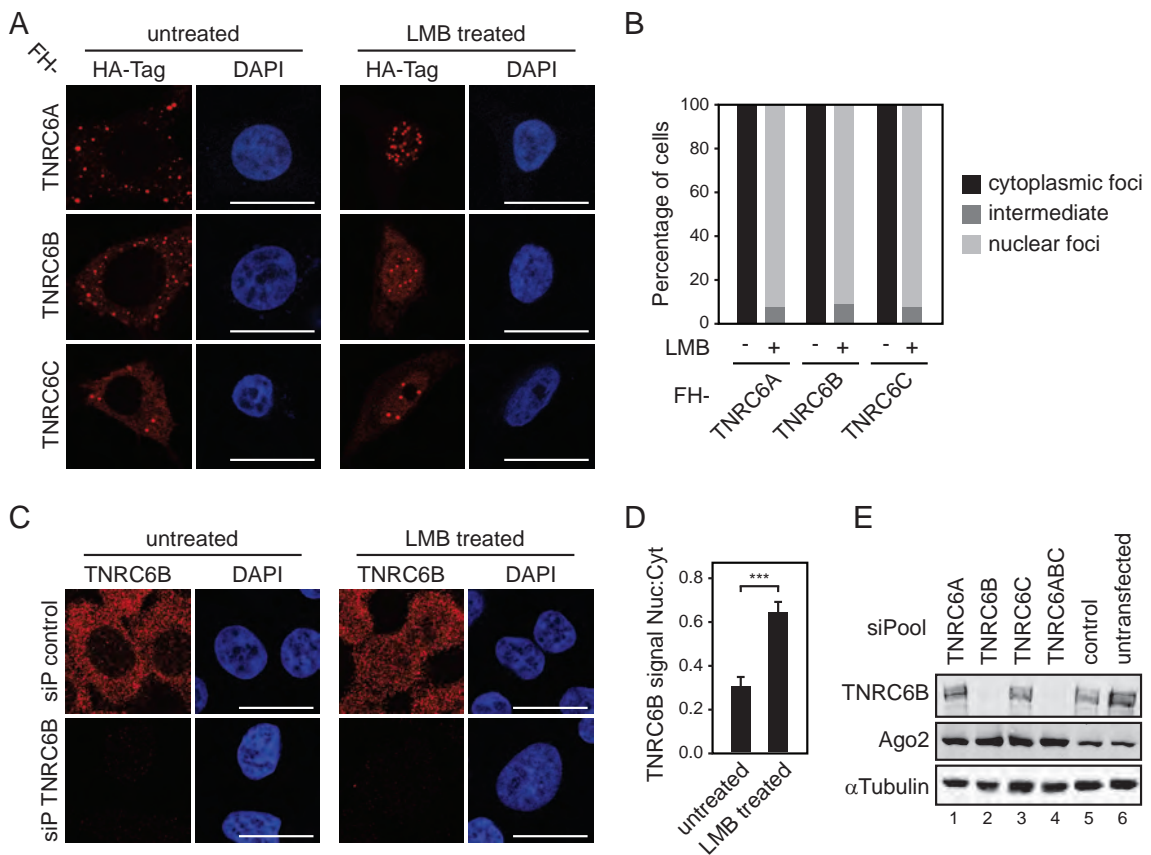


**Figure 3.3.9. Human TNRC6A-C are nucleo-cytoplasmic shuttling proteins.** **A** and **B**, HeLa cells were transfected with FH-TNRC6A, FH-TNRC6B or FH-TNRC6C and treated with Leptomycin B or not. TNRC6 proteins were detected with anti-HA antibody. Diagram in **B** shows the percentage of cells with cytoplasmic foci, nuclear foci or cells with foci in both compartments (intermediate). **C** and **D**, Endogenous TNRC6B was detected with monoclonal antibody in control or TNRC6B siPool transfected cells. TNRC6B signal intensity was determined and nucleus-to-cytoplasm ratio was calculated and shown in **D**. **E**, Western Blot of TNRC6A/B/C siPool transfected cells and detection of TNRC6B, Ago2 and  $\alpha$ Tubulin as loading control. FH, Flag/HA; LMB, Leptomycin B; siP, siPool. Scale bars in **A** and **C** represent 20  $\mu$ m. Data are represented as mean plus SEM. \*\*\*P < 0.0005.

TNRC6B pool to the nucleus as it was the case with overexpressed TNRC6B.

Taken together, all three human TNRC6 proteins shuttle between the nucleus and cytoplasm and their export route seems to be Crm1-dependent.

As nuclear trapped TNRC6A-C formed P-body like structures after overexpression, we investigated whether the observed nuclear foci resemble cytoplasmic P-bodies. This might provide information on possible nuclear TNRC6 functions. In addition, we were interested whether nuclear TNRC6 colocalizes with known nuclear compartments. We therefore performed colocalization experiments by confocal microscopy with nuclear trapped TNRC6A. As LMB treatment might affect localization of a broad spectrum of proteins, we specifically shifted TNRC6A into the nucleus by using a nuclear-trapped TNRC6A mutant, which contains mutations within the NES (Nishi et al., 2013). As expected, the mutant was exclusively nuclear and formed the expected nuclear foci (Figure 3.3.10 and Appendix Figure A4). We next tested colocalization with Ago2 (Figure 3.3.10 A). Ago2 partially colocalized with the nuclear TNRC6A foci, however non-colocalizing Ago2 and TNRC6A was also present, indicating that nuclear TNRC6A and Ago2 can interact but are also present as independent pools. We then investigated colocalization with other P-body components including YB-1, CNOT7 and Lsm4 (Appendix Figure A4 E). However, none of the mentioned factors were present in these foci, indicating that the nuclear TNRC6 foci are different compared to cytoplasmic P-bodies. Similarly, we did not find an overlap with diverse nuclear compartments including PML bodies, nuclear speckles, Cajal bodies, paraspeckles and heat shock granules (Appendix Figure A4 C). As antibodies were available, we also tested possible colocalization with DNA double-strand breaks, the exosome, RNA-polymerases and the ubiquitin-proteasome system, but did not find any overlap (Appendix Figure A4 D and E).

From these data, we conclude that the nuclear trapped TNRC6 proteins form foci in the nucleus, which lack typical P-body markers but can still interact with Ago proteins. Future studies will therefore be needed, to investigate the significance and possible function of these nuclear TNRC6 pool.

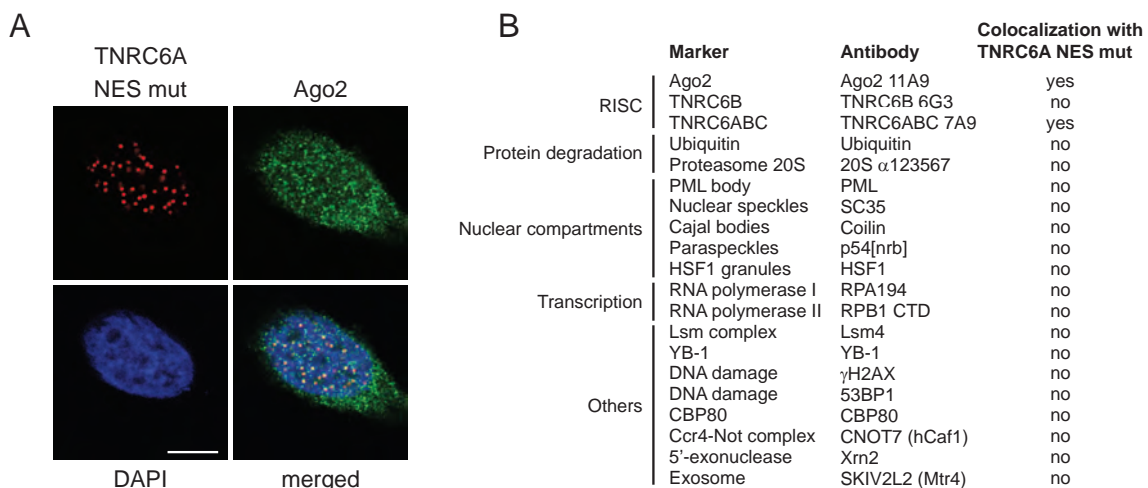


**Figure 3.3.10. Nuclear trapped TNRC6A colocalizes with Ago2.** **A** Colocalization of endogenous Ago2 with nuclear trapped TNRC6A NES mutant (NESmut). **B**, Tabular summary of the performed colocalization analyses as shown in Appendix Figure A4. Scale bars in **A** represent 20  $\mu$ m.

## 3.5. Nuclear import of TNRC6 proteins is mediated by Imp $\alpha$ and Imp $\beta$

### 3.5.1. Nuclear import of TNRC6 proteins requires Imp $\beta$

To elucidate the nuclear import pathway of TNRC6 proteins, we investigated which importins are needed for nuclear import of TNRC6 proteins by loss-of-function analysis. As a test system, we used the nuclear trapped TNRC6A NES mutant in a stably transfected inducible HEK 293T cell line (Figure 3.3.11). We screened this cell line with the previously established importin siRNA library. Two days after siRNA transfection, TNRC6A NES mutant expression was induced and 24 hours later, TNRC6A NES mutant was localized via its eGFP tag. Strikingly, we observed a strong decrease in nuclear localized TNRC6A NES mutant upon transfection of two independent Imp $\beta$  siRNAs. However, transfection of siRNAs against any other human Importin did not affect TNRC6A NES mutant localization (Figure 3.3.11, data shown for a representative subset of siRNAs). Therefore, we conclude that TNRC6A import requires Imp $\beta$  but is independent of other importins.

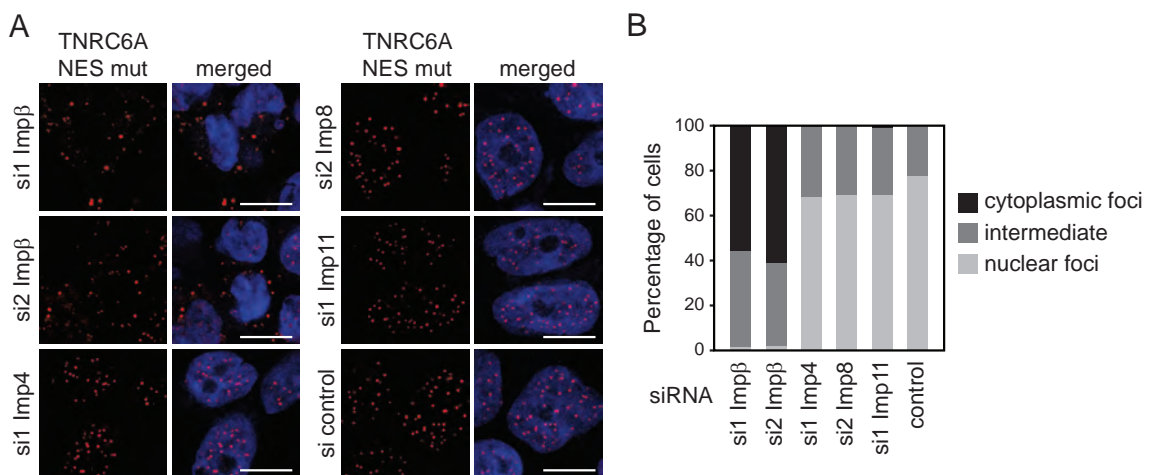


**Figure 3.3.11. Nuclear Import of TNRC6 proteins is facilitated by Imp $\beta$ .** **A**, HEK 293T cells with inducible nuclear trapped myc-GFP-TNRC6A NES mut were transfected with the Importin siRNA library. TNRC6A NES mut was localized by detection of GFP fluorescence. **B**, Diagram showing the percentage of cells with cytoplasmic or nuclear GFP foci and cells with foci in both compartments (intermediate). Scale bars in A represent 10  $\mu$ m.

To further verify this strict Imp $\beta$  dependency, we analyzed localization of endogenous TNRC6B after Imp $\beta$  knockdown (Figure 3.3.11). As the nuclear TNRC6B pool was very low under steady-state conditions, we additionally treated cells with LMB to investigate whether shuttling is Imp $\beta$ -dependent. As expected from our previous results, endogenous TNRC6B accumulates in the nucleus upon LMB treatment. Strikingly, when Imp $\beta$  was depleted by RNAi, nuclear accumulation of TNRC6B was not observable upon LMB treatment. This shows that Imp $\beta$  knockdown prevents nuclear import of endogenous TNRC6B. These data were reproduced using a second independent Imp $\beta$  siRNA (data not shown).

Taken together, we conclude that TNRC6 proteins are imported by an Imp $\beta$ -dependent pathway into the nucleus. In addition, as we did not observe effects of Imp $\beta$  on Ago2 nuclear import, we suggest that both TNRC6 and Ago proteins follow different import routes and are imported independently.

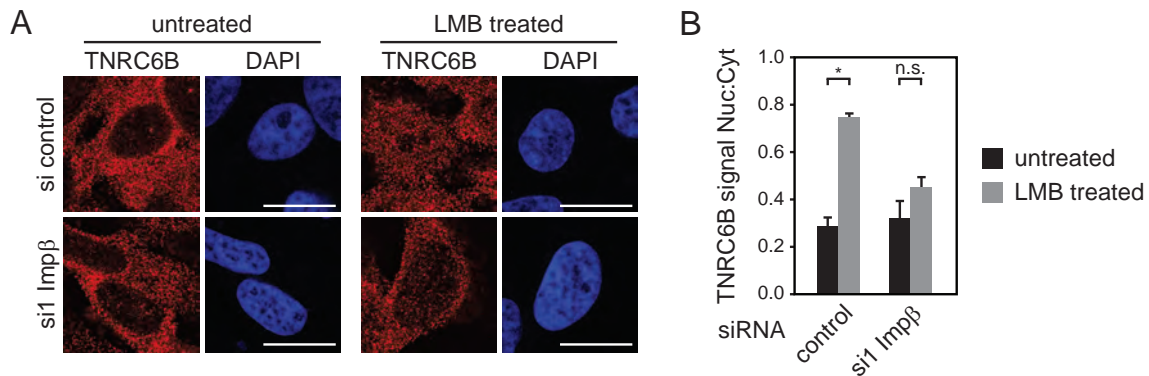


**Figure 3.3.12. Imp $\beta$  is needed for nuclear import of TNRC6B but not Ago2.** **A** and **B**, Endogenous TNRC6B was detected in untreated or Leptomycin B treated cells upon knockdown of Imp $\beta$  or transfection of a control siRNA. Diagram in **B** shows quantification of TNRC6B signal shown as nucleus-to-cytoplasm ratio. LMB, Leptomycin B. Scale bars in **A** and **C** represent 20  $\mu$ m. Data are represented as mean plus SEM. \* $P < 0.05$ ; n.s., not significant.

### 3.5.2. TNRC6 proteins interact with Imp $\alpha$ and Imp $\beta$

During classical import, Imp $\alpha$  binds an NLS of a cargo protein and recruits Imp $\beta$ , which facilitates translocation through the nuclear pore complex. In contrast, non-classical Imp $\beta$ -dependent import can be mediated by direct interaction of Imp $\beta$  with the cargo protein (Jäkel and Görlich, 1998, Görlich and Kutay, 1999). To test interactions between Imp $\alpha$ , Imp $\beta$  and TNRC6 proteins, we performed *in vitro* binding assays by pulldown of *in vitro* transcribed and translated TNRC6A with GST-tagged importins (Figure 3.3.13).

We first tested interactions for classical import with Imp $\alpha$  and Imp $\beta$ . Since Imp $\beta$  affects Imp $\alpha$ 's binding affinity to cargo proteins and *vice versa* (Fanara et al., 2000, Kobe, 1999), binding of both proteins was analyzed simultaneously (Figure 3.3.13 A). GST-Imp $\alpha$  family members (Imp $\alpha$ 1,  $\alpha$ 3,  $\alpha$ 4,  $\alpha$ 5,  $\alpha$ 7) were immobilized and incubated with His-Imp $\beta$  and radiolabeled TNRC6A. Strikingly, we found robust binding of TNRC6A for most Imp $\alpha$  family members in the presence of Imp $\beta$ . To validate specificity of the interaction, we performed binding experiments with TNRC6A containing mutations in the recently suggested NLS (Figure 3.3.13 B, Nishi et al., 2013). Indeed, binding of Imp $\alpha$ /Imp $\beta$  to this mutant appeared to be weakened compared to wildtype control, indicating that Imp $\alpha$ /Imp $\beta$  uses this NLS for binding. To validate that Imp $\alpha$  binds TNRC6A directly and independently of Imp $\beta$ , we performed pulldowns with GST-Imp $\alpha$  and radiolabeled TNRC6A alone (Figure 3.3.13 C). We still observed binding of Imp $\alpha$  to TNRC6A, albeit the amount of pulled down TNRC6A was different between the tested Imp $\alpha$  subtypes compared to the reactions with His-Imp $\beta$ . However, because our pulldowns were not quantitative, interpretations regarding affinities and direct comparison of different binding assays is not possible so far.

We next analyzed the non-classical import scenario by direct binding of Imp $\beta$  to TNRC6A. We also identified robust binding of GST-Imp $\beta$  alone to radiolabeled TNRC6A (Figure 3.3.13 A to C, lane 7). This binding seems to be independent of the reported NLS sequence in TNRC6A, because we did not observe an obvious decrease of GST-Imp $\beta$  pulled down TNRC6A NLS mut (Figure 3.3.13 A to C). As our experiments suggest that at least Imp $\beta$  can bind TNRC6A directly but independently of its previously identified NLS, we further validated the functionality of the reported NLS. We performed LMB treatments with TNRC6A NLS mutant and presuming that the identified NLS is sufficient for TNRC6A import, TNRC6A NLS mutant should remain cytoplasmic (Figure 3.3.14). While wildtype TNRC6A was trapped in the nucleus upon LMB treatment, the NLS mutated variant remained only partially cytoplasmic. Therefore, the reported NLS seems to

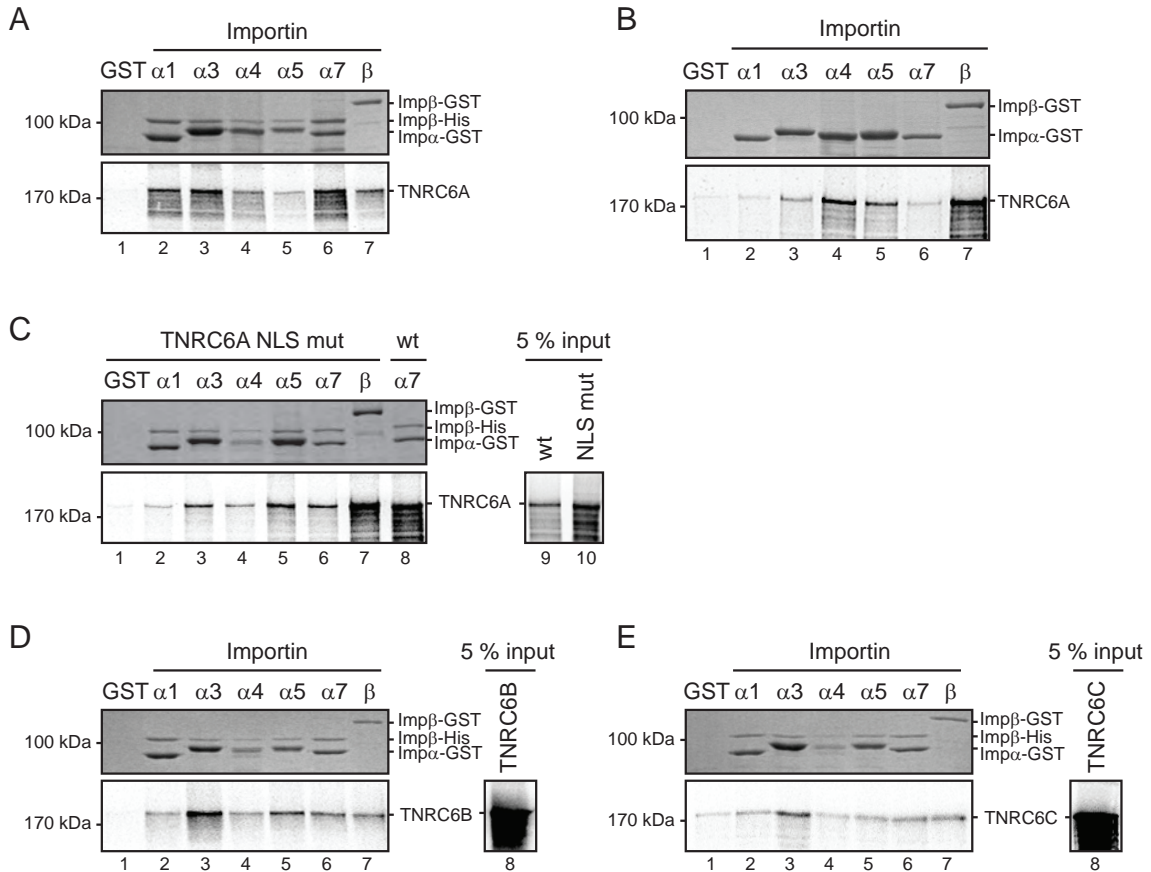


**Figure 3.3.13. TNRC6A-C interact with Imp $\alpha$  and Imp $\beta$ .** **A**, *In vitro* transcribed and translated TNRC6A was incubated with recombinant GST alone (lane 1), GST-tagged Imp $\alpha$ -family members and Imp $\beta$ -His (lane 2 to 6) or Imp $\beta$ -GST alone (lane 7) followed by GST-pull-down. TNRC6A was detected by autoradiography, recombinant proteins by Coomassie staining. **B**, Same experiment as described in A but with TNRC6A NLS mutant. Wildtype TNRC6A with Imp $\alpha$ 7 was loaded as control in lane 8. Inputs are shown in lane 9 and 10. **C**, Same experiment as described in A but without addition of Imp $\beta$ -His. **D** and **E**, Same experiment as described in A with *In vitro* transcribed and translated TNRC6B (D) and TNRC6C (E). NLS, nuclear localization sequence.

affect nuclear import of TNRC6A but does not fully abolish its import. This indicates that a so far unidentified second NLS might exist in TNRC6A.

To get insights into importin binding of TNRC6B, we performed binding experiments with Imp $\alpha$  and Imp $\beta$  (Figure 3.3.13 D and E). Of note, both TNRC6B and TNRC6C were not conserved in the NLS that is present and functional within TNRC6A. Similarly to TNRC6A, Imp $\beta$  alone or in combination with Imp $\alpha$  variants bound TNRC6B and TNRC6C. However, the amount of pulled down TNRC6B and TNRC6C were seemingly lower, but this has to be investigated further in quantitative experiments.

Taken together, our binding experiments suggest two different import routes for TNRC6 proteins. First, TNRC6 is imported via the classical Imp $\alpha$ /Imp $\beta$  pathway by directly binding Imp $\alpha$ . Second, we suggest a second non-classical import route by direct binding to Imp $\beta$  via a so far unknown second NLS.

### 3.5.3. miRNA-mediated gene silencing is affected by Imp $\beta$

We have established that nuclear import of TNRC6 proteins requires Imp $\beta$ . In addition, TNRC6 proteins can shuttle between the nucleus and the cytoplasm. During translocation through the nucleus, TNRC6 proteins should not be available for miRNA-mediated post-transcriptional gene

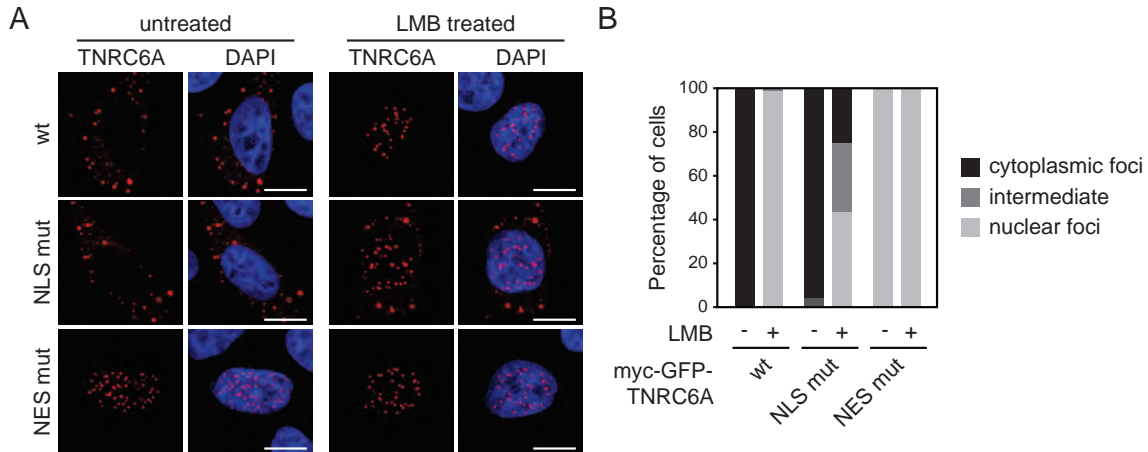


**Figure 3.3.14. LMB treatments with a TNRC6A NLS mutant suggest the existence of a second NLS in TNRC6A.** **A**, HeLa cells were transfected with myc-GFP-TNRC6A wildtype, NLS mut or NES mut. Cells were then treatment with Leptomycin B or control treatment. **B**, Diagram shows percentage of cells with cytoplasmic or nuclear GFP foci or foci in both compartments (intermediate). Scale bars in A represent 10  $\mu$ m.

silencing, a process that seems to take place in the cytoplasm. To test this hypothesis, we analyzed the efficiency of miRNA-mediated post-transcriptional gene silencing on an artificial miRNA reporter. This reporter contains firefly luciferase with Hmga2 3'-UTR, which harbors multiple miRNA binding sites including sites for the miRNA let-7. Therefore, firefly is under post-transcriptional control by the Hmga2 3'-UTR. Cells were transfected with siRNAs against Imp $\beta$  and the Hmga2 3'-UTR luciferase reporter plasmid (Figure 3.3.15). As control, we transfected inhibitors against let-7a, and as expected, inhibition of let-7a led to a strong derepression of the reporter (Figure 3.3.15). Interestingly, depletion of Imp $\beta$  resulted in an elevated silencing activity, suggesting that retention of TNRC6 proteins in the cytoplasm positively affects gene silencing by miRNAs. Therefore, the transition of TNRC6 proteins through the nuclear pore seems to directly influence cytoplasmic gene silencing by miRNAs.

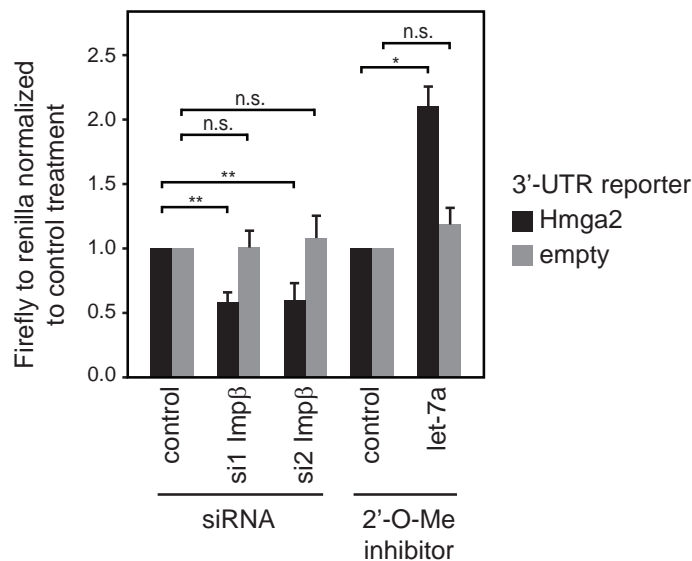


**Figure 3.3.15. Knockdown of Imp $\beta$  increases miRNA-mediated gene silencing.** HeLa cells were transfected with Imp $\beta$  siRNA or control siRNA and a Hmga2 3'-UTR reported or an empty reporter. As positive control, miRNA inhibitors against let-7a or control inhibitors were transfected. Firefly is under control of the Hmga2 3'-UTR. Firefly activity was normalized to renilla luciferase and control siRNA or control inhibitor. Data are shown as mean plus SEM. \*P < 0.05; \*\*P < 0.005; n.s., not significant.

## 3.6. Cytoplasmic Ago and TNRC6 levels influence nuclear localization

### 3.6.1. Cytoplasmic retention mechanisms of Argonaute and TNRC6

Both Ago and TNRC6 proteins can shuttle through the nucleus by presumably independent pathways. In addition, both proteins can interact with each other in the cytoplasm and the nucleus. Thus, we investigated whether both proteins can influence each others import. To do so, we coexpressed Ago2 and TNRC6A as wildtype proteins and different mutants (Figure 3.3.16). As expected, both wildtype proteins were found to colocalize in the cytoplasm. Strikingly, expression of the normally nuclear-trapped TNRC6A NES mutant with wildtype Ago2 resulted in an exclusively cytoplasmic TNRC6A NES mutant. This suggests that high levels of Ago2 retain TNRC6A in the cytoplasm. This cytoplasmic retention seems to depend on small RNA binding of Ago2 since

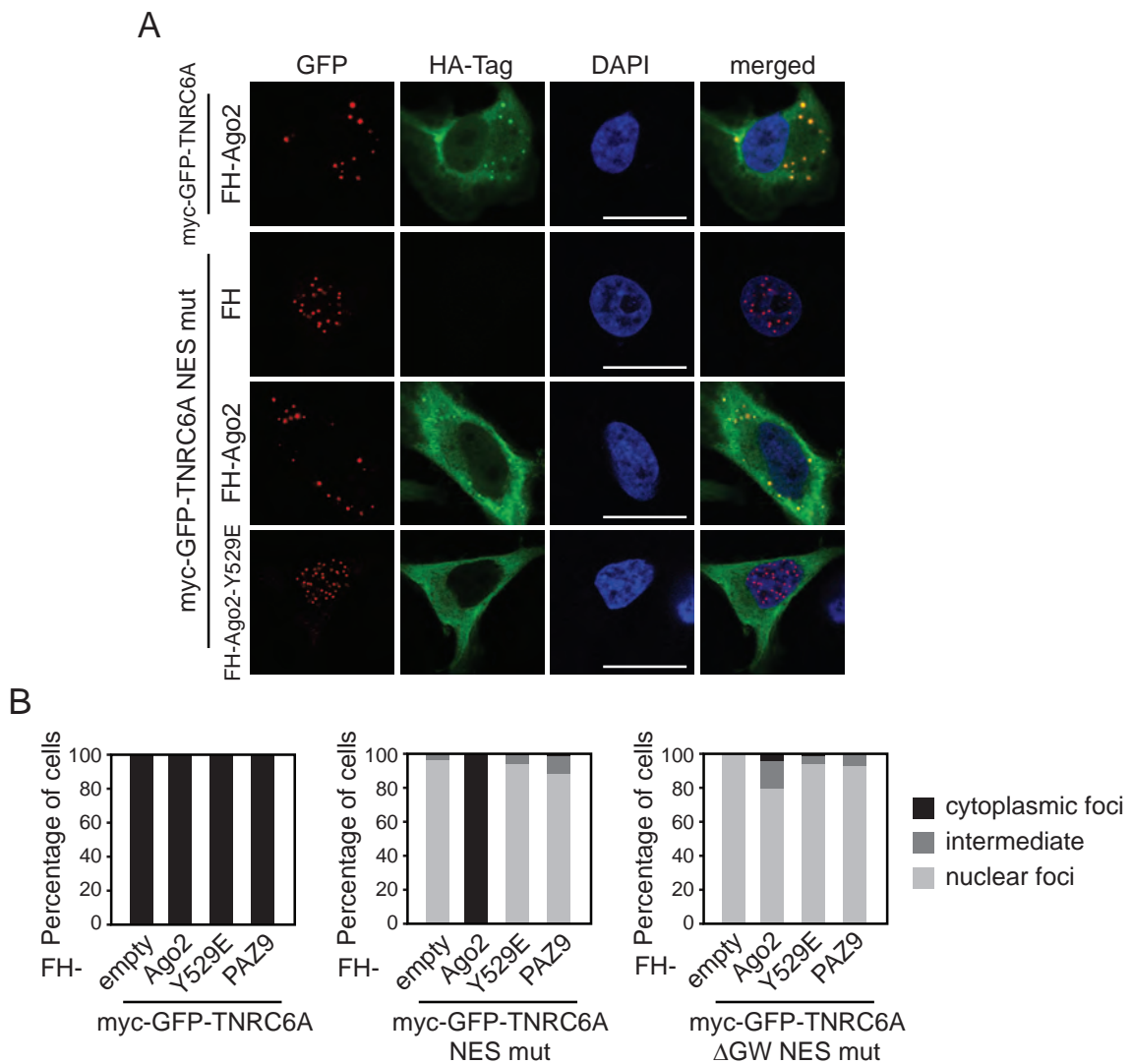


**Figure 3.3.16. Cytoplasmic retention of TNRC6 and Ago2.** **A**, Coexpression of myc-GFP-TNRC6A wildtype, NES mut or  $\Delta$ GW NES and FH-Ago2 wildtype, Y529E, PAZ9 or empty plasmid (FH). TNRC6A and its mutants were detected by GFP signal, Ago2 and its mutants with anti-HA antibody staining. **B**, Percentage of cells with cytoplasmic or nuclear GFP foci or foci in both compartments (intermediate). Ago2 PAZ9 and myc-GFP-TNRC6A  $\Delta$ GW NES are shown in the diagrams only. Scale bars in A represent 20  $\mu$ m.

Ago2 Y529E, which cannot bind miRNAs, does not retain TNRC6A in the cytoplasm. This was also observed for another miRNA binding deficient Ago2 mutant referred to as Ago2 PAZ9 (data not shown, Liu et al., 2005b). As negative control, we analyzed cytoplasmic retention with a TNRC6 protein that contains a deleted Ago2 binding motif together with the mutated NES (TNRC6A  $\Delta$ GW NESmut, Figure 3.3.16 B). As expected, this Ago2-binding deficient mutant still accumulates in the nucleus indicating that indeed binding of Ago2 mediates nuclear retention. Of note, the nuclear localization of TNRC6A  $\Delta$ GW NESmut further supports the finding, that both proteins are imported independently.

To support the identified nuclear retention mechanism, we investigated localization of the endogenous proteins upon knockdown of the respective interaction partner. Knockdown of single TNRC6 proteins did not significantly increase nuclear Ago2 levels. However, when TNRC6A-C were knocked down simultaneously, nuclear Ago2 levels increased significantly (Figure 3.3.17). Therefore, also TNRC6 can influence the nuclear localization of Ago2. Because the observed effects were only visible upon knockdown of all three TNRC6 proteins but not after separate knockdown, this finding indicates redundant functions of TNRC6 proteins in this retention mechanism. Surprisingly, upon knockdown of Ago1-4 we did not observe a significant increase of nuclear TNRC6B (data not shown). So far we can only speculate that the observed reduction of Ago protein to about 50% remaining protein might not be sufficient to observe the expected effects. However this has to be analyzed further in future studies.

Taken together, we observed that TNRC6 and Ago proteins influence each others import by a cytoplasmic retention mechanism. This mechanism depends on the interaction of both proteins in the cytoplasm and is regulated by miRNA-binding.

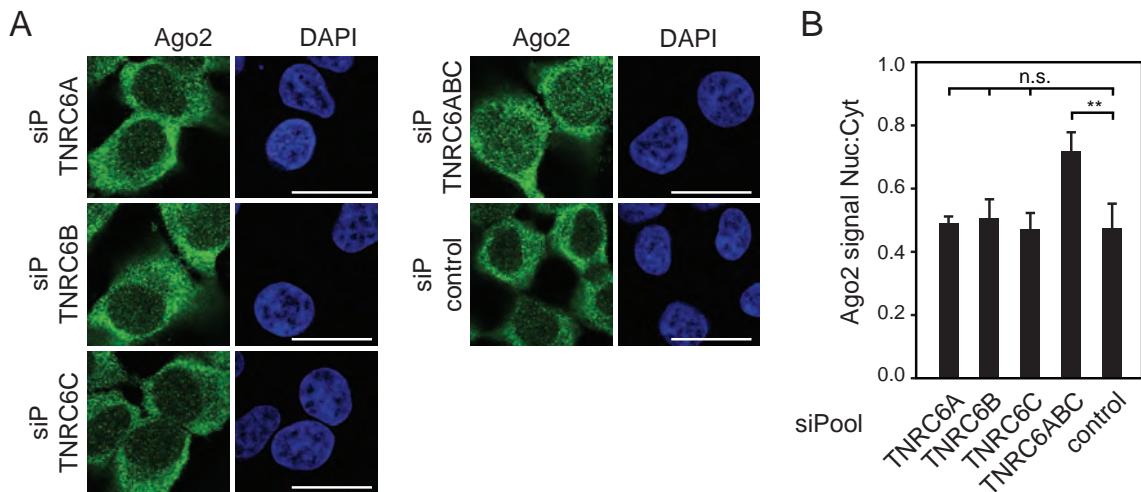


**Figure 3.3.17. Decreased levels of TNRC6A-C increase nuclear Ago2 pool.** **A**, HeLa cells were transfected with siPools to knockdown TNRC6A-C alone or simultaneously and endogenous Ago2 was detected by IF with anti-Ago2 antibody. **B**, Signal quantifications of cells as shown in **A** are presented as nucleus-to-cytoplasm ratios. Scale bars in **A** represent 20  $\mu$ m. Data in **B** are shown as mean plus SEM. \*\* $P < 0.005$ ; n.s., not significant.

### 3.6.2. Ago2 prevents binding of TNRC6A-importin interaction

Since the reported NLS in TNRC6A is close to the Ago2-binding domain, we asked whether importin and Ago2 binding to TNRC6 might be mutually exclusive (Figure 3.3.18 A). This could mechanistically explain the observed cytoplasmic retention mechanism. To test this hypothesis, GST-Imp $\beta$  alone or GST-Imp $\alpha$  with His-Imp $\beta$  was immobilized and incubated with radiolabeled

TNRC6A (Figure 3.3.18 B and C). In addition, recombinant HA-Ago2 was added to the reactions or not. Strikingly, when HA-Ago2 was present in the reactions, both the direct binding GST-Imp $\beta$  as well as GST-Imp $\alpha$ /His-Imp $\beta$  binding to TNRC6A was completely blocked by Ago2. Therefore, Ago2 seems to preferentially bind TNRC6A and can block accessibility of the importin binding sites. To exclude binding of recombinant Ago2 to Imp $\alpha$  and Imp $\beta$  in these assays, we performed direct Ago2 binding experiments (Figure 3.3.18 A). As expected, HA-Ago2 bound specifically to a TNRC6B peptide containing the Ago binding motif (TNRC6B 599-683, Pfaff et al., 2013), however binding to Imp $\alpha$  and Imp $\beta$  was not observed. This indicates that Ago2 blocks Imp $\alpha$  and Imp $\beta$  binding to TNRC6A via direct interaction with TNRC6A. In addition, this further supports the finding that Ago2 is not imported via Imp $\alpha$  and Imp $\beta$ .

Taken together, we have identified a mechanism of mutually exclusive binding of Imp $\alpha$ /Imp $\beta$  and Ago2 to TNRC6A. TNRC6A seems to preferentially bind Ago2 and bound Ago2 can mask accessibility of the identified classical NLS and the not yet identified second NLS. Consequently, Imp $\alpha$  and Imp $\beta$  cannot mediate import TNRC6 any more (Figure 3.3.16 A). However, when Ago2 is not present, the NLS sequences are accessible and can mediate nuclear import of TNRC6 via Imp $\beta$ - and Imp $\alpha$ /Imp $\beta$ -dependent pathways.

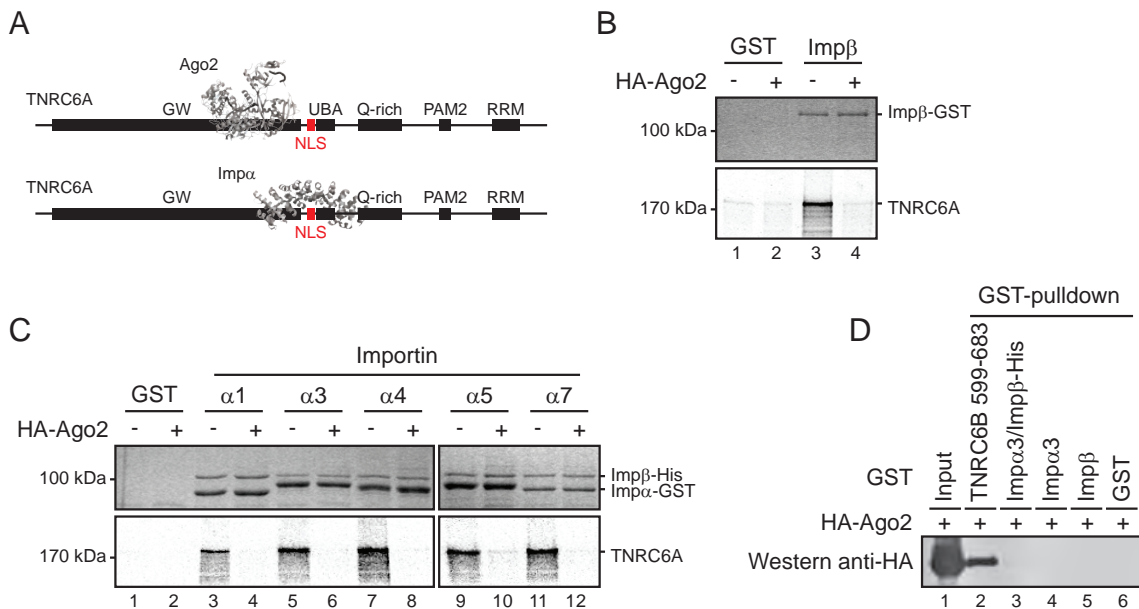


**Figure 3.3.18. Ago2 affects TNRC6A NLS accessibility.** **A**, Schematic representation of the proposed mechanism by which Ago2 blocks accessibility of TNRC6A NLS for Imp $\alpha$  and Imp $\beta$ . **B**, *In vitro* transcribed and translated TNRC6A was incubated with recombinant GST (lane 1 and 2) or Imp $\beta$ -GST (lane 3 and 4). Recombinant HA-Ago2 was added when indicated (even lanes). After GST-pulldown, TNRC6A was detected by autoradiography, recombinant proteins by Coomassie staining. **C**, GST-tagged Imp $\alpha$ -family members and Imp $\beta$ -His (lane 3 to 12) were mixed with *In vitro* transcribed and translated TNRC6A. Recombinant HA-Ago2 was added when indicated (even lanes). **D**, TNRC6B 599-683 (lane 2), Imp $\alpha$ 3-GST and Imp $\beta$ -His (lane 3), Imp $\alpha$ 3-GST (lane 4), Imp $\beta$ -His (lane 5) and recombinant GST (lane 6) were incubated with recombinant HA-Ago2. HA-Ago2 was detected in pulldowns by anti-HA antibody Western.

## 4. Discussion of Part III

Mammalian Ago proteins are key players in miRNA-mediated gene silencing processes in the cytoplasm. However, Ago proteins have also been implicated in various nuclear functions ranging from transcriptional regulation to DNA double-strand break repair and alternative splicing. Although still conversely discussed, those nuclear Ago functions might play important roles beyond cytoplasmic miRNA-mediated regulation. Furthermore, other gene silencing factors like TNRC6 proteins can localize to the nucleus as well, however, their nuclear functions have not been elucidated yet. Nuclear import is a prerequisite for nuclear functions and might provide an important regulatory mechanism that could affect cytoplasmic as well as nuclear Ago and TNRC6 functions. As nuclear import of Ago and TNRC6 proteins is almost totally uncharacterized so far, we wanted to identify nuclear import pathways of Ago and TNRC6 proteins and to unravel mechanisms that regulate nuclear import.

### **Nuclear localization and transport of Ago2**

To provide a solid basis for the analysis of nuclear transport pathways, we show that human Ago2 is indeed found in the nucleus and that we specifically detect Ago2 by immunofluorescent stainings. Nuclear localization of Ago proteins has been observed in numerous publications before by immunofluorescence or nucleo-cytoplasmic extractions (Meister et al., 2004b, Robb et al., 2005, Rüdél et al., 2008, Ohrt et al., 2008, Weinmann et al., 2009, Chu et al., 2010, Benhamed et al., 2012, Gagnon et al., 2014). Quantitative analysis of the obtained immunofluorescence data further suggested that only a minor portion of Ago2 is present in the nucleus in most human cell lines investigated. Although we only identified minor proportions of Ago2 in the nucleus, conditions might exist which accompany increased nuclear Ago2 localization. For example, it has been reported that Ago2 proteins are found in the nucleus upon senescence induction (Benhamed et al., 2012).

To show nuclear transport processes of Ago proteins *in vivo*, we directly measured nuclear import of Argonaute proteins in heterokaryon assays. We show that Ago2 travels into the nucleus in this system and therefore provide the first direct insight into nuclear Ago2 import.

Because Ago2 is imported into the nucleus but is mainly cytoplasmic under steady-state conditions, we investigated whether Ago2 can shuttle between the nucleus and cytoplasm. Using Leptomycin B (LMB) treatment, we show that nuclear Ago2 increases when Crm1-mediated export is inhibited. Importantly, however, we did not observe a complete shift of Ago2 into the nucleus, indicating that only a part of the cellular Ago pool shuttles between the nucleus and cytoplasm. Although LMB is thought to specifically inhibit Crm1-mediated export, it is also conceivable, that Ago proteins use additional export routes, which have not been analyzed in this study. One example would be nuclear export bound to mRNAs, a mechanism that should be investigated in future studies. Furthermore, direct interaction of Ago2 with Crm1 should be analyzed followed by identification of the necessary nuclear export signal in Ago2.

We were further able to validate these observations with heterokaryon assays using overex-

pressed and tagged Ago proteins. Similar as observed for LMB treatment, Ago2 shuttled through the nucleus in this assays when fused to a classical NLS. Of note, although we measured shuttling of Flag/HA-NLS-Ago2 in this assay, we did not observe shuttling of Flag/HA-Ago2 upon LMB treatment, a result which has not been shown. However, we do not know whether overexpression or the N-terminal tag might affect shuttling of Flag/HA-Ago2. Furthermore, we suggest that residual shuttling activity is retained in both Flag/HA-NLS-Ago2 and Flag/HA-Ago2, however, we only observed shuttling with the more sensitive heterokaryon assay.

The observed shuttling activity of Ago2 and its nuclear localization presumes active nuclear transport pathways, because Ago2 can not passively diffuse through the nuclear pore due to its size. The nuclear transport receptor Importin 8 (Imp8) has recently been implicated in the cytoplasmic function of miRNAs and was reported to eventually contribute to nuclear localization of mature miRNAs and Ago2 (Weinmann et al., 2009, Wei et al., 2014). However, by targeting the nuclear RNA 7sk, we find that knockdown of Imp8 did not affect nuclear RNA interference (RNAi) by Ago2-mediated cleavage of the nuclear target. We also did not observe a decrease of the nuclear Ago2 pool upon Imp8 knockdown. In addition to Imp8, none of the other tested import receptors changed nuclear RNAi efficiency and Ago2 localization. Using different biochemical assays, we further tried to directly identify Ago2-bound import receptors. Both in human cell extracts and *Xenopus* oocyte extracts, Ago2 did not coprecipitate with detectable importins. However, because only a minor pool of Ago2 seems to be imported into the nucleus, only a small proportion of Ago2 might transiently interact with importins, which might complicate biochemical identification. We therefore suggest that importins function redundantly and several import receptors can mediate nuclear import of Ago2. Such redundant import pathways have been found for several proteins before including the miRNA-biogenesis factor Dicer, which can be imported by redundant action of Imp $\beta$ , Imp7 and Imp8 (Doyle et al., 2013).

In addition to the tested import pathways, future analysis should analyze importin-independent transport by direct interaction with the nuclear pore. One might speculate, that Ago interacts with the phenylalanine residues of the FG-repeat meshwork in the nuclear pore in a similar way it binds tryptophan residues of TNRC6 proteins. Indeed, the tryptophan binding pockets mainly function by hydrophobic interactions rather than specific stacking interactions and have affinity to phenol (Schirle and MacRae, 2012). In addition, most phenylalanines within the FG-repeats are 10 to 20 amino acids apart, which is in the range of the distance needed to bind into both tryptophan binding pockets of Ago2 (Wente and Rout, 2010, Pfaff et al., 2013). Of note, this binding scenario would also provide an explanation how TNRC6 could mediate the observed cytoplasmic retention of Ago proteins, as both TNRC6 and the NPC FG-repeats would use the same binding mechanism.

### **Nuclear localization and transport of TNRC6 proteins**

Similar to Ago proteins, TNRC6 proteins localize predominantly to the cytoplasm as shown before by nucleocytoplasmic fractionations and immunofluorescent analysis of overexpressed TNRC6A-C (Meister et al., 2005, Jakymiw et al., 2005, Liu et al., 2005a, Lazzaretti et al., 2009, Gagnon et al., 2014).

Here, we clearly show that all three human TNRC6 proteins shuttle between the nucleus and cytoplasm and are trapped in the nucleus when Crm1-mediated export is inhibited by LMB. This has been observed for TNRC6A and TNRC6B before and a classical nuclear export signal (NES) for TNRC6A has been identified (Till et al., 2007, Nishi et al., 2013). To get insights into the in-

tracellular localization of endogenous TNRC6 and to validate the observed shuttling activity, we generated an antibody that detects TNRC6B in Western Blot and immunofluorescent stainings with high specificity. We show that endogenous TNRC6B is mainly cytoplasmic with similarly low nucleo-cytoplasmic ratios as observed for endogenous Ago2. Furthermore, endogenous TNRC6B partially accumulated in the nucleus upon LMB treatment and therefore, at least a part of endogenous TNRC6 proteins shuttles between the nucleus and cytoplasm.

We then took advantage of the nuclear localization of a TNRC6A nuclear export sequence (NES) mutant and found that Imp $\beta$  is needed for nuclear import of TNRC6A. Furthermore, none of the other tested import receptors affected nuclear localization of TNRC6A, indicating that TNRC6 import is strictly Imp $\beta$ -dependent. Imp $\beta$  did not affect nuclear Ago2 localization and function, indicating that both protein families are imported via different transport routes and are not co-imported. To further characterize the Imp $\beta$ -dependent nuclear transport routes of TNRC6 proteins, we used biochemical assays to directly show importin-TNRC6 binding. During classical nuclear import, Imp $\alpha$  binds an NLS on the cargo protein and associates with Imp $\beta$ , which facilitates transport through the nuclear pore complex (Görlich et al., 1995). Alternatively, Imp $\beta$  can directly contact cargo proteins and mediate non-classical import (Jäkel and Görlich, 1998). We find that Imp $\alpha$  binds a previously identified NLS on TNRC6A and that Imp $\beta$  participates in this interaction. In addition, Imp $\beta$  can contact TNRC6A-independently of Imp $\alpha$ , presumably via a so far unknown second NLS. Although the *in vitro* binding data should be further validated by co-immunoprecipitations, we suggest that Imp $\beta$  facilitates transport of TNRC6 proteins into the nucleus via a classical Imp $\alpha$ -dependent route and by direct interaction with TNRC6.

Interestingly, we and others found that overexpressed human TNRC6 proteins can form distinct foci in the nucleus. We analyzed these structures further and found that they neither resemble cytoplasmic P-bodies nor known nuclear structures. Furthermore, none of the other proteins investigated here were present in the nuclear TNRC6 foci. Only a sub-pool of nuclear Ago2 can be found in these structures. Therefore, we speculate that TNRC6 proteins can form these foci independent of any other cytoplasmic P-body component. This might be mediated by functioning as a scaffold protein which forms a meshwork by numerous interactions of the GW repeats in the large unstructured N-termini. Similar mechanisms might be responsible for the formation of RNA granules and also the better characterized FG-repeat meshwork of the nuclear pore complex (Frey and Görlich, 2007, Wentz and Rout, 2010, Han et al., 2012, Kato et al., 2012). Therefore, these nuclear foci might provide an interesting system to investigate P-body and RNA granule formation *in vivo* and to better understand the function of TNRC6 proteins in general. Of note, the comparison of endogenous Ago2 and TNRC6 stainings showed very similar granular patterns of the cytoplasmic signals. Because we only observed microscopically visible P-bodies upon overexpression of P-body components, we speculate that the observed granular pattern might represent submicroscopical P-bodies and that this granularity has functional implications for miRNA-mediated gene silencing. Therefore, future studies are needed to investigate this staining pattern with higher resolution.

### **Cytoplasmic retention of Ago and TNRC6 proteins**

We have shown that Ago and TNRC6 proteins are imported via different import routes. In addition, localization and quantification of the endogenous proteins revealed similar nucleo-cytoplasmic distributions of Ago and TNRC6 and both protein families partially accumulated in the nucleus upon LMB treatment. Therefore, we speculated whether Ago and TNRC6 proteins might influ-

ence each others nuclear transport pathways. We coexpressed Ago and TNRC6 proteins and different mutants thereof. Interestingly, when overexpressing Ago2, even the normally nuclear localized TNRC6A NES mutant remains in the cytoplasm. This suggested that Ago proteins can prevent nuclear import of TNRC6 proteins. In the cytoplasm, Ago2 and the TNRC6A NES mutant clearly colocalized, indicating that interaction of both proteins might affect nuclear transport. Interestingly, a miRNA-binding deficient Ago2 mutant was not able to retain TNRC6 in the cytoplasm, indicating that Ago and TNRC6 only stably interact when miRNAs are bound to Ago2. We further show that a loss of TNRC6 proteins results in an increased nuclear Ago2 pool, indicating that also TNRC6 proteins can prevent nuclear import of Ago proteins. In contrast to the proposed cytoplasmic retention mechanism, we found that Ago-binding deficient TNRC6 mutants are still mainly cytoplasmic (data not shown). This observation, however, might be explained by interaction with Ago1, 3 and 4 as it is not known whether Ago2-binding deficient TNRC6 mutants can still interact with the other Ago proteins (Baillat and Shiekhattar, 2009, Nishi et al., 2013, Pfaff et al., 2013). Alternatively, we suggest that not all Ago-free TNRC6 is immediately imported into the nucleus and that so far unknown regulatory processes exist to regulate TNRC6 or Ago import. One attractive possibility would be post-translational modifications, which have been shown to regulate NLS and NES function in diverse proteins (Nardozi et al., 2010).

Using biochemical assays, we further identified a mechanism by which Ago2 can regulate nuclear import of TNRC6 proteins. We found that Ago2-TNRC6 binding blocks the accessibility of the previously identified NLS and therefore prevents binding of Imp $\alpha$ /Imp $\beta$ . Furthermore, direct binding of Imp $\beta$  was also prevented in the presence of Ago2, indicating that both proposed nuclear transport mechanisms are regulated by Ago2 binding. How Ago2 blocks the NLS is not known so far, however the small distance between the Ago2 binding-site and the NLS might result in a sterical block of the NLS. In future studies, it will be interesting to see how Ago1, Ago3 and Ago4 might influence TNRC6-importin binding.

#### **A model for nuclear transport of Ago and TNRC6 proteins**

Our study provided first insights into nuclear import processes of Ago and TNRC6 proteins and show that both protein families are nucleo-cytoplasmic shuttling proteins. In addition we identified Imp $\beta$ -dependent import pathways of TNRC6 proteins and provide evidence for redundant transport pathways of Ago proteins. Finally, we uncovered a cytoplasmic retention mechanism by which both protein families can regulate each others import.

Figure 3.4.1 presents the proposed model for nucleo-cytoplasmic transport of Ago and TNRC6 proteins. In the cytoplasm, Ago and TNRC6 proteins function in miRNA-mediated post-transcriptional gene silencing. Free Argonaute and TNRC6 proteins instead can shuttle between the nucleus and cytoplasm. TNRC6 protein shuttling is mediated by import via classical Imp $\alpha$ / $\beta$ -dependent transport and non-classical Imp $\beta$ -dependent transport. Ago protein shuttling probably depends on several redundant import receptors. Both TNRC6 and Ago proteins can be exported again by the same Crm1-dependent export route. In the nucleus, Ago and TNRC6 proteins can interact and colocalize, but are also present in independent pools.

The proposed cytoplasmic retention mechanism suggests that Ago and TNRC6 proteins might travel through the nucleus in case they are not needed for miRNA-mediated gene silencing in the cytoplasm. Furthermore, it is tempting to speculate that nuclear import contributes to balanced cytoplasmic Ago and TNRC6 levels, which might be important for miRNA-mediated gene silencing in the cytoplasm. This hypothesis also includes, that rather than being imported for separate

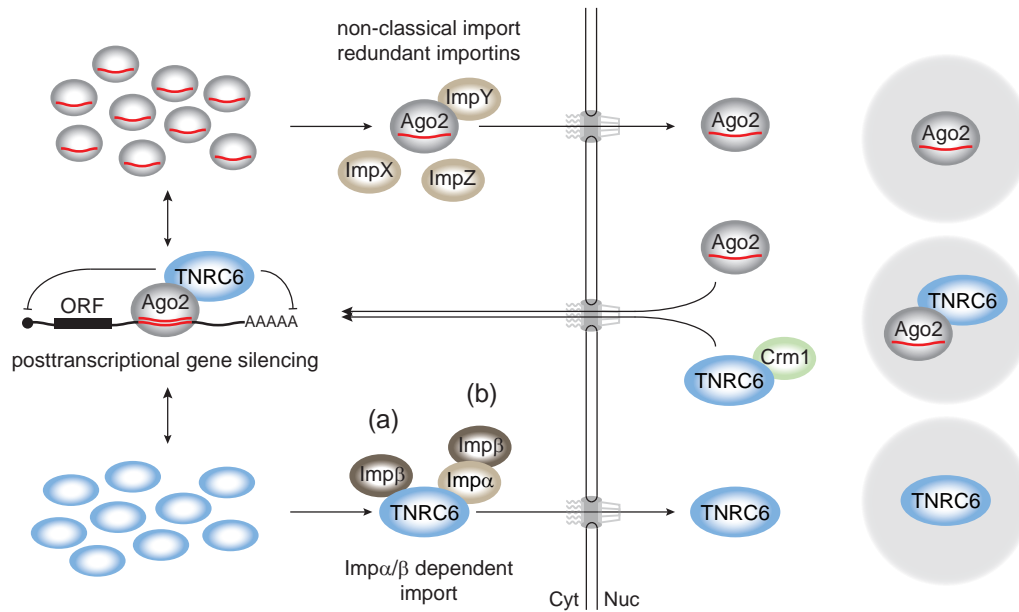


**Figure 3.4.1. A model for nuclear transport of Argonaute and TNRC6 proteins.** In the cytoplasm, Argonaute and TNRC6 proteins interact during post-transcriptional gene silencing. Free Argonaute and TNRC6 proteins instead can shuttle between the nucleus and cytoplasm which balances cytoplasmic levels. Nuclear import of TNRC6 proteins is mediated by classical Imp $\alpha/\beta$  pathway (A) as well as non-classical import via Imp $\beta$  (B). Nuclear import of Argonaute proteins instead is non-classical, Imp $\beta$ -independent and probably mediated by several redundant importins. Nuclear export of both Argonaute and TNRC6 proteins is mediated by Crm1. In the nucleus, Ago2 and TNRC6 can interact and colocalize, however, functions of these nuclear structures are not known.

nuclear functions, Ago and TNRC6 proteins might travel to the nucleus for storage. Upon increasing need of cytoplasmic gene silencing components, Ago and TNRC6 proteins can be exported again. Therefore, nuclear transport and localization of Ago and TNRC6 proteins might be a simple economic mechanism to balance cytoplasmic gene silencing components. In addition, the proposed cytoplasmic balancing model would explain why TNRC6 and Ago proteins shuttle and provides an alternative to the so far elusive functions of Ago and TNRC6 proteins in mammalian nuclei.

**Part IV.**

**Materials and Methods**

# 1. Materials

## 1.1. Chemicals and Enzymes

Unless stated otherwise, chemicals were purchased from Applichem (Darmstadt, Germany), Merck (Darmstadt, Germany), Roth (Karlsruhe, Germany) and Sigma Aldrich (Munich, Germany). All enzymes for cloning, DNA modification and RNA modification were purchased from Thermo Fisher Scientific (Waltham, USA) or New England Biolabs (Ipswich, USA). DNA oligonucleotides were ordered from Metabion (Martinsried, Germany). RNA oligonucleotides were synthesized by in-house synthesis service at Max-Planck-Institute of Biochemistry (Martinsried, Germany) or ordered at Biomers (Ulm, Germany).

## 1.2. Instruments

Instruments are described in chapter 2 to chapter 7 in the context of the respective application. All other instruments like centrifuges are listed here.

Polymax 2040	Heidolph (Schwabach, Germany)
Vortexer REAX top	Heidolph (Schwabach, Germany)
Screen Eraser-K	Bio-Rad (Hercules, USA)
Trans-Blot SD	Bio-Rad (Hercules, USA)
PowerPac HC Power Supply	Bio-Rad (Hercules, USA)
2720 Thermal Cycler	Applied Biosystems (Foster City, USA)
GeneAmp PCR System 9700	Applied Biosystems (Foster City, USA)
Mastercycler gradient	Eppendorf (Hamburg, Germany)
Thermomixer compact	Eppendorf (Hamburg, Germany)
Thermostat 5320	Eppendorf (Hamburg, Germany)
Centrifuge 5415D	Eppendorf (Hamburg, Germany)
Hybridization oven T 5042	Heraeus (Hanau, Germany)
Incubator Model B6200	Heraeus (Hanau, Germany)
Agilent 2100 Bioanalyzer	Agilent Technologies (Böblingen, Germany)
IKA MS3	Agilent Technologies (Böblingen, Germany)
Biofuge pico	Thermo Scientific (Rockford, USA)
Cytoperm	Thermo Scientific (Rockford, USA)
Fresco 17	Thermo Scientific (Rockford, USA)
HeraCell 240i CO2 Incubator	Thermo Scientific (Rockford, USA)
Megafuge 40R	Thermo Scientific (Rockford, USA)
HeraSafe KS	Thermo Scientific (Rockford, USA)
Branson Sonifier 450	Heinemann (Schwäbisch Gmünd, Germany)
Film Processor CP 1000	AGFA (Mortsel, Belgium)

Geiger Counter LB123 EG&G	Berthold (Bad Wildbad, Germany)
Power Supply EV233	Consort (Turnhout , Belgium)
Microscope Diavert	Leica (Wetzlar, Germany)
Milli-Q PLUS	Millipore (Billerica, USA)
Ultraspec 3300 pro	Amersham Biosciences (Little Chalfont, UK)
Avanti J-20 XP Centrifuge	Beckman Coulter (Krefeld, Germany)
Quantum ST4	PeqLab (Erlangen, Germany)

### 1.3. Buffers and Solutions

#### Phosphate buffered saline (PBS)

130 mM	NaCl
774 mM	Na <sub>2</sub> HPO <sub>4</sub>
226 mM	NaH <sub>2</sub> PO <sub>4</sub>

#### Tris/Borate/EDTA buffer (TBE)

89 mM	Tris pH 8,3
89 mM	Boric acid
2,5 mM	EDTA

#### Tris buffered saline (TBS)

10 mM	Tris pH 7,5
150 mM	NaCl

#### Western Blot blocking buffer

2 %	milk powder
0,01 %	Tween-20
add	TBS

#### Western Blot wash buffer

2 %	milk powder
0,01 %	Tween-20
add	TBS

#### Laemmli protein sample buffer

300 mM	Tris pH 6,8
50 %	Glycerol
10 %	SDS
0,01 %	Bromophenol blue

#### Proteinase K buffer

300 mM	NaCl
200 mM	Tris pH 7,5
25 mM	EDTA

2 % SDS

2 x RNA loading dye

99,9 % Formamide

0,05 % Xylene cyanol

0,05 % Bromphenol blue

Colloidal Coomassie solution

8,3 %  $H_3PO_4$

8,3 %  $(NH_4)_2SO_4$

20 % Methanol

1 g/L Coomassie Brilliant Blue G250

20 x SSC for Northern Blot

3 M NaCl

0,3 M NaCitrate pH 7,0

50 x Denhardt's Solution for Northern Blot

1 % Albumin Fraction V

1 % Polyvinylpyrrolidon K30

1 % Ficoll 400

Hybridization solution for Northern Blot

50 ml 20x SSC

4 ml 1 M  $Na_2HPO_4$  pH 7.2

140 ml 10 % SDS

4 ml 50X Denhardt's Solution

ad. 200 ml  $H_2O$

Wash Solution I for Northern Blot

5 x 20 x SSC

1 % (w/v) SDS

Wash Solution II for Northern Blot

1 x 20 x SSC

1 % (w/v) SDS

EDC crosslinking solution

2 ml  $H_2O$

61,25  $\mu$ l Methylimidazol

75  $\mu$ l 1 M HCl

188,25 mg 1-Ethyl-3(3-Dimethylaminopropyl)carbodiimide hydrochloride (EDC)

ad. 6 ml  $H_2O$

Elution buffer for RNA cloning

300 mM NaCl

2 mM EDTA

Firefly buffer for Luciferase assay

470 mM D-Luciferine (PJK GmbH, Kleinblitterdorf, Germany)  
530 mM ATP (PJK GmbH, Kleinblitterdorf, Germany)  
270 mM Coenzyme A (PJK GmbH, Kleinblitterdorf, Germany)  
20 mM Tricine  
5,34 mM  $\text{MgSO}_4 \cdot 7 \text{H}_2\text{O}$   
0,1 mM EDTA  
33,3 mM DTT

Renilla buffer for Luciferase assay

2.2 mM EDTA  
220 mM  $\text{K}_2\text{PO}_4$  pH 5,1  
0,44 mg/ml BSA  
1,1 M NaCl  
1,3 mM  $\text{NaN}_3$   
1,43 mM Coelenterazine (PJK GmbH, Kleinblitterdorf, Germany)

2 x HEPES for Calcium phosphate transfection

274 mM NaCl  
54,6 mM HEPES  
1,5 mM  $\text{Na}_2\text{HPO}_4$

10 % SDS-PAGE separation gel

10 % Acrylamide-Bis 37,5:1 30 % (w/v) (Serva, Heidelberg, Germany)  
400 mM Tris-HCl pH 8,8  
0,1 % SDS  
0,1 % APS  
0,05 % TEMED

5 % SDS-PAGE stacking gel

5 % Acrylamide-Bis 37,5:1 30 % (w/v) (Serva, Heidelberg, Germany)  
75 mM Tris-HCl pH 6.8  
0,1 % SDS  
0,1 % APS  
0,05 % TEMED

2 x siRNA annealing buffer

60 mM HEPES pH 7,4  
4 mM MgAc  
200 mM KAc

SDS running buffer

200 mM Glycine  
25 mM Tris pH 7,5

25 mM SDS

Towbin buffer

38,6 mM Glycine

48 mM Tris

0,0037 % (w/v) SDS

20 % Methanol

Nuclear lysis buffer

1 % SDS

10 mM EDTA

50 mM Tris pH 8,0

0,1 % Sodium deoxycholate

2 mM AEBSF

5 U/ml DNaseI

IP lysis buffer

150 mM KCl

25 mM Tris pH 7,5

2 mM EDTA

1 mM NaF

0,5 % NP-40

0,5 % DTT

0,5 % 4-(2-Aminoethyl)benzenesulfonyl fluoride (AEBSF)

IP wash buffer

300 mM NaCl

50 mM Tris pH 7,5

1 mM NaF

0,01 % NP-40

5 mM MgCl<sub>2</sub>

FACS buffer

1 % BSA

0,1 % NaN<sub>3</sub>

add PBS

PBS-A for IF

0,2 g KCl

0,2 g KH<sub>2</sub>PO<sub>4</sub>

8 g NaCl

2,2 g Na<sub>2</sub>HPO<sub>4</sub> • H<sub>2</sub>O

ad. 1 l H<sub>2</sub>O, adjust to pH 7,4

Fixation solution for IF

4 % paraformaldehyde (PFA)

add            PBS-A

Stopping solution for IF

100 mM       Glycine

add            PBS-A

Permeabilization solution for IF

0,1 %         Triton-X-100

add            PBS-A

Wash solution for IF

5 %            bovine serum albumin (BSA)

0,01 %       Triton-X-100

add            PBS-A

PEG solution for Heterokaryon Assay

50 % (w/v)   polyethylene glycol (PEG) 1500 (Sigma Aldrich, Munich, Germany)

add            PBS-A

DMEM/CHX solution for Heterokaryon Assay

1 % (v/v)     fetal bovine serum (FBS)

1x             penicillin/streptomycin mixture

75 µg/ml     cycloheximide (CHX) (Sigma Aldrich, Munich, Germany)

Buffer A for Ago2 purification

50 mM        HEPES pH 7,5

1 M            NaCl

0,1 %        NP-40

10 mM        imidazole

5 %            glycerol

1 mM         4-(2-aminoethyl)benzenesulfonyl fluoride (AEBSF)

5 U/ml        Benzonase

Buffer B for Ago2 purification

50 mM        HEPES pH 7,5

300 mM       NaCl

200 mM       imidazole

1 mM         DTT

Desalting buffer for Ago2 purification

50 mM        HEPES pH 7,5

1 M            NaCl

10 mM        Imidazole

Gelfiltration buffer for Ago2 purification

20 mM        HEPES pH 7,5

200 mM	KCl
2 mM	EDTA
1 mM	DTT
5 %	glycerol

Elution buffer for Importin purification

50 mM	Tris-HCl pH 8,0
10 mM	reduced glutathione

Dialysis buffer for Importin purification

50 mM	HEPES-KOH pH 7,5
200 mM	NaCl
5 %	glycerol)

Buffer A for Ran purification

20 mM	Tris pH 8,0
300 mM	NaCl
10 mM	Imidazole
1 mM	AEBSF
5 U/ml	Benzonase
5 µg/ml	Lysozyme

Buffer B for Ran purification

20 mM	Tris pH 8,0
300 mM	NaCl
250 mM	Imidazole
1 mM	AEBSF

Dialysis buffer for Ran purification

25 mM	Tris pH 7,5
150 mM	NaCl
1,5 mM	MgCl <sub>2</sub>
0,25 %	NP-40
1 mM	AEBSF
10 %	Glycerol

GST pulldown buffer for GST pulldowns

20 mM	HEPES pH 7,5
100 mM	KOAc
0,5 mM	EGTA
5 mM	MgOAc
250 mM	sucrose

Coupling buffer for antibody purification

0,1 M	NaHCO <sub>3</sub> pH 8,3
0,5 M	NaCl

## Wash buffer low pH for antibody purification

0,1 M NaAc pH 3-4

0,5 M NaCl

## Wash buffer high pH for antibody purification

0,1 M Tris pH 8-9

0,5 M NaCl

## Elution buffer for antibody purification

100 mM glycine pH 2,3

## Roeder A

10 mM HEPES pH 7,9

10 mM KCl

1,5 mM MgCl<sub>2</sub>

0,5 mM DTT

1 mM AEBSF

## Roeder B

300 mM HEPES pH 7,9

1,4 M KCl

30 mM MgCl<sub>2</sub>

0,5 mM DTT

1 mM AEBSF

## Roeder C

20 mM HEPES pH 7,9

420 mM KCl

1,5 mM MgCl<sub>2</sub>

0,2 mM EDTA

5 % glycerol

0,5 mM DTT

1 mM AEBSF

## Roeder D

20 mM HEPES pH 7,9

100 mM KCl

1,5 mM MgCl<sub>2</sub>

0,2 mM EDTA

5 % glycerol

0,5 mM DTT

1 mM AEBSF

## 1.4. DNA and RNA oligonucleotides

### 1.4.1. DNA oligonucleotides for molecular cloning

DNA oligonucleotides used for molecular cloning are listed in Table 1.1.

**Table 1.1. List of DNA oligonucleotides for molecular cloning.** Restriction enzyme substrate sequences are shown in bold.

Primer name	Sequence 5'→3'
CAMTA1 UTR SacI fwd	ATAC <b>GAGCTC</b> AGACATACAGCAGCATCCCTTAGCAATGTG
CAMTA1 UTR NaeI rev	ATAC <b>GCCGGC</b> GGAAATTTTCTTCATTTTAAATTACAGCAG
CAMTA pIRES EcoRV fwd	ATAC <b>GATATC</b> ATGTGGCGCGCGGAGGGGAAATG
CAMTA pIRES NotI rev	ATAT <b>GCGGCCGCT</b> CAAGTTCCCTTGGCCTTTTTCAATTCTTTCACTC
CAMTAdN pIRES RV fwd	ATAC <b>GATATC</b> ATGGGCAAGCCTTGGCGGCCCATCCTCTG
CAMTAdC pIRES rev	ATAT <b>GCGGCCGCT</b> CATTCATGATCAGACAGAGTGAGCTGAGC
CAMTAdN VP5 NotI fwd	TACT <b>GCGGCCGCT</b> ATGGGCAAGCCTTGGCGGCCCATCCTCTG
CAMTAdC VP5 Bam rev	ATAT <b>GGATCC</b> ATCATTGATCAGACAGAGTGAGCTGAGC
CAMTA1 VP5 NotI fwd	TACT <b>GCGGCCGCT</b> ATGTGGCGCGCGGAGGGGAAATG
CAMTA1 VP5 BamHI rev	ATAT <b>GGATCC</b> ATCAAGTTCCCTTGGCCTTTTTCAATTCTTTCACTC
CAMTA1 Sall rev2	TACT <b>GTCGACT</b> CACATTGCTAAGGGATGCTGCTGTATGTCTTCAAG
CAMTA1 f1 BamHI fwd	ATAT <b>GGATCC</b> ACAGGGGGGTACGGGAGCCACTCG
CAMTA1 f2 BamHI fwd	ATAT <b>GGATCC</b> CCCGGGGAGCGGAGCTTCAGCTTTAC
CAMTA1 f1/2 NotI rev	ATAT <b>GCGGCCGCT</b> TATTACAGCATGCCTAGGGTGCCCTGG
pFseI TNRC6A fwd	AGAG <b>GGCCGGCC</b> ATGAGAGAATTGGAAGCTAAAG
pAscl TNRC6A rev	AGAG <b>GGCGCGCCT</b> TACATGGACTCTCCACCC
pFseI NLS Ago2 fwd2	GAGAG <b>GGCCGGCC</b> CCAAAAAGAAGAGAAAGGTAGCTGGTATCATGTA
pFseI Ago2 fwd	AGAG <b>GGCCGGCC</b> ATGTA
pAscl Ago2 rev	AGAG <b>GGCGCGCCT</b> CAAGCAAAGTACATGGTGCG
phnRNPA1 NotI fwd	AGAG <b>GCGGCCGCT</b> ATGTCTAAGTCAGAGTCTCCTAAAGAGC
phnRNPA1 BamHI rev	AGAG <b>GGATCC</b> ATTAAATCTTCTGCCACTGCC
phnRNPC NotI fwd	AGAG <b>GCGGCCGCT</b> ATGGCCAGCAACGTTACC
phnRNPC BamHI rev	AGAG <b>GGATCC</b> ATTAAAGATCATCCTCGCCATT
pBam TEVHA fwd	AGAG <b>GGATCC</b> ATACCCTTATGACGTGCCCGATTACGCTCTCGAGATGTA
pAgo2 NotI rev	AGAG <b>GCGGCCGCT</b> TATCAAGCAAAGTACATGGTGCG
pTNRC6A SacI fwd	GAGAG <b>GAGCTC</b> ATGGATGCTGATTCTGCCTCC
pTNRC6A XhoI rev	GAG <b>ACTCGAGT</b> TACATGGACTCTCCACCCC
pTNRC6B BamHI fwd	GAGAG <b>GGATCC</b> ATGAGAGAGAAGGAGCAAGAAAG
pTNRC6B NotI rev	GAGAG <b>GCGGCCGCT</b> CAGATTGAATCCGACCCTCC
pTNRC6C SacI fwd	GAGAG <b>GAGCTC</b> ATGGCTACAGGGAGTGCCC
pTNRC6C XhoI rev	GAG <b>ACTCGAGT</b> TACAGGGACTCCCGCT
pRan FseI fwd	AGAG <b>GGCCGGCC</b> ATGGCTGCGCAGGGA
pRan Ascl rev	AGAG <b>GGCGCGCCT</b> CACAGGTATCATCCTCATC
pmycGFPTNRC6A fwd	AGAG <b>GGATCC</b> ATGGAACAAAACATCATCTCAGA
pmycGFPTNRC6A rev	AGAG <b>CTCGAGT</b> TACATGGACTCTCCACCC

Detailed information on molecular cloning strategy for each generated construct is given in subsection 2.1.3.

### 1.4.2. DNA oligonucleotides for quantitative real-time PCR

DNA oligonucleotides used for quantitative real-time PCR are listed in Table 1.2. All primers were designed against the human protein and to be exon-intron spanning.

**Table 1.2. List of DNA oligonucleotides for quantitative real-time PCR.** All primers are designed to detect the human mRNA.

Amplicon	Accession	Primer name	Sequence 5'→3'
GAPDH	NM_001256799	pRT GAPDH fwd	TGGTATCGTGGAAGGACTCATGAC
		pRT GAPDH rev	ATGCCAGTGAGCTTCCCGTTCAGC
β-Actin	NM_001101	pRT Actin fwd	GGACTTCGAGCAAGAGATGG
		pRT Actin rev	AGGAAGGAAGGCTGGAAGAG
Ile tRNA		Ile tRNA fwd	GGTACTTATATGACAGTGC
		Ile tRNA rev	TGCTCCAGGTGAGGATCGAAC
CAMTA1	NM_015215	CAMTA1 RT fwd	ATCCTTATCCAGAGCAAATTC
		CAMTA1 RT rev	AGTTTCTGTTGTACAATCACAG
NPPA	NM_006172	pRT NPPA fwd	CAGGATGGACAGGATTGGA
		pRT NPPA rev	TCTTCAGTACCGGAAGCTGTT
NPPB	NM_002521	pRT NPPB fwd	CTTTCCTGGGAGGTCGTTTC
		pRT NPPB rev	AGGGATGTCTGCTCCACCT
NPPC	NM_024409	pRT NPPC fwd	CTTGTCGCCCTTCTTCTGAC
		pRT NPPC rev	CTGCTCACGCTGCTCTCC
NPR-A	NM_000906	pRT NPR-A fwd	TCGAAACCACCAAACCTCCTC
		pRT NPR-A rev	AGTGGTGGGACTGAAGATGC
NPR-B	NM_003995	pRT NPR-B fwd	GGGGTTCTCGGTACGTGAT
		pRT NPR-B rev	TACCTGGATGTCTTTGGGGA
NPR-C	NM_000908	pRT NPR-C fwd	CATCGTGAATCCTTCAACA
		pRT NPR-C rev	GCATACTCGTCCCTCCAGAC
7sk		pRT 7sk fwd	CCTGCTAGAACCTCCAACAAG
		pRT 7sk rev	GCCTCATTTGGATGTGTCTG
Impβb	NM_002265	qRT Impb1 fwd	CAGCAGAACAAGGACGGCCCC
		qRT Impb1 rev	TGCTGCTTTCAGGGGTTCCA
Imp3	NM_013433	qRT Imp3 fwd	CAAGGCCTTCTTATCCGACA
		qRT Imp3 rev	GAGTGGGTGGTCAAGGAGTC
Imp4	NM_024658	qRT Imp4 fwd	TGTTGTCAGCCAGAATGAGG
		qRT Imp4 rev	GAGGACTTGGAGGAGTGGGT
Imp5	NM_002271	qRT Imp5 fwd2	GGAGATCAGCAAAGCTTTGGT
		qRT Imp5 rev2	AAAGGGACCATCAGTTTGACA
Imp7	NM_006391	qRT Imp7 fwd	ATGTCGGAACAGCTGGATTACCTG
		qRT Imp7 rev	CCCCTGGTGCTGTTTCTCGATCA

**Table 1.2. List of DNA oligonucleotides for quantitative real-time PCR, continued.**

Amplicon	Accession	Primer name	Sequence 5'→3'
Imp8	NM_006390	qRT Imp8 fwd	AGCCGAGAACGAGCTCAACCA
		qRT Imp8 rev	CGATCTGGCCAGTATTGTGTCCACCA
Imp9	NM_018085	qRT Imp9 fwd	GGCATCCGCACCCGCTCTAAG
		qRT Imp9 rev	CCTGGCGAGCGGCATTAGCC
Imp11	NM_016338	qRT Imp11 fwd	TCCTGTTTCAGGATCTTCCG
		qRT Imp11 rev	CTTTCAGCTTTGGCTTTGCT
Imp12	NM_012470	qRT Imp12 fwd	TTGGGGAGCTGCAGCGTTC
		qRT Imp12 rev	CATGAGAGTCTGTGGGGAGCTCA
Imp13	NM_014652	qRT Imp13 fwd	TCGACAGCAGTGTGGAGGCCA
		qRT Imp13 rev	TTCTGCACTGCCTGCCGCAG
TRPO1	NM_002270	qRT TRPO1 fwd	GGTTCTCTGGATGGTGGTGT
		qRT TRPO1 rev	GTCTGGGATGGTGTGGGA
forward primer		hsa-miR-9	TCTTTGGTTATCTAGCTGTATG
		hsa-miR-9*	ATAAAGCTAGATAACCGAAAG
		hsa-miR-34a	TGGCAGTGTCTTAGCTGGTTG
		U6 snRNA	GATGACACGCAAATTCGTGAAG
reverse primer		URT	AACGAGACGACGACAGACTTT

### 1.4.3. DNA oligonucleotides for Northern Blot

DNA oligonucleotides used as probes for Northern Blot are listed in Table 1.3. Probes were designed to correspond the exact antisense sequence for the miRNA strand of interest.

**Table 1.3. List of DNA oligonucleotides used as Northern Probes.**

Oligo name	Sequence 5'→3'
hsa-miR-9	TCATACAGCTAGATAACCAAAGA
hsa-miR-9*	ACTTTCGGTTGTCTAGCTTTAT
hsa-miR-17-5p	CTACCTGCTCTGTAAGCACTTTG
hsa-miR-106b	ATCTGCACTGTCAGCACTTTA
human U6	GAATTTGCGTGCATCCTTGCGCAGGGGCCATGCTAA
human Ile-tRNA	TGCTCCAGGTGAGGATCGAAC
human 7sk snRNA	ACTCGTATACCCTTGACCGAAGA

### 1.4.4. DNA oligonucleotides for mouse genotyping

DNA oligonucleotides for genotyping of CAMTA1<sup>fl/fl</sup> (Long et al., 2014) and Nes-cre/ERT2<sup>+0</sup> as well as the derived mouse strains are shown in Table 1.4.

**Table 1.4. List of DNA oligonucleotides used for mouse genotyping.**

Oligo name	Sequence 5'→3'	Reference
A1CKOsLA Seq	TGGTGGAGAGGGTCATCTCAGAAATCTC	Long et al., 2014
A1CKOASeq-6	CTCACACCTGATTCTGGCTGTGTAATG	Long et al., 2014
A1CKOfP-1	CTGGAAGAGCAGCTAGTGCTCTTAATTGC	Long et al., 2014
olMR1084 cre fwd	CTAGGCCACAGAATTGAAAGATCT	jaxmice.jax.org
olMR1085 cre rev	GTAGGTGGAAATTCTAGCATCATCC	jaxmice.jax.org

### 1.4.5. RNA oligonucleotides

### 1.4.6. siRNAs and siPools

RNA oligonucleotides that were used as siRNAs are listed in Table 1.5.

**Table 1.5. List of siRNAs.** Sense (s) and antisense (as) sequences are shown separately.

siRNA name	Sense sequence 5'→3'	Antisense sequence 5'→3'
CAMTA1 si1	CUACCGAAGUUUAAGAAUdT	UUUCUUUAACUUCGGUAGUdT
CAMTA1 si2	GAAUCAAGCAGGAGAAUUUdT	AAAUUCUCCUGCUUGAUUCGdT
si2 Impb1	GGAAAGAAGAGCCUAGUAAUdT	UUACUAGGCUCUUCUUCCUdT
si1 Impb1	CUGAAUGAGCUAAGGGAAUdT	UUUCCCUUAGCUCAUUCAGUdT
si1 Imp3	GGGCAGAGAUGCAGCCUUAUdT	UAAGGCUGCAUCUCUGCCUdT
si2 Imp3	GGGAUGAAGUACUCGGAAUdT	UUUCCGAGUACUUAUCCUdT
si1 Imp4	UGCGAUACGCAUACGUUUUdT	AAUACGUUAGCGUAUCGCAUdT
si1 Imp5	GAGAAUAGCAGGAGGAAUdT	AUUGCCUCGUGCAUUUCUCUdT
si2 Imp5	GUGCAAAUCCUUGGAAAUdT	UUUCCAAGGAUUUUGCACUdT
si1 Imp7	GGAAAGAGGUACUGCAAAUdT	UUUUGCAGUACCUUUCCUdT
si2 Imp7	GGAAGAAGAUGAUGCUGAAUdT	UUCAGCAUCAUCUUCUCCUdT
si2 Imp8	ACAAUAGUGUGGAUGAAUdT	UAUUCAUCCACACUUAUGUdT
si3 Imp8	UGAGCUCAAUCUAAGAAUdT	AUUUCUAGAUUGAGCUCAUdT
si1 Imp9	CCUAAUGGGUUGAGAGAAUdT	AUUCUCUACCCAUUAGGUdT
si2 Imp9	CCACAGAUUCCAGAAUGAUdT	UCAUUCUGGAAUCUGUGGUdT
si1 Imp11	GGAAGAUUGUUJAGAUAUdT	UAAUUCUAAACCAUCUCCUdT
si2 Imp11	GAUAAUGUGUGUAGAGAUdT	UAUCUCUACACAUUAUCUdT
si1 Imp12	ACGUGAAGAUUUAGACAAUdT	UUUGUCUAAAUCUUCACGUdT
si2 Imp12	GCACAGAAUUAJAGAAGAUdT	UCUUCUAAAUUUCUGUGCUdT
si1 Imp13	CCCUCUGAUGAGGAAUdT	AUAUCCUCAUCAGAAGGUdT
si2 Imp13	GGGAAAGGUGUACAGGAAUdT	UUCCUGUACCACCUUCCUdT
si1 Tnp01	GUAUAGAGAUUGCAGCCUdT	UAAGGCUGCAUCUCUAUACUdT
si2 Tnp01	GCCACAGGUUAUCAUUUdT	AUAAAUGAAUACCUGUGGUdT
si1 control	UUGUCUUGCAUUCGACUAAUdT	UUAGUCGAAUGCAAGACAAUdT

**Table 1.5. List of siRNAs, continued.**

siRNA name	Sense sequence 5'→3'	Antisense sequence 5'→3'
si2 control	UCGAAGUAUCCGCGUACGUdT	CGUACGCGGAAUACUUCGAUdT

As controls, si1 and si2 controls were used. si2 control is directed against firefly luciferase. All siRNAs were designed with Dharmacon siRNA Design Center and Whitehead siRNA selection tool which are publicly available online.

siPools were designed by and ordered at siTool Biotech (Martinsried, Germany). Following siTools were used during this study: siP TNRC6A, siP TNRC6C, siP TNRC6C, siP Ago1, siP Ago2, siP Ago3, siP Ago4, siP Neg.

### 1.4.7. miRNA inhibitors

RNA oligonucleotides that were used for miRNA inhibition experiments were synthesized as 2'-O-methylated RNAs and are listed in Table 1.6.

**Table 1.6. List of 2'-O-methylated miRNA inhibitors.**

Inhibitor name	Sequence 5'→3'
hsa-miR-9 antisense	UCAUACAGCUAGAUAAACCAAAGAT
hsa-miR-9* antisense	ACUUUCGGUUAUCUAGCUUUAT
hsa-miR-17-5p antisense	ACUACCUGCACUGUAAGCACUUUGT
hsa-miR-106b antisense	AUCUGCACUGUCAGCACUUUAT
hsa-miR-122 antisense	ACAAACACCAUUGUCACACUCCAT
hsa-miR-301 antisense	GCUUUGACAAUACUUAUUGCACUGT
hsa-miR-330 antisense	GCCUAAGACACAGGCCAGAGAT

### 1.4.8. miRNA mimics

RNA oligonucleotides that were used as miRNA mimics are listed in Table 1.7.

**Table 1.7. List of miRNA mimics.**

Oligo name	Sequence 5'→3'
hsa-miR-9/9* mimic sense	UCUUUGGUUAUCUAGCUGUAUGAT
hsa-miR-9/9* mimic antisense	AUAAAGCUAGAUAAACCGAAAGUT
hsa-miR-122 mimic sense	UGGAGUGUGACAAUGGUGUUUGT
hsa-miR-122 mimic antisense	AACGCCAUUAUCACACUAAAUAT

## 1.5. Plasmids

Following plasmids were available in advance of this work or purchased:

**pMIR-RL** Modified commercially available pMIR-REPORT (Thermo Scientific, Rockford, USA) in which *Renilla reniformis* luciferase under control of SV40 promoter has been inserted for dual luciferase assay. Modifications have been reported in Beitzinger et al., 2007.

**pIRESneo** Mammalian expression vector with CMV promoter and ECMV internal ribosome entry side for Cap-independent translation (Takara Bio, Otsu, Japan).

**pIRES-Flag/HA** Modified pIRESneo, which allows expression of N-terminal Flag/HA-tagged fusion proteins. Modifications have been reported in Meister et al., 2004b.

**pIRES-Flag/HA-FA** pIRES-Flag/HA with modified multiple cloning that contains FseI and Ascl sites for molecular cloning.

**pCS2-myc(6)** Published in Meister et al., 2004b.

**pCS2-myc(6)-FAME** Modified pCS2 plasmid, which encodes N-terminal 6 x myc-Tag and additional FseI/Ascl restriction sites for cloning. Modifications reported in Weinmann et al., 2009.

**pIRES-Flag/HA-eYFP** Plasmid expressing N-terminally Flag/HA-tagged eYFP from Meister et al., 2004b.

**pGEX-6P-1** Expression of N-terminal GST tagged fusion protein in bacteria (GE Healthcare, Little Chalfont, UK).

**pET28a** Commercially available from Novagen/Merck (Darmstadt, Germany).

**pIRES-Flag/HA-TNRC6B 599-683-eYFP** Plasmid containing TNRC6B fragment aa 599-683 of full length TNRC6B. Fragment is expressed as N-terminally Flag/HA-tagged and C-terminally eYFP-tagged fusion protein. Kindly provided by Judith Hauptmann.

**pIRES-Flag/HA-TNRC6B 599-683 mut-eYFP** Plasmid containing TNRC6B fragment aa 599-683 of full length TNRC6B. Kindly provided provided by Judith Hauptmann.

**pIRES-Flag/HA-eYFP** Plasmid containing eYFP. Cloning has been reported in Meister et al., 2004b.

**pcDNA5-FRT/TO** Commercially available from Life Technologies (Carlsbad, USA).

**pOG44** Commercially available from Life Technologies (Carlsbad, USA).

**VP5-Ago1, Ago2, Ago3, Ago4** Published in Meister et al., 2005.

**pCS2-myc(6)-Ago1, Ago2, Ago3, Ago4** Published in Meister et al., 2005.

**pCS2-myc(6)-Ago2 529E** Contains Ago2 with Y529E mutation, which interrupts miRNA binding. Published in Rüdél et al., 2011.

**pIRES-Flag/HA-TNRC6B** Contains 1724 aa TNRC6B ORF. Published in Pfaff et al., 2013.

**pIRES-Flag/HA-TNRC6C** Contains 1691 aa TNRC6C ORF. Cloned by Janina Pfaff, unpublished construct.

**pIRES-Flag/HA-TNRC6B W623A** Contains 1724 aa TNRC6B ORF with W623A mutation which prevents binding to Ago2 *in vitro*. Published in Pfaff et al., 2013.

**pcDNA3.1-myc-GFP-TNRC6A, NLS mut, NES mut,  $\delta$ GW,  $\delta$ GW NES mut** Contains 1709 aa TNRC6A ORF and mutant ORFs. 1709 aa TNRC6A variant doesn't contain the 254 aa N-terminal part of the longest annotated version of TNRC6A (1963 aa) including the Q-rich domain. Published in Nishi et al., 2013.

**pCS2-myc(6)-TNRC6A** Contains TNRC6A ORF, however it is not clear which variant of TNRC6A (sequencing never worked, but myc-tagged protein with size and distribution of 1709 TNRC6A version is expressed).

**pCS2-myc(6)-TNRC6B** Contains 1724 nt TNRC6B ORF. Published in Pfaff et al., 2013.

**pCS2-myc(6)-TNRC6C** Contains 1691 nt TNRC6C ORF. Cloned by Janina Pfaff, unpublished construct.

**pFastBac-HTa-3TEV-Ago2** Cloned by Lasse Weinmann to express 3 TEV sites between N-terminal His-tag and Ago2, unpublished construct.

**pET28a-Ago1, Ago2, Ago3, Ago4** Published in Weinmann et al., 2009.

## 1.6. Antibodies

Antibodies used for Western Blot, Immunoprecipitations and FACS analysis are listed in Table 1.8.

**Table 1.8. Antibodies used for Western Blot, immunoprecipitations and FACS.** Dilutions were shown for Western Blot applications. monocl, monoclonal antibody; polycl, polyclonal antibody; HS, hybridoma supernatand; pf, purified.

Antibody	Properties/Source	Dilution
rat-anti-Ago1	monocl, HS, clone 4B8, Beitzinger et al., 2007	1:10
rat-anti-Ago2	monocl, HS, clone 11A9, Rüdél et al., 2008	1:20
rat-anti-Ago3	monocl, HS, clone 5A3, Weinmann et al., 2009	1:20
rat-anti-TNRC6B	monocl, HS, clone 6G3, this work	1:10

**Table 1.8. Antibodies used for Western Blot, immunoprecipitations and FACS, continued.**

Antibody	Properties/Source	Dilution
rat-anti-TNRC6ABC	monocl, HS, clone 7A9, this work	1:10
mouse-anti-HA	monocl, clone 16B12, Covance (Princeton, USA)	1:1000
rabbit-anti-c-Myc	polycl, C3956, Sigma Aldrich (Munich, Germany)	1:1000
mouse-anti- $\alpha$ Tubulin	monocl, clone DM1A, Sigma Aldrich (Munich, Germany)	1:10000
rabbit-anti-Lamin A/C	polycl, H-110, Santa Cruz Biotechnology (Dallas, USA)	1:1000
mouse-anti-Tuj1	monocl, MMS-435p, Covance (Princeton, USA)	1:1000
mouse-anti- $\beta$ Actin	monocl, clone AC15, Abcam (Cambridge, UK)	1:10000
rabbit-anti-GFAP	monocl, clone 6F2, Dako (Eching, Germany)	1:2000
rabbit-anti-CAMTA1	polycl, rabbit #1886, Schraivogel et al., 2011	1:200
rabbit-anti-CAMTA1	polycl, rabbit #1901, this work	1:200
goat-anti-rabbit-HRP	secondary antibody, Sigma Aldrich (Munich, Germany)	1:5000
goat-anti-mouse-HRP	secondary antibody, Sigma Aldrich (Munich, Germany)	1:5000
goat-anti-rabbit 680	secondary antibody, Li-Cor Biosciences (Lincoln, USA)	1:10000
goat-anti-mouse 680	secondary antibody, Li-Cor Biosciences (Lincoln, USA)	1:10000
goat-anti-rat 680	secondary antibody, Li-Cor Biosciences (Lincoln, USA)	1:10000
goat-anti-rabbit 800	secondary antibody, Li-Cor Biosciences (Lincoln, USA)	1:10000
goat-anti-mouse 800	secondary antibody, Li-Cor Biosciences (Lincoln, USA)	1:10000
goat-anti-rat 800	secondary antibody, Li-Cor Biosciences (Lincoln, USA)	1:10000
anti-CD133/2-PE	FACS antibody, clone 293C3, Miltenyi (B. Gladbach, Germany)	

Antibody production and purification will be described in section 3.2.

Antibodies that were used for Immunofluorescence stainings are listed in Table 1.9

**Table 1.9. Antibodies used for Immunofluorescence stainings.** monocl, monoclonal antibody; polycl, polyclonal antibody; HS, hybridoma supernatand; pf, purified.

Antibody	Properties/Source	Dilution
rat-anti-Ago1	monocl, HS, clone 4B8, Beitzinger et al., 2007	1:10
rat-anti-Ago2	monocl, HS, clone 11A9, Rüdél et al., 2008	1:10
rat-anti-Ago2	monocl, pf, clone 11A9, Rüdél et al., 2008	1:1000
rabbit-anti-Ago2	polycl, HS, clone 1526, this work	1:100
rabbit-anti-Ago2	polycl, pf, clone 1526, this work	1:1000
mouse-anti-Ago2	polycl, 2E12-1C9, Abnova (Danvers, USA)	1:200
rabbit-anti-Ago2	polycl, C34C6, Cell Signalling (Danvers, USA)	1:200
rat-anti-Ago3	monocl, HS, clone 5A3, Weinmann et al., 2009	1:10
rat-anti-TNRC6B	monocl, HS, clone 6G3, this work	1:10
rat-anti-TNRC6ABC	monocl, HS, clone 7A9, this work	1:10
mouse-anti-HA	monocl, clone 16B12, Covance (Princeton, USA)	1:400
rabbit-anti-c-Myc	polycl, C3956, Sigma Aldrich (Munich, Germany)	1:400
chicken-anti-Lsm4	polycl, GW22314F, Sigma Aldrich (Munich, Germany)	1:500

**Table 1.9. Antibodies used for immunofluorescence stainings, continued.**

Antibody	Properties/Source	Dilution
rabbit-anti-YB1	polycl, ab12148, Abcam (Cambridge, UK)	1:400
mouse-anti-RPA194	monocl, C-1, Santa Cruz Biotechnology (Danvers, USA)	1:250
mouse-anti-RBP1 CTD	monocl, clone 8WG16, provided by Dirk Eick	1:10
rabbit-anti-Coilin	polycl, H-300, Santa Cruz Biotechnology (Dallas, USA)	1:50
mouse-anti-SC35	monocl, ab11862, Abcam (Cambridge, UK)	1:500
mouse-anti-p54nrb	monocl, clone 3, BD Biosciences (Franklin Lakes, USA)	1:200
mouse-anti-PML	polycl, H-238, Santa Cruz Biotechnology (Dallas, USA)	1:100
rabbit-anti-HSF1	monocl, D3L8I, Cell Signalling (Danvers, USA)	1:400
rabbit-anti-CBP80	polycl, ab42389, Abcam (Cambridge, UK)	1:100
rabbit-anti-CNOT7	provided by Laura Corbo, Chapat et al., 2013	1:100
rabbit-anti-SKIV2L2	polycl, Novus Biologicals (Littleton, USA)	1:100
rabbit-anti-Xrn2	provided by David Bentley, Brannan et al., 2012	1:400
mouse-anti-Ubiquitin	monocl, clone 6C1, Sigma Aldrich (Munich, Germany)	1:500
mouse-anti-Proteasome	monocl, MCP231, Enzo Lifesciences (Farmingdale, USA)	1:100
mouse-anti- $\gamma$ H2AX	polycl, clone JBW301, Millipore (Darmstadt, Germany)	1:100
rabbit-anti-53BP1	polycl, Novus Biologicals (Littleton, USA)	1:100
rabbit-anti-HSF1	polycl, #4356, Cell Signalling (Danvers, USA)	1:500
goat-anti-mouse 488	secondary antibody, Life Technologies (Carlsbad, USA)	1:500
goat-anti-rat 488	secondary antibody, Life Technologies (Carlsbad, USA)	1:500
goat-anti-rabbit 488	secondary antibody, Life Technologies (Carlsbad, USA)	1:500
goat-anti-chicken 488	secondary antibody, Life Technologies (Carlsbad, USA)	1:500
goat-anti-mouse 555	secondary antibody, Life Technologies (Carlsbad, USA)	1:500
goat-anti-rat 555	secondary antibody, Life Technologies (Carlsbad, USA)	1:500
goat-anti-rabbit 555	secondary antibody, Life Technologies (Carlsbad, USA)	1:500
goat-anti-chicken 555	secondary antibody, Life Technologies (Carlsbad, USA)	1:500
anti-CD133/2-PE	clone 293C3, Miltenyi (B. Gladbach, Germany)	

## 1.7. Bacterial Strains and Media

Following *Escherichia coli* strain was used for cloning:

**XL1-blue** recA1 endA1 gyrA96 thi-1 hsdR17 supE44 relA1 lac[F'proAB lacIqZ $\Delta$ M15 Tn10 (Tetr)]

Following *E. coli* strain was used for expression of CAMTA1 fragments:

**BL21** B F- dcm+ Hte ompT hsdS(rB- mB-) gal endA Hte

Liquid and solid media for cultivation of *E. coli* were composed as follows:

Lysogeny broth (LB) medium

5 g yeast extract

10 g Tryptone

10 g/l	NaCl
ad. 1 l	H <sub>2</sub> O

LB-Agar	
1 l	LB medium
16,4 g	Agar

Ampicillin (50 µg/ml) or Kanamycin (30 µg/ml) were added to LB medium for Mini and Midi preparations of plasmid DNA. Isopropylthio-β-galactoside (IPTG) for induction of recombinant protein expression from trp/lac hybrid promoter in pGEX was prepared as 0,1 M solution and added to growing cells to 0,1 mM final concentration.

## 1.8. Mammalian Cell lines and Media

### 1.8.1. Glioblastoma cell lines

Human glioblastoma cell lines that have been used during this work are listed below. Generation of cell lines has been described in Beier et al., 2007. All cell lines are derived from primary tumors of grade IV *Glioblastoma multiforme*. Type I cancer stem cell (CSC) lines are CD133-positive, show neurosphere growth, express proneural signature genes and are similar to fetal neural stem cell lines. Type II CSC lines are CD133-negative, show semi-adherent growth, express mesenchymal signature genes and are similar to adult neural stem cell lines. Classification of CSC lines has been done in Lottaz et al., 2010 and in Beier et al., 2012, mesenchymal-proneural classification was done in these studies according to signatures from Phillips et al., 2006. Interestingly, GBM derived cell lines are genetically stable during long-term cultivation in stem cell medium (Lee et al., 2006b), what can be confirmed for R28 and R11 by regular microarray analysis (Christoph Beier, personal communication).

**R8** human primary astrocytic GBM, Type II CSC, adherent growth pattern, established and described in Lottaz et al., 2010

**R11** human primary astrocytic GBM, Type I CSC, neurosphere-like growth, established and described in Lottaz et al., 2010

**R20** human primary GBM, origin not investigated, Schraivogel et al., 2011

**R28** human primary astrocytic GBM, Type I CSC, neurosphere-like growth, established and described in Lottaz et al., 2010

**R28-luc** R28 cell line stably transduced with a lentiviral vector expressing firefly luciferase under control of the constitutive spleen focus forming virus LTR promoter. Cell line was generated by Martina Anton (TU Munich, Institute of Experimental Oncology and Therapy Research, Munich, Germany) for Schraivogel et al., 2011. Detailed experimental procedures are presented in section 4.4.3.

**R40** human primary GBM, origin not investigated, Schraivogel et al., 2011

**R44** human primary GBM, origin not investigated, Type I CSC, neurosphere-like growth, established and described in Lottaz et al., 2010

**R52** human primary GBM, origin not investigated, Schraivogel et al., 2011

**R54** human primary GBM, origin not investigated, Type I CSC, neurosphere-like growth, established and described in Lottaz et al., 2010

Additional human and murine glioblastoma cell lines that were used for this work:

**LN-229** human glioblastoma cell line with adherent growth. Cells exhibit mutated TP53 (C98T) and homozygous deletions in p16 and p14ARF tumor suppressor genes. PTEN status is wildtype.

**SMA-560** murine glioma cell line which grows as adherent monolayer under standard growth conditions or as sphere culture in neural stem cell medium. Spontaneous murine anaplastic astrocytoma (SMA) 560 arose in a VM/Dk mouse strain followed by serial transplantations back into VM/Dk mice with stable tumorigenicity (Serano et al., 1980). SMA-560 have low S-100 expression, high expression of GFAP and glutamine synthetase and exhibit a CD133-positive subpopulation with cancer stem cell like properties (Oh et al., 2014; Ghazaleh Tabatabai, personal communication).

**T89G** human *Glioblastoma Multiforme* derived cell line with adherent growth.

**U87MG** human *Glioblastoma Multiforme* derived cell line with adherent growth.

## 1.8.2. Mammalian and murine cell lines

Human pulmonary artery smooth muscle cells (HPASMC) and endothelial cells (HPAEC) were purchased from Lonza (Basel, Switzerland). Primary keratinocytes were isolated as described in Kretz et al., 2013. Flp-In T-REx 293 cell line was purchased from Life Technologies (Carlsbad, USA).

All other cell lines are listed at ATCC: HeLa, HeLa S3 HEK 293T, NIH 3T3, U-2 OS, HCT116, Hep G2, HuH-7, A549, H1299, MCF7, T-47D, NCCIT, MRC-5, DU 145, GM5756, Ntera2 and Sk-Mel-28, Arpe-19, DLD-1, LNCaP.

## 1.8.3. Cell culture media

Following cell culture media were used for cells listed in sections 1.8.1 and 1.8.2.

Standard cell culture medium

Dulbecco's Modified Eagle Medium (DMEM) (Sigma Aldrich, Munich, Germany)

10 % FBS (Sigma Aldrich, Munich, Germany)

- 1 % penicillin/streptomycin (Sigma Aldrich, Munich, Germany)
- Tet-free DMEM Zeo/Blast medium  
DMEM
- 10 % Tetracycline-free FBS (Clontech, Saint-Germain-en-Laye, France)
- 1 % penicillin/streptomycin
- 100 µg/ml Zeocin (Life Technologies, Carlsbad, USA)
- 15 µg/ml Blasticidin (Applichem, Darmstadt, Germany)
- Tet-free DMEM HygB/Blast medium  
DMEM
- 10 % Tetracycline-free FBS
- 1 % penicillin/streptomycin
- 200 µg/ml Hygromycin B (Life Technologies, Carlsbad, USA)
- 15 µg/ml Blasticidin
- DMEM-F12 complete medium  
DMEM Nutrient Mixture F-12 (DMEM-F12) (PAN, Aidenbach, Germany)
- 10 % FBS
- 1 % penicillin/streptomycin
- RPMI complete medium  
RPMI-1640 (Sigma Aldrich, Munich, Germany)
- 10 % FBS
- 1 % penicillin/streptomycin
- Neural stem cell medium complete  
DMEM-F12
- 20 ng/ml epidermal growth factor (EGF) (R&D Systems, Minneapolis, USA)
- 20 ng/ml fibroblast growth factor (FGF) (R&D Systems, Minneapolis, USA)
- 20 ng/ml leukaemia inhibitory factor (LIF) (Millipore, Billerica, USA)
- 2 % B27 supplement (Life Technologies, Carlsbad, USA)
- 1 % penicillin/streptomycin
- 1 % MEM vitamins solution (Life Technologies, Carlsbad, USA)
- Neural stem cell medium incomplete  
DMEM-F12
- 1 % penicillin/streptomycin
- 1 % MEM vitamins solution
- SmBM complete  
Smooth muscle basal medium (SmBM) (Lonza, Basel, Switzerland)
- 10 % FBS (Lonza, Basel, Switzerland)
- 1 % SingleQuots Kit (Lonza, Basel, Switzerland)
- EBM-2 complete

	Endothelial basal medium 2 (EBM-2) (Lonza, Basel, Switzerland)
10 %	FBS (Lonza, Basel, Switzerland)
1 %	SingleQuots Kit

#### Keratinocyte medium

50 %	KSF-M (Gibco)
40 %	Medium 154 for keratinocytes (Gibco)
10 %	EGF
1 x	bovine pituitary extract

#### Minimum essential medium eagle Joklik Modification (Joklik's)

11,02 g/l	Joklik's dry powder (Sigma Aldrich, Munich, Germany)
0,29 g/l	L-glutamine
1 %	penicillin/streptomycin
1 %	non-essential amino acids
2 g/l	NaHCO <sub>3</sub>

#### Joklik's medium

	Joklik's
5 %	FBS

SingleQuots Kit contains human epidermal growth factor (hEGF), hydrocortisone, human recombinant fibroblast growth factor-Beta (hFGF- $\beta$ ), vascular endothelial growth factor (VEGF), insulin-like growth factor (R3-IGF-1), ascorbic acid, heparin, FBS, and gentamicin/amphotericin-B (GA).

The prepared stem cell medium contains human epidermal growth factor (EGF) and fibroblast growth factor (FGF), which have multiple effects by mainly preventing differentiation and apoptosis and accelerating cell growth (Pollard et al., 2009). B27 supplement includes a range of hormones, anti-oxidants and retinal acetate, transferrin, insulin, putrescine, progesterone and sodium selenate as formulated in Bottenstein and Sato, 1979 and Bottenstein and Sato, 1979 and was shown to support long-term survival of CNS derived non-neoplastic and GBM derived primary cell lines. B27 serum-free supplement was shown to increase survival of long-term cultivated primary GBM derived cell lines (Pollard et al., 2009).

All cell culture plates, dishes and wells were purchased from Sarstedt (Nümbrecht, Germany).

## 2. Molecular Biological Methods

### 2.1. DNA cloning

#### 2.1.1. General DNA cloning

Polymerase chain reaction (PCR) was performed with Phusion High-Fidelity DNA Polymerase (Thermo Scientific, Rockford, USA) according to the manufacturer's instructions. PCR fragments were purified by agarose gel electrophoresis according to Sambrook et al., 1989. Purification of PCR fragment from Agarose gels has been done using NucleoSpin Gel and PCR Clean-Up Kit (Macherey-Nagel, Düren, Germany). Fragments were then digested with restriction enzymes, purified again using NucleoSpin Gel and PCR Clean-Up Kit and used for ligation. Ligations were done for 2 h at RT or o/n at 16 °C.

Preparation and transformation of chemically competent *E. coli* has been described in Inoue et al., 1990. DNA isolation from *E. coli* was done by alkaline lysis according to Sambrook et al., 1989. Plasmids were then controlled by analytical digest with multi-cutting restriction enzyme. Positive clones were re-purified with NucleoBond Xtra PC20 gravity columns (Macherey-Nagel, Düren, Germany) and sent to sequencing. Sequencing has been done at GATC Biotech (Konstanz, Germany) or Macrogen (Amsterdam, Netherlands). DNA concentration and quality was determined using NanoDrop 1000 Spectrophotometer (Thermo Scientific, Rockford, USA). Midi preparations have been done using NucleoBond Xtra Midi Kit (Macherey-Nagel, Düren, Germany). For nucleofection experiments, plasmids were prepared using EndoFree Plasmid Midi Kit (Qiagen, Hilden, Germany).

#### 2.1.2. Site-directed mutagenesis

For site directed mutagenesis QuikChange II site-directed mutagenesis Kit (Agilent Technologies, Santa Clara, USA) was used according to the manufacturer's instructions. Mutagenesis was controlled by sequencing of the complete 3'-UTR.

#### 2.1.3. Cloning strategies for plasmids produced in this work

Following plasmids were cloned during this work. Primers are listed in Table 1.1.

**pMIR-RL-CAMTA1** The 3'-UTR of CAMTA1 mRNA was PCR amplified from R28 genomic DNA using primers *CAMTA1 UTR SacI fwd* and *CAMTA1 UTR NaeI rev* and cloned via SacI and NaeI into pMIR-RL.

**pMIR-RL-CAMTA1 miR-9 mut** For analysis of miR-9 binding sites, all sites predicted with TargetScan 5.0 and all seed matches conserved in mammals were mutated by site-directed mutagenesis from CAAA to GTTT.

**pMIR-RL-CAMTA1 miR-9\* mut** For analysis of miR-9\* binding sites, all sites predicted with TargetScan 5.0 and all seed matches conserved in mammals were mutated by site-directed mutagenesis from CTTT to GAAA.

**pIRES-CAMTA1** CAMTA1 cDNA was amplified from Marathon whole human brain cDNA library (BD Biosciences, Franklin Lakes, USA). CAMTA1 ORF was reamplified using primers *CAMTA pIRES EcoRV fwd* and *CAMTA pIRES NotI rev* and cloned via EcoRV and NotI into pIRES-neo. All CAMTA1 clones from Marathon whole human brain cDNA library contained an additional exon of 21 nt in size (AGCTGACATGGATAGCCTTGA) compared to the RefSeq sequence NM\_015215. The additional nucleotides are inserted after nt 4687 of NM\_015215 and encode for seven additional amino acids which localize to the predicted Calmodulin binding domain. Therefore, the used CAMTA1 construct encoded for a 1680 aa protein instead of the RefSeq 1673 aa protein.

**pIRES-CAMTA1  $\Delta$ N** N-terminally deleted CAMTA1 truncation lacking amino acids 1-188 (nt 1-564) which contain the predicted DNA binding domain. Fragment was PCR amplified from pIRES-CAMTA1 using primers *CAMTA $\Delta$ N pIRES RV fwd* and *CAMTA pIRES NotI rev* and cloned via EcoRV and NotI into pIRES-FH.

**pIRES-CAMTA1  $\Delta$ C** C-terminally deleted CAMTA1 truncation lacking the last 161 aa of full length 1680 aa CAMTA1. This results in deletion of the predicted IQ domain and Calmodulin binding domain. Fragment was PCR amplified from pIRES-CAMTA1 using primers *CAMTA pIRES EcoRV fwd* and *CAMTA $\Delta$ C pIRES rev* and cloned via EcoRV and NotI into pIRES-FH.

**pIRES-Flag/HA-CAMTA1** CAMTA1 was amplified with primer *CAMTA1 VP5 NotI fwd* and *CAMTA1 VP5 BamHI rev* from pIRES-CAMTA1 and cloned via NotI and BamHI into pIRES-Flag/HA.

**pIRES-Flag/HA-CAMTA1  $\Delta$ N** N-terminally deleted CAMTA1 fragment was amplified with primer *CAMTA $\Delta$ N VP5 NotI fwd* and *CAMTA1 VP5 BamHI rev* from pIRES-CAMTA1 and cloned via NotI and BamHI into pIRES-Flag/HA.

**pIRES-Flag/HA-CAMTA1  $\Delta$ C** C-terminally deleted CAMTA1 fragment was amplified with primer *CAMTA1 VP5 NotI fwd* and *CAMTA $\Delta$ C VP5 Bam rev* from pIRES-CAMTA1 and cloned via NotI and BamHI into pIRES-Flag/HA.

**pGEX-6P-1-CAMTA1 f1** Expression of N-terminal GST tagged 86 kDa CAMTA1 fragment containing aa 294-864 used for immunization of rabbits. Fragment was amplified from pIRES-CAMTA1 using primers *CAMTA1 f1 BamHI fwd* and *CAMTA1 f1/2 NotI rev* and cloned via into pGEX-6p-1.

**pGEX-6P-1-CAMTA1 f2** Expression of N-terminal GST tagged 63 kDa CAMTA1 fragment containing aa 516-864 used for immunization of rabbits. Fragment was amplified from pIRES-CAMTA1 using primers *CAMTA1 f2 BamHI fwd* and *CAMTA1 f1/2 NotI rev* and cloned via into pGEX-6p-1.

**pIRES-Flag/HA-TNRC6A** The 1709 aa TNRC6A ORF from pcDNA3.1-myc-GFP-TNRC6A was

amplified with primer *pFseI TNRC6A fwd* and *pAscl TNRC6A rev* and inserted into pIRES-Flag/HA-FA via FseI/Ascl.

**pIRES-Flag/HA-SV40NLS-Ago2 and Ago2 529E** Contains Ago2 with N-terminally fused SV40 large T-antigen NLS. Ago2 or its mutant was amplified from pIRES-Flag/HA-Ago2 and pIRES-Flag/HA-Ago2 529E using primer *pFseI NLS Ago2 fwd2* and *pAscl Ago2 rev* and cloned via FseI/Ascl into pIRES-Flag/HA-FA.

**pIRES-Flag/HA-Ago1 NLS mut and NES mut** Mutants of predicted Ago1 NLS and NES were generated by site directed mutagenesis. Ago1 putative NLS was mutated from MKRKYRV to MQQQYQV. Ago1 putative NES was mutated from EDLSYMVRELLIQ to EDVSYMVREVVIIQ.

**pIRES-Flag/HA-Ago2 NLS mut and NES mut** Mutants of predicted Ago2 NLS and NES were generated by site directed mutagenesis. Ago2 NLS was mutated from MKRKYRV to MQRKYRV and MKQKYRV. Ago2 putative NES was mutated from DLAAMVRELLIQ to DVAAMVREVVIIQ.

**pIRES-Flag/HA-Ago3 NLS mut** Mutants of predicted Ago3 NLS were generated by site directed mutagenesis. Ago3 NLS was mutated from MRRKYRV to MQQQYQV.

**pIRES-Flag/HA-Ago4 NLS mut** Mutants of predicted Ago4 NLS were generated by site directed mutagenesis. Ago4 NLS was mutated from MKRKYRV to MQQQYQV.

**pIRES-Flag/HA-Ago2 529E NLS mut and NES mut** Generation of combined Ago2 529E and putative NLS/NES mutations was done by ligation of ligating FseI/SphI digested PCR from pIRES-Flag/HA-Ago2 NLS/NES mut and SphI/Ascl digested PCR from pIRES-Flag/HA-Ago2 529E into pIRES-Flag/HA-FA. PCR was done with *pFseI Ago2 fwd* and *pAscl Ago2 rev*.

**pIRES-Flag/HA-hnRNPA1** hnRNPA1 ORF was amplified from HeLa cDNA with primer *phnRNPA1 NotI fwd* and *phnRNPA1 BamHI rev* and cloned via NotI/BamHI into pIRES-Flag/HA.

**pIRES-Flag/HA-hnRNPC** hnRNPC ORF was amplified from HeLa cDNA with primer *phnRNPC NotI fwd* and *phnRNPC BamHI rev* and cloned via NotI/BamHI into pIRES-Flag/HA.

**pFastBac-HTa-HA-Ago2** pFastBac-HTa-HA-Ago2 was cloned from pFastBac-HTa-3TEV-Ago2 (Lasse Weinmann, unpublished construct) by replacing 2 of the 3 TEV sites with HA-tag. Replacement was done by amplification of Ago2 from pIRES-Flag/HA-Ago2 with primer *pBam TEVHA fwd* and *pAgo2 NotI rev* and cloning via BamHI/NotI into pFastBac-HTa-3TEV-Ago2.

**pET28a-TNRC6A, NLS mut, NES mut, NLS/NES mut,  $\delta$ GW,  $\delta$ GW NES mut** TNRC6A or mutants ORFs were amplified from pcDNA3.1-myc-GFP-TNRC6A or mutant plasmids using primer *pTNRC6A SacI fwd* and *pTNRC6A XhoI rev* and cloned via SacI/XhoI into pET28a.

**pET28a-TNRC6B, W623A** TNRC6B or mutant ORFs were amplified from VP5-TNRC6B and mutant plasmid using primer *pTNRC6B BamHI fwd* and *pTNRC6B NotI rev* and cloned via BamHI/NotI into pET28a.

**pET28a-TNRC6C** TNRC6C ORF was amplified from VP5-TNRC6C using primer *pTNRC6C SacI fwd* and *pTNRC6C XhoI rev* and cloned via *SacI/XhoI* into pET28a.

**pET28a-Ran, Ran Q69L, Ran T24N** Ran and Ran mutant ORFs were amplified using primer *pRan FseI fwd* and *pRan AscI rev* from pCS2-Ran and Ran mutant plasmids.

**pcDNA5-FRT/TO-myc-GFP-TNRC6A, NES mut,  $\delta$ GW NES mut** myc-GFP-TNRC6A and mutant ORFs were amplified from pcDNA3.1-myc-GFP-TNRC6A or mutant plasmids using primer *pmycGFPTNRC6A fwd* and *pmycGFPTNRC6A rev* and cloned via *BamHI/XhoI* into pcDNA5-FRT/TO.

## 2.2. Working with RNA

### 2.2.1. RNA extraction

RNA extraction from cells for quantitative real-time PCR (qPCR) and microarray experiments has been done with NucleoSpin RNA Kit (Macherey-Nagel, Düren, Germany) following the manufacturer's protocol. RNA was resuspended and stored in H<sub>2</sub>O.

RNA extraction from cells for small RNA detection by Northern Blot and small RNA cloning has been done with TRIzol reagent (Life Technologies, Carlsbad, USA) essentially as described in the manufacturer's protocol. RNA precipitation from aqueous phase from samples with low amount of input material was supported by adding RNA grade glycogen (Life Technologies, Carlsbad, USA). After precipitation, pellet was washed with 80 % EtOH and finally resuspended in H<sub>2</sub>O.

For extraction of RNA from mouse organs, male or female animals of the mouse strain C57BL/6 were used. Tissue was prepared, snap frozen in liquid nitrogen and pulverized in a mortar with a pestle. Crushed tissue was lysed immediately using TRIzol reagent (Life Technologies, Carlsbad, USA), mixed rigorously and incubated for 10 min at RT. Further steps for RNA isolation with TRIzol were done as described above.

RNA extraction from Ago2-immunoprecipitations and R11 cells for miR-9\* target identification have been done as follows: R11 cells were lysed with IP lysis buffer and immunoprecipitation was done as described in section 3.1. Immunoprecipitation samples and corresponding samples of input material were proteinase K digested, followed by Roti-Phenol/Chloroform/Isoamyl alcohol extraction (Carl Roth, Karlsruhe, Germany), and precipitation of RNA in 80 % EtOH at -20 °C. RNA was pelleted, air dried and treated with DNaseI for 45 min at 37 °C, followed by thermal inactivation of DNaseI.

RNA concentration and quality for qPCR from cells and mouse tissues was determined using NanoDrop 1000 Spectrophotometer (Thermo Scientific, Rockford, USA). RNA quality for Northern Blot was additionally checked by nucleic acid staining of gels before Northern Blot in TBE supplemented with 5  $\mu$ l/100ml ethidium bromide. RNA for microarray analysis was analyzed using Bioanalyzer 2100 (Agilent Technologies, Santa Clara, USA).

### 2.2.2. Polyacrylamide urea gel electrophoresis of RNA

SequaGel UreaGel system (National Diagnostics, Atlanta, USA) was used to prepare polyacrylamide urea gels for electrophoresis of RNA. For small RNA detection, 12 % gels were prepared by mixing 29 ml concentrate, 25 ml diluent and 6 ml buffer with 24  $\mu$ l tetramethylethylenediamine (TEMED) and 480  $\mu$ l 10 % ammonium persulfate (APS). For 7sk and U6 detection after Importin knockdown, 6 % gels were prepared by mixing 14,4 ml concentrate, 39,6 ml diluent and 6 ml buffer with 24  $\mu$ l TEMED and 480  $\mu$ l 10 % APS. After polymerization for at least 1 h, gels were pre-run at 250 V for 20 min in TBE buffer prior to loading of RNA. Gel pockets were rinsed directly before loading to remove excess urea. 5 to 20  $\mu$ g RNA were mixed with 2x RNA sample buffer, heated for 2-3 min at 98 °C and loaded. Gels were run at 250 V until bromophenol blue band reaches a distance of 7 to 8 cm from pocket bottom. In 12 % denaturing polyacrylamide gels, bromophenol blue migrates at a size corresponding to about 10 nt ssRNA and xylene cyanol at about 70 nt. In 6 % gels, bromophenol blue migrates at about 26 nt and xylene cyanol at about 106 nt. No further marker for RNA length determination was used. Disassembled gels were ethidium bromide stained and used for Northern Blot as described in section 2.2.3.

### 2.2.3. Northern Blotting, probe labelling and RNA detection

Northern Blot was essentially performed as described in Pall and Hamilton, 2008. After disassembling polyacrylamide urea gels, RNA was blotted semi-dry onto a Hybond-N membrane (GE Healthcare, Little Chalfont, UK). For detection of miRNAs with 7sk or U6 as loading control, blot was done at 20 V for 30 min using H<sub>2</sub>O as transfer buffer. RNA was subsequently chemically crosslinked using EDC crosslinking solution for minimum 1 h to maximum 1,5 h at 50 °C. Membrane was shortly rinsed in water and pre-hybridized with hybridization solution. For detection of 7sk with U6 as loading control, blot was done at 20 V for 45 min. RNA was subsequently UV cross linked by exposing membrane from both sides for 30 sec each to high UV intensity from Quantum gel documentation system (Peqlab, Erlangen, Germany) and an additional chemical cross link done as described above.

Probe labeling was done using 20 pmol DNA oligonucleotide (listed in Table 1.3) with 20  $\mu$ Ci of  $\gamma$ -<sup>32</sup>P-ATP (Hartmann Analytics, Braunschweig, Germany) in a 20  $\mu$ l T4 PNK reaction according to the manufacturer's protocol (Life Technologies, Carlsbad, USA). Reaction was incubated for 30 min at 37 °C. The reaction was directly added onto a Illustra MicroSpin G-25 columns (GE Healthcare, Little Chalfont, UK) and flow through was mixed with 30  $\mu$ l 30 mM EDTA to stop PNK reaction. Radioactivity of the labeled oligo was determined.

The radioactively labeled probe was added to the pre-hybridized membrane and incubated o/n at 50 °C on rating wheel with about 50 ml hybridization solution. From U6 probe, only a fifth of one labeling reaction was used per membrane, all other reactions were used completely for one hybridization reaction. The membrane was washed twice with wash solution I and once with wash solution II for Northern Blot, incubating each wash step for 15 min on a turning wheel at 50 °C. Liquid was discarded and membrane was wrapped in saran for exposure. Signals were detected either by exposure to a Imaging Screen-K (Kodak, Rochester, USA) and read out with Personal Molecular Imager System (Bio-Rad, Hercules, USA) or exposure to BioMax MS films (Kodak, Rochester, USA) using an intensifying screen (GE Healthcare, Little Chalfont, UK) and subsequent film development. Signal quantifications were done using Personal Molecular Imager System.

For repeated hybridization of different probes on the same blot membrane, the current probe was stripped off the membrane. H<sub>2</sub>O was boiled, membrane was added to water to be completely covered and 10 % SDS was added to a final concentration of 0,1 %. After 30 min incubation at RT on a rocker, membrane was wrapped in saran end exposed to check efficiency of probe removal. Procedure was repeated if stripping was not effective.

## 2.3. cDNA synthesis and quantitative real-time PCR

### 2.3.1. qPCR for mRNA quantification

RNA was prepared for cDNA synthesis by performing an additional DNaseI digest (Life Technologies, Carlsbad, USA) using 1 µg RNA per reaction as given in the manufacturer's protocol. Reaction was incubated for 30 min at 37 °C and stopped by adding 1 µl 100 mM EDTA and heat inactivation at 72 °C for 10 min. The complete 1 µg RNA reaction was used for cDNA synthesis using First Strand cDNA Synthesis Kit (Thermo Scientific, Rockford, USA). RNA was mixed with 1 µl random hexamer primer, filled up to 11 µl with H<sub>2</sub>O and incubated for 65 °C for 5 min. Samples were chilled on ice and mixed with 4 µl 5 x reaction buffer, 1 µl 2 U/µl RiboLock RNase inhibitor, 2 µl 1 mM dNTP mix and 2 µl 20 U/µl M-MuLV reverse transcriptase. Reaction was mixed, incubated for 5 min at 25 °C and subsequently 60 min at 37 °C. Reaction was then terminated by heating to 70 °C for 5 min.

qPCR was done with Sso Fast Eva Green Mix (Bio-Rad, Hercules, USA), 0,4 µM forward and 0,4 µM reverse primer and cDNA from 50 ng RNA as template. qPCR primer sequences are shown in table 1.2. qPCRs were run on a CFX96 cycler (Bio-Rad, Hercules, USA) using standard program as given in the SsoFast EvaGreen SuperMix manual with denaturation and annealing/extension times of 5 sec, 40 cycles and a 65-95 °C melt curve. Data were evaluated using  $\Delta\Delta C_t$  method (Livak and Schmittgen, 2001) with GAPDH or  $\beta$ -Actin as reference mRNA and normalized to control sample. Error bars were calculated from three biological replicates.

### 2.3.2. qPCR for miRNA quantification

For miRNA quantification, DNaseI treated RNA samples were poly(A)-tailed using Poly(A) Tailing Kit (Life Technologies, Carlsbad, USA) according to the manufacturer's protocol. Samples were then reverse transcribed with First Strand cDNA Synthesis Kit (Thermo Scientific, Rockford, USA) using URT primer (1.2, Hurteau et al., 2006).

## 2.4. miRNA target identification

miRNA target identification has been done as described previously in Beitzinger et al., 2007 and Schraivogel et al., 2011. The experimental procedure described here has been taken in parts from Schraivogel et al., 2011. In short, RNA from anti-Ago2 IP and input samples was extracted as described in section 2.2.1. RNA was further processed using the SuperAmp RNA amplification protocol (Miltenyi, Bergisch Gladbach, Germany). cDNA integrity was checked via Bioanalyzer. 250 ng of each cDNA was labelled with Cy3 dye (Miltenyi, Bergisch Gladbach, Germany) according to the manufacturer's protocol. Samples were then hybridized to Whole Human Genome 4x44

K Oligo Microarrays (Agilent Technologies, Santa Clara, USA). Fluorescence signals for Cy3 were detected using Microarray Scanner System (Agilent Technologies, Santa Clara, USA).

Microarray data were analyzed using Genespring software (Agilent Technologies, Santa Clara, USA) and further processed using Excel. Expression values  $< 0,01$  were set to  $0,01$ . Each measurement was divided by the 50th percentile of all measurements in that sample. All IP samples were normalized to the corresponding input RNA samples. The IP sample from control and miR-9\* inhibitor transfected cells was normalized against the median of the corresponding input RNA samples. For normalization, each measurement for each gene in the IP samples was divided by the median of that gene's measurements in the corresponding input RNA samples. IP to input ratios from miR-9\* inhibitor transfected samples were then divided by the IP to input ratios from control transfected sample.

Using this normalization procedure, the normalized expression value of each transcript in the IP samples reflects its fold enrichment in the immunoprecipitated transcript pool relative to the input RNA pool. All transcripts that were more than 5-fold enriched in IPs from control inhibitor transfected cells were isolated to filter for potential miRNA target mRNAs bound by Ago2. Transcripts with a  $> 10$ -fold decrease in miR-9\* inhibitor transfected cells compared to control-transfected cells were selected as potential targets of miR-9\*.

## 2.5. Transcriptome analysis after CAMTA1 overexpression

To analyze transcriptome response after CAMTA1 overexpression, LN-229 cells were transfected with pIRES-CAMTA or pIRES using Lipofectamine 2000 as described in section 4.3. RNA was prepared using column-based preparation with NucleoSpin RNA Kit (Macherey-Nagel) and RNA quality was determined by measuring A260/A280 ratio with NanoDrop (Thermo Scientific). RNA samples were processed and hybridized on GeneChip Human Gene 1.1 ST Arrays (Affymetrix) at KFB Regensburg in biological duplicates. Those arrays are designed to cover the whole human transcriptome with probes against about 30000 protein-coding and 11000 long intergenic non-coding RNA transcripts (lincRNAs). Fold change for each biological duplicate was calculated. Heat map was built with GiTools 2.2.1.

## 2.6. Generation of small RNA libraries and Deep sequencing

### 2.6.1. Small RNA libraries and Deep sequencing from CD133-sorted R11 cells

The following procedure has been previously reported in Schraivogel et al., 2011 and partially adopted. Small RNA libraries were generated by Vertis Biotechnology (Freising, Germany) and sequenced by 454 pyrosequencing as previously described (Tarasov et al., 2007). Known miRNAs were identified by comparing the sequencing results with annotated miRNAs from the *H. sapiens* miRBase release 10.0 (08/2007) using Microsoft Excel software. Several miRNA reads were found to contain sequencing errors, typically starting from nucleotides 18 to 25 that were possibly due to the procedure of library preparation and/or pyrosequencing. Most errors were poly(A) insertions at the 3'-end of the reads. Therefore, those reads that were fully complementary to a known miRNAs from nucleotides 1 to 18 but had additional poly(A) insertions at the 3'-end were re-annotated as miRNAs. Read numbers for each miRNA were normalized to the total number

of reads of the corresponding library. For calculation of miRNA expression, the normalized read numbers from the CD133-negative cell library were divided by the normalized read numbers from the CD133-negative library.

### **2.6.2. Generation of small RNA libraries from cells with DNA damages**

Nuclear RNAs were isolated from cells and cloned essentially as described in Dueck et al., 2012 without size selection for 21 nt small RNAs prior to RNA cloning. 2  $\mu$ g RNA were used as input material for 3'-adapter and 5'-adapter ligation. After cloning and extraction from gel, cluster generation, sequencing and FastQ file generation were carried out at sequencing core facility at Center of Excellence for Fluorescent Bioanalytics (KFB) at Regensburg University. Datasets were analyzed in the department of Rainer Spang at Regensburg University.

## **3. Proteinbiochemical methods**

### **3.1. Immunoprecipitations**

#### **3.1.1. Ago2 immunoprecipitation for miRNA target identification**

To identify miR-9\* target mRNAs, immunoprecipitation of Ago2 for enrichment of Ago2-associated mRNAs was done as described in Schraivogel et al., 2011. R11 cells were transfected with miR-9\* and control inhibitors for 2 days in four 10 cm plates per inhibitor. Cells were then lysed in 2 ml IP lysis buffer supplemented with 1  $\mu$ l/ml Ribolock (Life Technologies, Carlsbad, USA) by incubation for 20 min at 4 °C. Lysate was cleared by centrifugation at 16000 g for 10 min. In advance, 3 ml of anti-Ago2 11A9 hybridoma supernatant was coupled to 100  $\mu$ l Protein-G Sepharose beads (GE Healthcare, Little Chalfont, UK) for over night at 4 °C. All centrifugation steps with beads were done for 1 min at 1000 g. Coupled beads were washed twice with PBS. Beads were subsequently incubated with cell lysate for 4 h at 4 °C. All IP samples were washed twice with IP wash buffer, transferred into a new 1,5 ml tube and washed again once with IP wash buffer and once with PBS.

### **3.2. Protein expression, purification and antibody production**

#### **3.2.1. Proteins for immunization of rats and rabbits**

CAMTA1 fragments were expressed in BL21 as N-terminal GST fusions and directly used for immunization of rabbits. TNRC6A, B and C RRM domains were expressed in *E. coli* and used for immunization of rats.

#### **3.2.2. HA-tagged Ago2**

Human HA-tagged Ago2 was expressed in Sf-21 cells as described in section 4.2. Purification has essentially been done as described in Pfaff et al., 2013. pFastBac-HTa-HA-Ago2 was used for virus production. Purification was done from 2,5 l culture infected with viral stock and cultivated for 72 hours at 27,5 °C. Cells were harvested at 300 g for 10 min at RT and lysed using 120 ml Buffer A and additional sonification. Lysate was cleared by centrifugation at 40.000 g for 60 min at 4 °C. Cleared lysate was filtered through a 45  $\mu$ m filter and loaded onto a Ni-loaded HiTrap IMAC FF 5 ml column (GE Healthcare, Little Chalfont, UK). After binding, column was washed extensively with 10 column volumes of Buffer A and 5 column volumes 5 % Buffer B. Elution was done with 100 % Buffer B and eluate was collected from peak fractions, supplemented with tobacco etch virus (TEV) protease (kindly provided by Leonhard Jakob) and incubated over night. Sample was loaded on a HiPrep 26/60 desalting column (GE Healthcare, Little Chalfont, UK) using desalting buffer to increase salt concentration. Peak fractions were collected and applied again onto Ni-loaded HiTrap IMAC FF 5 ml column and unbound flow-through was collected.

Two different Ago2 stocks were produced with different properties: Flow through from second IMAC was collected, concentrated and resolved by size-exclusion chromatography with a HiLoad Superdex 200 26/60 column (GE Healthcare, Little Chalfont, UK) in gelfiltration buffer. Fractions corresponding to HA-Ago2 were collected, pooled and concentrated (Stock I). Due to incomplete TEV cleavage, TEV cleavage was repeated from bound fractions of second IMAC. All steps after TEV cleavage were repeated as described above. However, as TEV cleavage was again incomplete, bound and unbound peak fractions were collected after elution from second IMAC. Bound and unbound peak fractions were pooled, concentrated and resolved by size-exclusion chromatography as described above. Fractions corresponding to His-HA-Ago2 and HA-Ago2 were collected, pooled and concentrated (Stock II).

Stock I containing pure HA-Ago2 was used for anti-Flag-pulldowns from *Xenopus laevis* oocytes. Stock II containin HA-Ago2 as well as His-HA-Ago2 was used for GST-pulldowns with TNRC6A and Import factors.

### 3.2.3. GST- and His-tagged Importins and Nucleoplasmin

Recombinant human Importin  $\alpha$  subtypes were expressed as GST- and His-fusion proteins and purified as described in Depping et al., 2008. Proteins were expressed in *E. coli* BL21. Cells were grown and expression was induced by IPTG for 4 h at 25 °C. Cells were harvested and lyzed in a French Press. Lysate was cleared for 1 h at 22.000 rpm in a SS-34 rotor. Cleared lysate was incubated for 2-3 h at 4 °C with glutathion sepharose beads (GE Healthcare, Little Chalfont, UK). Beads were washed 3 times and protein was subsequently eluted with elution buffer. Protein samples were dialyzed against dialysis buffer and concentrated if necessary. His-tagged Importins and Nucleoplasmin were purified by metal affinity chromatography using BD TALON metal affinity resin (Clontech-Takara Bio Europe, Saint-Germain-en-Laye, France) according to the manufacturer's instructions and as described in Depping et al., 2008.

### 3.2.4. His-tagged Ran and Ran mutants

His-tagged human Ran and GTPase defective mutant RanQ69L were expressed in *E. coli* BL21. Cells were grown to OD600 = 0,5 and expression was induced adding IPTG for 13 h at 37 °C. Cells were harvested and lyzed in 100 ml Buffer A and additional sonification. Lysates were cleared for 40 min at 22.000 rpm, supernatant was filtered through a 45  $\mu$ m filter and applied onto a Ni-loaded HiTrap IMAC FF 5 ml column (GE Healthcare, Little Chalfont, UK). Column was washed with mixed buffer A and B resulting in 22 mM Imidazole. Elution was done with 100 % Buffer B. Fractions containing Ran were pooled, dialyzed against 2 l Dialysis buffer over night in a dialysis tube with a MWCO of 12 kDa (Carl Roth, Karlsruhe, Germany). Dialysate was concentrated in a Centricon 10k (Merck Millipore, Darmstadt, Germany) and protein concentration was determined using Bradford assay (Bio-Rad, Hercules, USA). Dialysis was set up to largely match IP lysis buffer.

### 3.3. Antibody production and purification

#### 3.3.1. Antibody production from immunized rats and rabbits

Immunization of rats and production of hybridoma clones was done as described in Beitzinger et al., 2007. All steps were done by Elisabeth Kremmer at Helmholtz Zentrum Munich and provided as hybridoma supernatants. Polyclonal antibodies were generated by immunization of rabbits as described in Weinmann et al., 2009. All steps were done at core facility of Max-Planck-Institute of Biochemistry Martinsried/Munich and provided as blood serum.

#### 3.3.2. Antibody purification

Monoclonal antibodies were purified with CnBr activated sepharose 4 fast flow (GE Healthcare, Little Chalfont, UK) coupled recombinant antigen used for immunization. Sepharose columns were prepared by swelling 300 mg sepharose powder in 1 mM HCl for 30 min on ice. 300 mg sepharose was directly transferred into 10 ml gravity flow columns (Bio-Rad, Hercules, USA). Column was allowed to empty by gravity flow and washed once with about 10 ml coupling buffer until flow through was at pH 8,4. In advance, purified recombinant antigen was dialyzed against 1 l of coupling buffer over night at 4 °C. Dialysate was applied to column and incubated over night at 4 °C or for 4 h at RT on turning wheel. After incubation, column was emptied by gravity flow and washed with 5 packed column volumes (pcv) coupling buffer. Sepharose was resuspended in 1 M ethanolamine pH 8,0 and incubated for 2 h at room temperature to block unused activated CnBr. Column was washed 8 x with 3 pcv wash buffer using alternate low and high pH wash buffer. Column was then washed once with 10 ml PBS and completely emptied by gravity flow. Hybridoma supernatant or rabbit blood serum was freed from debris by centrifugation at 4000 rpm for 5 min and supernatant was added to coupled sepharose. Coupling was done by incubation over night at 4 °C. After incubation, column was emptied by gravity flow and washed two times with 1 pcv PBS. Coupled antibody was eluted with elution buffer and immediately mixed with 100 µl 1 M Tris pH 8,8 per 1 ml eluate. Antibody, yield and concentration was checked by Coomassie staining and NanoDrop measurement.

Polyclonal antibodies were purified by HiTrap Protein A FF columns by affinity purification. Purification was done by Nicholas Putz.

### 3.4. *in vitro* transcription/translation

Coupled *in vitro* transcription/translation of human GW182 proteins were performed using TNT Coupled Reticulocyte Lysate System (Promega, Madison, USA) according to the manufacturer's protocol. pET28a plasmids were used for T7-dependent transcription containing TNRC6A, TNRC6B, TNRC6C wildtype and mutant coding sequences. Sequences were transcribed and translated *in vitro* in the presence of [<sup>35</sup>S]-methionine (Hartmann Analytics, Braunschweig, Germany).

## 3.5. Preparation of cell extracts

### 3.5.1. Preparation of whole cell extracts

Cell extracts for analysis of Ago2 and TNRC6A and corresponding controls, cells were lysed with IP lysis buffer. About  $1 \times 10^6$  cells were thoroughly resuspended in 100  $\mu$ l IP lysis buffer by pipetting and incubated on ice for 20 min with vortexing time by time. Lysates were then cleared by centrifugation at highest speed for 15 min at 4 °C in a table top centrifuge. Supernatant was supplemented with Laemmli buffer or used for Immunoprecipitations.

Whole cell extracts for analysis of CAMTA1 and corresponding controls were generated by cell lysis in nuclear lysis buffer for 20 min and subsequent sonification for 10 s using a Sonopuls HD2070 sonifier (Bandelin Electronic, Berlin, Germany). SDS and other components of nuclear lysis buffer ensure complete dissociation of the cell. Lysates were then cleared by centrifugation at highest speed for 15 min at 4 °C in a table top centrifuge. Supernatant was supplemented with Laemmli buffer.

For direct and fast lysis of whole cells, cells were scraped off the wells in PBS, centrifuged for 4 min at 100-200 g and resuspended in 1 x Laemmli buffer. After sonification for 15 sec, samples were loaded on Western Blot.

### 3.5.2. Preparation of subcellular extracts

Nucleo-cytoplasmic fractionations were done from HeLa S3 suspension cultures according to Dignam et al., 1983 with some slight modifications. Cells were harvested for 20 min at 500 g, washed once with PBS and packed cell volume (pcv) was detected (1 l HeLa S3 suspension culture at  $1 \times 10^6$  cells/ml gives a pcv of about 2,5 ml). Cells washed once carefully with 5 pcv Roeder A, centrifuged for 5 min at 1000 g and resuspended in 3 pcv Roeder A. Cells were incubated for 15 min on ice for swelling and transferred into a douncer with a Type B pestle. Cells were dounced until Trypan-blue exclusion staining revealed 90 to 95 % positive cells. Lysate was centrifuged for 10 min at 3000 g. Supernatant was taken, volume was determined and supplemented with 0,1 vol Roeder B which gave the raw cytoplasmic extract. Raw cytoplasmic extract was cleared by high speed centrifugation for 60 min at 100000 g, lipid film was completely taken off from the top of the supernatant and remaining supernatant was saved as cleared cytoplasmic extract. Nucleus pellet was washed twice with 5 pcv Roeder A and resuspended in 3 ml/ $10^9$  cells Roeder C. Nuclei were lysed by 10 strokes with type B pestle and 30 min incubation at 4 °C on a magnetic stirrer. Extract was crude nuclear extract. Soluble and insoluble nuclear extracts were generated from crude nuclear extract by centrifugation for 20 min at 25000 g. Supernatant and pellet were separated, pellet was resuspended in 3 ml/ $10^9$  cells Roeder C and sonified. Both fractions were cleared by high speed centrifugation for 20 min at 25000 g and declared as cleared nuclear soluble and insoluble extract. Samples were analyzed by Western Blot and detection of nuclear Lamin A/C and cytoplasmic  $\alpha$ Tubulin.

## 3.6. GST pulldowns

GST pulldowns were done essentially as described in Steinhoff et al., 2009. Proteins were expressed and purified as described in section 3.2.3 and 3.2.2. Coupled *in vitro* transcription/translation was described in section 3.4.

Purified His-Importin  $\beta$ , HA-Ago2 or Nucleoplasmin was added to Importin  $\alpha$  if needed. [ $^{35}\text{S}$ ]-labelled protein was added to the reaction and incubated at 4 °C for 1 h with GST pulldown buffer pre-equilibrated glutathion sepharose beads (GE Healthcare, Little Chalfont, UK). After incubation, samples were washed three times with GST pulldown buffer and elution was done by adding 1 x Laemmli buffer. To detect [ $^{35}\text{S}$ ]-labeled proteins, the dried gels were autoradiographed and binding was visualized by analyzing the data with a CR 35 BIO (Dürr Medical, Bietigheim-Bissingen, Germany) and the Aida Image Analyser v 4.27 (Raytest, Straubenhardt, Germany).

### 3.7. SDS-PAGE and Western-Blot

SDS-PAGE gels were prepared with a 10 % separation gel and 5 % stacking gel. After polymerization, gels were stored at 4 °C until use. Samples were mixed with 4x Laemmli buffer and heated for 5 min at 95 °C. After gel run with SDS running buffer, proteins were blotted semi-dry onto a Hybond-ECL membrane (GE Healthcare, Little Chalfont, UK) using Towbin buffer for 2 h at 13 V. Membrane was blocked using Western Blot blocking buffer. Antibodies were incubated using Western Blot wash buffer. Between 1st and 2nd antibody, membrane was washed three times for 10 min with Western Blot wash buffer. After 2nd antibody, membrane was washed once with Western blot wash buffer and twice for 10 min with PBS. Antibodies are listed in table 1.8. 2nd antibody was peroxidase coupled and signal was produced using enhanced chemiluminescence (ECL) substrate as described in Sambrook et al., 1989.

## 4. Cell Biological Methods

### 4.1. Cultivation of mammalian cells

All cells except for HeLa S3 spinner cultures were cultivated at 37 °C in a humidified chamber with air atmosphere and addition of 5 % CO<sub>2</sub>. HeLa spinner cultures were cultivated at 37 °C in air atmosphere. HPAEC were grown on gelatine coated surface, all other cell lines were cultivated on uncoated plastic surface.

Human glioblastoma cell lines (except for immortal glioblastoma cell lines) were cultivated in 6-well formate with 2 ml neural stem cell medium complete per well. Cells were passaged all 3 to 5 days by detaching with a pipette. In all, 50 % of the medium was substituted twice weekly and cells were transferred into new wells after each passage. Cell lines were not used for experiments directly after isolation from patients but were passaged frequently before. The number of passages is not known.

HeLa, HEK 293T, NIH 3T3, U-2 OS, HCT116, Hep G2, HuH-7, A549, H1299, MCF7, T-47D, NCCIT, MRC-5, DU 145, GM5756, Ntera2, LN-229, U87MG, T98G, SMA-560 and Sk-Mel-28 were cultivated in standard cell culture medium. Arpe-19 was cultivated in DMEM-F12 complete medium. DLD-1 and LNCaP were cultivated in RPMI complete medium. Cells were passaged twice weekly using trypsinization. Trypsin was purchased as 1x solution from Sigma Aldrich (Munich, Germany).

Human pulmonary artery smooth muscle cells (HPASMC) were cultivated in SmBM complete and human pulmonary artery endothelial cells (HPAEC) were cultivated in EBM-2 complete. Primary keratinocytes were cultivated in Keratinocyte medium. Cells were passaged twice weekly using trypsinization.

For growing HeLa S3 cells in suspension cultures, 10 15 cm plates of adherent HeLa S3 were detached by trypsinization, pelleted by centrifugation at 200 g for 5 min and used to inoculate 150 of Joklik's medium in a spinner flask (Corning). Suspension culture adapted cells were then frozen and new suspension cultures were directly inoculated from frozen cells. Cells were cultivated with closed lids, allowing atmosphere to refresh every 48 h. Cells were diluted twice weekly to concentrations of 0,5 x 10<sup>6</sup> cells/ml and maximum cell density before splitting was 1,0 to 1,2 x 10<sup>6</sup> cells/ml.

For transfections with Lipofectamine 2000 or Nucleofection, cells were cultivated without penicillin/streptomycin 1 d before transfection.

### 4.2. Cultivation of insect cells and baculovirus production

Recombinant baculovirus production and cultivation of insect cells was done as described in the Bac-to-Bac manual and guide to baculovirus expression vector systems and insect cell culture techniques manual provided by Life Technologies (Carlsbad, USA).

### 4.3. Cell transfections

R11 and R8 were transfected with 2'-O-methylated miRNA inhibitors, miRNA mimics and siRNAs using Lipofectamine 2000 (Life Technologies, Carlsbad, USA).  $4 \times 10^5$  cells were used per transfection and final concentrations of 100 nM for 2'-O-methylated miRNA inhibitors or 40 nM for siRNAs and miRNA mimics were used. Transfections were done in 6-well format using 5  $\mu$ l Lipofectamine 2000, 10 cm format using 25  $\mu$ l Lipofectamine 2000 or T75 flasks using 60  $\mu$ l Lipofectamine 2000. Transfection premixes containing OptiMEM with siRNA/miRNA/inhibitor and OptiMEM with Lipofectamine 2000 were prepared and incubated for 5 min, mixed and incubated for further 20 min before cells were added. For cotransfection of two different 2'-O-methylated miRNA inhibitors into R11, each oligo was added to 50 nM final concentration, to give an overall concentration of 100 nM. Transfection mix was removed 24 h post-transfection and fresh SCM was added.

R28, R11, LN-229 and SMA-560 were transfected with plasmids by electroporation using Nucleofector Device I and Nucleofector Kit R (both from Lonza, Basel, Switzerland). 3 Mio cells LN-229 and SMA-560 and 100.000 cells R28 and R11 were used per transfection. 5  $\mu$ g plasmid were transfected using program A-33 and cells were plated out on 10 cm plates. For nucleofection, plasmids were prepared using EndoFree Plasmid Midi Kit (Qiagen, Hilden, Germany) to ensure optimal cell viability after transfection.

T98G was cotransfected with plasmids and 2'-O-methylated miRNA inhibitors using Lipofectamine 2000 (Life Technologies, Carlsbad, USA) as given by the manufacturer's forward protocol. Inhibitors were used at 80 nM final concentration, siRNAs at 40 nM final concentration and pMIR-RL plasmids were transfected with 100 ng/48-well well. All transfections were done in 48-well format.

HEK 293T was transfected with plasmids using Lipofectamine 2000 (Life Technologies, Carlsbad, USA) according to the manufacturer's forward protocol and 90 % confluent cells in different plate formats.

### 4.4. Preparation of stable cell lines

#### 4.4.1. Generation of stable HeLa cell lines

For generation of stable HeLa cell line expressing FH-SV40NLS-Ago2, HeLa was transfected with pIRES-Flag/HA-SV40NLS-Ago2 in 6-well format. Cells were split one day post transfection into one 15 cm plate and selection was started with 400  $\mu$ g/ml G418 (GE Healthcare/PAA). Clones were picked 4 weeks after transfection and tested for expression by Western and Immunofluorescence. Stable clones were maintained in the same medium as used for selection.

#### 4.4.2. Generation of stable inducible HEK 293T cell lines

For generation of stable inducible Flp-In T-REx 293 cell lines, cells were grown for 24 h without Zeocin and Blasticidin until transfection. Cells were cotransfected with pOG44 and pcDNA5-FRT/TO in a 9:1 ratio in 6-well format and split to one 10 cm plate one day post-transfection. Selection was started two days post-transfection by splitting cells into two 15 cm plates and addition of 15  $\mu$ g/ml Blasticidin and 200  $\mu$ g/ml Hygromycin B (Life Technologies). Clones were picked two weeks later and tested for Zeocin sensitivity, inducibility and expression levels. Expression

was induced for 24 h with 1  $\mu\text{g/ml}$  Tetracycline (Sigma Aldrich). Stable clones were maintained in the same medium as used for selection. Stable T-REx 293 cell lines were generated by Kerrin Hansen Intana.

#### **4.4.3. Generation of a stable Luciferase expressing R28 cell line**

Third-generation packaging, VSV-pseudotyped, self-inactivating lentiviral vectors were produced by transient transfection of HEK 293T cells using standard protocols (Wübbenhorst et al., 2010). Medium was changed to stem cell medium after 24 h. Supernatants were filtered through 0,45  $\mu\text{m}$  filter and used for spin infection (Leisegang et al., 2008). Individual wells of a 24-well plate were coated with 400  $\mu\text{l}$  RetroNectin (Takara Bio, Otsu, Japan) at 12,5 mg/ml final concentration for 2 h at room temperature, subsequently incubated for 30 min at 37 °C with bovine serum albumine (2 % in PBS) and washed with PBS prior to addition of cells.  $1 \times 10^5$  cells/ml suspension cells were added onto RetroNectin coated wells. 1 ml virus containing supernatant supplemented with protamine sulphate at 4 mg/ml final concentration was added to each well and infection was enhanced by 90 min centrifugation at 32 °C and 800 g. Cells were incubated at 37 °C. The next day, cells were washed off the wells, spun down, resuspended in 5 ml fresh SCM and further cultivated.

Cell line was tested by detection of Luciferase activity on a Mithras LB 940 luminometer (Berthold Technologies, Bad Wildbad, Germany). Luciferase substrate reagents were purchased from PJK (Kleinbittersdorf, Germany).

### **4.5. Investigation of nucleocytoplasmic transport processes**

#### **4.5.1. Heterokaryon Assay**

$2 \times 10^5$  HeLa cells, stable monoclonal HeLa or HEK 293T TRex FLP/IN were plated out on cover slips in 24-well plates one day before assay. HEK TRex FLP/IN cell lines were induced 24 h before addition of NIH 3T3 cells. 2 h before addition of NIH 3T3 cells, medium was changed to DMEM/CHX solution.  $4 \times 10^4$  cells NIH 3T3 were added to wells and cocultured with HeLa for 2 to 4 h until attachment of NIH 3T3. Cells were then treated with 1 ml PEG solution for 2 min at room temperature followed by 5 washing steps with PBS-A. Then, DMEM/CHX solution was added again to cells for 4 hours. Assay was stopped by adding IF Fixation solution. For detection of endogenous Ago2 or FH-NLS-Ago2, cells were used for immunofluorescence staining as described in section 5.1. For detection of eGFP-Ago2 or eGFP-Ago2 Y529E, cells were directly mounted after Fixation solution, Stopping solution and one PBS-A wash.

#### **4.5.2. Leptomycin B treatments**

Leptomycin B was purchased from Cayman Chemicals (Ann Arbor, USA) as 0,1 mg/ml solution in Ethanol. Leptomycin B was added to cells to 10 ng/ml final concentration in standard cultivation medium. Ethanol was added to control cells without Leptomycin B. Treatments were done for 4 h and stopped by addition of Fixation solution for IF and subsequent immunofluorescence staining as described in section 5.1.

## 4.6. Flow cytometry

### 4.6.1. Fluorescence-activated cell sorting and analysis

Cells were trypsinized and washed with DMEM-F12 and FACS buffer. FACS staining has essentially been done as described in anti-CD133-PE manual (Miltenyi, Bergisch Gladbach, Germany). In short,  $10^7$  cells were resuspended in 80 ml FACS buffer containing 10 % FcR blocking reagent (Miltenyi, Bergisch Gladbach, Germany) and incubated for 5 min on ice. In all, 10  $\mu$ l anti-CD133-PE was added, and cells were incubated for 10 min on ice in the dark. Cells were pelleted and washed once with FACS buffer. Stained cells were sorted on an FACS Aria system (BD Biosciences, Franklin Lakes, USA). Cell debris were gated out using a forward scatter/sideward scatter dot plot. CD133-negative and CD133-positive cell populations were identified using unstained cells as control.

### 4.6.2. Cell cycle progression analysis

Cells were harvested by trypsinization, Trypsin was neutralized with standard cell culture medium and  $2 \times 10^6$  cells were collected by centrifugation at 200 g for 5 min at 4 °C. Cells were washed once with 4 °C PBS and resuspended in 300  $\mu$ l 4 °C PBS. Cells were fixed by dropwise addition of 700  $\mu$ l ice cold 70 % EtOH while gently vortexing and subsequently incubated for 1 h at 4 °C. Cells were collected again by centrifugation, washed once with 1 ml PBS and resuspended in 1 ml PBS with 100  $\mu$ g/ml RNase A. After incubation for 1 h at 4 °C, 50  $\mu$ l 1 mg/ml Propidium Iodide (Sigma Aldrich, Munich, Germany) was added to cells. Cells were then stored in the dark at 4 °C and analyzed using CyFlow Space (Partec, Münster, Germany) at 488 nm.

## 4.7. Neurosphere-formation assays

Analysis of neurosphere-formation in primary glioblastoma cell lines have been done following transfection with miRNA inhibitors, miRNA mimics or siRNAs using Lipofectamine 2000 or plasmids using Nucleofection. Transfections have been done as described in section 4.3. For effects of miRNA mimics, inhibitors and siRNAs, cells were transfected twice with 7 d between 1st and 2nd transfection. Single transfections did not lead to significant effects by miRNA inhibitors and miRNA mimics, presumably due to transient activity of the transfected RNA. Plasmid transfection have been done only once.

$1 \times 10^5$  cells R11 were transfected in 6-well plates. For the second transfection, cells in control transfected sample was counted and again  $1 \times 10^5$  cells were used for transfection. From non-control samples, the same proportion of cells as in the control sample was used.

1 to 4 weeks after the last transfection or as soon as clear neurospheres (clearly distinguishable from not growing cell clumps) appeared, spheres were counted under inverted microscope. For each 6-well well, cells were counted as follows: Cells in the microscope field of view were counted throughout a complete well diameter and diameters were counted in duplicates per well with 90° between the two diameter lines. The ratio of spheres in control versus non-control samples was constant during late and early timepoints of counting.

## 4.8. Luciferase Reporter Assays

Dual luciferase reporter assays have been done with T98G and HeLa cells. pMIR-RL encodes for firefly (*Photinus pyralis*) and renilla (*Renilla reniformis*) luciferases. Firefly luciferase expression is initiated from constitutive CMV promoter and a 3'-UTR was cloned downstream of firefly open reading frame, which controls expression of firefly. Renilla is under control of constitutive SV40 promoter. Cells were cotransfected with 250 ng pMIR-RL and miRNA inhibitors, siRNAs and siPools. For cotransfection with other plasmids, 125 ng of each plasmid was transfected. Transfections have been done in 48-well format as described in section 4.3. T98G was analyzed 24 h post-transfection. HeLa was analyzed 48 or 72 h post-transfection. T98G was used as it was the glioblastoma cell line with highest transfection efficiency and high firefly and renilla expression levels. Cells were lysed in passive lysis buffer (Promega, Madison, USA). Luciferase activities were measured on a Mithras LB 940 luminometer (Berthold Technologies, Bad Wildbad, Germany). Luciferase substrate reagents were purchased from PJK (Kleinbittersdorf, Germany). Coelenterazine and DTT were added freshly before use. All samples were assayed in 3 technical and 3-6 biological replicates. Data were analyzed by calculating firefly/renilla ratio for each well and normalization of the ratios to control transfected samples.

# 5. Microscopy

## 5.1. Immunofluorescence stainings

Fixation solution was prepared as 1x stock and frozen at -20 °C until use. PBS-A, Fixation solution and Stopping solution were prewarmed to 37 °C before addition to cells to prevent damage of cell morphology prior to fixation. For immunofluorescence stainings, cells were cultivated 1 day before staining in 24-well plates with 12 mm diameter cover slips of thickness #1,5 (0,15-0,19 mm) for confocal microscopy (Carl Roth, Karlsruhe, Germany). All steps were done in 24-well format with 500 µl volumes for all washing steps or 300 µl for antibody containing solutions. During all wash steps, the time in which sample was exposed to air was minimized by addition of new wash solution directly after aspirating the wash step before.

Cells were washed once with PBS-A and fixed with Fixation solution for 10 min at 37 °C. Fixation of cells expressing eGFP or related fluorescent proteins which will be detected later on was reduced to 8 min at 37 °C to prevent protein damage. Fixation was stopped adding Stopping solution for 5 min. All following steps were done at room temperature. Cells were washed once with PBS-A and permeabilized with Permeabilization solution for 30 min. Permeabilization solution was thoroughly vortexed before adding to cell in order to reduce detergent micelle size allowing consistent and efficient permeabilization while preventing morphology changes. After washing off detergent by one wash step with PBS-A, cells were blocked with Wash solution containing 5 % BSA for 30 min. First antibody incubation was done in Wash solution for 1 h at room temperature or over night at 4 °C. After three washing steps with Wash solution and incubation for 5 min at RT between wash step 2 and 3, secondary antibody was added for 1 h at room temperature or 4 °C over night. Cells were then washed once with Wash solution and thrice with PBS-A and incubated for 5 min between PBS-A wash 2 and 3 and between 3 and 4. Cells were then mounted using Prolong Gold with 4',6-diamidino-2-phenylindole (DAPI) (Life Technologies, Carlsbad, USA): 11 µl mounting medium was placed on a microscope slide, excess liquid was removed from cover slip by dipping on paper and cover slip was placed inverted on the mounting medium drop. Mounting medium was allowed to dry for minimum 12 h.

## 5.2. Microscopy

Confocal microscopy has been done with a TCS SP8 (Leica Microsystems, Mannheim, Germany) inverted microscope equipped with acousto-optical beam splitter, 405 nm laser (for DAPI), Argon laser (488 nm for Alexa 488 and GFP) and DPSS laser 561 nm (for Alexa 555). All confocal images were recorded using objective HC PL APO 63x/1,30 GLYC CORR CS2 and focusing to the z section with the biggest nucleus diameter. Images for quantifications have been recorded with HyD SP GaAsP detectors (Leica Microsystems, Mannheim, Germany). Images were recorded using following microscope and scanning settings: Format 1024 x 1024; scan speed 700, 1000 or 1400 Hz; unidirectional scanning; pinhole size of 1 AU calculated by LAS AF for emission  $\lambda = 580$

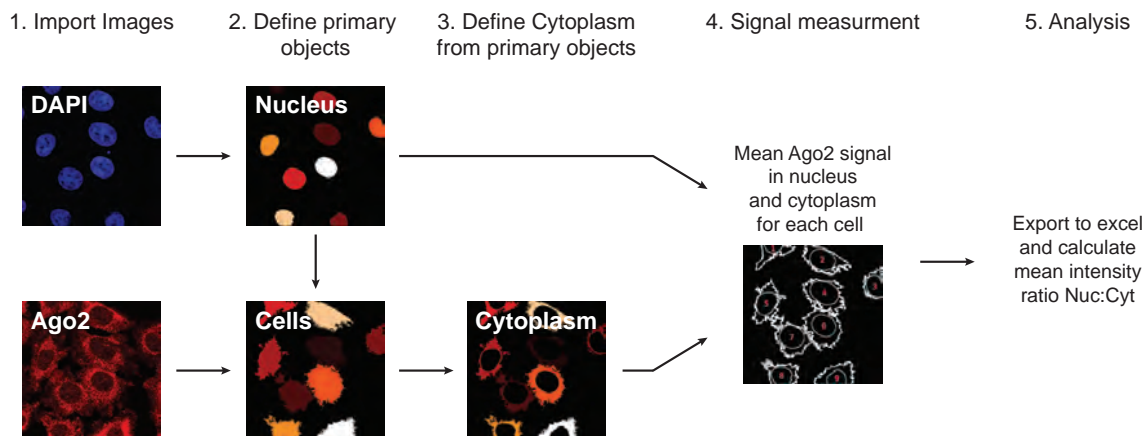


**Figure 4.5.1. Schematic demonstration of CellProfiler pipeline generated for measurement of cytoplasmic to nuclear protein distribution.** Pipeline is shown using the example of an Ago2 staining with anti-Ago2 11A9 antibody and HeLa cells.

nm; 3 line averages. PMT detector gain was set to 750 V and offset was reduced until 50 % of all image background pixels showed no signal. HyD detectors were set to standard mode and were not changed from initial company settings. Scan speed and not the zoom mode was changed to record either large or small field of views. Following procedures were done to prevent cross talk between dyes: Dye combinations were chosen which show clearly separated extinction and emission spectra (Alexa Fluor 488, 555 and 594); all channels were recorded separately using sequential scanning mode. Cross talk was controlled by recording samples without primary or secondary antibodies. Background detection was reduced by initial adjustment of laser power and detector gain to detect minimal or no signal from samples without primary antibody.

Fluorescence microscopy was done with a Axiovert 200 inverse microscope (Zeiss Microscopy, Jena, Germany) with Axiovision software (Zeiss Microscopy, Jena, Germany) or on a Eclipse TE2000 inverted microscope (Nikon Instruments, Düsseldorf, Germany) equipped with a Zeiss camera and Axiovision software.

### 5.3. Microscopy data analysis and quantifications

Quantifications were done from tif files exported from LAS AF software (Leica Microsystems, Mannheim, Germany). Quantification was automated using CellProfiler v. 2.1.0 (Carpenter et al., 2006). CellProfiler pipeline is shown in Figure 4.5.1. In a first step, the pipeline detects nuclei from DAPI pictures. Cytoplasm was detected from anti-Ago2 or anti-TNRC6B antibody staining around nucleus objects. Then nuclear and cytoplasmic objects were separated with a margin of 10 pixels around the nuclear envelope from where no signal was included into analysis. Signal from antibody staining was then measured as a mean pixel value from nuclear and cytoplasmic objects and exported to a Excel file. Nucleo-cytoplasmic ratio was calculated with excel and normalized to control sample or shown as absolute ratios. The nucleo-cytoplasmic ratio does represent the ratio in the recorded z section and should therefore also represent the mean ratio of the whole cell. However, due to the detection of mean signal intensities this method does not measure total protein levels and does not normalize to different nuclear and cytoplasmic compartment volumes and therefore does not show total nucleo-cytoplasmic ratios of proteins.

Nuclear and cytoplasmic TNRC6A foci were manually counted from 100 randomly picked cells

per sample and cells were classified into cells with nuclear, intermediate and cytoplasmic foci. A cell is classified as "nuclear" ("cytoplasmic"), if more than 80 % of the foci are nuclear (cytoplasmic). Cells which show 21 to 79 % foci in the nucleus or cytoplasm are classified as "intermediate".

For figure images, representative cells were selected, picture was cropped and contrast was increased to the same extend for all pictures of one panel.

## 6. *In vivo* Experiments

### 6.1. Mouse strains

Following mouse strains were used or generated during this study:

**C57BL/6** obtained from local ZTL maintained stock.

**NMRI:nu/nu** full name Crl:NMRI-Foxn1<sup>nu</sup> was obtained from Charles River.

**Nes-Cre/ERT2<sup>+0</sup>** full name C57BL/6-Tg(Nes-cre/ERT2)KEisc/J was obtained from Jackson Laboratories, stock number 016261 (Lagace et al., 2007).

**CAMTA1<sup>fl/fl</sup>** full name not known but has mixed genetic background of 129 and C57BL/6. Obtained and previously characterized in Long et al., 2014.

**CAMTA1<sup>fl/fl</sup> / Nes-Cre/ERT2<sup>+0</sup>** was generated by crossing Nes-Cre/ERT2<sup>+0</sup> and CAMTA1<sup>fl/fl</sup>. F1 animals were genotyped and Nes-Cre/ERT2<sup>+0</sup> and CAMTA1<sup>fl/0</sup> animals were selected and paired again to obtain CAMTA1<sup>fl/fl</sup> / Nes-Cre/ERT2<sup>+0</sup>.

### 6.2. Murine xenograft model for CAMTA1 overexpression

Transfection of R28-luc was done by Nucleofection as described in section 4.3. 1 day before, cells were cultivated in SCM without penicillin/streptomycin. Three hours after transfection, cell viability was determined by trypan blue exclusion and 140.000 viable cells were resuspended in PBS to give total concentration of 140.000 viable cells in 3  $\mu$ l PBS.

Intracranial glioblastoma xenografts were established in 10 week old male NMRI:nu/nu mice (Charles River, Wilmington, USA) essentially as described in Beier et al., 2007. All experimental procedures were conducted in accordance with German laws governing animal care. Group size was 15 mice, i.e. 15 mice were injected per sample. A burr hole was drilled 2 mm dorsal to the midline and 4 mm anterior to bregma. Transfected tumour cells were stereotactically injected to a depth of 3 mm from the dura, using a manual Hamilton syringe and an injection volume of about 3  $\mu$ l over 1 min. The burr hole was closed with cement.

Tumor size was analyzed 15 days after implantation by bioluminescence detection. 15 days were chosen as successfully developed tumors show stable growth after 15 days without severely affecting the animal. Mice were observed continuously after injection and animal was killed as soon as clear pain expression was observed. 1 min after injection of 150 mg/kg D-luciferin (Biosynth, Staad, Switzerland), mice were anaesthetized and emitted photons were registered for 5 min using Xenogen IVIS Lumina Imaging System (Caliper Life Sciences, Hopkinton, USA). The

signal was corrected to background signal and mice without detectable tumours were excluded from the analysis.

### 6.3. Isolation of neural stem cells

For isolation of neural stem cells, mice were killed with CO<sub>2</sub>. Mice were decapitated and brain was isolated and stored in PBS on ice. Dissection was done under dissection microscope as described in Walker and Kempermann, 2014 to isolate subventricular zone (SVZ), dentate gyrus (DG), cortex and cerebellum. Tissue samples of approximately similar size were minced using a scalpel for 1 min and transferred into 3 ml 0,05 % Trypsin-EDTA or Accutase (Life Technologies) followed by 20 min incubation at 37 °C in water bath. Cells were pipetted time by time with 1 ml pipet. Cells were then filled up to 15 ml with SCM incomplete and spin down at 300 g for 5 min at RT. Supernatant was discarded and pellet thoroughly resuspended in 10 ml SCM complete. Cells were finally passaged through a 70 µm filter and plated on 10 cm plates. Neurospheres started to develop 5 to 7 days post isolation and continued to increase in size rapidly. Cells were passaged every five days with 50 % medium exchange and singularization by pipetting. Short spins at very low g-force were done to separate spheres from dead cells that remained from isolation if necessary. Pure isolation of brain regions was not controlled but neurospheres only developed from SVZ samples.

### 6.4. Mouse genotyping

Genomic DNA preparation by NaOH extraction was done as follows from mouse tail tip biopsies or brain tissue samples. Brain tissue samples were snap frozen with liquid nitrogen and sheared with a mortar in liquid nitrogen in advance. Tail or mortared tissue was mixed with 75 µl 25 mM NaOH / 0,2 mM EDTA and placed in a thermocycler at 98 °C for 1 hour. Then temperature was reduced to 15 °C. 75 µl 40 mM Tris pH 5,5 were added and mixed. After centrifugation at 4000 rpm for 3 min, an aliquot of 1 µl was used as template for genotyping PCR. Multiplexed PCR for detection of Cre-allele and various CAMTA1 alleles was set up using Taq DNA polymerase (Life Technologies) in the following reaction:

2,5 µl	10 x Taq buffer with (NH <sub>4</sub> ) <sub>2</sub> SO <sub>4</sub> without MgCl <sub>2</sub>
0,125 µl	10 mM dNTP mix
0,125 µl	A1CKOsLA Seq
0,125 µl	A1CKOASeq-6
0,125 µl	A1CKOfP-1
0,125 µl	oIMR1084 cre fwd
0,125 µl	oIMR1085 cre rev
2 µl	25 mM MgCl <sub>2</sub>
1 µl	template DNA from NaOH extraction
18,625 µl	H <sub>2</sub> O
0,125 µl	5 U/µl recombinant Taq DNA Polymerase

PCR was done as follows:

---

95 °C	2 min
95 °C	30 sec
55 °C	30 sec
72 °C	45 sec
72 °C	7 min
4 °C	infinite

Following bands correspond to either Cre or CAMTA1 alleles and were analyzed by agarose gel electrophoresis on a 1 % agarose gel:

390 nt	CAMTA1 <sup>wt</sup> (C57BL/6 were used)
390 + 495 nt	CAMTA1 <sup>fl/wt</sup>
495 nt	CAMTA1 <sup>fl/fl</sup>
700 nt	CAMTA1 <sup>fl/fl</sup> floxed allele
no band	Nes-Cre/ERT2 <sup>0/0</sup>
100 nt	Nes-Cre/ERT2 <sup>+/0</sup>

Of note, in some cases multiplexing of Cre and CAMTA1 specific primers resulted in a decrease in CAMTA1 specific bands. If this was observed, two separate PCRs were set up, one with A1CKOsLA Seq/A1CKOASeq-6/A1CKOfP-1, the second with oIMR1084 cre fwd/oIMR1085 cre rev.

# 7. Computational methods and statistical analyses

## 7.1. Analysis of glioblastoma patient data

### 7.1.1. GBM patient data copy number variation analysis

For genomic copy number variation analyses around CAMTA1 genomic locus in patients suffering from *Glioblastoma multiforme*, a published dataset from 587 *Glioblastoma multiforme* samples (TCGA, 2008) was accessed via the UCSC Cancer Browser. Copy number profile was determined by analyzing SNP and copy-number markers from an Affymetrix Genome-Wide Human SNP Array 6.0 (TCGA, 2008).

### 7.1.2. GBM patient data gene expression and survival analysis

Repository for Molecular Brain Neoplasia Data (REMBRANDT) is a publicly available brain tumor dataset managed by the National Cancer Institute. REMBRANDT contains clinical and molecular data from clinical trial patients suffering from grade II, III and IV gliomas, i.e. not only high grade *Glioblastoma multiforme* but also lower grade gliomas.

Analysis of CAMTA1 expression in glioma patients and analysis of survival data have been done with REMBRANDT (June 2009). Higher order analysis was performed and patients suffering from *Glioblastoma multiforme*, oligodendroglioma and astrocytoma have been included into analysis. Analysis with *Glioblastoma multiforme* alone was not informative due to low number of patients with differential expression of CAMTA1. P values, gene expression data for box-whisker plot and Kaplan-Meier survival curves were generated by REMBRANDT.

For analysis of natriuretic peptide hormone system components in glioma patients, query search function was used with REMBRANDT version 1.5.9 (November 2013) and patients with *Glioblastoma multiforme* only were included into analysis. P values and Kaplan-Meier survival curves were generated by REMBRANDT.

## 7.2. Prediction of classical NLS and NES sequences

Prediction of classical nuclear localization sequences (NLS) and nuclear export sequences (NES) have been performed using eukaryotic linear motif resource (ELM) tool (Dinkel et al., 2014). ELM contains a collection of short linear motifs analyzed against input protein sequences. NLS identifiers look for monopartite (TRG\_NLS\_MonoCore\_2, TRG\_NLS\_MonoExtC\_3, TRG\_NLS\_MonoExtN\_4) or bipartite (TRG\_NLS\_Bipartite\_1) basically charged NLSs which are typical substrates for import factor Imp $\alpha$ . NES identifiers (TRG\_NES\_CRM1\_1) looks for Leucine-rich motifs that are binding substrates to the export factor Crm1 (Exp1). Other NLS and NES sequences which are used by non-classical import and export pathways can not be solidly predicted.

### **7.3. Statistical analyses**

All experiments were performed in minimum 3 biological replicates. Error bars represent the plus/minus standard error of the mean calculated from biological replicates. Significance was calculated from biological replicates using two-sided Student's t-test for unequal sample variance. P values were classified into "\*" for  $P < 0,05$ , "\*\*" for  $P < 0,005$ , "\*\*\*" for  $P < 0,0005$  and "n.s." for  $P > 0,05$ .

# Appendix

**Figure A1 CAMTA1 multiple sequence alignment.** Alignment was done with Clustal W2 including human and mouse CAMTA1 and CAMTA2. JNet secondary structure prediction is indicated in the lower row for hsCAMTA1. Color scheme represents percentage of conservation between all four sequences. Figure is split in three parts 1-3. hs, *Homo sapiens* mm; *Mus musculus*.

**Figure A2 Generation of the CAMTA1 conditional knockout mouse.** Schematic representation the knockout strategy for CAMTA1<sup>fl/fl</sup> from Long et al., 2014. Domain organization of CAMTA1 protein is shown on the top, below the CAMTA1 locus on mouse chr 4. Exon 9, directly upstream of the TIG domain was flanked with loxP sites for Cre-mediated recombination. Recombination generates a premature stop codon within Exon 10. The mutant allele can generate a truncated protein product with the N-terminal CG-1 domain. CAMTA1<sup>fl/fl</sup> mice were used for experiments described in this study. Figure adapted from Long et al., 2014.

**Figure A3 Ago2 localization in 26 different human cell lines from various tissue origins.** Confocal microscopy with anti-Ago2 antibody was done in 26 different cell lines from different tissue origins. Figure contains two parts. Scale bar represents 20  $\mu\text{m}$ .

**Figure A4 Colocalization of the nuclear trapped TNRC6A NES mut with various factors. A to E,** Confocal microscopy with HEK cells stably expressing TNRC6A NES mut. TNRC6A NES mut was detected via its GFP tag, the different factors were costained by secondary immunofluorescence. These factors include components of cytoplasmic P-bodies (A and E), protein degradation machinery (B), nuclear compartments (C), RNA polymerases (D). Figure contains three parts. Scale bar represents 10  $\mu\text{m}$ .

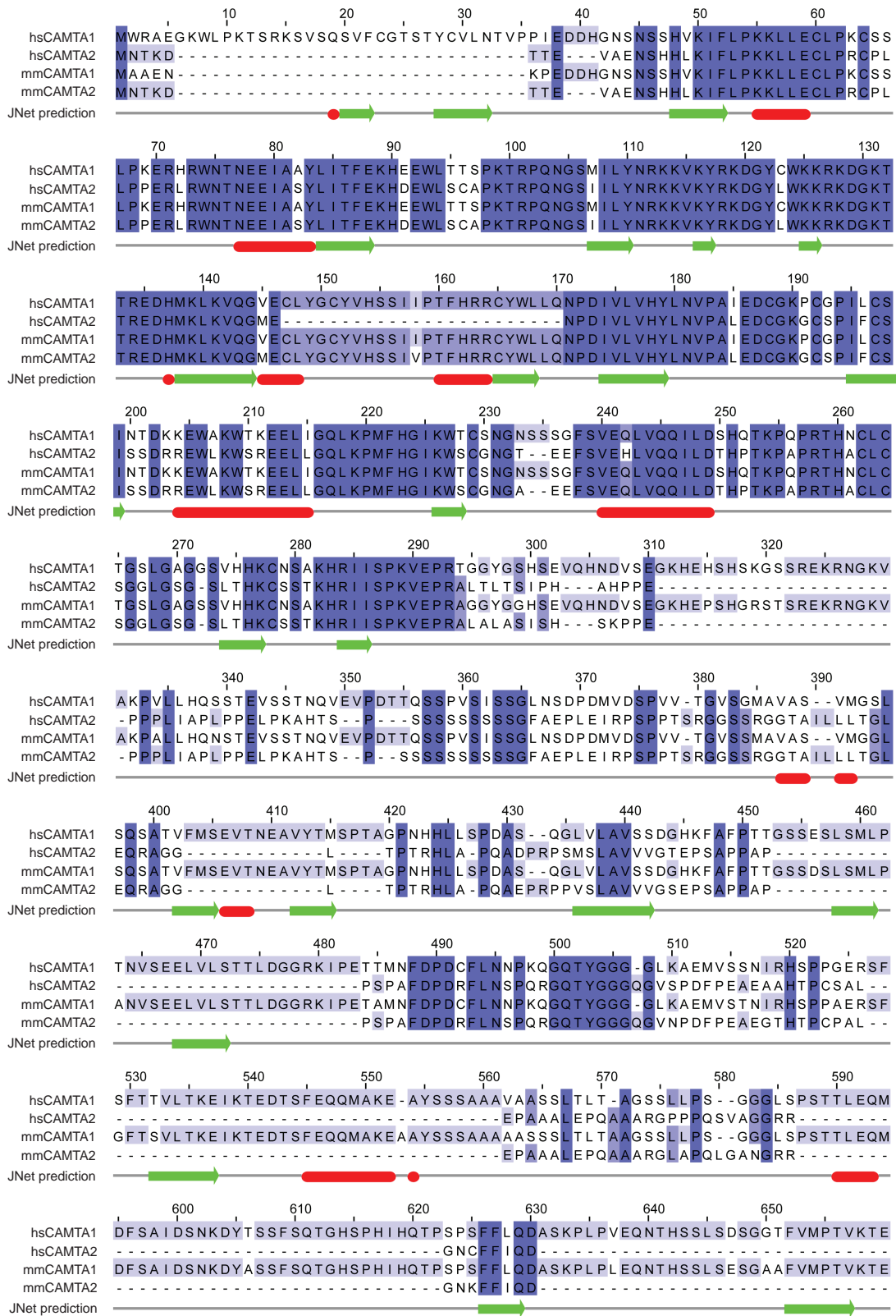


Figure A1. part 1

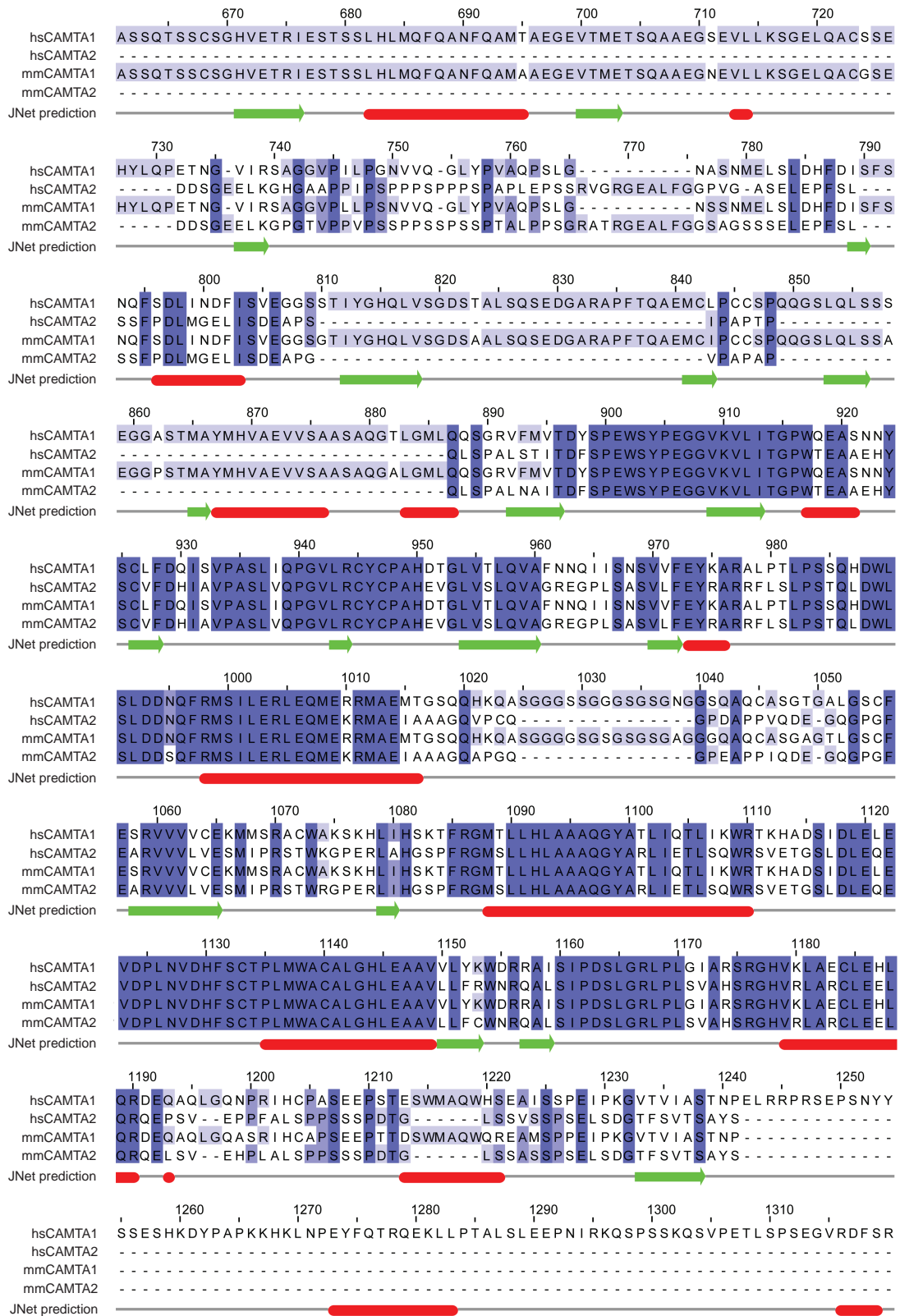


Figure A1 part 2

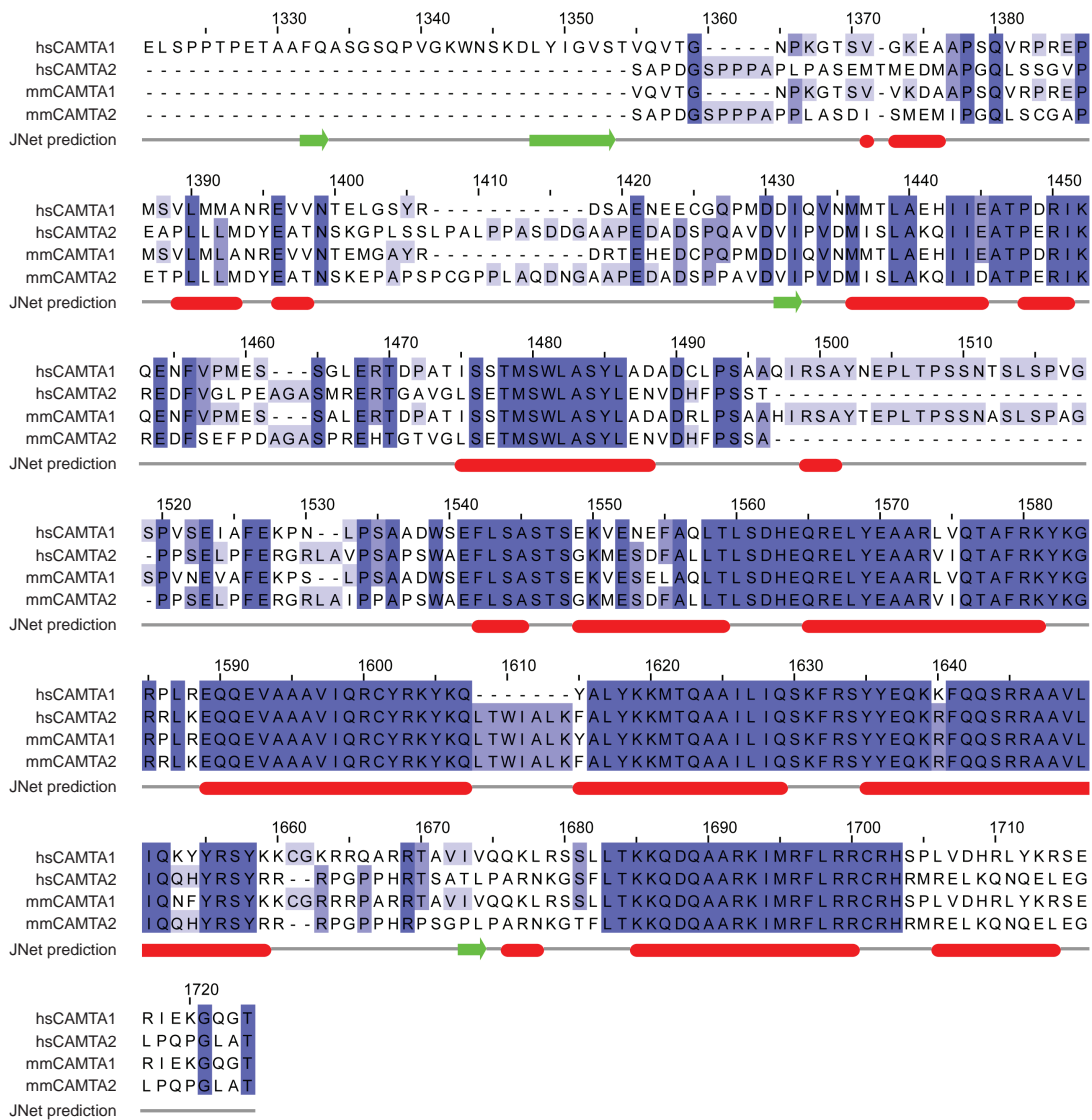


Figure A1 part 3

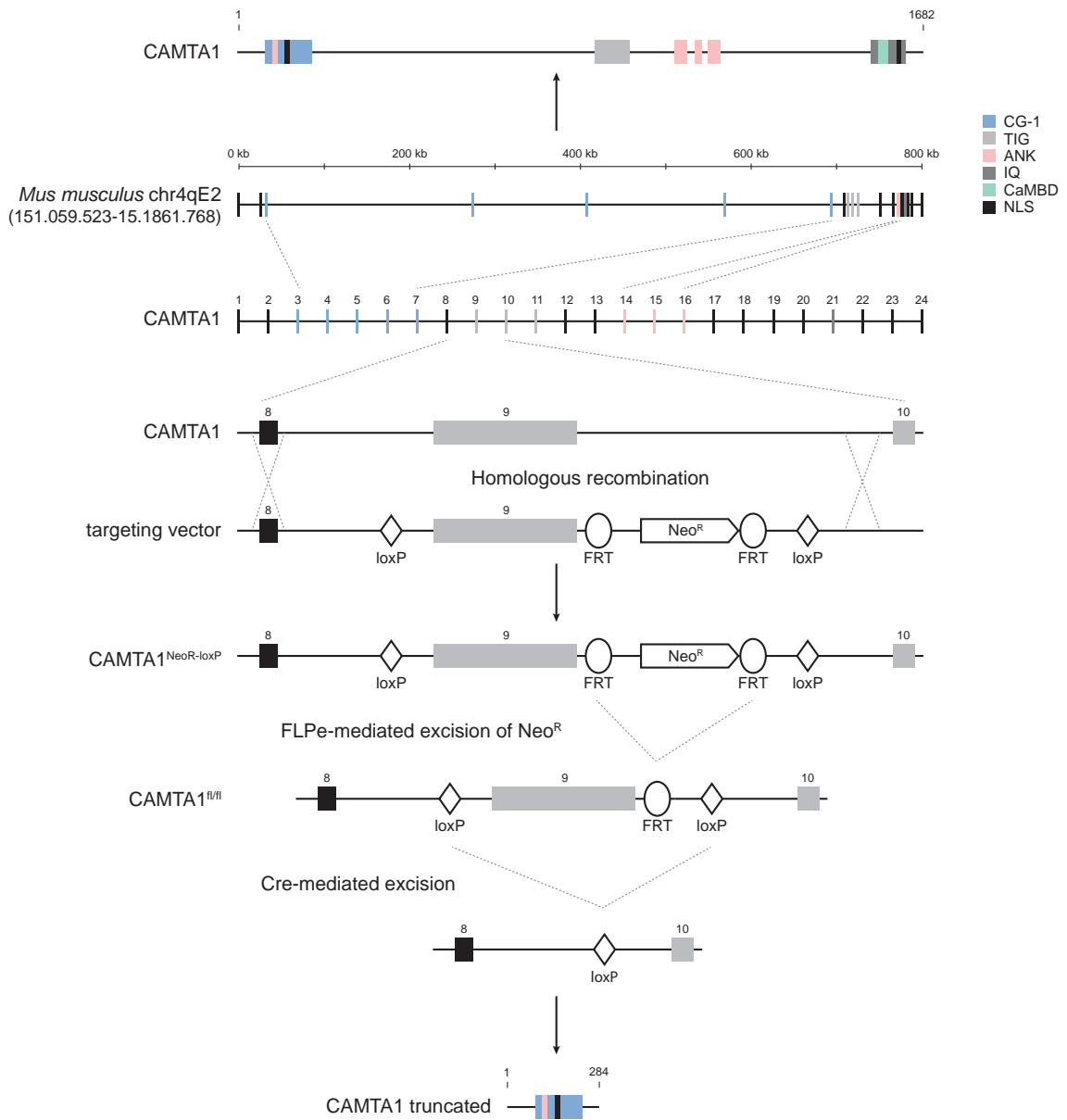


Figure A2.

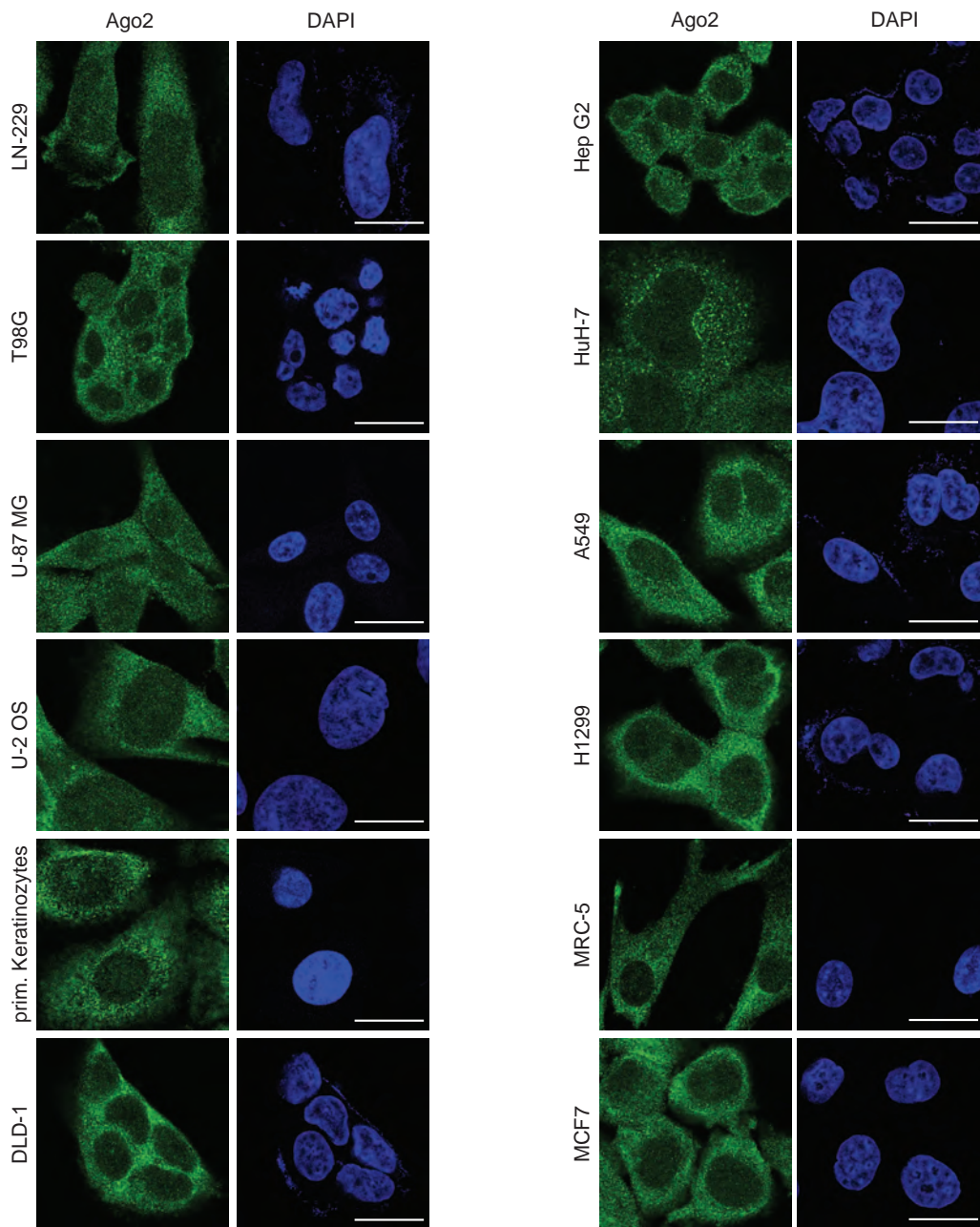


Figure A3. part 1

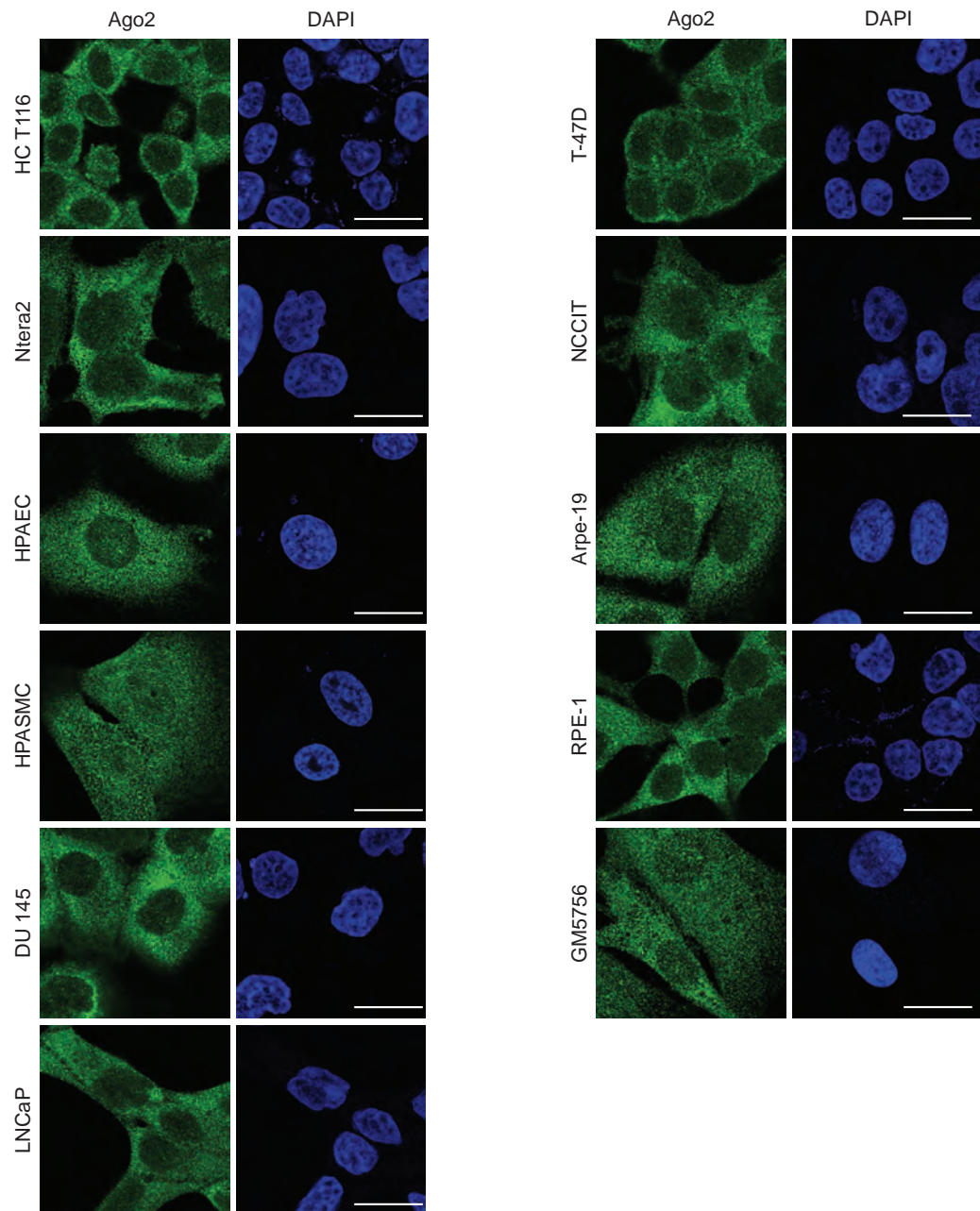
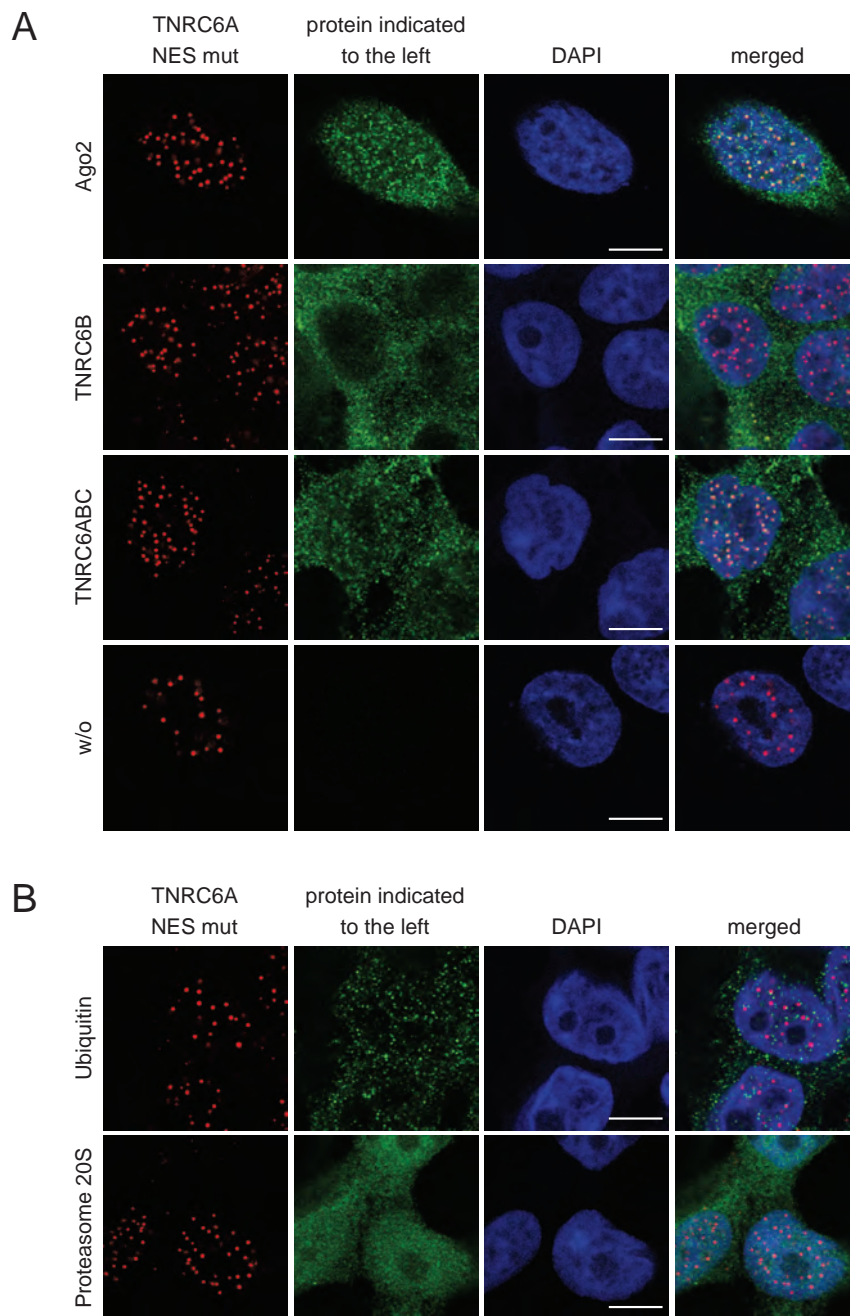


Figure A3 part 2

**Figure A4.** part 1

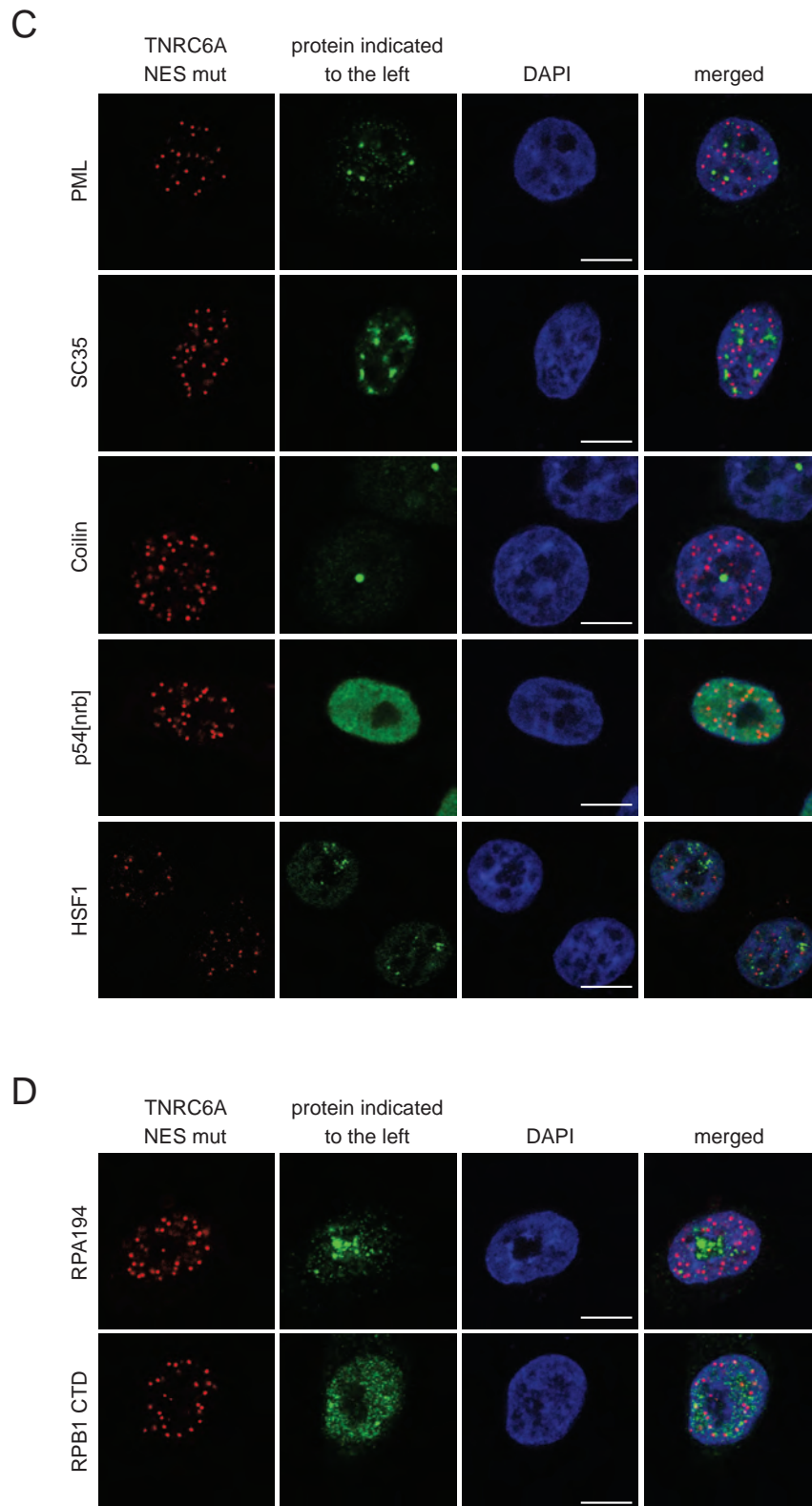


Figure A4 part 2

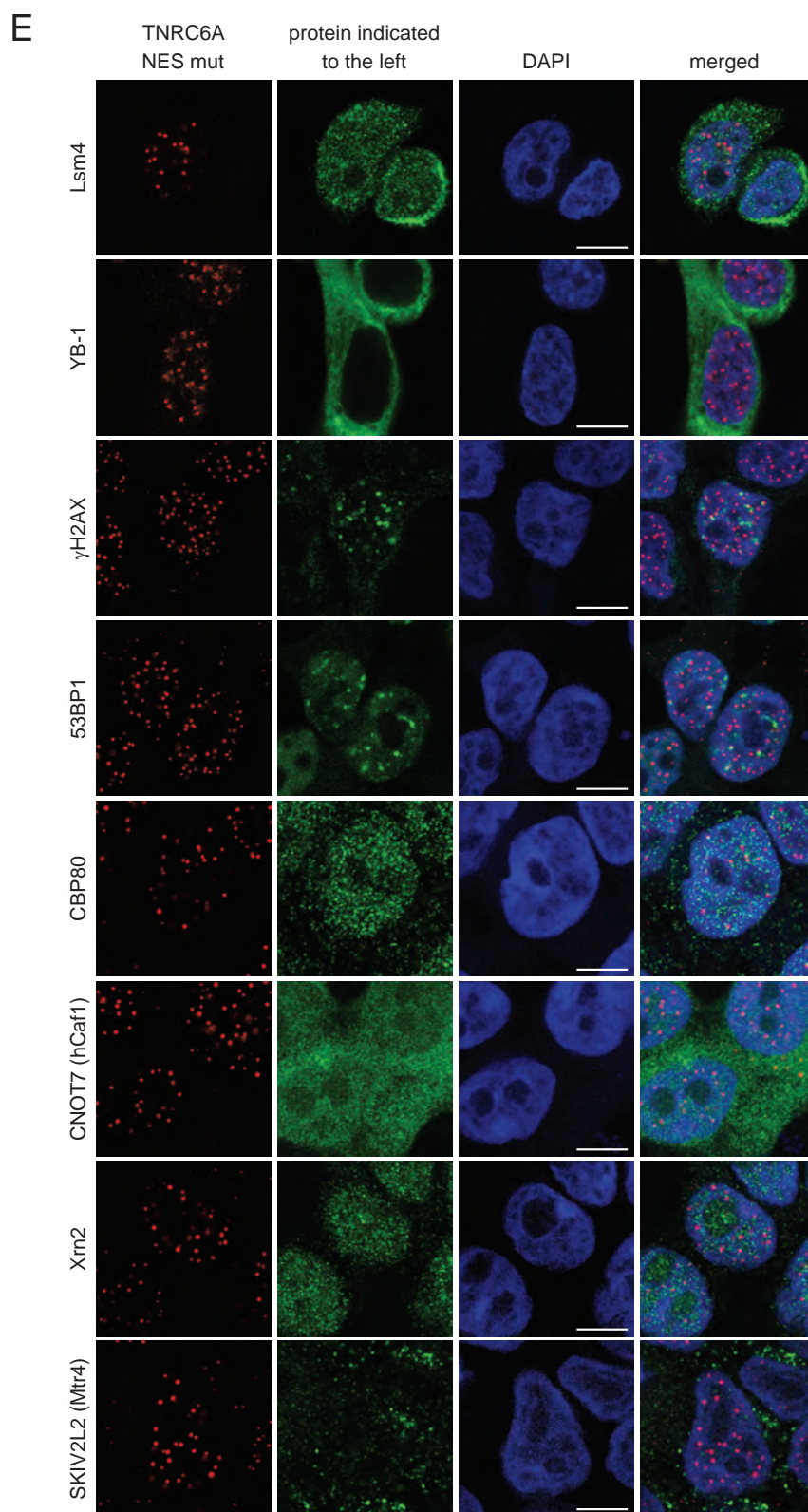


Figure A4 part 3

# Contributions

## **Part I: miR-9/9\* regulate CAMTA1 in glioblastoma stem cells**

The results of part I of this work have been published in parts in Schraivogel et al., 2011. Figures of section 3 were partially adapted from Schraivogel et al., 2011 I contributed to experiments presented in Figures 2.3.3, 2.3.4, 2.3.7, 2.3.9C, 2.3.11, 2.3.12C, 2.3.13, 2.3.14 and 2.3.15 and analyzed data in Figures 2.3.2 and 2.3.6.

## **Part II: Nuclear transport of Argonaute and TNRC6 proteins**

In part II of this work, I contributed all data except for pulldowns from oocyte extracts presented in Figure 3.3.8D where I analyzed data and the GST-pulldown experiments in Figures 3.3.13 and 3.3.18B-D.

# List of Figures

1.2.1.	MiRNA processing pathway . . . . .	16
1.2.2.	Sources of siRNAs . . . . .	20
1.3.1.	Structure of human Ago2 . . . . .	23
1.3.2.	Domain organization of TNRC6 proteins . . . . .	25
1.4.1.	Post-transcriptional gene silencing mechanism . . . . .	30
2.1.1.	Aberrations in GBM . . . . .	38
2.1.2.	Molecular subclasses of GBM . . . . .	39
2.1.3.	Sources of intratumoral heterogeneity . . . . .	40
2.3.1.	Small RNA profiling of glioblastoma cancer stem cells . . . . .	46
2.3.2.	miR-9/9* in different primary GBM cell lines . . . . .	47
2.3.3.	miR-9/9* inhibition affects neurosphere-formation . . . . .	48
2.3.4.	miR-9/9* mimics increase neurosphere-formation . . . . .	49
2.3.5.	miR-9/9* inhibition affects GSC population. . . . .	49
2.3.6.	Identification of miR-9* target mRNAs . . . . .	51
2.3.7.	CAMTA1 domain structure and genomic localization . . . . .	52
2.3.8.	Validation of CAMTA1 as miR-9/9* target . . . . .	53
2.3.9.	CAMTA1 has tumor suppressor activity <i>in vitro</i> . . . . .	54
2.3.10.	CAMTA1 knockdown rescues miR-9/9* inhibition effects . . . . .	55
2.3.11.	CAMTA1 functions as a tumor suppressor <i>in vivo</i> . . . . .	56
2.3.12.	CAMTA1 expression correlates with patient survival . . . . .	57
2.3.13.	NPPA and NPR-A are regulated by CAMTA1 . . . . .	58
2.3.14.	NPPA expression correlates with patient survival . . . . .	59
2.3.15.	Transcriptome response after CAMTA1 overexpression . . . . .	60
2.4.1.	A model for miR-9/9*-CAMTA1-NPPA function . . . . .	66
3.1.1.	TGS in <i>S. pombe</i> . . . . .	69
3.1.2.	General principles of nuclear transport pathways . . . . .	73
3.1.3.	Properties of nuclear import pathways . . . . .	74
3.1.4.	Importin structure . . . . .	75
3.1.5.	Nuclear import of <i>C. elegans</i> NRDE-3 . . . . .	78
3.1.6.	Shuttling of <i>S. pombe</i> Dcr1 . . . . .	79
3.3.1.	Ago2 localization in different cell lines . . . . .	81
3.3.2.	Modified HK shows nuclear import of Ago2 . . . . .	82
3.3.3.	Ago2 is a shuttling protein . . . . .	83

---

3.3.4.	Classical HK shows Ago2 shuttling . . . . .	84
3.3.5.	7sk assay to identify Ago2 Import factors . . . . .	86
3.3.6.	Experimental validation of Ago2 NLS and NES . . . . .	88
3.3.7.	Ago2 shuttling is Imp $\beta$ -independent . . . . .	89
3.3.8.	Biochemical identification of Ran-dependent Ago2 interactors . . . . .	90
3.3.9.	TNRC6 proteins are shuttling proteins . . . . .	91
3.3.10.	TNRC6 proteins only colocalize with Ago2 . . . . .	92
3.3.11.	Identification of import factors for TNRC6A . . . . .	93
3.3.12.	Shuttling of TNRC6B is Imp $\beta$ -dependent . . . . .	94
3.3.13.	TNRC6A-C interact with Imp $\alpha$ and Imp $\beta$ . . . . .	95
3.3.14.	TNRC6A NLS mut localization suggests a second NLS . . . . .	96
3.3.15.	miRNA-mediated gene silencing is affected by Imp $\beta$ . . . . .	96
3.3.16.	Cytoplasmic retention of TNRC6A and Ago2 . . . . .	97
3.3.17.	TNRC6 knockdown increases nuclear Ago2 . . . . .	98
3.3.18.	Ago2 blocks TNRC6A NLS accessibility . . . . .	99
3.4.1.	Ago2 and TNRC6 nuclear transport model . . . . .	104
4.5.1.	Cell Profiler pipeline . . . . .	146
A1.	CAMTA1 multiple sequence alignment . . . . .	154
A2.	Generation of CAMTA1 knockout mouse . . . . .	157
A3.	Ago2 localization in different cell lines . . . . .	158
A4.	Colocalization of nuclear TNRC6A . . . . .	160

# List of Tables

1.1. DNA oligonucleotides for cloning . . . . .	114
1.2. DNA oligonucleotides for qPCR . . . . .	115
1.3. Northern Blot probes . . . . .	116
1.4. Oligonucleotides for mouse genotyping . . . . .	117
1.5. List of siRNAs . . . . .	117
1.6. 2'-O-methylated miRNA inhibitors . . . . .	118
1.7. List of miRNA mimics . . . . .	118
1.8. Antibodies used for Western, IP and FACS . . . . .	120
1.9. Antibodies used for IF . . . . .	121

# List of Abbreviations

AEBSF	4-(2-Aminoethyl)benzenesulfonyl fluoride
Ago	Argonaute
<i>A. thaliana</i>	<i>Arabidopsis thaliana</i>
ATP	Adenosine triphosphate
bp	base pair
BSA	bovine serum albumin
<i>C. elegans</i>	<i>Caenorhabditis elegans</i>
Ci	Curie
CSC	cancer stem cell
CoIP	co-immunoprecipitation
Da	Dalton
Δ	Deletion
<i>D. melanogaster</i>	<i>Drosophila melanogaster</i>
DMEM	Dulbecco's Modified Eagle Medium
DNA	deoxyribonucleic acid
dNTP	2"-deoxyribonucleoside triphosphate
ds	double-stranded
dsRBD	double-stranded RNA binding domain
dT	desoxythymidine
DTT	1,4-Dithiothreitol
DUF	domain of unknown function
<i>E. coli</i>	<i>Escherichia coli</i>
EDTA	Ethylendiamintetraacetic acid
Exp	Exportin
F	phenylalanine
FH	Flag-HA
G	glycine
g	gram
g	gravitational constant
GFP	green fluorescent protein
GDP	guanosine diphosphate
GTP	guanosine triphosphate
h	hour
His	hexa-histidine tag
<i>H. sapiens</i>	<i>Homo sapiens</i>
Imp	Importin
IP	immunoprecipitation
IRES	internal ribosome entry site
k	kilo

---

l	liter
LOH	loss of heterozygosity
M	molar
MCS	multiple cloning site
min	minute
Mio	million, 10 <sup>6</sup>
miRISC	miRNA induced silencing complex
miRNA	microRNA
miRNP	micro-ribonucleoprotein
mRNA	messenger RNA
NES	nuclear localization signal
NLS	nuclear export signal
nt	nucleotide(s)
NSC	neural stem cell
o/n	over night
ORF	open reading frame
P-bodies	processing bodies
PBS	Phosphate buffered saline
PCR	polymerase chain reaction
piRNA	Piwi-interacting RNA
pre-miRNA	precursor miRNA
pri-miRNA	primary miRNA
qRT-PCR	quantitative real-time polymerase chain reaction
PTGS	post-transcriptional gene silencing
RISC	RNA-induced silencing complex
RNA	ribonucleic acid
RNAi	RNA interference
RNP	ribonucleoprotein
rpm	revolutions per minute
RT	room temperature
<i>S. cerevisiae</i>	<i>Saccharomyces cerevisiae</i>
<i>S. pombe</i>	<i>Schizosaccharomyces pombe</i>
sec	second
shRNA	short hairpin RNA
siRNA	small interfering RNA
snoRNA	small nucleolar RNA
ss	single-stranded
TBE	Tris/Borate/EDTA buffer
TBS	Tris buffered saline
tRNA	transfer RNA
UTP	uridine triphosphate
UTR	untranslated region
W	tryptophan
w/v	weight per volume
wt	wild type

# Bibliography

- Ahlenstiel, C. L., Lim, H. G. W., Cooper, D. A., Ishida, T., Kelleher, A. D., and Suzuki, K. (2012). Direct evidence of nuclear Argonaute distribution during transcriptional silencing links the actin cytoskeleton to nuclear RNAi machinery in human cells. *Nucleic Acids Res*, 40(4):1579–1595.
- Aizer, A., Brody, Y., Ler, L. W., Sonenberg, N., Singer, R. H., and Shav-Tal, Y. (2008). The dynamics of mammalian P body transport, assembly, and disassembly in vivo. *Mol Biol Cell*, 19(10):4154–4166.
- Alló, M., Buggiano, V., Fededa, J. P., Petrillo, E., Schor, I., de la Mata, M., Agirre, E., Plass, M., Eyraes, E., Elela, S. A., Klinck, R., Chabot, B., and Kornblihtt, A. R. (2009). Control of alternative splicing through siRNA-mediated transcriptional gene silencing. *Nat Struct Mol Biol*, 16(7):717–724.
- Altuvia, Y., Landgraf, P., Lithwick, G., Elefant, N., Pfeffer, S., Aravin, A., Brownstein, M. J., Tuschl, T., and Margalit, H. (2005). Clustering and conservation patterns of human microRNAs. *Nucleic Acids Res*, 33(8):2697–2706.
- Ameyar-Zazoua, M., Rachez, C., Souidi, M., Robin, P., Fritsch, L., Young, R., Morozova, N., Fenouil, R., Descostes, N., Andrau, J.-C., Mathieu, J., Hamiche, A., Ait-Si-Ali, S., Muchardt, C., Batsché, E., and Harel-Bellan, A. (2012). Argonaute proteins couple chromatin silencing to alternative splicing. *Nat Struct Mol Biol*, 19(10):998–1004.
- Anand-Srivastava, M. B. (2005). Natriuretic peptide receptor-C signaling and regulation. *Peptides*, 26(6):1044–1059.
- Anderson, P. and Kedersha, N. (2008). Stress granules: the Tao of RNA triage. *Trends Biochem Sci*, 33(3):141–150.
- Antic, D., Lu, N., and Keene, J. D. (1999). ELAV tumor antigen, Hel-N1, increases translation of neurofilament M mRNA and induces formation of neurites in human teratocarcinoma cells. *Genes Dev*, 13(4):449–461.
- Azuma-Mukai, A., Oguri, H., Mituyama, T., Qian, Z. R., Asai, K., Siomi, H., and Siomi, M. C. (2008). Characterization of endogenous human Argonautes and their miRNA partners in RNA silencing. *Proc Natl Acad Sci U S A*, 105(23):7964–7969.
- Babiarz, J. E., Ruby, J. G., Wang, Y., Bartel, D. P., and Blelloch, R. (2008). Mouse ES cells express endogenous shRNAs, siRNAs, and other Microprocessor-independent, Dicer-dependent small RNAs. *Genes Dev*, 22(20):2773–2785.
- Baillat, D. and Shiekhattar, R. (2009). Functional dissection of the human TNRC6 (GW182-related) family of proteins. *Mol Cell Biol*, 29(15):4144–4155.

- Bao, S., Wu, Q., McLendon, R. E., Hao, Y., Shi, Q., Hjelmeland, A. B., Dewhirst, M. W., Bigner, D. D., and Rich, J. N. (2006). Glioma stem cells promote radioresistance by preferential activation of the DNA damage response. *Nature*, 444(7120):756–760.
- Barbashina, V., Salazar, P., Holland, E. C., Rosenblum, M. K., and Ladanyi, M. (2005). Allelic losses at 1p36 and 19q13 in gliomas: correlation with histologic classification, definition of a 150-kb minimal deleted region on 1p36, and evaluation of CAMTA1 as a candidate tumor suppressor gene. *Clin Cancer Res*, 11(3):1119–1128.
- Barraud, P., Banerjee, S., Mohamed, W. I., Jantsch, M. F., and Allain, F. H.-T. (2014). A bimodular nuclear localization signal assembled via an extended double-stranded RNA-binding domain acts as an RNA-sensing signal for transportin 1. *Proc Natl Acad Sci U S A*, 111(18):E1852–E1861.
- Barraud, P., Emmerth, S., Shimada, Y., Hotz, H.-R., Allain, F. H.-T., and Bühler, M. (2011). An extended dsRBD with a novel zinc-binding motif mediates nuclear retention of fission yeast Dicer. *EMBO J*, 30(20):4223–4235.
- Bartel, D. P. (2004). MicroRNAs: genomics, biogenesis, mechanism, and function. *Cell*, 116(2):281–297.
- Bayliss, R., Littlewood, T., and Stewart, M. (2000). Structural basis for the interaction between FxFG nucleoporin repeats and importin-beta in nuclear trafficking. *Cell*, 102(1):99–108.
- Bayne, E. H., White, S. A., Kagansky, A., Bijos, D. A., Sanchez-Pulido, L., Hoe, K.-L., Kim, D.-U., Park, H.-O., Ponting, C. P., Rappsilber, J., and Allshire, R. C. (2010). Stc1: a critical link between RNAi and chromatin modification required for heterochromatin integrity. *Cell*, 140(5):666–677.
- Bazzini, A. A., Lee, M. T., and Giraldez, A. J. (2012). Ribosome profiling shows that miR-430 reduces translation before causing mRNA decay in zebrafish. *Science*, 336(6078):233–237.
- Behm-Ansmant, I., Rehwinkel, J., Doerks, T., Stark, A., Bork, P., and Izaurralde, E. (2006). mRNA degradation by miRNAs and GW182 requires both CCR4:NOT deadenylase and DCP1:DCP2 decapping complexes. *Genes Dev*, 20(14):1885–1898.
- Beier, C. P., Kumar, P., Meyer, K., Leukel, P., Bruttel, V., Aschenbrenner, I., Riemenschneider, M. J., Fragoulis, A., Rümmele, P., Lamszus, K., Schulz, J. B., Weis, J., Bogdahn, U., Wischhusen, J., Hau, P., Spang, R., and Beier, D. (2012). The cancer stem cell subtype determines immune infiltration of glioblastoma. *Stem Cells Dev*, 21(15):2753–2761.
- Beier, D., Hau, P., Proescholdt, M., Lohmeier, A., Wischhusen, J., Oefner, P. J., Aigner, L., Brawanski, A., Bogdahn, U., and Beier, C. P. (2007). CD133(+) and CD133(-) glioblastoma-derived cancer stem cells show differential growth characteristics and molecular profiles. *Cancer Res*, 67(9):4010–4015.
- Beier, D., Wischhusen, J., Dietmaier, W., Hau, P., Proescholdt, M., Brawanski, A., Bogdahn, U., and Beier, C. P. (2008). CD133 expression and cancer stem cells predict prognosis in high-grade oligodendroglial tumors. *Brain Pathol*, 18(3):370–377.
- Beitzinger, M., Peters, L., Zhu, J. Y., Kremmer, E., and Meister, G. (2007). Identification of human microRNA targets from isolated argonaute protein complexes. *RNA Biol*, 4(2):76–84.

- Benhamed, M., Herbig, U., Ye, T., Dejean, A., and Bischof, O. (2012). Senescence is an endogenous trigger for microRNA-directed transcriptional gene silencing in human cells. *Nat Cell Biol*, 14(3):266–275.
- Béthune, J., Artus-Revel, C. G., and Filipowicz, W. (2012). Kinetic analysis reveals successive steps leading to miRNA-mediated silencing in mammalian cells. *EMBO Rep*, 13(8):716–723.
- Bhattacharyya, S. N., Habermacher, R., Martine, U., Closs, E. I., and Filipowicz, W. (2006). Relief of microRNA-mediated translational repression in human cells subjected to stress. *Cell*, 125(6):1111–1124.
- Bischoff, F. R., Klebe, C., Kretschmer, J., Wittinghofer, A., and Ponstingl, H. (1994). RanGAP1 induces GTPase activity of nuclear Ras-related Ran. *Proc Natl Acad Sci U S A*, 91(7):2587–2591.
- Bischoff, F. R. and Ponstingl, H. (1991). Catalysis of guanine nucleotide exchange on Ran by the mitotic regulator RCC1. *Nature*, 354(6348):80–82.
- Bohnsack, M. T., Czaplinski, K., and Gorlich, D. (2004). Exportin 5 is a RanGTP-dependent dsRNA-binding protein that mediates nuclear export of pre-miRNAs. *RNA*, 10(2):185–191.
- Bologna, N. G. and Voinnet, O. (2014). The diversity, biogenesis, and activities of endogenous silencing small RNAs in Arabidopsis. *Annu Rev Plant Biol*, 65:473–503.
- Bottenstein, J. E. and Sato, G. H. (1979). Growth of a rat neuroblastoma cell line in serum-free supplemented medium. *Proc Natl Acad Sci U S A*, 76(1):514–517.
- Bouché, N., Scharlat, A., Snedden, W., Bouchez, D., and Fromm, H. (2002). A novel family of calmodulin-binding transcription activators in multicellular organisms. *J Biol Chem*, 277(24):21851–21861.
- Brannan, K., Kim, H., Erickson, B., Glover-Cutter, K., Kim, S., Fong, N., Kiemele, L., Hansen, K., Davis, R., Lykke-Andersen, J., and Bentley, D. L. (2012). mRNA decapping factors and the exonuclease Xrn2 function in widespread premature termination of RNA polymerase II transcription. *Mol Cell*, 46(3):311–324.
- Braun, J. E., Huntzinger, E., Fauser, M., and Izaurralde, E. (2011). GW182 proteins directly recruit cytoplasmic deadenylase complexes to miRNA targets. *Mol Cell*, 44(1):120–133.
- Braun, J. E., Huntzinger, E., and Izaurralde, E. (2013). The role of GW182 proteins in miRNA-mediated gene silencing. *Adv Exp Med Biol*, 768:147–163.
- Bregues, M., Teixeira, D., and Parker, R. (2005). Movement of eukaryotic mRNAs between polysomes and cytoplasmic processing bodies. *Science*, 310(5747):486–489.
- Brennan, C. W., Verhaak, R. G. W., McKenna, A., Campos, B., Noushmehr, H., et al. (2013). The somatic genomic landscape of glioblastoma. *Cell*, 155(2):462–477.
- Brohawn, S. G., Partridge, J. R., Whittle, J. R. R., and Schwartz, T. U. (2009). The nuclear pore complex has entered the atomic age. *Structure*, 17(9):1156–1168.
- Brueckner, B., Stresemann, C., Kuner, R., Mund, C., Musch, T., Meister, M., Sültmann, H., and Lyko, F. (2007). The human let-7a-3 locus contains an epigenetically regulated microRNA gene with oncogenic function. *Cancer Res*, 67(4):1419–1423.

- Bühler, M., Haas, W., Gygi, S. P., and Moazed, D. (2007). RNAi-dependent and -independent RNA turnover mechanisms contribute to heterochromatic gene silencing. *Cell*, 129(4):707–721.
- Bushati, N. and Cohen, S. M. (2007). microRNA functions. *Annu Rev Cell Dev Biol*, 23:175–205.
- Cai, X., Hagedorn, C. H., and Cullen, B. R. (2004). Human microRNAs are processed from capped, polyadenylated transcripts that can also function as mRNAs. *RNA*, 10(12):1957–1966.
- Calabrese, C., Poppleton, H., Kocak, M., Hogg, T. L., Fuller, C., Hamner, B., Oh, E. Y., Gaber, M. W., Finklestein, D., Allen, M., Frank, A., Bayazitov, I. T., Zakharenko, S. S., Gajjar, A., Davidoff, A., and Gilbertson, R. J. (2007). A perivascular niche for brain tumor stem cells. *Cancer Cell*, 11(1):69–82.
- Calin, G. A., Dumitru, C. D., Shimizu, M., Bichi, R., Zupo, S., Noch, E., Aldler, H., Rattan, S., Keating, M., Rai, K., Rassenti, L., Kipps, T., Negrini, M., Bullrich, F., and Croce, C. M. (2002). Frequent deletions and down-regulation of micro- RNA genes miR15 and miR16 at 13q14 in chronic lymphocytic leukemia. *Proc Natl Acad Sci U S A*, 99(24):15524–15529.
- Calin, G. A., Ferracin, M., Cimmino, A., Di Leva, G., Shimizu, M., et al. (2005). A MicroRNA signature associated with prognosis and progression in chronic lymphocytic leukemia. *N Engl J Med*, 353(17):1793–1801.
- Carmody, S. R. and Wentz, S. R. (2009). mRNA nuclear export at a glance. *Journal of cell science*, 122(12):1933–1937.
- Carpenter, A. E., Jones, T. R., Lamprecht, M. R., Clarke, C., Kang, I. H., Friman, O., Guertin, D. A., Chang, J. H., Lindquist, R. A., Moffat, J., Golland, P., and Sabatini, D. M. (2006). CellProfiler: image analysis software for identifying and quantifying cell phenotypes. *Genome Biol*, 7(10):R100.
- Carro, M. S., Lim, W. K., Alvarez, M. J., Bollo, R. J., Zhao, X., Snyder, E. Y., Sulman, E. P., Anne, S. L., Doetsch, F., Colman, H., Lasorella, A., Aldape, K., Califano, A., and Iavarone, A. (2010). The transcriptional network for mesenchymal transformation of brain tumours. *Nature*, 463(7279):318–325.
- Castel, S. E. and Martienssen, R. A. (2013). RNA interference in the nucleus: roles for small RNAs in transcription, epigenetics and beyond. *Nat Rev Genet*, 14(2):100–112.
- Chan, J. A., Krichevsky, A. M., and Kosik, K. S. (2005). MicroRNA-21 is an antiapoptotic factor in human glioblastoma cells. *Cancer Res*, 65(14):6029–6033.
- Chan, X. H. D., Nama, S., Gopal, F., Rizk, P., Ramasamy, S., Sundaram, G., Ow, G. S., Ivshina, A. V., Tanavde, V., Haybaeck, J., Kuznetsov, V., and Sampath, P. (2012). Targeting glioma stem cells by functional inhibition of a prosurvival oncomiR-138 in malignant gliomas. *Cell Rep*, 2(3):591–602.
- Chang, T.-C., Wentzel, E. A., Kent, O. A., Ramachandran, K., Mullendore, M., Lee, K. H., Feldmann, G., Yamakuchi, M., Ferlito, M., Lowenstein, C. J., Arking, D. E., Beer, M. A., Maitra, A., and Mendell, J. T. (2007). Transactivation of miR-34a by p53 broadly influences gene expression and promotes apoptosis. *Mol Cell*, 26(5):745–752.

- Chapat, C., Kolytcheff, C., Le Romancer, M., Auboeuf, D., De La Grange, P., Chettab, K., Sentis, S., and Corbo, L. (2013). hCAF1/CNOT7 regulates interferon signalling by targeting STAT1. *EMBO J*, 32(5):688–700.
- Chaulk, S. G., Thede, G. L., Kent, O. A., Xu, Z., Gesner, E. M., Veldhoen, R. A., Khanna, S. K., Goping, I. S., MacMillan, A. M., Mendell, J. T., Young, H. S., Fahlman, R. P., and Glover, J. N. M. (2011). Role of pri-miRNA tertiary structure in miR-17 92 miRNA biogenesis. *RNA Biol*, 8(6):1105–1114.
- Chekulaeva, M., Mathys, H., Zipprich, J. T., Attig, J., Colic, M., Parker, R., and Filipowicz, W. (2011). miRNA repression involves GW182-mediated recruitment of CCR4-NOT through conserved W-containing motifs. *Nat Struct Mol Biol*, 18(11):1218–1226.
- Chekulaeva, M., Parker, R., and Filipowicz, W. (2010). The GW/WG repeats of Drosophila GW182 function as effector motifs for miRNA-mediated repression. *Nucleic Acids Res*, 38(19):6673–6683.
- Cheloufi, S., Dos Santos, C. O., Chong, M. M. W., and Hannon, G. J. (2010). A dicer-independent miRNA biogenesis pathway that requires Ago catalysis. *Nature*, 465(7298):584–589.
- Chen, C.-Y. A., Zheng, D., Xia, Z., and Shyu, A.-B. (2009). Ago-TNRC6 triggers microRNA-mediated decay by promoting two deadenylation steps. *Nat Struct Mol Biol*, 16(11):1160–1166.
- Chen, J., Li, Y., Yu, T.-S., McKay, R. M., Burns, D. K., Kernie, S. G., and Parada, L. F. (2012a). A restricted cell population propagates glioblastoma growth after chemotherapy. *Nature*, 488(7412):522–526.
- Chen, J., McKay, R. M., and Parada, L. F. (2012b). Malignant glioma: lessons from genomics, mouse models, and stem cells. *Cell*, 149(1):36–47.
- Chen, R., Nishimura, M. C., Bumbaca, S. M., Kharbanda, S., Forrest, W. F., et al. (2010). A hierarchy of self-renewing tumor-initiating cell types in glioblastoma. *Cancer Cell*, 17(4):362–375.
- Chen, Y., Boland, A., Kuzuolu-Ozturk, D., Bawankar, P., Loh, B., Chang, C.-T., Weichenrieder, O., and Izaurralde, E. (2014). A DDX6-CNOT1 complex and W-binding pockets in CNOT9 reveal direct links between miRNA target recognition and silencing. *Mol Cell*, 54(5):737–750.
- Chendrimada, T. P., Gregory, R. I., Kumaraswamy, E., Norman, J., Cooch, N., Nishikura, K., and Shiekhattar, R. (2005). TRBP recruits the Dicer complex to Ago2 for microRNA processing and gene silencing. *Nature*, 436(7051):740–744.
- Cheng, J.-X., Liu, B.-L., and Zhang, X. (2009). How powerful is CD133 as a cancer stem cell marker in brain tumors? *Cancer Treat Rev*, 35(5):403–408.
- Chin, L. J., Ratner, E., Leng, S., Zhai, R., Nallur, S., et al. (2008). A SNP in a let-7 microRNA complementary site in the KRAS 3' untranslated region increases non-small cell lung cancer risk. *Cancer Res*, 68(20):8535–8540.
- Chook, Y. M. and Blobel, G. (2001). Karyopherins and nuclear import. *Curr Opin Struct Biol*, 11(6):703–715.

- Chook, Y. M. and Süel, K. E. (2011). Nuclear import by karyopherin- $\beta$ s: recognition and inhibition. *Biochim Biophys Acta*, 1813(9):1593–1606.
- Christie, M., Boland, A., Huntzinger, E., Weichenrieder, O., and Izaurralde, E. (2013). Structure of the PAN3 pseudokinase reveals the basis for interactions with the PAN2 deadenylase and the GW182 proteins. *Mol Cell*, 51(3):360–373.
- Chu, C.-y. and Rana, T. M. (2006). Translation repression in human cells by microRNA-induced gene silencing requires RCK/p54. *PLoS Biol*, 4(7):e210.
- Chu, Y., Yue, X., Younger, S. T., Janowski, B. A., and Corey, D. R. (2010). Involvement of argonaute proteins in gene silencing and activation by RNAs complementary to a non-coding transcript at the progesterone receptor promoter. *Nucleic Acids Res*, 38(21):7736–7748.
- Cifuentes, D., Xue, H., Taylor, D. W., Patnode, H., Mishima, Y., Cheloufi, S., Ma, E., Mane, S., Hannon, G. J., Lawson, N. D., Wolfe, S. A., and Giraldez, A. J. (2010). A novel miRNA processing pathway independent of Dicer requires Argonaute2 catalytic activity. *Science*, 328(5986):1694–1698.
- Cikaluk, D. E., Tahbaz, N., Hendricks, L. C., DiMattia, G. E., Hansen, D., Pilgrim, D., and Hobman, T. C. (1999). GERp95, a membrane-associated protein that belongs to a family of proteins involved in stem cell differentiation. *Mol Biol Cell*, 10(10):3357–3372.
- Cingolani, G., Petosa, C., Weis, K., and Müller, C. W. (1999). Structure of importin-beta bound to the IBB domain of importin-alpha. *Nature*, 399(6733):221–229.
- Cloughesy, T. F., Cavenee, W. K., and Mischel, P. S. (2014). Glioblastoma: from molecular pathology to targeted treatment. *Annu Rev Pathol*, 9:1–25.
- Codega, P., Silva-Vargas, V., Paul, A., Maldonado-Soto, A. R., Deleo, A. M., Pastrana, E., and Doetsch, F. (2014). Prospective identification and purification of quiescent adult neural stem cells from their in vivo niche. *Neuron*, 82(3):545–559.
- Colmenares, S. U., Buker, S. M., Buhler, M., Dlakić, M., and Moazed, D. (2007). Coupling of double-stranded RNA synthesis and siRNA generation in fission yeast RNAi. *Mol Cell*, 27(3):449–461.
- Colwell, L. J., Brenner, M. P., and Ribbeck, K. (2010). Charge as a selection criterion for translocation through the nuclear pore complex. *PLoS Comput Biol*, 6(4):e1000747.
- Conti, E., Uy, M., Leighton, L., Blobel, G., and Kuriyan, J. (1998). Crystallographic analysis of the recognition of a nuclear localization signal by the nuclear import factor karyopherin alpha. *Cell*, 94(2):193–204.
- Coolen, M., Katz, S., and Bally-Cuif, L. (2013). miR-9: a versatile regulator of neurogenesis. *Frontiers in cellular neuroscience*, 7.
- Cougot, N., Molza, A.-E., Giudice, E., Cavalier, A., Thomas, D., and Gillet, R. (2013). Structural organization of the polysomes adjacent to mammalian processing bodies (P-bodies). *RNA Biol*, 10(2):314–320.
- Couvillion, M. T., Bounova, G., Purdom, E., Speed, T. P., and Collins, K. (2012). A Tetrahymena Piwi bound to mature tRNA 3' fragments activates the exonuclease Xrn2 for RNA processing in the nucleus. *Mol Cell*, 48(4):509–520.

- Croce, C. M. (2009). Causes and consequences of microRNA dysregulation in cancer. *Nat Rev Genet*, 10(10):704–714.
- Cuddapah, V. A., Robel, S., Watkins, S., and Sontheimer, H. (2014). A neurocentric perspective on glioma invasion. *Nat Rev Neurosci*, 15(7):455–465.
- Daxinger, L., Kanno, T., Bucher, E., van der Winden, J., Naumann, U., Matzke, A. J. M., and Matzke, M. (2009). A stepwise pathway for biogenesis of 24-nt secondary siRNAs and spreading of DNA methylation. *EMBO J*, 28(1):48–57.
- de la Mata, M., Alonso, C. R., Kadener, S., Fededa, J. P., Blaustein, M., Pelisch, F., Cramer, P., Bentley, D., and Kornblihtt, A. R. (2003). A slow RNA polymerase II affects alternative splicing in vivo. *Mol Cell*, 12(2):525–532.
- Delalay, C., Liu, L., Lee, J.-A., Su, H., Shen, F., Yang, G.-Y., Young, W. L., Ivey, K. N., and Gao, F.-B. (2010). MicroRNA-9 coordinates proliferation and migration of human embryonic stem cell-derived neural progenitors. *Cell Stem Cell*, 6(4):323–335.
- Denli, A. M., Tops, B. B. J., Plasterk, R. H. A., Ketting, R. F., and Hannon, G. J. (2004). Processing of primary microRNAs by the Microprocessor complex. *Nature*, 432(7014):231–235.
- Depping, R., Steinhoff, A., Schindler, S. G., Friedrich, B., Fagerlund, R., Metzen, E., Hartmann, E., and Köhler, M. (2008). Nuclear translocation of hypoxia-inducible factors (HIFs): involvement of the classical importin alpha/beta pathway. *Biochim Biophys Acta*, 1783(3):394–404.
- DeSano, J. T. and Xu, L. (2009). MicroRNA regulation of cancer stem cells and therapeutic implications. *AAPS J*, 11(4):682–692.
- Detzer, A., Engel, C., Wünsche, W., and Sczakiel, G. (2011). Cell stress is related to re-localization of Argonaute 2 and to decreased RNA interference in human cells. *Nucleic Acids Res*, 39(7):2727–2741.
- Di Leva, G., Garofalo, M., and Croce, C. M. (2014). MicroRNAs in cancer. *Annu Rev Pathol*, 9:287–314.
- Dignam, J. D., Lebovitz, R. M., and Roeder, R. G. (1983). Accurate transcription initiation by RNA polymerase II in a soluble extract from isolated mammalian nuclei. *Nucleic Acids Res*, 11(5):1475–1489.
- Ding, S.-W. and Voinnet, O. (2007). Antiviral immunity directed by small RNAs. *Cell*, 130(3):413–426.
- Dinkel, H., Van Roey, K., Michael, S., Davey, N. E., Weatheritt, R. J., Born, D., Speck, T., Krüger, D., Grebnev, G., Kuban, M., Strumillo, M., Uyar, B., Budd, A., Altenberg, B., Seiler, M., Chemes, L. B., Glavina, J., Sánchez, I. E., Diella, F., and Gibson, T. J. (2014). The eukaryotic linear motif resource ELM: 10 years and counting. *Nucleic Acids Res*, 42(Database issue):D259–D266.
- Djuranovic, S., Nahvi, A., and Green, R. (2012). miRNA-mediated gene silencing by translational repression followed by mRNA deadenylation and decay. *Science*, 336(6078):237–240.
- Dong, X., Biswas, A., Süel, K. E., Jackson, L. K., Martinez, R., Gu, H., and Chook, Y. M. (2009). Structural basis for leucine-rich nuclear export signal recognition by CRM1. *Nature*, 458(7242):1136–1141.

- Dong, Z., Pang, J.-S., Ng, M., Poon, W., Zhou, L., and Ng, H. (2004). Identification of two contiguous minimally deleted regions on chromosome 1p36. 31–p36. 32 in oligodendroglial tumours. *British journal of cancer*, 91(6):1105–1111.
- Doyle, M., Badertscher, L., Jaskiewicz, L., Güttinger, S., Jurado, S., Hugenschmidt, T., Kutay, U., and Filipowicz, W. (2013). The double-stranded RNA binding domain of human Dicer functions as a nuclear localization signal. *RNA*, 19(9):1238–1252.
- Dueck, A. and Meister, G. (2014). Assembly and function of small RNA - argonaute protein complexes. *Biol Chem*, 395(6):611–629.
- Dueck, A., Ziegler, C., Eichner, A., Berezikov, E., and Meister, G. (2012). microRNAs associated with the different human Argonaute proteins. *Nucleic Acids Res*, 40(19):9850–9862.
- Easow, G., Teleman, A. A., and Cohen, S. M. (2007). Isolation of microRNA targets by miRNP immunopurification. *RNA*, 13(8):1198–1204.
- Eichhorn, S. W., Guo, H., McGeary, S. E., Rodriguez-Mias, R. A., Shin, C., Baek, D., Hsu, S.-H., Ghoshal, K., Villén, J., and Bartel, D. P. (2014). mRNA destabilization is the dominant effect of mammalian microRNAs by the time substantial repression ensues. *Mol Cell*, 56(1):104–115.
- Elbashir, S. M., Harborth, J., Lendeckel, W., Yalcin, A., Weber, K., and Tuschl, T. (2001). Duplexes of 21-nucleotide RNAs mediate RNA interference in cultured mammalian cells. *Nature*, 411(6836):494–498.
- Elkayam, E., Kuhn, C.-D., Tocilj, A., Haase, A. D., Greene, E. M., Hannon, G. J., and Joshua-Tor, L. (2012). The structure of human argonaute-2 in complex with miR-20a. *Cell*, 150(1):100–110.
- Emmerth, S., Schober, H., Gaidatzis, D., Roloff, T., Jacobsen, K., and Bühler, M. (2010). Nuclear retention of fission yeast dicer is a prerequisite for RNAi-mediated heterochromatin assembly. *Dev Cell*, 18(1):102–113.
- Ernst, A., Campos, B., Meier, J., Devens, F., Liesenberg, F., Wolter, M., Reifenberger, G., Herold-Mende, C., Lichter, P., and Radlwimmer, B. (2010). De-repression of CTGF via the miR-17-92 cluster upon differentiation of human glioblastoma spheroid cultures. *Oncogene*, 29(23):3411–3422.
- Esquela-Kerscher, A. and Slack, F. J. (2006). Oncomirs—microRNAs with a role in cancer. *Nature Reviews Cancer*, 6(4):259–269.
- Eulalio, A., Behm-Ansmant, I., and Izaurralde, E. (2007a). P bodies: at the crossroads of post-transcriptional pathways. *Nat Rev Mol Cell Biol*, 8(1):9–22.
- Eulalio, A., Behm-Ansmant, I., Schweizer, D., and Izaurralde, E. (2007b). P-body formation is a consequence, not the cause, of RNA-mediated gene silencing. *Mol Cell Biol*, 27(11):3970–3981.
- Eulalio, A., Helms, S., Fritsch, C., Fauser, M., and Izaurralde, E. (2009a). A C-terminal silencing domain in GW182 is essential for miRNA function. *RNA*, 15(6):1067–1077.
- Eulalio, A., Tritschler, F., Büttner, R., Weichenrieder, O., Izaurralde, E., and Truffault, V. (2009b). The RRM domain in GW182 proteins contributes to miRNA-mediated gene silencing. *Nucleic Acids Res*, 37(9):2974–2983.

- Eulalio, A., Tritschler, F., and Izaurralde, E. (2009c). The GW182 protein family in animal cells: new insights into domains required for miRNA-mediated gene silencing. *RNA*, 15(8):1433–1442.
- Eystathiou, T., Chan, E. K. L., Mahler, M., Luft, L. M., Fritzier, M. L., and Fritzier, M. J. (2003a). A panel of monoclonal antibodies to cytoplasmic GW bodies and the mRNA binding protein GW182. *Hybrid Hybridomics*, 22(2):79–86.
- Eystathiou, T., Chan, E. K. L., Tenenbaum, S. A., Keene, J. D., Griffith, K., and Fritzier, M. J. (2002). A phosphorylated cytoplasmic autoantigen, GW182, associates with a unique population of human mRNAs within novel cytoplasmic speckles. *Mol Biol Cell*, 13(4):1338–1351.
- Eystathiou, T., Jakymiw, A., Chan, E. K. L., Séraphin, B., Cougot, N., and Fritzier, M. J. (2003b). The GW182 protein colocalizes with mRNA degradation associated proteins hDcp1 and hLSm4 in cytoplasmic GW bodies. *RNA*, 9(10):1171–1173.
- Fabian, M. R., Cieplak, M. K., Frank, F., Morita, M., Green, J., Srikumar, T., Nagar, B., Yamamoto, T., Raught, B., Duchaine, T. F., and Sonenberg, N. (2011). miRNA-mediated deadenylation is orchestrated by GW182 through two conserved motifs that interact with CCR4-NOT. *Nat Struct Mol Biol*, 18(11):1211–1217.
- Fabian, M. R., Mathonnet, G., Sundermeier, T., Mathys, H., Zipprich, J. T., Svitkin, Y. V., Rivas, F., Jinek, M., Wohlschlegel, J., Doudna, J. A., Chen, C.-Y. A., Shyu, A.-B., Yates, 3rd, J. R., Hannon, G. J., Filipowicz, W., Duchaine, T. F., and Sonenberg, N. (2009). Mammalian miRNA RISC recruits CAF1 and PABP to affect PABP-dependent deadenylation. *Mol Cell*, 35(6):868–880.
- Fabian, M. R. and Sonenberg, N. (2012). The mechanics of miRNA-mediated gene silencing: a look under the hood of miRISC. *Nat Struct Mol Biol*, 19(6):586–593.
- Fabian, M. R., Sonenberg, N., and Filipowicz, W. (2010). Regulation of mRNA translation and stability by microRNAs. *Annu Rev Biochem*, 79:351–379.
- Fanara, P., Hodel, M. R., Corbett, A. H., and Hodel, A. E. (2000). Quantitative analysis of nuclear localization signal (NLS)-importin alpha interaction through fluorescence depolarization. Evidence for auto-inhibitory regulation of NLS binding. *J Biol Chem*, 275(28):21218–21223.
- Feuerborn, A., Srivastava, P. K., Küffer, S., Grandy, W. A., Sijmonsma, T. P., Gretz, N., Brors, B., and Gröne, H.-J. (2011). The Forkhead factor FoxQ1 influences epithelial differentiation. *J Cell Physiol*, 226(3):710–719.
- Finkler, A., Ashery-Padan, R., and Fromm, H. (2007). CAMTAs: calmodulin-binding transcription activators from plants to human. *FEBS Lett*, 581(21):3893–3898.
- Fire, A., Xu, S., Montgomery, M. K., Kostas, S. A., Driver, S. E., and Mello, C. C. (1998). Potent and specific genetic interference by double-stranded RNA in *Caenorhabditis elegans*. *Nature*, 391(6669):806–811.
- Fontes, M. R., Teh, T., and Kobe, B. (2000). Structural basis of recognition of monopartite and bipartite nuclear localization sequences by mammalian importin-alpha. *J Mol Biol*, 297(5):1183–1194.
- Fornerod, M., Ohno, M., Yoshida, M., and Mattaj, I. W. (1997). CRM1 is an export receptor for leucine-rich nuclear export signals. *Cell*, 90(6):1051–1060.

- Fox, J. L., Dews, M., Minn, A. J., and Thomas-Tikhonenko, A. (2013). Targeting of TGF $\beta$  signature and its essential component CTGF by miR-18 correlates with improved survival in glioblastoma. *RNA*, 19(2):177–190.
- Francia, S., Michelini, F., Saxena, A., Tang, D., de Hoon, M., Anelli, V., Mione, M., Carninci, P., and d'Adda di Fagagna, F. (2012). Site-specific DICER and DROSHA RNA products control the DNA-damage response. *Nature*, 488(7410):231–235.
- Frank, F., Sonenberg, N., and Nagar, B. (2010). Structural basis for 5'-nucleotide base-specific recognition of guide RNA by human AGO2. *Nature*, 465(7299):818–822.
- Frey, S. and Görlich, D. (2007). A saturated FG-repeat hydrogel can reproduce the permeability properties of nuclear pore complexes. *Cell*, 130(3):512–523.
- Friedmann-Morvinski, D. and Verma, I. M. (2014). Dedifferentiation and reprogramming: origins of cancer stem cells. *EMBO Rep*, 15(3):244–253.
- Frohn, A., Eberl, H. C., Stöhr, J., Glasmacher, E., Rüdell, S., Heissmeyer, V., Mann, M., and Meister, G. (2012). Dicer-dependent and -independent Argonaute2 protein interaction networks in mammalian cells. *Mol Cell Proteomics*, 11(11):1442–1456.
- Fukuda, M., Asano, S., Nakamura, T., Adachi, M., Yoshida, M., Yanagida, M., and Nishida, E. (1997). CRM1 is responsible for intracellular transport mediated by the nuclear export signal. *Nature*, 390(6657):308–311.
- Fukunaga, R., Han, B. W., Hung, J.-H., Xu, J., Weng, Z., and Zamore, P. D. (2012). Dicer partner proteins tune the length of mature miRNAs in flies and mammals. *Cell*, 151(3):533–546.
- Gabriely, G., Yi, M., Narayan, R. S., Niers, J. M., Wurdinger, T., Imitola, J., Ligon, K. L., Kesari, S., Esau, C., Stephens, R. M., Tannous, B. A., and Krichevsky, A. M. (2011). Human glioma growth is controlled by microRNA-10b. *Cancer Res*, 71(10):3563–3572.
- Gagnon, K. T., Li, L., Chu, Y., Janowski, B. A., and Corey, D. R. (2014). RNAi factors are present and active in human cell nuclei. *Cell Rep*, 6(1):211–221.
- Gal, H., Pandi, G., Kanner, A. A., Ram, Z., Lithwick-Yanai, G., Amariglio, N., Rechavi, G., and Givol, D. (2008). MIR-451 and Imatinib mesylate inhibit tumor growth of Glioblastoma stem cells. *Biochem Biophys Res Commun*, 376(1):86–90.
- Gama-Carvalho, M. and Carmo-Fonseca, M. (2001). The rules and roles of nucleocytoplasmic shuttling proteins. *FEBS Lett*, 498(2-3):157–163.
- Gangaraju, V. K. and Lin, H. (2009). MicroRNAs: key regulators of stem cells. *Nat Rev Mol Cell Biol*, 10(2):116–125.
- Gao, M., Wei, W., Li, M.-M., Wu, Y.-S., Ba, Z., Jin, K.-X., Li, M.-M., Liao, Y.-Q., Adhikari, S., Chong, Z., Zhang, T., Guo, C.-X., Tang, T.-S., Zhu, B.-T., Xu, X.-Z., Mailand, N., Yang, Y.-G., Qi, Y., and Rendtlew Danielsen, J. M. (2014). Ago2 facilitates Rad51 recruitment and DNA double-strand break repair by homologous recombination. *Cell Res*, 24(5):532–541.
- Gent, J. I., Lamm, A. T., Pavelec, D. M., Maniar, J. M., Parameswaran, P., Tao, L., Kennedy, S., and Fire, A. Z. (2010). Distinct phases of siRNA synthesis in an endogenous RNAi pathway in *C. elegans* soma. *Mol Cell*, 37(5):679–689.

- Gibbins, D., Mostowy, S., Jay, F., Schwab, Y., Cossart, P., and Voinnet, O. (2012). Selective autophagy degrades DICER and AGO2 and regulates miRNA activity. *Nat Cell Biol*, 14(12):1314–1321.
- Gilbert, M. R. (2011). Recurrent glioblastoma: a fresh look at current therapies and emerging novel approaches. In *Seminars in oncology*, volume 38, pages S21–S33. Elsevier.
- Godlewski, J., Nowicki, M. O., Bronisz, A., Williams, S., Otsuki, A., Nuovo, G., Raychaudhury, A., Newton, H. B., Chiocca, E. A., and Lawler, S. (2008). Targeting of the Bmi-1 oncogene/stem cell renewal factor by microRNA-128 inhibits glioma proliferation and self-renewal. *Cancer Res*, 68(22):9125–9130.
- Görlich, D., Kostka, S., Kraft, R., Dingwall, C., Laskey, R. A., Hartmann, E., and Prehn, S. (1995). Two different subunits of importin cooperate to recognize nuclear localization signals and bind them to the nuclear envelope. *Curr Biol*, 5(4):383–392.
- Görlich, D. and Kutay, U. (1999). Transport between the cell nucleus and the cytoplasm. *Annu Rev Cell Dev Biol*, 15:607–660.
- Gravendeel, L. A. M., Kouwenhoven, M. C. M., Gevaert, O., de Rooi, J. J., Stubbs, A. P., et al. (2009). Intrinsic gene expression profiles of gliomas are a better predictor of survival than histology. *Cancer Res*, 69(23):9065–9072.
- Greaves, M. and Maley, C. C. (2012). Clonal evolution in cancer. *Nature*, 481(7381):306–313.
- Gregory, R. I., Chendrimada, T. P., Cooch, N., and Shiekhattar, R. (2005). Human RISC couples microRNA biogenesis and posttranscriptional gene silencing. *Cell*, 123(4):631–640.
- Gregory, R. I., Yan, K.-P., Amuthan, G., Chendrimada, T., Doratotaj, B., Cooch, N., and Shiekhattar, R. (2004). The Microprocessor complex mediates the genesis of microRNAs. *Nature*, 432(7014):235–240.
- Grossman, E., Medalia, O., and Zwerger, M. (2012). Functional architecture of the nuclear pore complex. *Annu Rev Biophys*, 41:557–584.
- Gruber, A. J. and Zavolan, M. (2013). Modulation of epigenetic regulators and cell fate decisions by miRNAs. *Epigenomics*, 5(6):671–683.
- Guang, S., Bochner, A. F., Burkhart, K. B., Burton, N., Pavelec, D. M., and Kennedy, S. (2010). Small regulatory RNAs inhibit RNA polymerase II during the elongation phase of transcription. *Nature*, 465(7301):1097–1101.
- Guang, S., Bochner, A. F., Pavelec, D. M., Burkhart, K. B., Harding, S., Lachowiec, J., and Kennedy, S. (2008). An Argonaute transports siRNAs from the cytoplasm to the nucleus. *Science*, 321(5888):537–541.
- Guessous, F., Zhang, Y., Kofman, A., Catania, A., Li, Y., Schiff, D., Purow, B., and Abounader, R. (2010). microRNA-34a is tumor suppressive in brain tumors and glioma stem cells. *Cell Cycle*, 9(6):1031–1036.
- Günther, H. S., Schmidt, N. O., Phillips, H. S., Kemming, D., Kharbanda, S., Soriano, R., Modrusan, Z., Meissner, H., Westphal, M., and Lamszus, K. (2008). Glioblastoma-derived stem cell-enriched cultures form distinct subgroups according to molecular and phenotypic criteria. *Oncogene*, 27(20):2897–2909.

- Ha, M. and Kim, V. N. (2014). Regulation of microRNA biogenesis. *Nat Rev Mol Cell Biol*, 15(8):509–524.
- Haase, A. D., Jaskiewicz, L., Zhang, H., Lainé, S., Sack, R., Gatignol, A., and Filipowicz, W. (2005). TRBP, a regulator of cellular PKR and HIV-1 virus expression, interacts with Dicer and functions in RNA silencing. *EMBO Rep*, 6(10):961–967.
- Hafner, M., Landthaler, M., Burger, L., Khorshid, M., Hausser, J., Berninger, P., Rothballer, A., Ascano, Jr, M., Jungkamp, A.-C., Munschauer, M., Ulrich, A., Wardle, G. S., Dewell, S., Zavolan, M., and Tuschl, T. (2010). Transcriptome-wide identification of RNA-binding protein and microRNA target sites by PAR-CLIP. *Cell*, 141(1):129–141.
- Hammond, S. M., Bernstein, E., Beach, D., and Hannon, G. J. (2000). An RNA-directed nuclease mediates post-transcriptional gene silencing in *Drosophila* cells. *Nature*, 404(6775):293–296.
- Han, J., Gong, P., Reddig, K., Mitra, M., Guo, P., and Li, H.-S. (2006a). The fly CAMTA transcription factor potentiates deactivation of rhodopsin, a G protein-coupled light receptor. *Cell*, 127(4):847–858.
- Han, J., Lee, Y., Yeom, K.-H., Kim, Y.-K., Jin, H., and Kim, V. N. (2004). The Drosha-DGCR8 complex in primary microRNA processing. *Genes Dev*, 18(24):3016–3027.
- Han, J., Lee, Y., Yeom, K.-H., Nam, J.-W., Heo, I., Rhee, J.-K., Sohn, S. Y., Cho, Y., Zhang, B.-T., and Kim, V. N. (2006b). Molecular basis for the recognition of primary microRNAs by the Drosha-DGCR8 complex. *Cell*, 125(5):887–901.
- Han, T. W., Kato, M., Xie, S., Wu, L. C., Mirzaei, H., Pei, J., Chen, M., Xie, Y., Allen, J., Xiao, G., and McKnight, S. L. (2012). Cell-free formation of RNA granules: bound RNAs identify features and components of cellular assemblies. *Cell*, 149(4):768–779.
- Hanahan, D. and Weinberg, R. A. (2011). Hallmarks of cancer: the next generation. *Cell*, 144(5):646–674.
- Hannus, M., Beitzinger, M., Engelmann, J. C., Weickert, M.-T., Spang, R., Hannus, S., and Meister, G. (2014). siPools: highly complex but accurately defined siRNA pools eliminate off-target effects. *Nucleic Acids Res*, 42(12):8049–8061.
- Hatch, E. and Hetzer, M. (2014). Breaching the nuclear envelope in development and disease. *J Cell Biol*, 205(2):133–141.
- Hauptmann, J. and Meister, G. (2013). Argonaute regulation: two roads to the same destination. *Dev Cell*, 25(6):553–554.
- Hausser, J., Syed, A. P., Bilén, B., and Zavolan, M. (2013). Analysis of CDS-located miRNA target sites suggests that they can effectively inhibit translation. *Genome Res*, 23(4):604–615.
- Havecker, E. R., Wallbridge, L. M., Hardcastle, T. J., Bush, M. S., Kelly, K. A., Dunn, R. M., Schwach, F., Doonan, J. H., and Baulcombe, D. C. (2010). The Arabidopsis RNA-directed DNA methylation argonautes functionally diverge based on their expression and interaction with target loci. *Plant Cell*, 22(2):321–334.

- He, L., He, X., Lim, L. P., de Stanchina, E., Xuan, Z., Liang, Y., Xue, W., Zender, L., Magnus, J., Ridzon, D., Jackson, A. L., Linsley, P. S., Chen, C., Lowe, S. W., Cleary, M. A., and Hannon, G. J. (2007). A microRNA component of the p53 tumour suppressor network. *Nature*, 447(7148):1130–1134.
- Heddleston, J. M., Wu, Q., Rivera, M., Minhas, S., Lathia, J. D., Sloan, A. E., Iliopoulos, O., Hjelmeland, A. B., and Rich, J. N. (2012). Hypoxia-induced mixed-lineage leukemia 1 regulates glioma stem cell tumorigenic potential. *Cell Death Differ*, 19(3):428–439.
- Henrich, K.-O., Bauer, T., Schulte, J., Ehemann, V., Deubzer, H., Gogolin, S., Muth, D., Fischer, M., Benner, A., König, R., Schwab, M., and Westermann, F. (2011). CAMTA1, a 1p36 tumor suppressor candidate, inhibits growth and activates differentiation programs in neuroblastoma cells. *Cancer Res*, 71(8):3142–3151.
- Henriksen, M., Johnsen, K. B., Andersen, H. H., Pilgaard, L., and Duroux, M. (2014). MicroRNA expression signatures determine prognosis and survival in glioblastoma multiforme—a systematic overview. *Mol Neurobiol*, 50(3):896–913.
- Hiraguri, A., Itoh, R., Kondo, N., Nomura, Y., Aizawa, D., Murai, Y., Koiwa, H., Seki, M., Shinozaki, K., and Fukuhara, T. (2005). Specific interactions between Dicer-like proteins and HYL1/DRB-family dsRNA-binding proteins in *Arabidopsis thaliana*. *Plant Mol Biol*, 57(2):173–188.
- Höck, J. and Meister, G. (2008). The Argonaute protein family. *Genome Biol*, 9(2):210.
- Huang, V. and Li, L.-C. (2014). Demystifying the nuclear function of Argonaute proteins. *RNA Biol*, 11(1):18–24.
- Huang, V., Zheng, J., Qi, Z., Wang, J., Place, R. F., Yu, J., Li, H., and Li, L.-C. (2013). Ago1 interacts with RNA polymerase II and binds to the promoters of actively transcribed genes in human cancer cells. *PLoS Genet*, 9(9):e1003821.
- Huber, J., Cronshagen, U., Kadokura, M., Marshallsay, C., Wada, T., Sekine, M., and Lührmann, R. (1998). Snurportin1, an m3G-cap-specific nuclear import receptor with a novel domain structure. *EMBO J*, 17(14):4114–4126.
- Huntzinger, E., Braun, J. E., Heimstädt, S., Zekri, L., and Izaurralde, E. (2010). Two PABPC1-binding sites in GW182 proteins promote miRNA-mediated gene silencing. *EMBO J*, 29(24):4146–4160.
- Huntzinger, E. and Izaurralde, E. (2011). Gene silencing by microRNAs: contributions of translational repression and mRNA decay. *Nat Rev Genet*, 12(2):99–110.
- Huntzinger, E., Kuzuoglu-Öztürk, D., Braun, J. E., Eulalio, A., Wohlbold, L., and Izaurralde, E. (2013). The interactions of GW182 proteins with PABP and deadenylases are required for both translational repression and degradation of miRNA targets. *Nucleic Acids Res*, 41(2):978–994.
- Hurteau, G. J., Spivack, S. D., and Brock, G. J. (2006). Potential mRNA degradation targets of hsa-miR-200c, identified using informatics and qRT-PCR. *Cell Cycle*, 5(17):1951–1956.
- Huse, J. T., Brennan, C., Hambarzumyan, D., Wee, B., Pena, J., Rouhanifard, S. H., Sohn-Lee, C., le Sage, C., Agami, R., Tuschl, T., and Holland, E. C. (2009). The PTEN-regulating microRNA miR-26a is amplified in high-grade glioma and facilitates gliomagenesis in vivo. *Genes Dev*, 23(11):1327–1337.

- Huse, J. T., Phillips, H. S., and Brennan, C. W. (2011). Molecular subclassification of diffuse gliomas: seeing order in the chaos. *Glia*, 59(8):1190–1199.
- Hutvagner, G. and Simard, M. J. (2008). Argonaute proteins: key players in RNA silencing. *Nat Rev Mol Cell Biol*, 9(1):22–32.
- Ichimura, K., Vogazianou, A., Liu, L., Pearson, D., Bäcklund, L., Plant, K., Baird, K., Langford, C., Gregory, S., and Collins, V. (2007). 1p36 is a preferential target of chromosome 1 deletions in astrocytic tumours and homozygously deleted in a subset of glioblastomas. *Oncogene*, 27(14):2097–2108.
- Iki, T., Yoshikawa, M., Nishikiori, M., Jaudal, M. C., Matsumoto-Yokoyama, E., Mitsuhara, I., Meshi, T., and Ishikawa, M. (2010). In vitro assembly of plant RNA-induced silencing complexes facilitated by molecular chaperone HSP90. *Mol Cell*, 39(2):282–291.
- Inoue, H., Nojima, H., and Okayama, H. (1990). High efficiency transformation of *Escherichia coli* with plasmids. *Gene*, 96(1):23–28.
- Ipsaro, J. J. and Joshua-Tor, L. (2015). From guide to target: molecular insights into eukaryotic RNA-interference machinery. *Nat Struct Mol Biol*, 22(1):20–28.
- Iwasaki, S., Kobayashi, M., Yoda, M., Sakaguchi, Y., Katsuma, S., Suzuki, T., and Tomari, Y. (2010). Hsc70/Hsp90 chaperone machinery mediates ATP-dependent RISC loading of small RNA duplexes. *Mol Cell*, 39(2):292–299.
- Jackson, R. J., Hellen, C. U. T., and Pestova, T. V. (2010). The mechanism of eukaryotic translation initiation and principles of its regulation. *Nat Rev Mol Cell Biol*, 11(2):113–127.
- Jain, R. K., di Tomaso, E., Duda, D. G., Loeffler, J. S., Sorensen, A. G., and Batchelor, T. T. (2007). Angiogenesis in brain tumours. *Nat Rev Neurosci*, 8(8):610–622.
- Jäkel, S. and Görlich, D. (1998). Importin beta, transportin, RanBP5 and RanBP7 mediate nuclear import of ribosomal proteins in mammalian cells. *EMBO J*, 17(15):4491–4502.
- Jakymiw, A., Lian, S., Eystathioy, T., Li, S., Satoh, M., Hamel, J. C., Fritzler, M. J., and Chan, E. K. L. (2005). Disruption of GW bodies impairs mammalian RNA interference. *Nat Cell Biol*, 7(12):1267–1274.
- Janowski, B. A. and Corey, D. R. (2010). Minireview: Switching on progesterone receptor expression with duplex RNA. *Mol Endocrinol*, 24(12):2243–2252.
- Janowski, B. A., Huffman, K. E., Schwartz, J. C., Ram, R., Nordsell, R., Shames, D. S., Minna, J. D., and Corey, D. R. (2006). Involvement of AGO1 and AGO2 in mammalian transcriptional silencing. *Nat Struct Mol Biol*, 13(9):787–792.
- Jansson, M. D. and Lund, A. H. (2012). MicroRNA and cancer. *Mol Oncol*, 6(6):590–610.
- Jeang, K.-T. (2012). RNAi in the regulation of mammalian viral infections. *BMC Biol*, 10:58.
- Jeffries, C. D., Fried, H. M., and Perkins, D. O. (2011). Nuclear and cytoplasmic localization of neural stem cell microRNAs. *RNA*, 17(4):675–686.

- Jinek, M., Fabian, M. R., Coyle, S. M., Sonenberg, N., and Doudna, J. A. (2010). Structural insights into the human GW182-PABC interaction in microRNA-mediated deadenylation. *Nat Struct Mol Biol*, 17(2):238–240.
- Johnson, S. M., Grosshans, H., Shingara, J., Byrom, M., Jarvis, R., Cheng, A., Labourier, E., Reinert, K. L., Brown, D., and Slack, F. J. (2005). RAS is regulated by the let-7 microRNA family. *Cell*, 120(5):635–647.
- Johnston, M., Geoffroy, M.-C., Sobala, A., Hay, R., and Hutvagner, G. (2010). HSP90 protein stabilizes unloaded argonaute complexes and microscopic P-bodies in human cells. *Mol Biol Cell*, 21(9):1462–1469.
- Karginov, F. V., Conaco, C., Xuan, Z., Schmidt, B. H., Parker, J. S., Mandel, G., and Hannon, G. J. (2007). A biochemical approach to identifying microRNA targets. *Proc Natl Acad Sci U S A*, 104(49):19291–19296.
- Kataoka, N., Fujita, M., and Ohno, M. (2009). Functional association of the Microprocessor complex with the spliceosome. *Mol Cell Biol*, 29(12):3243–3254.
- Kato, M., Han, T. W., Xie, S., Shi, K., Du, X., Wu, L. C., Mirzaei, H., Goldsmith, E. J., Longgood, J., Pei, J., Grishin, N. V., Frantz, D. E., Schneider, J. W., Chen, S., Li, L., Sawaya, M. R., Eisenberg, D., Tycko, R., and McKnight, S. L. (2012). Cell-free formation of RNA granules: low complexity sequence domains form dynamic fibers within hydrogels. *Cell*, 149(4):753–767.
- Katsushima, K. and Kondo, Y. (2014). Non-coding RNAs as epigenetic regulator of glioma stem-like cell differentiation. *Front Genet*, 5:14.
- Kedde, M., van Kouwenhove, M., Zwart, W., Oude Vrielink, J. A. F., Elkon, R., and Agami, R. (2010). A Pumilio-induced RNA structure switch in p27-3' UTR controls miR-221 and miR-222 accessibility. *Nat Cell Biol*, 12(10):1014–1020.
- Ketting, R. F. (2011). The many faces of RNAi. *Dev Cell*, 20(2):148–161.
- Ketting, R. F., Fischer, S. E., Bernstein, E., Sijen, T., Hannon, G. J., and Plasterk, R. H. (2001). Dicer functions in RNA interference and in synthesis of small RNA involved in developmental timing in *C. elegans*. *Genes Dev*, 15(20):2654–2659.
- Khorovova, A., Reynolds, A., and Jayasena, S. D. (2003). Functional siRNAs and miRNAs exhibit strand bias. *Cell*, 115(2):209–216.
- Kim, B. S., Jung, J. S., Jang, J. H., Kang, K. S., and Kang, S. K. (2011a). Nuclear Argonaute 2 regulates adipose tissue-derived stem cell survival through direct control of miR10b and selenoprotein N1 expression. *Aging Cell*, 10(2):277–291.
- Kim, D. H., Villeneuve, L. M., Morris, K. V., and Rossi, J. J. (2006). Argonaute-1 directs siRNA-mediated transcriptional gene silencing in human cells. *Nat Struct Mol Biol*, 13(9):793–797.
- Kim, H., Huang, W., Jiang, X., Pennicooke, B., Park, P. J., and Johnson, M. D. (2010). Integrative genome analysis reveals an oncomir/oncogene cluster regulating glioblastoma survivorship. *Proc Natl Acad Sci U S A*, 107(5):2183–2188.
- Kim, T.-M., Huang, W., Park, R., Park, P. J., and Johnson, M. D. (2011b). A developmental taxonomy of glioblastoma defined and maintained by MicroRNAs. *Cancer Res*, 71(9):3387–3399.

- Kim, V. N., Han, J., and Siomi, M. C. (2009). Biogenesis of small RNAs in animals. *Nat Rev Mol Cell Biol*, 10(2):126–139.
- Kim, Y., Yeo, J., Lee, J. H., Cho, J., Seo, D., Kim, J.-S., and Kim, V. N. (2014a). Deletion of Human tarbp2 Reveals Cellular MicroRNA Targets and Cell-Cycle Function of TRBP. *Cell Rep*, 9(3):1061–1074.
- Kim, Y. J., Maizel, A., and Chen, X. (2014b). Traffic into silence: endomembranes and post-transcriptional RNA silencing. *EMBO J*, 33(9):968–980.
- Kim, Y.-K. and Kim, V. N. (2007). Processing of intronic microRNAs. *EMBO J*, 26(3):775–783.
- Kobe, B. (1999). Autoinhibition by an internal nuclear localization signal revealed by the crystal structure of mammalian importin alpha. *Nat Struct Biol*, 6(4):388–397.
- Köhler, A. and Hurt, E. (2007). Exporting RNA from the nucleus to the cytoplasm. *Nat Rev Mol Cell Biol*, 8(10):761–773.
- Köhler, M., Speck, C., Christiansen, M., Bischoff, F. R., Prehn, S., Haller, H., Görlich, D., and Hartmann, E. (1999). Evidence for distinct substrate specificities of importin alpha family members in nuclear protein import. *Mol Cell Biol*, 19(11):7782–7791.
- Kreso, A. and Dick, J. E. (2014). Evolution of the cancer stem cell model. *Cell Stem Cell*, 14(3):275–291.
- Kretz, M., Siprashvili, Z., Chu, C., Webster, D. E., Zehnder, A., Qu, K., Lee, C. S., Flockhart, R. J., Groff, A. F., Chow, J., Johnston, D., Kim, G. E., Spitale, R. C., Flynn, R. A., Zheng, G. X. Y., Aiyer, S., Raj, A., Rinn, J. L., Chang, H. Y., and Khavari, P. A. (2013). Control of somatic tissue differentiation by the long non-coding RNA TINCR. *Nature*, 493(7431):231–235.
- Kudo, N., Matsumori, N., Taoka, H., Fujiwara, D., Schreiner, E. P., Wolff, B., Yoshida, M., and Horinouchi, S. (1999). Leptomycin B inactivates CRM1/exportin 1 by covalent modification at a cysteine residue in the central conserved region. *Proc Natl Acad Sci U S A*, 96(16):9112–9117.
- Kulkarni, M., Ozgur, S., and Stoecklin, G. (2010). On track with P-bodies. *Biochem Soc Trans*, 38(Pt 1):242–251.
- Kumar, M. S., Pester, R. E., Chen, C. Y., Lane, K., Chin, C., Lu, J., Kirsch, D. G., Golub, T. R., and Jacks, T. (2009). Dicer1 functions as a haploinsufficient tumor suppressor. *Genes Dev*, 23(23):2700–2704.
- Kumeta, M., Yamaguchi, H., Yoshimura, S. H., and Takeyasu, K. (2012). Karyopherin-independent spontaneous transport of amphiphilic proteins through the nuclear pore. *J Cell Sci*, 125(Pt 21):4979–4984.
- Kutay, U., Bischoff, F. R., Kostka, S., Kraft, R., and Görlich, D. (1997). Export of importin alpha from the nucleus is mediated by a specific nuclear transport factor. *Cell*, 90(6):1061–1071.
- Kwanhian, W., Lenze, D., Alles, J., Motsch, N., Barth, S., Döll, C., Imig, J., Hummel, M., Tinguely, M., Trivedi, P., Lulitanond, V., Meister, G., Renner, C., and Grässer, F. A. (2012). MicroRNA-142 is mutated in about 20 lymphoma. *Cancer Med*, 1(2):141–155.

- Lagace, D. C., Whitman, M. C., Noonan, M. A., Ables, J. L., DeCarolis, N. A., Arguello, A. A., Donovan, M. H., Fischer, S. J., Farnbauch, L. A., Beech, R. D., DiLeone, R. J., Greer, C. A., Mandyam, C. D., and Eisch, A. J. (2007). Dynamic contribution of nestin-expressing stem cells to adult neurogenesis. *J Neurosci*, 27(46):12623–12629.
- Lagos-Quintana, M., Rauhut, R., Lendeckel, W., and Tuschl, T. (2001). Identification of novel genes coding for small expressed RNAs. *Science*, 294(5543):853–858.
- Lagos-Quintana, M., Rauhut, R., Yalcin, A., Meyer, J., Lendeckel, W., and Tuschl, T. (2002). Identification of tissue-specific microRNAs from mouse. *Curr Biol*, 12(9):735–739.
- Lambertz, I., Nittner, D., Mestdagh, P., Denecker, G., Vandesompele, J., Dyer, M. A., and Marine, J.-C. (2010). Monoallelic but not biallelic loss of Dicer1 promotes tumorigenesis in vivo. *Cell Death Differ*, 17(4):633–641.
- Landgraf, P., Rusu, M., Sheridan, R., Sewer, A., Iovino, N., et al. (2007). A mammalian microRNA expression atlas based on small RNA library sequencing. *Cell*, 129(7):1401–1414.
- Landthaler, M., Gaidatzis, D., Rothballer, A., Chen, P. Y., Soll, S. J., Dinic, L., Ojo, T., Hafner, M., Zavolan, M., and Tuschl, T. (2008). Molecular characterization of human Argonaute-containing ribonucleoprotein complexes and their bound target mRNAs. *RNA*, 14(12):2580–2596.
- Landthaler, M., Yalcin, A., and Tuschl, T. (2004). The human DiGeorge syndrome critical region gene 8 and its D. melanogaster homolog are required for miRNA biogenesis. *Curr Biol*, 14(23):2162–2167.
- Larsson, O. and Nadon, R. (2013). Re-analysis of genome wide data on mammalian microRNA-mediated suppression of gene expression. *Translation*, 1(1):e24557.
- Lau, N. C., Lim, L. P., Weinstein, E. G., and Bartel, D. P. (2001). An abundant class of tiny RNAs with probable regulatory roles in *Caenorhabditis elegans*. *Science*, 294(5543):858–862.
- Lazzaretti, D., Tournier, I., and Izaurralde, E. (2009). The C-terminal domains of human TNRC6A, TNRC6B, and TNRC6C silence bound transcripts independently of Argonaute proteins. *RNA*, 15(6):1059–1066.
- Lee, B. J., Cansizoglu, A. E., Süel, K. E., Louis, T. H., Zhang, Z., and Chook, Y. M. (2006a). Rules for nuclear localization sequence recognition by karyopherin beta 2. *Cell*, 126(3):543–558.
- Lee, H. Y., Zhou, K., Smith, A. M., Noland, C. L., and Doudna, J. A. (2013). Differential roles of human Dicer-binding proteins TRBP and PACT in small RNA processing. *Nucleic Acids Res*, 41(13):6568–6576.
- Lee, J., Kotliarova, S., Kotliarov, Y., Li, A., Su, Q., Donin, N. M., Pastorino, S., Purow, B. W., Christopher, N., Zhang, W., Park, J. K., and Fine, H. A. (2006b). Tumor stem cells derived from glioblastomas cultured in bFGF and EGF more closely mirror the phenotype and genotype of primary tumors than do serum-cultured cell lines. *Cancer Cell*, 9(5):391–403.
- Lee, R. C. and Ambros, V. (2001). An extensive class of small RNAs in *Caenorhabditis elegans*. *Science*, 294(5543):862–864.
- Lee, R. C., Feinbaum, R. L., and Ambros, V. (1993). The *C. elegans* heterochronic gene *lin-4* encodes small RNAs with antisense complementarity to *lin-14*. *cell*, 75(5):843–854.

- Lee, Y., Hur, I., Park, S.-Y., Kim, Y.-K., Suh, M. R., and Kim, V. N. (2006c). The role of PACT in the RNA silencing pathway. *EMBO J*, 25(3):522–532.
- Lee, Y., Kim, M., Han, J., Yeom, K.-H., Lee, S., Baek, S. H., and Kim, V. N. (2004). MicroRNA genes are transcribed by RNA polymerase II. *EMBO J*, 23(20):4051–4060.
- Lee, Y. S. and Dutta, A. (2007). The tumor suppressor microRNA let-7 represses the HMGGA2 oncogene. *Genes Dev*, 21(9):1025–1030.
- Leisegang, M., Engels, B., Meyerhuber, P., Kieback, E., Sommermeyer, D., Xue, S.-A., Reuss, S., Stauss, H., and Uckert, W. (2008). Enhanced functionality of T cell receptor-redirection T cells is defined by the transgene cassette. *J Mol Med (Berl)*, 86(5):573–583.
- Leung, A. K. L., Calabrese, J. M., and Sharp, P. A. (2006). Quantitative analysis of Argonaute protein reveals microRNA-dependent localization to stress granules. *Proc Natl Acad Sci U S A*, 103(48):18125–18130.
- Leung, A. K. L. and Sharp, P. A. (2013). Quantifying Argonaute proteins in and out of GW/P-bodies: implications in microRNA activities. *Adv Exp Med Biol*, 768:165–182.
- Lewis, B. P., Shih, I.-h., Jones-Rhoades, M. W., Bartel, D. P., and Burge, C. B. (2003). Prediction of mammalian microRNA targets. *Cell*, 115(7):787–798.
- Li, A., Walling, J., Ahn, S., Kotliarov, Y., Su, Q., Quezado, M., Oberholtzer, J. C., Park, J., Zenklusen, J. C., and Fine, H. A. (2009). Unsupervised analysis of transcriptomic profiles reveals six glioma subtypes. *Cancer Res*, 69(5):2091–2099.
- Li, S., Wang, L., Fu, B., Berman, M. A., Diallo, A., and Dorf, M. E. (2014). TRIM65 regulates microRNA activity by ubiquitination of TNRC6. *Proc Natl Acad Sci U S A*, 111(19):6970–6975.
- Li, Y., Lu, J., Han, Y., Fan, X., and Ding, S.-W. (2013). RNA interference functions as an antiviral immunity mechanism in mammals. *Science*, 342(6155):231–234.
- Lima, W. F., Wu, H., Nichols, J. G., Sun, H., Murray, H. M., and Crooke, S. T. (2009). Binding and cleavage specificities of human Argonaute2. *J Biol Chem*, 284(38):26017–26028.
- Lin, J., Teo, S., Lam, D. H., Jeyaseelan, K., and Wang, S. (2012). MicroRNA-10b pleiotropically regulates invasion, angiogenicity and apoptosis of tumor cells resembling mesenchymal subtype of glioblastoma multiforme. *Cell Death Dis*, 3:e398.
- Liu, B., Liu, M., Wang, J., Zhang, X., Wang, X., Wang, P., Wang, H., Li, W., and Wang, Y. (2015). DICER-dependent biogenesis of let-7 miRNAs affects human cell response to DNA damage via targeting p21/p27. *Nucleic Acids Res*.
- Liu, C. and Tang, D. G. (2011). MicroRNA regulation of cancer stem cells. *Cancer Res*, 71(18):5950–5954.
- Liu, J., Carmell, M. A., Rivas, F. V., Marsden, C. G., Thomson, J. M., Song, J.-J., Hammond, S. M., Joshua-Tor, L., and Hannon, G. J. (2004). Argonaute2 is the catalytic engine of mammalian RNAi. *Science*, 305(5689):1437–1441.
- Liu, J., Hu, J., and Corey, D. R. (2012). Expanding the action of duplex RNAs into the nucleus: redirecting alternative splicing. *Nucleic Acids Res*, 40(3):1240–1250.

- Liu, J., Rivas, F. V., Wohlschlegel, J., Yates, 3rd, J. R., Parker, R., and Hannon, G. J. (2005a). A role for the P-body component GW182 in microRNA function. *Nat Cell Biol*, 7(12):1261–1266.
- Liu, J., Valencia-Sanchez, M. A., Hannon, G. J., and Parker, R. (2005b). MicroRNA-dependent localization of targeted mRNAs to mammalian P-bodies. *Nat Cell Biol*, 7(7):719–723.
- Liu, Z., Yang, X., Li, Z., McMahon, C., Sizer, C., Barenboim-Stapleton, L., Bliskovsky, V., Mock, B., Ried, T., London, W. B., Maris, J., Khan, J., and Thiele, C. J. (2011). CASZ1, a candidate tumor-suppressor gene, suppresses neuroblastoma tumor growth through reprogramming gene expression. *Cell Death Differ*, 18(7):1174–1183.
- Livak, K. J. and Schmittgen, T. D. (2001). Analysis of relative gene expression data using real-time quantitative PCR and the 2<sup>(-Delta Delta C(T))</sup> Method. *Methods*, 25(4):402–408.
- Long, C., Grueter, C. E., Song, K., Qin, S., Qi, X., Kong, Y. M., Shelton, J. M., Richardson, J. A., Zhang, C.-L., Bassel-Duby, R., and Olson, E. N. (2014). Ataxia and Purkinje cell degeneration in mice lacking the CAMTA1 transcription factor. *Proc. Natl. Acad. Sci. U. S. A.*
- Lottaz, C., Beier, D., Meyer, K., Kumar, P., Hermann, A., Schwarz, J., Junker, M., Oefner, P. J., Bogdahn, U., Wischhusen, J., Spang, R., Storch, A., and Beier, C. P. (2010). Transcriptional profiles of CD133+ and CD133- glioblastoma-derived cancer stem cell lines suggest different cells of origin. *Cancer Res*, 70(5):2030–2040.
- Lu, J., Getz, G., Miska, E. A., Alvarez-Saavedra, E., Lamb, J., Peck, D., Sweet-Cordero, A., Ebert, B. L., Mak, R. H., Ferrando, A. A., Downing, J. R., Jacks, T., Horvitz, H. R., and Golub, T. R. (2005). MicroRNA expression profiles classify human cancers. *Nature*, 435(7043):834–838.
- Lund, E., Güttinger, S., Calado, A., Dahlberg, J. E., and Kutay, U. (2004). Nuclear export of microRNA precursors. *Science*, 303(5654):95–98.
- Lytle, J. R., Yario, T. A., and Steitz, J. A. (2007). Target mRNAs are repressed as efficiently by microRNA-binding sites in the 5' UTR as in the 3' UTR. *Proc Natl Acad Sci U S A*, 104(23):9667–9672.
- Ma, L., Young, J., Prabhala, H., Pan, E., Mestdagh, P., Muth, D., Teruya-Feldstein, J., Reinhardt, F., Onder, T. T., Valastyan, S., Westermann, F., Speleman, F., Vandesompele, J., and Weinberg, R. A. (2010). miR-9, a MYC/MYCN-activated microRNA, regulates E-cadherin and cancer metastasis. *Nat Cell Biol*, 12(3):247–256.
- Macrae, I. J., Zhou, K., Li, F., Repic, A., Brooks, A. N., Cande, W. Z., Adams, P. D., and Doudna, J. A. (2006). Structural basis for double-stranded RNA processing by Dicer. *Science*, 311(5758):195–198.
- Madhavan, S., Zenklusen, J.-C., Kotliarov, Y., Sahni, H., Fine, H. A., and Buetow, K. (2009). Rembrandt: helping personalized medicine become a reality through integrative translational research. *Mol Cancer Res*, 7(2):157–167.
- Maillard, P. V., Ciaudo, C., Marchais, A., Li, Y., Jay, F., Ding, S. W., and Voinnet, O. (2013). Antiviral RNA interference in mammalian cells. *Science*, 342(6155):235–238.
- Malik, H. S., Eickbush, T. H., and Goldfarb, D. S. (1997). Evolutionary specialization of the nuclear targeting apparatus. *Proc Natl Acad Sci U S A*, 94(25):13738–13742.

- Malzkorn, B., Wolter, M., Liesenberg, F., Grzendowski, M., Stühler, K., Meyer, H. E., and Reifemberger, G. (2010). Identification and functional characterization of microRNAs involved in the malignant progression of gliomas. *Brain Pathol*, 20(3):539–550.
- Maniataki, E. and Mourelatos, Z. (2005). A human, ATP-independent, RISC assembly machine fueled by pre-miRNA. *Genes Dev*, 19(24):2979–2990.
- Marfori, M., Lonhienne, T. G., Forwood, J. K., and Kobe, B. (2012). Structural basis of high-affinity nuclear localization signal interactions with importin- $\alpha$ . *Traffic*, 13(4):532–548.
- Martinez, N. J., Chang, H.-M., Borrajo, J. d. R., and Gregory, R. I. (2013). The co-chaperones Fkbp4/5 control Argonaute2 expression and facilitate RISC assembly. *RNA*, 19(11):1583–1593.
- Martinez, N. J. and Gregory, R. I. (2013). Argonaute2 expression is post-transcriptionally coupled to microRNA abundance. *RNA*, 19(5):605–612.
- Mathys, H., Basquin, J., Ozgur, S., Czarnocki-Cieciura, M., Bonneau, F., Aartse, A., Dziembowski, A., Nowotny, M., Conti, E., and Filipowicz, W. (2014). Structural and biochemical insights to the role of the CCR4-NOT complex and DDX6 ATPase in microRNA repression. *Mol Cell*, 54(5):751–765.
- Matsui, M., Chu, Y., Zhang, H., Gagnon, K. T., Shaikh, S., Kuchimanchi, S., Manoharan, M., Corey, D. R., and Janowski, B. A. (2013). Promoter RNA links transcriptional regulation of inflammatory pathway genes. *Nucleic Acids Res*, 41(22):10086–10109.
- Matzke, M. A. and Mosher, R. A. (2014). RNA-directed DNA methylation: an epigenetic pathway of increasing complexity. *Nature Reviews Genetics*.
- Mayr, C. and Bartel, D. P. (2009). Widespread shortening of 3'UTRs by alternative cleavage and polyadenylation activates oncogenes in cancer cells. *Cell*, 138(4):673–684.
- Mayr, C., Hemann, M. T., and Bartel, D. P. (2007). Disrupting the pairing between let-7 and Hmga2 enhances oncogenic transformation. *Science*, 315(5818):1576–1579.
- Meister, G. (2013). Argonaute proteins: functional insights and emerging roles. *Nat Rev Genet*, 14(7):447–459.
- Meister, G., Landthaler, M., Dorsett, Y., and Tuschl, T. (2004a). Sequence-specific inhibition of microRNA- and siRNA-induced RNA silencing. *RNA*, 10(3):544–550.
- Meister, G., Landthaler, M., Patkaniowska, A., Dorsett, Y., Teng, G., and Tuschl, T. (2004b). Human Argonaute2 mediates RNA cleavage targeted by miRNAs and siRNAs. *Mol Cell*, 15(2):185–197.
- Meister, G., Landthaler, M., Peters, L., Chen, P. Y., Urlaub, H., Lührmann, R., and Tuschl, T. (2005). Identification of novel argonaute-associated proteins. *Curr Biol*, 15(23):2149–2155.
- Melo, S. A., Moutinho, C., Roperio, S., Calin, G. A., Rossi, S., Spizzo, R., Fernandez, A. F., Davalos, V., Villanueva, A., Montoya, G., et al. (2010). A genetic defect in exportin-5 traps precursor microRNAs in the nucleus of cancer cells. *Cancer cell*, 18(4):303–315.
- Mingot, J. M., Kostka, S., Kraft, R., Hartmann, E., and Görlich, D. (2001). Importin 13: a novel mediator of nuclear import and export. *EMBO J*, 20(14):3685–3694.

- Mizoguchi, M., Guan, Y., Yoshimoto, K., Hata, N., Amano, T., Nakamizo, A., and Sasaki, T. (2012). MicroRNAs in Human Malignant Gliomas. *J Oncol*, 2012:732874.
- Modzelewski, A. J., Holmes, R. J., Hilz, S., Grimson, A., and Cohen, P. E. (2012). AGO4 regulates entry into meiosis and influences silencing of sex chromosomes in the male mouse germline. *Dev Cell*, 23(2):251–264.
- Møller, H. G., Rasmussen, A. P., Andersen, H. H., Johnsen, K. B., Henriksen, M., and Duroux, M. (2013). A systematic review of microRNA in glioblastoma multiforme: micro-modulators in the mesenchymal mode of migration and invasion. *Mol Neurobiol*, 47(1):131–144.
- Monecke, T., Güttler, T., Neumann, P., Dickmanns, A., Görlich, D., and Ficner, R. (2009). Crystal structure of the nuclear export receptor CRM1 in complex with Snurportin1 and RanGTP. *Science*, 324(5930):1087–1091.
- Monecke, T., Haselbach, D., Voß, B., Russek, A., Neumann, P., Thomson, E., Hurt, E., Zachariae, U., Stark, H., Grubmüller, H., Dickmanns, A., and Ficner, R. (2013). Structural basis for cooperativity of CRM1 export complex formation. *Proc Natl Acad Sci U S A*, 110(3):960–965.
- Moore, M. S. and Blobel, G. (1993). The GTP-binding protein Ran/TC4 is required for protein import into the nucleus. *Nature*, 365(6447):661–663.
- Morita, S., Horii, T., Kimura, M., Goto, Y., Ochiya, T., and Hatada, I. (2007). One Argonaute family member, Eif2c2 (Ago2), is essential for development and appears not to be involved in DNA methylation. *Genomics*, 89(6):687–696.
- Morlando, M., Ballarino, M., Gromak, N., Pagano, F., Bozzoni, I., and Proudfoot, N. J. (2008). Primary microRNA transcripts are processed co-transcriptionally. *Nat Struct Mol Biol*, 15(9):902–909.
- Moroianu, J., Blobel, G., and Radu, A. (1996). The binding site of karyopherin alpha for karyopherin beta overlaps with a nuclear localization sequence. *Proc Natl Acad Sci U S A*, 93(13):6572–6576.
- Morris, K. V., Chan, S. W.-L., Jacobsen, S. E., and Looney, D. J. (2004). Small interfering RNA-induced transcriptional gene silencing in human cells. *Science*, 305(5688):1289–1292.
- Morris, K. V., Santoso, S., Turner, A.-M., Pastori, C., and Hawkins, P. G. (2008). Bidirectional transcription directs both transcriptional gene activation and suppression in human cells. *PLoS Genet*, 4(11):e1000258.
- Motamedi, M. R., Verdel, A., Colmenares, S. U., Gerber, S. A., Gygi, S. P., and Moazed, D. (2004). Two RNAi complexes, RITS and RDRC, physically interact and localize to noncoding centromeric RNAs. *Cell*, 119(6):789–802.
- Murray, M. J., Saini, H. K., Siegler, C. A., Hanning, J. E., Barker, E. M., et al. (2013). LIN28 Expression in malignant germ cell tumors downregulates let-7 and increases oncogene levels. *Cancer Res*, 73(15):4872–4884.
- Nachury, M. V. and Weis, K. (1999). The direction of transport through the nuclear pore can be inverted. *Proc Natl Acad Sci U S A*, 96(17):9622–9627.

- Naim, B., Zbaida, D., Dagan, S., Kapon, R., and Reich, Z. (2009). Cargo surface hydrophobicity is sufficient to overcome the nuclear pore complex selectivity barrier. *EMBO J*, 28(18):2697–2705.
- Nardozi, J. D., Lott, K., and Cingolani, G. (2010). Phosphorylation meets nuclear import: a review. *Cell Commun Signal*, 8:32.
- Nass, D., Rosenwald, S., Meiri, E., Gilad, S., Tabibian-Keissar, H., Schlosberg, A., Kuker, H., Sion-Vardy, N., Tobar, A., Kharenko, O., et al. (2009). MiR-92b and miR-9/9\* are specifically expressed in brain primary tumors and can be used to differentiate primary from metastatic brain tumors. *brain pathology*, 19(3):375–383.
- Nishi, K., Nishi, A., Nagasawa, T., and Ui-Tei, K. (2013). Human TNRC6A is an Argonaute-navigator protein for microRNA-mediated gene silencing in the nucleus. *RNA*, 19(1):17–35.
- Nishi, K., Yoshida, M., Fujiwara, D., Nishikawa, M., Horinouchi, S., and Beppu, T. (1994). Leptomycin B targets a regulatory cascade of crm1, a fission yeast nuclear protein, involved in control of higher order chromosome structure and gene expression. *J Biol Chem*, 269(9):6320–6324.
- Nishihara, T., Zekri, L., Braun, J. E., and Izaurralde, E. (2013). miRISC recruits decapping factors to miRNA targets to enhance their degradation. *Nucleic Acids Res*, 41(18):8692–8705.
- Noland, C. L., Ma, E., and Doudna, J. A. (2011). siRNA repositioning for guide strand selection by human Dicer complexes. *Mol Cell*, 43(1):110–121.
- Noto, T., Kurth, H. M., Kataoka, K., Aronica, L., DeSouza, L. V., Siu, K. W. M., Pearlman, R. E., Gorovsky, M. A., and Mochizuki, K. (2010). The Tetrahymena argonaute-binding protein Giw1p directs a mature argonaute-siRNA complex to the nucleus. *Cell*, 140(5):692–703.
- Nowak, J. S., Choudhury, N. R., de Lima Alves, F., Rappsilber, J., and Michlewski, G. (2014). Lin28a regulates neuronal differentiation and controls miR-9 production. *Nat Commun*, 5:3687.
- Oh, T., Fakurnejad, S., Sayegh, E. T., Clark, A. J., Ivan, M. E., Sun, M. Z., Safaee, M., Bloch, O., James, C. D., and Parsa, A. T. (2014). Immunocompetent murine models for the study of glioblastoma immunotherapy. *J Transl Med*, 12:107.
- Ohgaki, H. and Kleihues, P. (2007). Genetic pathways to primary and secondary glioblastoma. *Am J Pathol*, 170(5):1445–1453.
- Ohrt, T., Mütze, J., Staroske, W., Weinmann, L., Höck, J., Crell, K., Meister, G., and Schwill, P. (2008). Fluorescence correlation spectroscopy and fluorescence cross-correlation spectroscopy reveal the cytoplasmic origination of loaded nuclear RISC in vivo in human cells. *Nucleic Acids Res*, 36(20):6439–6449.
- Okada, C., Yamashita, E., Lee, S. J., Shibata, S., Katahira, J., Nakagawa, A., Yoneda, Y., and Tsukihara, T. (2009). A high-resolution structure of the pre-microRNA nuclear export machinery. *Science*, 326(5957):1275–1279.
- Olivieri, D., Sykora, M. M., Sachidanandam, R., Mechtler, K., and Brennecke, J. (2010). An in vivo RNAi assay identifies major genetic and cellular requirements for primary piRNA biogenesis in *Drosophila*. *EMBO J*, 29(19):3301–3317.
- Olsen, P. H. and Ambros, V. (1999). The lin-4 regulatory RNA controls developmental timing in *Caenorhabditis elegans* by blocking LIN-14 protein synthesis after the initiation of translation. *Dev Biol*, 216(2):671–680.

- Orban, T. I. and Izaurralde, E. (2005). Decay of mRNAs targeted by RISC requires XRN1, the Ski complex, and the exosome. *RNA*, 11(4):459–469.
- Orom, U. A., Nielsen, F. C., and Lund, A. H. (2008). MicroRNA-10a binds the 5'UTR of ribosomal protein mRNAs and enhances their translation. *Mol Cell*, 30(4):460–471.
- Pall, G. S. and Hamilton, A. J. (2008). Improved northern blot method for enhanced detection of small RNA. *Nat Protoc*, 3(6):1077–1084.
- Paraskeva, E., Izaurralde, E., Bischoff, F. R., Huber, J., Kutay, U., Hartmann, E., Lührmann, R., and Görlich, D. (1999). CRM1-mediated recycling of snurportin 1 to the cytoplasm. *J Cell Biol*, 145(2):255–264.
- Pare, J. M., LaPointe, P., and Hobman, T. C. (2013). Hsp90 cochaperones p23 and FKBP4 physically interact with hAgo2 and activate RNA interference-mediated silencing in mammalian cells. *Mol Biol Cell*, 24(15):2303–2310.
- Park, J., Freitag, S. I., Young, P. G., and Hobman, T. C. (2012). The karyopherin Sal3 is required for nuclear import of the core RNA interference pathway protein Rdp1. *Traffic*, 13(4):520–531.
- Parrish, S., Fleenor, J., Xu, S., Mello, C., and Fire, A. (2000). Functional anatomy of a dsRNA trigger: differential requirement for the two trigger strands in RNA interference. *Mol Cell*, 6(5):1077–1087.
- Parsons, D. W., Jones, S., Zhang, X., Lin, J. C.-H., Leary, R. J., et al. (2008). An integrated genomic analysis of human glioblastoma multiforme. *Science*, 321(5897):1807–1812.
- Parton, R. M., Davidson, A., Davis, I., and Weil, T. T. (2014). Subcellular mRNA localisation at a glance. *Journal of cell science*, 127(10):2127–2133.
- Pasquinelli, A. E., Reinhart, B. J., Slack, F., Martindale, M. Q., Kuroda, M. I., Maller, B., Hayward, D. C., Ball, E. E., Degnan, B., Müller, P., et al. (2000). Conservation of the sequence and temporal expression of let-7 heterochronic regulatory RNA. *Nature*, 408(6808):86–89.
- Patel, A. P., Tirosh, I., Trombetta, J. J., Shalek, A. K., Gillespie, S. M., Wakimoto, H., Cahill, D. P., Nahed, B. V., Curry, W. T., Martuza, R. L., Louis, D. N., Rozenblatt-Rosen, O., Suvà, M. L., Regev, A., and Bernstein, B. E. (2014). Single-cell RNA-seq highlights intratumoral heterogeneity in primary glioblastoma. *Science*, 344(6190):1396–1401.
- Pauley, K. M., Eystathioy, T., Jakymiw, A., Hamel, J. C., Fritzler, M. J., and Chan, E. K. L. (2006). Formation of GW bodies is a consequence of microRNA genesis. *EMBO Rep*, 7(9):904–910.
- Pawlicki, J. M. and Steitz, J. A. (2008). Primary microRNA transcript retention at sites of transcription leads to enhanced microRNA production. *J Cell Biol*, 182(1):61–76.
- Peruzzi, P., Bronisz, A., Nowicki, M. O., Wang, Y., Ogawa, D., Price, R., Nakano, I., Kwon, C.-H., Hayes, J., Lawler, S. E., Ostrowski, M. C., Chiocca, E. A., and Godlewski, J. (2013). MicroRNA-128 coordinately targets Polycomb Repressor Complexes in glioma stem cells. *Neuro Oncol*, 15(9):1212–1224.
- Peters, L. and Meister, G. (2007). Argonaute proteins: mediators of RNA silencing. *Mol Cell*, 26(5):611–623.

- Pfaff, J., Hennig, J., Herzog, F., Aebersold, R., Sattler, M., Niessing, D., and Meister, G. (2013). Structural features of Argonaute-GW182 protein interactions. *Proc Natl Acad Sci U S A*, 110(40):E3770–E3779.
- Pfaff, J. and Meister, G. (2013). Argonaute and GW182 proteins: an effective alliance in gene silencing. *Biochem Soc Trans*, 41(4):855–860.
- Phillips, H. S., Kharbanda, S., Chen, R., Forrester, W. F., Soriano, R. H., Wu, T. D., Misra, A., Nigro, J. M., Colman, H., Soroceanu, L., et al. (2006). Molecular subclasses of high-grade glioma predict prognosis, delineate a pattern of disease progression, and resemble stages in neurogenesis. *Cancer cell*, 9(3):157–173.
- Pillai, R. S., Bhattacharyya, S. N., Artus, C. G., Zoller, T., Cougot, N., Basyuk, E., Bertrand, E., and Filipowicz, W. (2005). Inhibition of translational initiation by Let-7 MicroRNA in human cells. *Science*, 309(5740):1573–1576.
- Piñol-Roma, S. and Dreyfuss, G. (1992). Shuttling of pre-mRNA binding proteins between nucleus and cytoplasm. *Nature*, 355(6362):730–732.
- Pollard, S. M., Yoshikawa, K., Clarke, I. D., Danovi, D., Stricker, S., Russell, R., Bayani, J., Head, R., Lee, M., Bernstein, M., Squire, J. A., Smith, A., and Dirks, P. (2009). Glioma stem cell lines expanded in adherent culture have tumor-specific phenotypes and are suitable for chemical and genetic screens. *Cell Stem Cell*, 4(6):568–580.
- Pollard, V. W., Michael, W. M., Nakielnny, S., Siomi, M. C., Wang, F., and Dreyfuss, G. (1996). A novel receptor-mediated nuclear protein import pathway. *Cell*, 86(6):985–994.
- Pyhtila, B. and Rexach, M. (2003). A gradient of affinity for the karyopherin Kap95p along the yeast nuclear pore complex. *J Biol Chem*, 278(43):42699–42709.
- Radu, A., Blobel, G., and Moore, M. S. (1995). Identification of a protein complex that is required for nuclear protein import and mediates docking of import substrate to distinct nucleoporins. *Proc Natl Acad Sci U S A*, 92(5):1769–1773.
- Ramalingam, P., Palanichamy, J. K., Singh, A., Das, P., Bhagat, M., Kassab, M. A., Sinha, S., and Chattopadhyay, P. (2014). Biogenesis of intronic miRNAs located in clusters by independent transcription and alternative splicing. *RNA*, 20(1):76–87.
- Rasmussen, K. D., Simmini, S., Abreu-Goodger, C., Bartonicek, N., Di Giacomo, M., Bilbao-Cortes, D., Horos, R., Von Lindern, M., Enright, A. J., and O'Carroll, D. (2010). The miR-144/451 locus is required for erythroid homeostasis. *J Exp Med*, 207(7):1351–1358.
- Rathod, S. S., Rani, S. B., Khan, M., Muzumdar, D., and Shiras, A. (2014). Tumor suppressive miRNA-34a suppresses cell proliferation and tumor growth of glioma stem cells by targeting Akt and Wnt signaling pathways. *FEBS Open Bio*, 4:485–495.
- Rehwinkel, J., Behm-Ansmant, I., Gatfield, D., and Izaurralde, E. (2005). A crucial role for GW182 and the DCP1:DCP2 decapping complex in miRNA-mediated gene silencing. *RNA*, 11(11):1640–1647.
- Reinhart, B. J., Slack, F. J., Basson, M., Pasquinelli, A. E., Bettinger, J. C., Rougvie, A. E., Horvitz, H. R., and Ruvkun, G. (2000). The 21-nucleotide let-7 RNA regulates developmental timing in *Caenorhabditis elegans*. *nature*, 403(6772):901–906.

- Reuter, M., Chuma, S., Tanaka, T., Franz, T., Stark, A., and Pillai, R. S. (2009). Loss of the Mili-interacting Tudor domain-containing protein-1 activates transposons and alters the Mili-associated small RNA profile. *Nat Struct Mol Biol*, 16(6):639–646.
- Reynolds, B. A. and Weiss, S. (1992). Generation of neurons and astrocytes from isolated cells of the adult mammalian central nervous system. *Science*, 255(5052):1707–1710.
- Ricci-Vitiani, L., Pallini, R., Biffoni, M., Todaro, M., Invernici, G., Cenci, T., Maira, G., Parati, E. A., Stassi, G., Larocca, L. M., and De Maria, R. (2010). Tumour vascularization via endothelial differentiation of glioblastoma stem-like cells. *Nature*, 468(7325):824–828.
- Robb, G. B., Brown, K. M., Khurana, J., and Rana, T. M. (2005). Specific and potent RNAi in the nucleus of human cells. *Nat Struct Mol Biol*, 12(2):133–137.
- Rodriguez, A., Griffiths-Jones, S., Ashurst, J. L., and Bradley, A. (2004). Identification of mammalian microRNA host genes and transcription units. *Genome Res*, 14(10A):1902–1910.
- Rüdel, S., Flatley, A., Weinmann, L., Kremmer, E., and Meister, G. (2008). A multifunctional human Argonaute2-specific monoclonal antibody. *RNA*, 14(6):1244–1253.
- Rüdel, S., Wang, Y., Lenobel, R., Körner, R., Hsiao, H.-H., Urlaub, H., Patel, D., and Meister, G. (2011). Phosphorylation of human Argonaute proteins affects small RNA binding. *Nucleic Acids Res*, 39(6):2330–2343.
- Ryan, B. M., Robles, A. I., and Harris, C. C. (2010). Genetic variation in microRNA networks: the implications for cancer research. *Nature Reviews Cancer*, 10(6):389–402.
- Saito, K., Inagaki, S., Mituyama, T., Kawamura, Y., Ono, Y., Sakota, E., Kotani, H., Asai, K., Siomi, H., and Siomi, M. C. (2009). A regulatory circuit for piwi by the large Maf gene traffic jam in *Drosophila*. *Nature*, 461(7268):1296–1299.
- Sakurai, K., Amarzguioui, M., Kim, D.-H., Alluin, J., Heale, B., Song, M.-s., Gagnon, A., Behlke, M. A., and Rossi, J. J. (2011). A role for human Dicer in pre-RISC loading of siRNAs. *Nucleic Acids Res*, 39(4):1510–1525.
- Sambrook, J., Fritsch, E. F., Maniatis, T., et al. (1989). *Molecular cloning*, volume 2. Cold spring harbor laboratory press New York.
- Sanai, N., Alvarez-Buylla, A., and Berger, M. S. (2005). Neural stem cells and the origin of gliomas. *N Engl J Med*, 353(8):811–822.
- Schauer, S. E., Jacobsen, S. E., Meinke, D. W., and Ray, A. (2002). DICER-LIKE1: blind men and elephants in *Arabidopsis* development. *Trends Plant Sci*, 7(11):487–491.
- Schirle, N. T. and MacRae, I. J. (2012). The crystal structure of human Argonaute2. *Science*, 336(6084):1037–1040.
- Schirle, N. T., Sheu-Gruttadauria, J., and MacRae, I. J. (2014). Gene regulation. Structural basis for microRNA targeting. *Science*, 346(6209):608–613.
- Schraivogel, D. and Meister, G. (2014). Import routes and nuclear functions of Argonaute and other small RNA-silencing proteins. *Trends Biochem Sci*.

- Schraivogel, D., Weinmann, L., Beier, D., Tabatabai, G., Eichner, A., Zhu, J. Y., Anton, M., Sixt, M., Weller, M., Beier, C. P., and Meister, G. (2011). CAMTA1 is a novel tumour suppressor regulated by miR-9/9\* in glioblastoma stem cells. *EMBO J*, 30(20):4309–4322.
- Schwartz, J. C., Younger, S. T., Nguyen, N.-B., Hardy, D. B., Monia, B. P., Corey, D. R., and Janowski, B. A. (2008). Antisense transcripts are targets for activating small RNAs. *Nat Struct Mol Biol*, 15(8):842–848.
- Schwarz, D. S., Hutvagner, G., Du, T., Xu, Z., Aronin, N., and Zamore, P. D. (2003). Asymmetry in the assembly of the RNAi enzyme complex. *Cell*, 115(2):199–208.
- Schwarz, D. S., Tomari, Y., and Zamore, P. D. (2004). The RNA-induced silencing complex is a Mg<sup>2+</sup>-dependent endonuclease. *Curr Biol*, 14(9):787–791.
- Seidel, S., Garvalov, B. K., Wirta, V., von Stechow, L., Schänzer, A., Meletis, K., Wolter, M., Sommerlad, D., Henze, A.-T., Nistér, M., Reifenberger, G., Lundeberg, J., Frisé, J., and Acker, T. (2010). A hypoxic niche regulates glioblastoma stem cells through hypoxia inducible factor 2 alpha. *Brain*, 133(Pt 4):983–995.
- Sempere, L. F., Freemantle, S., Pitha-Rowe, I., Moss, E., Dmitrovsky, E., and Ambros, V. (2004). Expression profiling of mammalian microRNAs uncovers a subset of brain-expressed microRNAs with possible roles in murine and human neuronal differentiation. *Genome biology*, 5(3):R13.
- Sen, G. L. and Blau, H. M. (2005). Argonaute 2/RISC resides in sites of mammalian mRNA decay known as cytoplasmic bodies. *Nat Cell Biol*, 7(6):633–636.
- Serano, R. D., Pegram, C. N., and Bigner, D. D. (1980). Tumorigenic cell culture lines from a spontaneous VM/Dk murine astrocytoma (SMA). *Acta Neuropathol*, 51(1):53–64.
- Shan, F., Li, J., and Huang, Q.-Y. (2014). HIF-1 alpha-induced up-regulation of miR-9 contributes to phenotypic modulation in pulmonary artery smooth muscle cells during hypoxia. *J Cell Physiol*, 229(10):1511–1520.
- Sharma, M., Jamieson, C., Johnson, M., Molloy, M. P., and Henderson, B. R. (2012). Specific armadillo repeat sequences facilitate  $\beta$ -catenin nuclear transport in live cells via direct binding to nucleoporins Nup62, Nup153, and RanBP2/Nup358. *J Biol Chem*, 287(2):819–831.
- Shen, Q. and Temple, S. (2009). Fine control: microRNA regulation of adult neurogenesis. *Nature neuroscience*, 12(4):369–370.
- Shenoy, A. and Blelloch, R. H. (2014). Regulation of microRNA function in somatic stem cell proliferation and differentiation. *Nat Rev Mol Cell Biol*, 15(9):565–576.
- Shibata, M., Nakao, H., Kiyonari, H., Abe, T., and Aizawa, S. (2011). MicroRNA-9 regulates neurogenesis in mouse telencephalon by targeting multiple transcription factors. *J Neurosci*, 31(9):3407–3422.
- Siddiqui, N., Mangus, D. A., Chang, T.-C., Palermينو, J.-M., Shyu, A.-B., and Gehring, K. (2007). Poly(A) nuclease interacts with the C-terminal domain of polyadenylate-binding protein domain from poly(A)-binding protein. *J Biol Chem*, 282(34):25067–25075.

- Siegel, R., Ma, J., Zou, Z., and Jemal, A. (2014). Cancer statistics, 2014. *CA Cancer J Clin*, 64(1):9–29.
- Silber, J., Lim, D. A., Petritsch, C., Persson, A. I., Maunakea, A. K., Yu, M., Vandenberg, S. R., Ginzinger, D. G., James, C. D., Costello, J. F., Bergers, G., Weiss, W. A., Alvarez-Buylla, A., and Hodgson, J. G. (2008). miR-124 and miR-137 inhibit proliferation of glioblastoma multiforme cells and induce differentiation of brain tumor stem cells. *BMC Med*, 6:14.
- Singh, S. K., Hawkins, C., Clarke, I. D., Squire, J. A., Bayani, J., Hide, T., Henkelman, R. M., Cusimano, M. D., and Dirks, P. B. (2004). Identification of human brain tumour initiating cells. *Nature*, 432(7015):396–401.
- Siomi, H. and Siomi, M. C. (2010). Posttranscriptional regulation of microRNA biogenesis in animals. *Mol Cell*, 38(3):323–332.
- Siomi, M. C., Sato, K., Pezic, D., and Aravin, A. A. (2011). PIWI-interacting small RNAs: the vanguard of genome defence. *Nat Rev Mol Cell Biol*, 12(4):246–258.
- Song, K., Backs, J., McAnally, J., Qi, X., Gerard, R. D., Richardson, J. A., Hill, J. A., Bassel-Duby, R., and Olson, E. N. (2006). The transcriptional coactivator CAMTA2 stimulates cardiac growth by opposing class II histone deacetylases. *Cell*, 125(3):453–466.
- Stalder, L., Heusermann, W., Sokol, L., Trojer, D., Wirz, J., Hean, J., Fritzsche, A., Aeschmann, F., Pfanzagl, V., Basselet, P., Weiler, J., Hintersteiner, M., Morrissey, D. V., and Meisner-Kober, N. C. (2013). The rough endoplasmic reticulum is a central nucleation site of siRNA-mediated RNA silencing. *EMBO J*, 32(8):1115–1127.
- Steinhoff, A., Pientka, F. K., Möckel, S., Kettelhake, A., Hartmann, E., Köhler, M., and Depping, R. (2009). Cellular oxygen sensing: Importins and exportins are mediators of intracellular localisation of prolyl-4-hydroxylases PHD1 and PHD2. *Biochem Biophys Res Commun*, 387(4):705–711.
- Stephens, P. J., Greenman, C. D., Fu, B., Yang, F., Bignell, G. R., Mudie, L. J., Pleasance, E. D., Lau, K. W., Beare, D., Stebbings, L. A., et al. (2011). Massive genomic rearrangement acquired in a single catastrophic event during cancer development. *Cell*, 144(1):27–40.
- Stewart, M. (2007). Molecular mechanism of the nuclear protein import cycle. *Nat Rev Mol Cell Biol*, 8(3):195–208.
- Stiles, C. D. and Rowitch, D. H. (2008). Glioma stem cells: a midterm exam. *Neuron*, 58(6):832–846.
- Stupp, R. and Hegi, M. E. (2007). Targeting brain-tumor stem cells. *Nat Biotechnol*, 25(2):193–194.
- Stupp, R., Mason, W. P., van den Bent, M. J., Weller, M., Fisher, B., et al. (2005). Radiotherapy plus concomitant and adjuvant temozolomide for glioblastoma. *N Engl J Med*, 352(10):987–996.
- Su, H., Trombly, M. I., Chen, J., and Wang, X. (2009). Essential and overlapping functions for mammalian Argonautes in microRNA silencing. *Genes Dev*, 23(3):304–317.
- Subtelny, A. O., Eichhorn, S. W., Chen, G. R., Sive, H., and Bartel, D. P. (2014). Poly(A)-tail profiling reveals an embryonic switch in translational control. *Nature*, 508(7494):66–71.

- Sun, Q., Carrasco, Y. P., Hu, Y., Guo, X., Mirzaei, H., Macmillan, J., and Chook, Y. M. (2013). Nuclear export inhibition through covalent conjugation and hydrolysis of Leptomycin B by CRM1. *Proc Natl Acad Sci U S A*, 110(4):1303–1308.
- Sundar, S. J., Hsieh, J. K., Manjila, S., Lathia, J. D., and Sloan, A. (2014). The role of cancer stem cells in glioblastoma. *Neurosurg Focus*, 37(6):E6.
- Suva, M. L., Rheinbay, E., Gillespie, S. M., Patel, A. P., Wakimoto, H., et al. (2014). Reconstructing and reprogramming the tumor-propagating potential of glioblastoma stem-like cells. *Cell*, 157(3):580–594.
- Swarts, D. C., Makarova, K., Wang, Y., Nakanishi, K., Ketting, R. F., Koonin, E. V., Patel, D. J., and van der Oost, J. (2014). The evolutionary journey of Argonaute proteins. *Nat Struct Mol Biol*, 21(9):743–753.
- Takahashi, K. and Yamanaka, S. (2006). Induction of pluripotent stem cells from mouse embryonic and adult fibroblast cultures by defined factors. *Cell*, 126(4):663–676.
- Takahashi, R.-u., Miyazaki, H., and Ochiya, T. (2013). The role of microRNAs in the regulation of cancer stem cells. *Frontiers in genetics*, 4.
- Takimoto, K., Wakiyama, M., and Yokoyama, S. (2009). Mammalian GW182 contains multiple Argonaute-binding sites and functions in microRNA-mediated translational repression. *RNA*, 15(6):1078–1089.
- Tam, O. H., Aravin, A. A., Stein, P., Girard, A., Murchison, E. P., Cheloufi, S., Hodges, E., Anger, M., Sachidanandam, R., Schultz, R. M., and Hannon, G. J. (2008). Pseudogene-derived small interfering RNAs regulate gene expression in mouse oocytes. *Nature*, 453(7194):534–538.
- Tarasov, V., Jung, P., Verdoodt, B., Lodygin, D., Epanchintsev, A., Menssen, A., Meister, G., and Hermeking, H. (2007). Differential regulation of microRNAs by p53 revealed by massively parallel sequencing: miR-34a is a p53 target that induces apoptosis and G1-arrest. *Cell Cycle*, 6(13):1586–1593.
- Taylor, D. W., Ma, E., Shigematsu, H., Cianfrocco, M. A., Noland, C. L., Nagayama, K., Nogales, E., Doudna, J. A., and Wang, H.-W. (2013). Substrate-specific structural rearrangements of human Dicer. *Nat Struct Mol Biol*, 20(6):662–670.
- TCGA, C. G. A. R. N. (2008). Comprehensive genomic characterization defines human glioblastoma genes and core pathways. *Nature*, 455(7216):1061–1068.
- Thome, M. (2008). Multifunctional roles for MALT1 in T-cell activation. *Nat Rev Immunol*, 8(7):495–500.
- Till, S., Lejeune, E., Thermann, R., Bortfeld, M., Hothorn, M., Enderle, D., Heinrich, C., Hentze, M. W., and Ladurner, A. G. (2007). A conserved motif in Argonaute-interacting proteins mediates functional interactions through the Argonaute PIWI domain. *Nat Struct Mol Biol*, 14(10):897–903.
- Tolia, N. H. and Joshua-Tor, L. (2007). Slicer and the argonautes. *Nat Chem Biol*, 3(1):36–43.
- Van Stry, M., Oguin, 3rd, T. H., Cheloufi, S., Vogel, P., Watanabe, M., Pillai, M. R., Dash, P., Thomas, P. G., Hannon, G. J., and Bix, M. (2012). Enhanced susceptibility of Ago1/3 double-null mice to influenza A virus infection. *J Virol*, 86(8):4151–4157.

- Verdel, A., Jia, S., Gerber, S., Sugiyama, T., Gygi, S., Grewal, S. I. S., and Moazed, D. (2004). RNAi-mediated targeting of heterochromatin by the RITS complex. *Science*, 303(5658):672–676.
- Verhaak, R. G. W., Hoadley, K. A., Purdom, E., Wang, V., Qi, Y., et al. (2010). Integrated genomic analysis identifies clinically relevant subtypes of glioblastoma characterized by abnormalities in PDGFRA, IDH1, EGFR, and NF1. *Cancer Cell*, 17(1):98–110.
- Vesely, B. A., Alli, A. A., Song, S. J., Gower, Jr, W., Sanchez-Ramos, J., and Vesely, D. L. (2005). Four peptide hormones' specific decrease (up to 97 prostate carcinoma cells. *Eur J Clin Invest*, 35(11):700–710.
- Vesely, B. A., Eichelbaum, E. J., Alli, A. A., Sun, Y., Gower, Jr, W. R., and Vesely, D. L. (2007). Four cardiac hormones eliminate 4-fold more human glioblastoma cells than the green mamba snake peptide. *Cancer Lett*, 254(1):94–101.
- Virden, R. A., Thiele, C. J., and Liu, Z. (2012). Characterization of critical domains within the tumor suppressor CASZ1 required for transcriptional regulation and growth suppression. *Mol Cell Biol*, 32(8):1518–1528.
- Völler, D., Reinders, J., Meister, G., and Bosserhoff, A.-K. (2013). Strong reduction of AGO2 expression in melanoma and cellular consequences. *Br J Cancer*, 109(12):3116–3124.
- von Bohlen Und Halbach, O. (2007). Immunohistological markers for staging neurogenesis in adult hippocampus. *Cell Tissue Res*, 329(3):409–420.
- Walker, T. L. and Kempermann, G. (2014). One mouse, two cultures: isolation and culture of adult neural stem cells from the two neurogenic zones of individual mice. *J Vis Exp*, 25(84):e51225.
- Wang, R., Chadalavada, K., Wilshire, J., Kowalik, U., Hovinga, K. E., Geber, A., Fligelman, B., Leversha, M., Brennan, C., and Tabar, V. (2010). Glioblastoma stem-like cells give rise to tumour endothelium. *Nature*, 468(7325):829–833.
- Watanabe, T., Totoki, Y., Toyoda, A., Kaneda, M., Kuramochi-Miyagawa, S., Obata, Y., Chiba, H., Kohara, Y., Kono, T., Nakano, T., Surani, M. A., Sakaki, Y., and Sasaki, H. (2008). Endogenous siRNAs from naturally formed dsRNAs regulate transcripts in mouse oocytes. *Nature*, 453(7194):539–543.
- Wei, W., Ba, Z., Gao, M., Wu, Y., Ma, Y., Amiard, S., White, C. I., Rendtlew Danielsen, J. M., Yang, Y.-G., and Qi, Y. (2012). A role for small RNAs in DNA double-strand break repair. *Cell*, 149(1):101–112.
- Wei, Y., Li, L., Wang, D., Zhang, C.-Y., and Zen, K. (2014). Importin 8 regulates the transport of mature microRNAs into the cell nucleus. *J Biol Chem*, 289(15):10270–10275.
- Weick, E.-M. and Miska, E. A. (2014). piRNAs: from biogenesis to function. *Development*, 141(18):3458–3471.
- Weinberg, R. (2013). *The biology of cancer*. Garland Science.
- Weinmann, L., Höck, J., Ivacevic, T., Ohrt, T., Mütze, J., Schwille, P., Kremmer, E., Benes, V., Urlaub, H., and Meister, G. (2009). Importin 8 is a gene silencing factor that targets argonaute proteins to distinct mRNAs. *Cell*, 136(3):496–507.

- Weitzer, S. and Martinez, J. (2007). The human RNA kinase hCIP1 is active on 3 transfer RNA exons and short interfering RNAs. *Nature*, 447(7141):222–226.
- Weller, M., Felsberg, J., Hartmann, C., Berger, H., Steinbach, J. P., et al. (2009). Molecular predictors of progression-free and overall survival in patients with newly diagnosed glioblastoma: a prospective translational study of the German Glioma Network. *J Clin Oncol*, 27(34):5743–5750.
- Wente, S. R. and Rout, M. P. (2010). The nuclear pore complex and nuclear transport. *Cold Spring Harb Perspect Biol*, 2(10):a000562.
- Wierzbicki, A. T., Cocklin, R., Mayampurath, A., Lister, R., Rowley, M. J., Gregory, B. D., Ecker, J. R., Tang, H., and Pikaard, C. S. (2012). Spatial and functional relationships among Pol V-associated loci, Pol IV-dependent siRNAs, and cytosine methylation in the Arabidopsis epigenome. *Genes Dev*, 26(16):1825–1836.
- Wierzbicki, A. T., Haag, J. R., and Pikaard, C. S. (2008). Noncoding transcription by RNA polymerase Pol IVb/Pol V mediates transcriptional silencing of overlapping and adjacent genes. *Cell*, 135(4):635–648.
- Wightman, B., Ha, I., and Ruvkun, G. (1993). Posttranscriptional regulation of the heterochronic gene *lin-14* by *lin-4* mediates temporal pattern formation in *C. elegans*. *Cell*, 75(5):855–862.
- Wilczynska, A. and Bushell, M. (2015). The complexity of miRNA-mediated repression. *Cell Death Differ*, 22(1):22–33.
- Wilson, R. C., Tambe, A., Kidwell, M. A., Noland, C. L., Schneider, C. P., and Doudna, J. A. (2015). Dicer-TRBP Complex Formation Ensures Accurate Mammalian MicroRNA Biogenesis. *Mol Cell*, 57(3):397–407.
- Wolf, J., Valkov, E., Allen, M. D., Meineke, B., Gordiyenko, Y., McLaughlin, S. H., Olsen, T. M., Robinson, C. V., Bycroft, M., Stewart, M., and Passmore, L. A. (2014). Structural basis for Pan3 binding to Pan2 and its function in mRNA recruitment and deadenylation. *EMBO J*, 33(14):1514–1526.
- Woolcock, K. J., Gaidatzis, D., Punga, T., and Bühler, M. (2011). Dicer associates with chromatin to repress genome activity in *Schizosaccharomyces pombe*. *Nat Struct Mol Biol*, 18(1):94–99.
- Woolcock, K. J., Stunnenberg, R., Gaidatzis, D., Hotz, H.-R., Emmerth, S., Barraud, P., and Bühler, M. (2012). RNAi keeps Atf1-bound stress response genes in check at nuclear pores. *Genes Dev*, 26(7):683–692.
- Wübbenhorst, D., Dumler, K., Wagner, B., Wexel, G., Imhoff, A., Gansbacher, B., Vogt, S., and Anton, M. (2010). Tetracycline-regulated bone morphogenetic protein 2 gene expression in lentivirally transduced primary rabbit chondrocytes for treatment of cartilage defects. *Arthritis Rheum*, 62(7):2037–2046.
- Xia, H., Cheung, W. K. C., Ng, S. S., Jiang, X., Jiang, S., Sze, J., Leung, G. K. K., Lu, G., Chan, D. T. M., Bian, X.-W., Kung, H.-f., Poon, W. S., and Lin, M. C. (2012). Loss of brain-enriched miR-124 microRNA enhances stem-like traits and invasiveness of glioma cells. *J Biol Chem*, 287(13):9962–9971.

- Yang, J.-S., Maurin, T., Robine, N., Rasmussen, K. D., Jeffrey, K. L., Chandwani, R., Papapetrou, E. P., Sadelain, M., O'Carroll, D., and Lai, E. C. (2010). Conserved vertebrate mir-451 provides a platform for Dicer-independent, Ago2-mediated microRNA biogenesis. *Proc Natl Acad Sci U S A*, 107(34):15163–15168.
- Yang, Z., Jakymiw, A., Wood, M. R., Eystathiou, T., Rubin, R. L., Fritzler, M. J., and Chan, E. K. L. (2004). GW182 is critical for the stability of GW bodies expressed during the cell cycle and cell proliferation. *J Cell Sci*, 117(Pt 23):5567–5578.
- Ye, R., Wang, W., Iki, T., Liu, C., Wu, Y., Ishikawa, M., Zhou, X., and Qi, Y. (2012). Cytoplasmic assembly and selective nuclear import of Arabidopsis Argonaute4/siRNA complexes. *Mol Cell*, 46(6):859–870.
- Yi, R., Qin, Y., Macara, I. G., and Cullen, B. R. (2003). Exportin-5 mediates the nuclear export of pre-microRNAs and short hairpin RNAs. *Genes Dev*, 17(24):3011–3016.
- Yoo, A. S., Staahl, B. T., Chen, L., and Crabtree, G. R. (2009). MicroRNA-mediated switching of chromatin-remodelling complexes in neural development. *Nature*, 460(7255):642–646.
- Yoshimura, S. H., Kumeta, M., and Takeyasu, K. (2014). Structural Mechanism of Nuclear Transport Mediated by Importin  $\beta$  and Flexible Amphiphilic Proteins. *Structure*.
- Zamore, P. D., Tuschl, T., Sharp, P. A., and Bartel, D. P. (2000). RNAi: double-stranded RNA directs the ATP-dependent cleavage of mRNA at 21 to 23 nucleotide intervals. *Cell*, 101(1):25–33.
- Zekri, L., Huntzinger, E., Heimstädt, S., and Izaurralde, E. (2009). The silencing domain of GW182 interacts with PABPC1 to promote translational repression and degradation of microRNA targets and is required for target release. *Mol Cell Biol*, 29(23):6220–6231.
- Zekri, L., Kuzuolu-Ozturk, D., and Izaurralde, E. (2013). GW182 proteins cause PABP dissociation from silenced miRNA targets in the absence of deadenylation. *EMBO J*, 32(7):1052–1065.
- Zhang, H., Kolb, F. A., Jaskiewicz, L., Westhof, E., and Filipowicz, W. (2004). Single processing center models for human Dicer and bacterial RNase III. *Cell*, 118(1):57–68.
- Zhao, C., Sun, G., Li, S., and Shi, Y. (2009). A feedback regulatory loop involving microRNA-9 and nuclear receptor TLX in neural stem cell fate determination. *Nat Struct Mol Biol*, 16(4):365–371.
- Zheng, X., Zhu, J., Kapoor, A., and Zhu, J.-K. (2007). Role of Arabidopsis AGO6 in siRNA accumulation, DNA methylation and transcriptional gene silencing. *EMBO J*, 26(6):1691–1701.
- Zhou, X., Zhang, J., Jia, Q., Ren, Y., Wang, Y., Shi, L., Liu, N., Wang, G., Pu, P., You, Y., and Kang, C. (2010). Reduction of miR-21 induces glioma cell apoptosis via activating caspase 9 and 3. *Oncol Rep*, 24(1):195–201.
- Zipprich, J. T., Bhattacharyya, S., Mathys, H., and Filipowicz, W. (2009). Importance of the C-terminal domain of the human GW182 protein TNRC6C for translational repression. *RNA*, 15(5):781–793.
- Zong, H., Verhaak, R. G. W., and Canoll, P. (2012). The cellular origin for malignant glioma and prospects for clinical advancements. *Expert Rev Mol Diagn*, 12(4):383–394.

# Publications and Presentations

## Publications

**Schraivogel D**<sup>1</sup>, Weinmann L<sup>1</sup>, Beier D, Tabatabai G, Eichner A, Zhu JY, Anton M, Sixt M, Weller M, Beier CP, Meister G. CAMTA1 is a novel tumour suppressor regulated by miR-9/9\* in glioblastoma stem cells. *EMBO J.* 2011 Aug 19;30(20):4309-22. doi:10.1038/emboj.2011.301

**Schraivogel D**, Meister G. Import routes and nuclear functions of Argonaute and other small RNA-silencing proteins. *Trends Biochem Sci.* 2014 Sep 39(9):420-31. doi:10.1016/j.tibs.2014.07.004

Bassler J<sup>1</sup>, Patergona H<sup>1</sup>, Holdermann I, Thoms M, Granneman S, Barrio-Garcia C, Nyarko A, Stier G, Clark S, **Schraivogel D**, Kallas M, Beckmann R, Tollervey D, Barbar E, Sinning I, Hurt E. A network of assembly factors is involved in remodeling rRNA elements during preribosome maturation. *JCB* 2014 Nov 207(4):481-98. doi:10.1083/jcb.201408111

**Schraivogel D**, Schindler S, Danner J, Kremmer E, Pfaff J, Depping R, Meister G. Importin- $\beta$  facilitates nuclear import of human GW proteins and balances cytoplasmic gene silencing protein levels. [Manuscript under revision]

Hauptmann J, **Schraivogel D**, Bruckmann A, Manickavel S, Jakob L, Eichner N, Pfaff J, Hafner M, Tuschl T, Deutzmann R, Meister G. Ago-APP: A GW peptide-based Argonaute affinity capture strategy. [Manuscript in preparation]

Codo P, Weller M, Wolter M, **Schraivogel D**, Meister G, Roth P. Control of glioma cell migration and invasiveness by GDF-15. [Manuscript submitted]

---

<sup>1</sup>These authors contributed equally to this work.

## **Presentations**

**Schraivogel D**, Meister G. Nuclear Import of Argonaute Proteins. Poster presented at EMBO/EMBL Symposium The Non-Coding Genome, Heidelberg, 2010

**Schraivogel D**, Strieder N, Weinmann L, Meister G. Nuclear Import of Argonaute Proteins. Poster presented at Keystone Symposium on Non-coding RNA, Utah, USA, 2012

**Schraivogel D**, Weinmann L, Eichner A, Beier C, Beier D, Meister G. CAMTA1 is a novel tumor suppressor that is regulated by miR-9/9\* in glioblastoma stem cells. Poster presented at Microsymposium on RNA, Vienna, Austria 2012

# Curriculum vitae

## Personal information

Name Daniel Florian Schraivogel  
Nationality German  
Date of birth 22. February 1984  
Place of birth Ochsenhausen

## Scholar education

1990 to 1994 Basic school Ochsenhausen  
1994 to 2003 Gymnasium Ochsenhausen (Abitur)  
Grade: 2,3

## Academic education

2003 to 2009 Studies of Biology (Diploma) at Ulm University  
Grade: 1,1  
2008 to 2009 Diploma thesis at Heidelberg University Biochemistry Center  
in the laboratory of Prof. Ed Hurt  
Topic: *Characterizing the Interaction of Nsa2 and Rsa4,  
which are essential factors in 60S biogenesis*  
2009 to 2015 Doctoral thesis at Max-Planck-Institute of Biochemistry (Munich)  
and Regensburg University in the laboratory of Prof. G. Meister  
Topics: *miR-9/9\* regulate the tumor suppressor CAMTA1  
in glioblastoma cancer stem cells and  
Nuclear transport of Argonaute and TNRC6 proteins*

## Extracurricular skills and activities

Teaching Tutor for practical physiology training for medical students  
Supervision of 2 diploma, 2 bachelor and 3 master students  
Languages German, English, French  
Computer Standard applications (Windows, Office, Photoshop, Illustrator)  
Basic programming knowledge  
University FELASA accredited course type B, Regensburg University  
Genetic engineering law course, Regensburg University  
Hobbies Football, Skiing, Squash

# Acknowledgements

First and foremost, I want to thank Gunter Meister for the great opportunity to conduct my doctoral research in his department. I thank him for his constant support, his enthusiasm, many inspiring discussions and for enabling experimental freedom. My future career will - without a doubt - profit a lot from your mentorship and far-reaching scientific experience.

I am very thankful to Peter Hau, Frank Sprenger, Herbert Tschochner and Richard Warth for being in my thesis examination committee.

Many thanks goes to the entire Meister laboratory at Max-Planck Institute and Regensburg. Special thanks goes to Anne for critically reading my dissertation and for many fruitful discussions. Furthermore, I thank Mathias, Inga, Sam, Johannes, Sebastian, Melina and all the others for being great colleagues and friends. I am also very grateful to Jan for many discussions in- and outside the lab.

I especially thank following collaborators and facilities: Dagmar and Christoph Beier for providing the xenograft mouse model; Michael Weller and Ghazaleh Tabatabai for cooperation on glioblastoma-associated projects; Reinhard Depping for performing GST-pulldown experiments; Mathias Stotz for his help during Ago2-purification; Oliver Gruss for performing Ago2-pulldowns from oocyte extracts; Elisabeth Kremmer and Johannes Danner for generating TNRC6-antibodies; Frank Sprenger for access to CyFlow; Regensburg animal facility members Daniel Wagner and Peter Karl.

Many thanks to my friends including Mario, Andreas and Wolfgang. Further more, I want to thank my former fellow students and colleagues from Ulm and Heidelberg.

Last but not least, I want to express my gratitude to my great parents and my precious brother incl. Julia. Thank you for your unconditional support, for always being there as a fixed point and for giving new impulses when they are needed. That was without a doubt crucial for this work.

